
**Imaging atherosclerotic plaque inflammation with
[¹⁸F]- fluorodeoxyglucose positron emission
tomography**

A dissertation submitted to The University of Cambridge for the degree of
Doctor of Philosophy

James H.F. Rudd

January 2003

Wolfson College
and
Division of Cardiovascular Medicine
Department of Medicine
University of Cambridge

DECLARATION

All of the work reported in this thesis is my own. Where any assistance with technical matters was obtained, those providing expertise are acknowledged in the text. No part of this dissertation has been submitted for a degree, diploma or other qualification at any other university.

James H F Rudd

January 2003

ACKNOWLEDGEMENTS

I am extremely grateful to Professor Peter Weissberg for supervising the work described in this thesis. His assistance, from initial grant application to journal publication and all stops in between has been invaluable, and this work would not have come to fruition without his guidance and enthusiasm.

I would also like to express sincere thanks to Dr Tim Fryer, whose help, often at unearthly hours, with the analysis of PET data was essential to the project, and whose ready wit and wisdom were essential to my continued sanity.

In this work, which crosses many specialist boundaries, cooperation between departments was vital for success. I would particularly like to mention the following who advised and helped to make things happen within their respective departments : Dr Liz Warburton whose enthusiasm is infectious, Dr Hazel Jones, Dr John Clark, Dr Jonathan Gillard, Dr Peter Johnstrom, Dr Anthony Davenport, Dr Nagui Antoun, Dr Barbara Arch, Dr Hugh Richards, Mr Peter Kirkpatrick and thanks especially to Dr Laszlo Hegyi who provided me with training and supervision for the microPet work in Chapter 6. I am also grateful to Nikki Figg and Carl Atkinson for their expert assistance with immunohistochemistry. Thanks also for the patience and humour of those working alongside me in the ACCI – Mike, Steve, Afshin, Denise, Joe, Diane, Nicola, John, Clive, Chandike, Alastair, Rhiannon and Cassie.

Finally, I would like to express my heartfelt gratitude to my family who have been unconditional in supporting me over the last 33 years. Particular mention is due to Emma, who has put up with all the highs and lows of the last three years without a grumble. For this, and for everything else, I am unable to express truly the extent of my thanks and admiration.

LIST OF ABBREVIATIONS

^{11}C	11-Carbon
^{18}F	18-Fluorine
(k/M)Bq	(kilo/mega) Bequerel
C_b	Concentration of bound tracer
C_f	Concentration of free tracer
C_p	Plasma concentration of tracer
C_T	Total concentration of tracer
CI	Confidence interval
CO_2	Carbon dioxide
CRP	C-reactive protein
CT	Computed tomography
DPM	Decays per minute
eNOS	Endothelial nitric oxide synthase
EDTA	Ethylene diamine tetra-acetic acid
ETL	Echo train length
FDG	2-[^{18}F]fluoro-2-deoxy-D-glucose
FOV	Field of view
FWHM	Full width half maximum
GLUT	Glucose transporter protein
H and E	Haematoxylin and eosin
HDG	2-Deoxy-D-[1- ^3H]glucose
HDL	High density lipoprotein
HRMR	High-resolution magnetic resonance
ICAM-1	Intercellular adhesion molecule-1
IFN	Interferon gamma
IL-1 β	Interleukin-1 beta
IVUS	Intravascular ultrasound
(m/ μ)l	(milli/micro)litre
LDL	Low density lipoprotein
LPS	Lipopolysaccharide
M199	Medium 199
MR	Magnetic resonance
MMP	Matrix metalloproteinase
MCP-1	Monocyte chemoattractant protein-1
MRGlc	Metabolic rate for glucose
NEX	Number of excitations
NO	Nitric oxide
NZWR	New Zealand white rabbit
p	Probability
PBMC	Peripheral blood mononuclear cells
PBS	Phosphate-buffered saline
PDGF	Platelet-derived growth factor
PDW	Proton density-weighted
PET	Positron emission tomography
PK11195	1-(2-chlorophenyl)-N-methyl-N-(1-methylpropyl)-1-isoquinolone carboxamide
PMA	Phorbol myristate acetate
ROI	Region of interest

SE	Standard error
SEM	Standard error of the mean
SMA	Smooth muscle actin
t	Time
T	Tesla
T1W	T1-weighted
T2W	T2-weighted
TAC	Time activity curve
TBS	Tris-buffered saline
TE	Echo time
TIA	Transient ischaemic attack
TNF- α	Tumour necrosis factor alpha
VCAM-1	Vascular cell adhesion molecule-1
VOI	Volume of interest
VSMC	Vascular smooth muscle cell
v/v	Volume/volume

Atherosclerotic Plaque Inflammation Imaging Using Fluorodeoxyglucose Positron Emission Tomography (FDG-PET)

James H F Rudd

Inflammation is important in both the pathogenesis and outcome of atherosclerosis. Plaques containing numerous inflammatory cells, particularly macrophages, have a high risk of rupture, whereas those with fewer inflammatory cells are at lower risk. The current 'gold standard' technique for imaging atherosclerosis is x-ray contrast angiography, which provides high-resolution definition of the site and severity of luminal stenoses, but no information about plaque inflammation.

Quantification of plaque inflammation is desirable both to predict risk of plaque rupture and to monitor the effects of atheroma-modifying therapies. This is important since recent studies strongly suggest that HMG Co-A reductase inhibitors promote plaque stability by decreasing plaque macrophage content and activity without substantially reducing plaque size and therefore angiographic appearance. FDG is a glucose analogue that is taken up by cells in proportion to their metabolic activity.

In this work, the central hypothesis was that plaque inflammation could be visualised and quantified non-invasively using FDG-PET.

Initially, THP-1 monocytes and buffy-coat macrophages were stimulated with cellular activators, and the effect on deoxyglucose uptake was observed. It was demonstrated that both types of cell accumulated deoxyglucose in proportion to their metabolic activity. Next, FDG uptake was assessed in endarterectomy specimens from patients with symptomatic carotid disease. Autoradiography of excised plaques confirmed accumulation of deoxyglucose in macrophage-rich areas.

Subsequently, co-registered FDG-PET imaging was performed in patients with transient ischaemic attack. FDG accumulated within carotid plaques, with

significantly more FDG being taken up into symptomatic plaques than contralateral asymptomatic lesions.

Finally, a rabbit model of atherosclerosis was established to investigate two related questions: firstly, whether an animal PET scanner (MicroPet) might detect atheroma, and secondly whether FDG-PET could image and perhaps quantify both atheroma progression and regression. Aortic atheroma was identified by FDG-PET, but full quantification was not possible, because the microPet system is currently unable to perform studies with attenuation correction.

In summary, it has been shown, both *in vitro* and *in vivo*, that inflammation within atherosclerotic plaques can be successfully imaged by FDG-PET. In addition, pilot data from an experimental study of atherosclerosis in rabbits suggested that serial imaging with this technique might be useful for monitoring the effects of anti-atheroma drugs.

TABLE OF CONTENTS

	DECLARATION	i
	ACKNOWLEDGEMENTS	ii
	LIST OF ABBREVIATIONS	iii
	SUMMARY	v
	TABLE OF CONTENTS	vii
	LIST OF FIGURES	xi
	LIST OF TABLES	xiii
1	INTRODUCTION	1
1.1	Atherosclerosis	1
1.1.1	The epidemiology of atherosclerosis.....	1
1.1.2	The pathology of atherosclerosis.....	3
1.1.2.1	The structure of the healthy artery.....	5
1.1.2.2	The pathology of the atherosclerotic artery.....	6
1.1.3	Theories of atherogenesis.....	7
1.1.3.1	Lipid hypothesis.....	7
1.1.3.2	Thrombogenic hypothesis.....	7
1.1.3.3	The response to injury hypothesis.....	8
1.1.3.4	The modified response to injury hypothesis.....	8
1.1.3.5	Atherosclerosis as an inflammatory disease.....	9
1.2	Cellular roles in atherosclerosis	10
1.2.1	The endothelium.....	10
1.2.1.1	The role of nitric oxide.....	10
1.2.2	Lipids and inflammatory cells.....	12
1.2.3	Vascular smooth muscle cells.....	14
1.2.4	Cellular interactions and lesions stability.....	15
1.2.5	Two forms of plaque disruption – fibrous cap rupture and endothelial erosion.....	17
1.2.6	Inflammatory markers in atherosclerosis.....	18
1.2.7	The balance of atherosclerosis.....	20
1.3	Carotid artery atherosclerosis	22
1.4	Imaging the atherosclerotic plaque	24
1.4.1	Invasive imaging.....	24
1.4.1.1	X-ray contrast angiography.....	24
1.4.1.2	Intravascular ultrasound.....	25
1.4.1.3	Intravascular angioscopy.....	25
1.4.1.4	Thermography.....	26
1.4.2	Non-invasive imaging.....	26
1.4.2.1	Surface ultrasound.....	26
1.4.2.2	Electron beam computed tomography.....	27
1.4.2.3	Nuclear scintigraphy.....	27
1.4.2.4	Magnetic resonance imaging.....	28
1.4.2.4.1	Plaque characterisation with MR.....	29
1.4.2.4.2	Atherosclerosis imaging with MR in humans.....	30

1.5	Introduction to PET	32
1.5.1	Positron emission.....	33
1.5.2	PET scanner.....	33
1.5.3	Data corrections.....	34
1.5.4	PET tracers.....	35
1.5.5	Metabolic pathway of FDG.....	35
1.5.6	Quantification of cellular FDG accumulation.....	36
1.5.6.1	Qualitative image analysis.....	36
1.5.6.2	Quantative image analysis.....	37
1.5.6.2.1	Time activity curves.....	37
1.5.6.2.2	Standard uptake value.....	37
1.5.6.3	Absolute quantification.....	38
1.5.6.3.1	Full kinetic modelling.....	38
1.5.6.3.2	Patlak plot.....	39
1.5.7	Partial volume effect.....	41
1.6	Project design	42
1.7	References	44
2	MATERIALS AND METHODS	56
2.1	Materials	56
2.1.1	General laboratory reagents.....	56
2.1.2	Materials for imaging experiments.....	57
2.2	General stock solutions	57
2.3	Experimental methods	58
2.3.1	Histology protocols.....	58
2.3.1.1	Anti-smooth muscle cell immunochemistry for animal studies.....	58
2.3.1.2	Anti-macrophage immunochemistry for animal studies.....	59
2.3.1.3	Anti-macrophage and smooth muscle cell immunochemistry for human studies.....	60
2.3.2	Haematoxylin and eosin staining.....	61
2.4	Statistical analysis	61
2.5	References	63
3	THE CHARACTERISTICS OF HDG UPTAKE IN A MONOCYTE CELL LINE (THP-1) AND IN HUMAN MACROPHAGES IN CULTURE	64
3.1	Introduction	64
3.2	Methods	66
3.2.1	General cell culture techniques.....	66
3.2.2	Culture of THP-1 cells.....	66
3.2.3	Isolation of peripheral blood-derived mononuclear cells.....	67
3.2.4	Purification of monocyte fraction.....	67
3.2.5	Immunocytochemical characterisation of monocytes.....	67
3.2.6	Analysis of HDG uptake over time in THP-1 cells.....	68
3.2.7	Analysis of HDG uptake over time in human macrophages.....	69
3.2.8	Analysis of HDG uptake in THP-1 cells after stimulation with PMA.....	69
3.2.9	Analysis of HDG uptake in human macrophages after activation with various agonists...	70
3.3	Results	71

3.3.1	Visual morphology of THP-1 cells in culture.....	71
3.3.2	Visual morphology of monocyte/macrophage cells in culture.....	71
3.3.3	Immunocytochemical characterisation of monocytes.....	71
3.3.4	Analysis of HDG uptake over time in THP-1 cells.....	72
3.3.5	Effect of PMA stimulation on HDG uptake in THP-1 cells.....	72
3.3.6	Analysis of HDG uptake over time in macrophages.....	72
3.3.7	Effect of various cytokine and non-cytokine activators on macrophage HDG uptake.....	73
3.3.7.1	Effect of treatment with IFN and TNF- α on macrophage HDG uptake.....	74
3.3.7.2	Effect of native and oxidised LDL on HDG uptake by macrophages.....	75
3.3.7.3	Effect of serum withdrawal, and the effect of IFN and LPS in combination, on HDG uptake in macrophages.....	76
3.4	Discussion.....	77
3.5	References.....	79
4	THE UPTAKE OF FDG IN ATHEROSCLEROSIS <i>IN VITRO</i>.....	83
4.1	Introduction.....	83
4.2	Methods.....	84
4.2.1	Phosphor imaging technique.....	84
4.2.2	Phosphor imaging of carotid atherosclerosis.....	85
4.2.3	Plaque histological characterisation.....	86
4.2.4	Correlation between plaque FDG uptake and cellular composition.....	86
4.2.5	Tritiated deoxyglucose autoradiography of carotid atherosclerosis.....	86
4.3	Results.....	87
4.3.1	Phosphor imaging of carotid atherosclerosis.....	87
4.3.2	Correlation between plaque FDG uptake and cellular composition.....	87
4.3.3	Tritiated deoxyglucose autoradiography of carotid atherosclerosis.....	89
4.4	Discussion.....	91
4.5	References.....	94
5	THE UPTAKE OF FDG IN HUMAN ATHEROSCLEROSIS.....	95
5.1	Introduction.....	95
5.2	Methods.....	97
5.2.1	Patient recruitment.....	97
5.2.2	Computed tomography protocol.....	98
5.2.3	PET protocols.....	98
5.2.3.1	Pilot 2-D dynamic imaging protocol.....	98
5.2.3.2	Late imaging protocol.....	98
5.2.3.3	3-D dynamic imaging protocol.....	99
5.2.4	Image co-registration.....	99
5.2.5	Quantification of plaque FDG concentration in late imaging studies.....	99
5.2.6	Quantification of plaque FDG concentration in 3-D dynamic studies.....	101
5.2.7	High resolution magnetic resonance (HRMR) protocol.....	101
5.2.8	Plaque histological characterisation.....	102
5.3	Results.....	103
5.3.1	Patient characteristics.....	103
5.3.2	Late imaging protocol.....	103

5.3.3	Dynamic imaging PET protocol.....	105
5.3.4	FDG-PET/HRMR imaging.....	106
5.4	Discussion	107
5.5	References	111
6	THE UPTAKE OF FDG IN AN EXPERIMENTAL MODEL OF ATHEROSCLEROSIS	114
6.1	Introduction	114
6.1.1	Background to the model of atherosclerosis.....	115
6.1.2	MicroPet system.....	115
6.2	Methods	118
6.2.1	Rabbit housing and diet.....	118
6.2.2	Lipid measurements.....	118
6.2.3	Anaesthesia	119
6.2.4	Aortic balloon injury.....	119
6.2.5	FDG-PET imaging protocols.....	120
6.2.5.1	Control imaging (Day 29).....	120
6.2.5.2	Atheroma Progression imaging (Day 170).....	120
6.2.5.3	Atheroma Regression imaging.....	121
6.2.6	Data corrections.....	121
6.2.7	Assessment of plaque FDG concentration.....	121
6.2.8	Perfusion fixation.....	122
6.3	Results	124
6.3.1	Lipid profiles.....	124
6.3.2	Aortic histology.....	125
6.3.3	Control FDG-PET imaging.....	125
6.3.4	Atheroma Progression FDG-PET imaging.....	125
6.3.5	Atheroma Regression FDG-PET imaging.....	127
6.4	Discussion	129
6.5	References	132
7	CONCLUSIONS AND FUTURE DIRECTIONS	134
7.1	References	137

LIST OF FIGURES

CHAPTER 1

1.1	The process of positron emission.....	33a
1.2	The metabolic pathway of FDG.....	35a

CHAPTER 3

3.1	THP-1 cells in culture – unstimulated.....	71a
3.2	THP-1 cells in culture – stimulated.....	71b
3.3	Monocytes in culture.....	71c
3.4	Macrophages in culture.....	71d
3.5	CD14 immunocytochemistry.....	71e
3.6	The uptake of HDG in THP-1 cells over time.....	72a
3.7	HDG uptake in THP-1 cells after PMA stimulation.....	72b
3.8	HDG uptake in human macrophages over time.....	72c
3.9	The effect of agonists on HDG uptake in human macrophages (1).....	74a
3.10	The effect of agonists on HDG uptake in human macrophages (2).....	75a
3.11	The effect of agonists on HDG uptake in human macrophages (3).....	76a

CHAPTER 4

4.1	Plaque FDG phosphor imaging.....	87a
4.2	Plaque HDG autoradiography (1).....	89a
4.3	Plaque HDG autoradiography (2).....	89b
4.4	Plaque HDG autoradiography (3).....	90a
4.5	Plaque HDG autoradiography (4).....	90b

CHAPTER 5

5.1	PET imaging of symptomatic carotid atherosclerosis.....	103a
5.2	PET imaging of asymptomatic carotid atherosclerosis.....	103b
5.3	Unilateral carotid FDG uptake.....	103c
5.4	Carotid plaque histology.....	105a
5.5	Histology of ruptured carotid plaque.....	105b
5.6	Pilot 2-D dynamic FDG-PET images.....	105c
5.7	3-D dynamic carotid FDG-PET imaging.....	105d
5.8	Patlak plot-symptomatic lesion.....	105e
5.9	Patlak plot-asymptomatic lesion.....	105f
5.10	HRMR carotid plaque imaging.....	106a
5.11	HRMR/FDG-PET carotid plaque imaging.....	106b
5.12	HRMR carotid plaque imaging.....	106c
5.13	HRMR/FDG-PET carotid plaque imaging.....	106d

CHAPTER 6

6.1	Plasma cholesterol concentrations over time.....	124a
6.2	Histological representation of a typical plaque generated by the NZWR model.....	125a
6.3	FDG-PET imaging of control NZWR.....	125b
6.4	FDG-PET imaging of NZWR atherosclerosis during high lipid diet (1).....	126a
6.5	FDG-PET imaging of NZWR atherosclerosis during high lipid diet (2).....	126b

6.6	Graphical representation of average aortic FDG uptake after subtraction of FDG signal within the bloodstream.....	126c
6.7	FDG-PET imaging of NZWR atherosclerosis, after change to low cholesterol diet (1)....	127a
6.8	FDG-PET imaging of NZWR atherosclerosis, after change to low cholesterol diet (2)....	127b
6.9	FDG-PET imaging of NZWR atherosclerosis, after change to low cholesterol diet, and subsequent histology.....	127c
6.10	FDG-PET imaging of NZWR atherosclerosis, after continued high cholesterol diet.....	127d
6.11	FDG-PET imaging of NZWR atherosclerosis, with continued high cholesterol diet, and subsequent histology.....	127e
6.12	FDG-PET imaging of NZWR atherosclerosis, after continued high cholesterol diet.....	128a
6.13	FDG-PET imaging of NZWR atherosclerosis, with continued high cholesterol diet, and subsequent histology.....	128b
6.14	Graphical representation of average aortic FDG uptake after the dietary split after subtraction of FDG signal within the bloodstream.....	128c

LIST OF TABLES

CHAPTER 1

1.1	Plaque characterisation with MR.....	29
-----	--------------------------------------	----

CHAPTER 4

4.1	Correlation between FDG uptake and plaque macrophage area.....	88
4.2	Correlation between FDG uptake and plaque smooth muscle cell area.....	88

CHAPTER 5

5.1	Characteristics of patients undergoing late and FDG-PET dynamic imaging.....	103a
5.2	Early and late net FDG accumulation rate for late protocol FDG-PET patients.....	104a

CHAPTER 6

6.1	Technical specifications of the Concorde microPet P4 model, taken from Concorde Microsystems website	116a
6.2	Timeline of experiments.....	118a
6.3	Mean total cholesterol profiles of NZWR.....	124a
6.4	Cholesterol profiles of individual NZWR.....	124b

Chapter 1

CHAPTER 1

INTRODUCTION

1.1 ATHEROSCLEROSIS

1.1.1 The epidemiology of atherosclerosis

Atherosclerosis, with its complications, is the leading cause of mortality and morbidity in the developed world. In the United States alone, a snapshot of the population would reveal that 60 million adults suffer from atherosclerotic cardiovascular disease, which accounts for 42% of all deaths annually, at a cost to the nation of 128 billion dollars. Vascular disease (including cardiovascular and cerebrovascular disease) is also the leading cause of mortality in the United Kingdom, leading to nearly 260,000 deaths per annum (Office of National Statistics, 1997). Fortunately, despite this catastrophic burden of disease, much evidence has emerged over the last decade suggesting that the progression of atherosclerosis can be slowed or even reversed with appropriate lifestyle and drug interventions.

The origin of the current epidemic of atherosclerotic cardiovascular disease can be traced back to the time of industrialisation in the 1700's. The three factors largely responsible for this were an increase in the use of tobacco products, reduced physical activity and the adoption of a diet high in fat, calories and cholesterol. This rising tide of cardiovascular disease continued into the 20th century, but began to recede when data from the Framingham study identified a number of modifiable risk factors including cigarette smoking, hypertension and hypercholesterolaemia (Wong et al., 1991).

The number of deaths per 100,000 population attributable to cardiovascular disease peaked in the western world in 1964-5, since which time there has been a gradual decline in death rates (NHLBI, 1998). The age-adjusted coronary heart disease mortality in the US has dropped by more than 40% and cerebrovascular disease mortality by more than

50%, with the greatest reductions being seen among whites and males. This reduction has occurred despite a quadrupling of the proportion of the population aged over 65 years, and has been due to a number of factors, particularly efforts by the US and the British governments, both of whom launched major health promotion campaigns aimed at reducing the prevalence of risk factors defined by the Framingham study (Wilson et al., 1987). Indeed, there has been a substantial change in the prevalence of cardiovascular risk factors in the population as a whole over the last thirty years. The war is not won however, and the decline in the death rate from cardiovascular disease slowed in the 1990's. This is likely to be due to a large increase in the prevalence of both obesity and type 2 diabetes mellitus, as well as a resurgence of cigarette smoking in some sections of society (Cooper et al., 2000). Female death rates from cardiovascular disease overtook male in 1984, and have shown a smaller decline over the last thirty years (McGovern et al., 1996). The consequences of atherosclerosis are also beginning to be felt in less well-developed regions of the globe (Knopp, 1999), with atherosclerotic cardiovascular disease set to replace infection as the leading cause of death in the third world in the near future.

1.1.2 The pathophysiology of atherosclerosis

Traditionally, atherosclerosis has been viewed as a degenerative disease, affecting predominantly older people, slowly progressing over many years, and eventually leading to symptoms through mechanical effects on blood flow. The perceived insidious and relentless nature of its development has meant that a somewhat pessimistic view of the potential to modify its progression by medical therapy has held sway. There has been little emphasis on the diagnosis and treatment of high-risk asymptomatic patients. Disease management has instead been dominated by interventional re-vascularisation approaches, targeting the largest and most visible or symptomatic lesions with angioplasty, bypass surgery or endarterectomy.

Recently, for three reasons, this defeatist view of the pathogenesis and progression of atherosclerosis has begun to change. Firstly, because careful descriptive studies of the underlying pathology of atherosclerosis have revealed that atherosclerotic plaques differ in their cellular composition, and that the cell types predominating in the plaque can determine the risk of fatal clinical events. Secondly, recent cellular and molecular biological research has emphasised the importance of inflammatory cells and inflammatory mediators in the pathogenesis of atherosclerosis. The third, and most important reason is because several large-scale clinical trials have reported that drugs, in particular HMG-CoA reductase inhibitors (statins), are able to reduce the number of clinical events in patients with established atherosclerosis, and to do so without necessarily affecting the size of atherosclerotic plaques. These three strands of evidence have shown that, rather than being an irreversibly progressive disease, atherosclerosis is a dynamic, inflammatory process that may be amenable to medical therapy. Understanding the cellular and molecular interactions that determine the development and progression of atherosclerosis brings with it opportunities to develop novel therapeutic agents targeting key molecular and cellular interactions in its aetiology. In addition, the recognition that the clinical consequences of atherosclerosis depend almost entirely on plaque composition argues for a new approach to diagnosis, with less emphasis placed on the

degree of lumen narrowing, and more attention focused on the cellular composition of the plaque.

1.1.2.1 The structure of the healthy artery

The normal artery consists of three histologically distinct layers. Innermost and lining the lumen is the tunica intima, which comprises a single layer of endothelial cells in close proximity to the internal elastic lamina. The tunica media surrounds the internal elastic lamina and its composition varies depending on the type of artery. The tunica media of the smallest arterial vessels, arterioles, comprises a single layer of vascular smooth muscle cells (VSMCs). Small arteries have a similar structure but with a thicker layer of medial VSMCs. Arterioles and small arteries are termed resistance vessels, because they contribute significantly to vascular resistance and hence directly affect blood pressure. At the opposite end of the spectrum are large elastic or conduit arteries, named for the high proportion of elastin in the tunica media. The tunica media of all arteries is contained within a connective tissue layer, rich in blood vessels and nerves, known as the tunica adventitia. In healthy arteries, the vessel lumen diameter can be altered by contraction and relaxation of the medial VSMCs, in response to a variety of systemic and locally released signals.

1.1.2.2 The pathology of the atherosclerotic artery

Atherosclerosis is primarily a disease affecting the intimal layer of elastic arteries. For reasons that remain largely unknown, some arterial beds appear more prone than others. Coronary, carotid, cerebral, renal arteries and the aorta are most often affected. The arteries supplying the lower limb are also vulnerable to disease. Interestingly, the internal mammary and radial arteries are almost always spared, making them invaluable vessels for coronary bypass surgery.

Atherosclerotic lesions develop slowly over many years, passing through several stages. Histologically, the earliest sign is a subendothelial accumulation of lipid-laden macrophage foam cells and associated T- lymphocytes known as a fatty streak. Fatty streaks are asymptomatic and non-stenotic. Post-mortem examinations have shown that they are present in the aorta at the end of the first decade of life, in the coronary arteries by the second and begin to appear in the cerebral circulation by the third decade. With time, the lesion progresses and the core of the early plaque becomes necrotic, containing cellular debris, crystalline cholesterol and inflammatory cells, particularly macrophage foam cells. This necrotic core becomes bounded on its luminal aspect by an endothelialised fibrous cap, consisting of vascular smooth muscle cells embedded in an extensive collagenous extracellular matrix. Inflammatory cells are also present in the fibrous cap, concentrated particularly in the 'shoulder' regions, where T cells, mast cells and especially macrophages have a tendency to accumulate (Kaartinen et al., 1994; Kaartinen et al., 1998). Advanced lesions become increasingly complex, showing evidence of calcification, ulceration, new vessel formation and fibrous cap rupture or erosion.

Thus, the composition of atherosclerotic plaques is variable and complex, and it is the interaction between the various cell types within a plaque that determines the progression, complications and outcome of the disease. Carotid artery atherosclerosis is the form of the disease most relevant to this thesis, and it is discussed later in this Chapter in Section 1.3.

1.1.3 Theories of atherogenesis

Over the years, several theories have been advanced to explain atherogenesis. None of these is able to account for all aspects of the disease. The most recent, which views atherosclerosis as a consequence of inflammation in the vessel wall, is however, supported by the results of large-scale clinical trials.

1.1.3.1 Lipid hypothesis

This theory, proposed initially in 1913 (Anitschkow, 1913), held that the development of atherosclerosis was the result of the gradual accumulation of lipid in the arterial wall, with its presence at that site being responsible for the generation of the characteristic tissue changes of atheroma. In animal models, hyperlipidaemia, as a result of either a high fat diet or genetic modification, reliably leads to the development of atherosclerotic lesions in many species. The lipid hypothesis is supported by the wealth of evidence that links elevated serum lipids with the risk of development of atherosclerotic lesions in humans (Berliner et al., 1995).

1.1.3.2 Thrombogenic hypothesis

This theory (Rokitansky, 1855) hypothesises that atherosclerotic lesions grow by the gradual incorporation of luminal thrombus into the arterial wall. It is supported by the finding of fibrin (Bini et al., 1989) and platelet-derived proteins in both developing and mature atherosclerotic plaques (Wilcox et al., 1988). In addition, thrombus contains large amounts of platelet-derived growth factor, a potent VSMC mitogen. However, this theory is difficult to prove because plaque infiltration by immature blood vessels is common in advanced lesions, and consequently haemorrhage and thrombosis occur frequently. Therefore, thrombus may appear as a result of atherosclerosis rather than be a causative factor.

The initiating factor for atherosclerosis formation in both of the above theories can be considered to be endothelial dysfunction. In the lipid hypothesis, a defective endothelial cell barrier permits the gradual seepage of lipid into the arterial intima, allowing plaque formation to begin. In the thrombogenic theory, a dysfunctional endothelium allows local platelet aggregation and clot formation which might subsequently become incorporated into the arterial wall. The idea that endothelial dysfunction is central to the origin of atherosclerosis has dominated recent thinking on the subject.

1.1.3.3 The response to injury hypothesis

This was initially proposed by Virchow (Virchow, 1858), who believed that the degenerative changes associated with atherosclerosis were due to a healing response of the arterial intima as a result of a prior mechanical injury. The theory was subsequently revised as shown below.

1.1.3.4 The modified response to injury hypothesis

One hundred and fifteen years after it was first proposed, Ross and Glomset published a modified version of the response to injury hypothesis (Ross et al., 1973). They noted histological similarities between advanced native atherosclerotic plaques and those created in monkeys' aortas by balloon injury of the endothelium. It was suggested that atherosclerosis was the result of excessive vascular smooth muscle cell proliferation in response to a prior endothelial injury. This idea was later revised, and subsequent versions of the theory implied that endothelial dysfunction from any cause, not necessarily mechanical injury, was crucial for the development of atherosclerosis (Ross, 1986; Ross, 1993). These injurious agents are what are today regarded as risk factors for atherosclerosis, and include hypertension, hyperlipidaemia and cigarette smoking.

1.1.3.5 Atherosclerosis as an inflammatory disease

In his final review of the pathogenesis of atherosclerosis (Ross, 1999), Ross emphasised the importance of endothelial dysfunction, but also highlighted the role played by inflammation at every step of both the disease and its complications. The key parts played in this process by endothelial, inflammatory and vascular smooth muscle cells are discussed below.

1.2 CELLULAR ROLES IN ATHEROSCLEROSIS

1.2.1 The endothelium

1.2.1.1 The role of nitric oxide

The endothelium plays a central role in maintaining vascular health, by virtue of its anti-inflammatory and anticoagulant properties. Most of these characteristics are mediated by the molecule nitric oxide (NO). NO was discovered in the 1980s, having been isolated from lipopolysaccharide-primed macrophages (Palmer et al., 1987). It is synthesized by endothelial cells under the control of the enzyme endothelial nitric oxide synthase (eNOS), and has a number of anti-atherogenic properties. Firstly, it acts as a powerful inhibitor of platelet aggregation on endothelial cells (Radomski et al., 1987). Secondly, it can reduce inflammatory cell recruitment into the intima by reducing the expression of genes involved in this process, such as those encoding intercellular adhesion molecule-1 (ICAM-1), vascular cell adhesion molecule-1 (VCAM-1), P-selectin and monocyte chemoattractant protein-1 (MCP-1) (Tsao et al., 1997; Gauthier et al., 1995; Tsao et al., 1996). There is some evidence that NO may also reduce lipid entry into the arterial intima (Cardona-Sanclemente et al., 1995). NO is also a potent anti-inflammatory molecule, and, depending on concentration, may be either a scavenger or a producer of potentially destructive oxygen free radicals, such as peroxynitrite (Hobbs et al., 1999; Anggard, 1994; Bhagat et al., 1996).

One of the earliest detectable manifestations of atherosclerosis is a decrease in the bioavailability of NO in response to pharmacological or haemodynamic stimuli (Ross, 1999). This may occur for two reasons: either there may be decreased manufacture of NO because of endothelial cell dysfunction, or there may be increased NO breakdown. There is evidence that both mechanisms might be important in different situations (Li et al., 2000). Many atherosclerosis risk factors can lead to impaired endothelial function and reduced NO bioavailability. For example, hyperlipidaemic patients have normal forearm blood at rest, but a blunted response to NO-dependent vasodilatation. This abnormality is

reversed when patients are treated with lipid-lowering medication (Stroes et al., 1995). Patients with diabetes mellitus also have impaired endothelial function, occurring primarily as a result of impaired NO production. There is, however, some evidence to suggest that increased oxidative stress leading to enhanced NO breakdown may also be a factor (Williams et al., 1996). Similarly, other risk factors for atherosclerosis, such as hypertension and cigarette smoking, are associated with reduced NO bioavailability (Panza et al., 1995; Heitzer et al., 1996). In cigarette smokers, endothelial impairment is thought to be due to enhanced NO degradation by oxygen-derived free radical agents such as the superoxide ion. There are also other consequences of an increased reactivity between NO and superoxide species. The product of their interaction, peroxynitrite (ONOO^-), is a powerful oxidising agent, and can reach high concentrations in atherosclerotic lesions where it can cause cellular oxidative injury.

Another consequence of endothelial cell dysfunction that occurs in early atherosclerosis is the expression of surface-bound selectins and adhesion molecules, including P-selectin, ICAM-1 and VCAM-1. These molecules attract and capture circulating inflammatory cells, and facilitate their migration into the subendothelial space (Ross, 1999). Healthy endothelial cells do not express these molecules, but their appearance may be induced by abnormal arterial shear stress, subendothelial oxidised lipid and, in diabetic patients, advanced glycosylation products in the arterial wall (Ross, 1993). The importance of selectins and adhesion molecules in the development of atherosclerosis is demonstrated by experiments using mice which lack their expression. These animals develop smaller lesions, with lower lipid content and fewer inflammatory cells than control mice when fed a lipid-rich diet (Nakashima et al., 1994). Animal models have reinforced the importance of inflammatory cell recruitment in the pathogenesis of atherosclerosis, but since inflammatory cells are never seen in the intima in the absence of lipid, it seems likely that subendothelial lipid accumulation is also necessary for the development of atherosclerosis.

The tendency for atherosclerosis to occur preferentially at particular sites may be explained by subtle variations in endothelial function. This is probably caused by

variations in local blood flow patterns, especially conditions of low flow, which can influence expression of a number of endothelial cell genes including those encoding ICAM-1 and eNOS (Resnick et al., 1997; Topper et al., 1996). In addition to flow speed, the type of flow can have a direct affect on cell morphology. In areas of laminar flow, endothelial cells tend to have an elliptoid shape, contrasting with the situation found at vessel branch points and curves where turbulent flow induces a conformational change towards polygonal shaped cells. Such cells have an increased permeability to LDL cholesterol and may promote lesion formation (Gimbrone, Jr., 1999).

These data are consistent with the idea that the primary event in atherogenesis is endothelial dysfunction. The endothelium can be damaged by a variety of means, leading to dysfunction and subsequent subendothelial lipid accumulation. In this situation, the normal homeostatic features of the endothelium break down; it becomes more adhesive to inflammatory cells and platelets, it loses its anticoagulant properties and there is reduced bioavailability of NO. Importantly, endothelial function is improved by drugs that have been shown to substantially reduce death from vascular disease, including statins and angiotensin converting enzyme inhibitors (LIPID Study Group, 1998; Yusuf et al., 2000).

1.2.2 Lipids and inflammatory cells

The vascular endothelium provides a continuous boundary lining the vasculature, and is characterised by the presence of tight junctions at the margin of each endothelial cell. These tight junctions restrict the passage of macromolecules from blood to subendothelial space. However, a transcytotic route exists, via which certain macromolecules may be transported across the endothelial cell layer. It is through this system that LDL is thought to be transported from the blood into the vessel wall. This accumulation of subendothelial lipid, particularly when partly oxidised, stimulates the local inflammatory reaction that initiates and maintains the activation of overlying endothelial cells. The activated cells express a variety of selectins and adhesion molecules and also produce a number of chemokines, in particular MCP-1, whose expression is upregulated by the presence of oxidised LDL in the subendothelial space (Boring et al., 1998). Interestingly, the

protective effect of HDL against atherosclerotic vascular disease may be partly explained by its ability to block endothelial cell expression of adhesion molecules (Xia et al., 1999; Calabresi et al., 1997). Chemokines are pro-inflammatory cytokines that are responsible for chemoattraction, migration and subsequent activation of leukocytes. Mice lacking the MCP-1 gene develop smaller atherosclerotic lesions than wild-type animals (Gosling et al., 1999).

The first stage of inflammatory cell recruitment to the intima is the initiation of 'rolling' of monocytes and T-cells along the endothelial cell layer. This phenomenon is mediated by the selectin molecules which selectively bind ligands found on the inflammatory cells. Having been slowed down by interactions with selectins, the subsequent firm adhesion to, and migration of leukocytes through the endothelial cell layer is dependent upon the endothelial expression of adhesion molecules such as ICAM-1 and VCAM-1, and their binding to appropriate receptors on inflammatory cells. Once present in the intima, monocytes differentiate into macrophages under the influence of chemokines such as macrophage colony stimulating factor. Such molecules also stimulate the expression of the scavenger receptors that allow macrophages to ingest oxidised lipid and to develop into macrophage foam cells, the predominant cell in an early atherosclerotic lesion. The formation of scavenger receptors is also regulated by peroxisome proliferator-activated receptor- γ , a nuclear transcription factor expressed at high levels in foam cells (Tontonoz et al., 1998).

In early atherosclerosis at least, the macrophage can be thought of as performing a predominantly beneficial role as a 'neutraliser', ingesting potentially harmful oxidised lipid components in the vessel wall. This removal prevents ongoing activation of the overlying endothelial cells by modified LDL. Unfortunately, the inflammatory process itself can have significant effects on lipoprotein movement into the arterial wall. Specifically, inflammatory mediators such as tumour necrosis factor alpha (TNF- α) and interleukin-1 may increase binding of LDL to endothelium. Other cytokines produced by macrophages have beneficial effects on the evolution of the plaque. Some of these factors are chemoattractant for VSMCs, for example osteopontin (Shanahan et al., 1994; Liaw et

al., 1994), others are growth enhancing, such as platelet-derived growth factor. Under the influence of these cytokines, VSMC migrate from the media to the intima, where they adopt a synthetic phenotype, well suited to matrix production and protective fibrous cap formation. This can be thought of as a useful 'plaque stabilising' function of macrophages.

However, activated macrophages have a high rate of apoptosis. Once dead, their lipid content is released and becomes part of the core of the plaque, contributing to its enlargement. The apoptotic cells also contain high concentrations of tissue factor, which may invoke thrombosis if exposed to circulating platelets (Zaman et al., 2000).

Immunohistochemical studies have demonstrated that T-lymphocytes are present in atheromatous plaques, located predominantly in the subendothelial space. The cells are in an activated state, as evidenced by their expression of HLA-DR, CD25 (interleukin-2 receptor) and CD30 (de Boer et al., 2000). The cells are mainly of the T-helper type 1 class, characterised by the production of interleukin-2 and interferon gamma (IFN). These factors can up-regulate adhesion molecule expression by endothelial cells, thereby recruiting more cells to join the inflammatory process.

It is now generally recognised that the pathological progression and consequences of atherosclerotic lesions are determined by dynamic interactions between inflammatory cells recruited in response to subendothelial lipid accumulation, and the local reparative 'wound healing' response of surrounding VSMCs (Farzaneh-Far et al., 2001).

1.2.3 Vascular smooth muscle cells

VSMCs reside mostly in the media of healthy adult arteries, where their role is to regulate vascular tone. Thus, medial VSMCs contain large amounts of contractile proteins, including myosin, tropomyosin and alpha-actin. Continued expression of this 'contractile' phenotype is maintained by the influence of extracellular proteins in the media, which act via integrins in the VSMC membrane. In atherosclerosis, however, the

cells become influenced by cytokines produced by activated macrophages and endothelial cells. Under these influences, VSMCs migrate to the intima and undergo a phenotypic change characterised by a reduction in content of contractile proteins and a large increase in the number of synthetic organelles. This migration of VSMCs from the media to the intima, and the consequent change from a 'contractile' to a 'synthetic' phenotype, was previously thought to be a crucial step in the development of atherosclerosis in the modified response to injury hypothesis. More recently, it has been recognised that intimal VSMCs in atherosclerotic plaques bear a remarkable similarity to VSMCs found in early developing blood vessels (Shanahan et al., 1998), suggesting that intimal VSMCs may be performing a beneficial, reparative role rather than a destructive one in atherosclerosis.

VSMC are well equipped for this action. Firstly, they can express the proteinases that they require to break free from the medial basement membrane and allow them to migrate to the site of inflammation or injury in response to chemokines. Secondly, they can produce various growth factors, including vascular endothelial growth factor and platelet-derived growth factor, that act in an autocrine loop to facilitate their proliferation at the site of injury. Finally, and most importantly, they produce large quantities of matrix proteins, in particular glycosaminoglycans, elastin and collagen isoforms 1 and 3, necessary to repair the vessel and form a fibrous cap over the lipid rich core of the lesion. This fibrous cap separates the highly thrombogenic lipid-rich core from circulating platelets and the proteins of the coagulation cascade, and also confers structural stability to the atherosclerotic lesion. And since the VSMC is the only cell capable of synthesizing this cap, it follows that VSMCs play a pivotal role in maintaining plaque stability and protecting against the potentially fatal thrombotic consequences of atherosclerosis (Libby, 1995).

1.2.4 Cellular interactions and lesion stability

Generally, early atherosclerosis progresses without symptoms until a lesion declares itself in one of two ways. As discussed above, macrophage foam cells may undergo apoptosis, especially in the presence of high concentrations of oxidised LDL. Their cellular

remnants then become part of an enlarging lipid-rich core. In this manner, plaque size increases, and there may be a consequent reduction in vessel lumen area. At times of increased demand, such as during exercise, this may be sufficient to cause ischaemic symptoms such as angina. More hazardous is if the plaque first presents with disruption of its fibrous cap, leading to exposure of the thrombogenic lipid core to the flowing blood. This is likely to result in subsequent platelet accumulation and activation, fibrin deposition and intravascular thrombosis. Depending on several factors, such as the extent of arterial thrombus, local fibrinolytic activity and collateral blood supply, the end result may be arterial occlusion and downstream necrosis.

However, by studying the pathology of rupture plaques, several characteristics have been identified that seem to be predictive of the risk of rupture in individual lesions (Galis et al., 1994). Plaques that are vulnerable to rupture tend to have thin fibrous caps with a high ratio of inflammatory cells to VSMCs, and to contain a lipid core that occupies more than 50% of the volume of the plaque (Boyle, 1997; van der Wal et al., 1994). Of these, the most important is the cellular composition of the fibrous cap. Plaques containing a heavy inflammatory cell infiltrate and relatively few VSMCs have the highest risk of rupture (Davies, 1996).

Inflammatory cells in plaques act to promote plaque rupture in a number of synergistic ways. Firstly, activated T-cells produce pro-inflammatory cytokines, typified by IFN, that directly inhibit VSMC proliferation (Warner et al., 1989) and almost completely shut down collagen synthesis (Amento et al., 1991; Libby et al., 1995). Thus, VSMC in the vicinity of activated T-cells in plaques are poorly able to lay down or repair extracellular matrix. Secondly, macrophage-derived inflammatory cytokines, in particular interleukin 1- β (IL-1 β) and TNF- α along with IFN from T-cells are synergistically cytotoxic for VSMCs, causing depletion in cell number by apoptosis (Geng et al., 1996). These cytokines are found at high levels in vulnerable plaques (Sukhova et al., 1999). Thirdly, activated macrophages can induce VSMC apoptosis by direct cell to cell contact (Boyle et al., 2000). Finally, and probably most importantly, macrophages secrete a variety of matrix metalloproteinases (MMPs) that degrade the matrix components of the fibrous cap

by proteolytic cleavage of its protein components (Libby, 1995). The production of MMPs is upregulated by inflammatory mediators such as TNF- α . As well as being under threat from this array of insults, VSMCs themselves within the fibrous cap of a mature plaque have a reduced ability to proliferate (Ross et al., 1984; Bennett et al., 1998) and an enhanced susceptibility to apoptosis (Bennett et al., 1997; Geng et al., 1997). Thus, inflammatory cells can destroy the fabric of the fibrous cap, and resident VSMCs are poorly equipped to compensate, particularly in the presence of inhibitory inflammatory cytokines. Importantly, all these features can be present in small, haemodynamically insignificant plaques that are clinically silent and angiographically invisible. Thus, plaque composition is far more important than plaque size in determining outcome.

1.2.5 Two forms of plaque disruption – fibrous cap rupture and endothelial erosion

Atherosclerotic plaques become life-threatening when they initiate clot formation in the vessel lumen and disturb blood flow. This can occur in two different ways. Either there can be fibrous cap rupture, with consequent exposure of the thrombogenic extracellular matrix of the cap and the tissue factor-rich lipid core to circulating blood, or less commonly, there is erosion of the endothelial cell layer covering the fibrous cap, also potentially leading to the build-up of platelet-rich thrombus in the artery. Endothelial erosion probably accounts for around 30% of acute coronary syndromes overall, and seems particularly common in females (Farb et al., 1996). Both forms of plaque disruption invariably lead to local platelet accumulation and activation. This may result in triggering of the clotting cascade, thrombus formation and, if extensive, vessel occlusion. Platelet-rich thrombus contains chemokines and mitogens, in particular platelet-derived growth factor, thrombin and transforming growth factor beta, that induce migration and proliferation of VSMCs from the arterial media to the plaque and initiate healing of the disrupted lesion (McNamara et al., 1996). Platelets also express CD40 on their cell membrane, which causes local endothelial cell activation, resulting in the recruitment of more inflammatory cells to the lesion and perpetuating the cycle of inflammation, plaque rupture and thrombosis. However, fibrous cap rupture or erosion does not invariably lead

to vessel occlusion. Up to 70% of plaques causing high-grade stenosis contain histological evidence of previous, sub-clinical plaque rupture with subsequent repair (Davies, 1995). This is particularly likely to occur if high blood flow through the vessel prevents the accumulation of a large occlusive thrombus. Thus, non-occlusive plaque rupture induces formation of a new fibrous cap over the organising thrombus which restabilises the lesion, but at the expense of increasing its size. Since this occurs suddenly, there is little opportunity for adaptive remodelling of the artery and the healed lesion may now impede flow sufficiently to produce ischaemic symptoms. This explains why patients with previously normal exercise tolerance may suddenly develop symptoms of stable angina pectoris. It also follows that, if lesions can grow as a consequence of repeated episodes of silent rupture and repair, a reduction of plaque rupture rate will slow the progression of atherosclerosis.

In summary, therefore, atheromatous plaques may become larger by two methods: the first is a gradual increase in size as a consequence of macrophage foam cell apoptosis and incorporation into an enlarging necrotic lipid-laden plaque core. The second is a stepwise increase in size because of repeated, often silent episodes of plaque rupture or erosion with subsequent VSMC-driven repair.

1.2.6 Inflammatory markers in atherosclerosis

The cell biology of plaque development and rupture illustrates that atherosclerosis is fundamentally an inflammatory condition. Confirmation of this inflammatory basis has come from several landmark studies that have all demonstrated a correlation between serum levels of markers of systemic inflammation, principally C-reactive protein (CRP), and risk of a clinical event due to plaque rupture, including myocardial infarction, stroke, and sudden death (Ridker et al., 2000a; Albert et al., 2002; Sacks et al., 1999; Ridker et al., 1997; Ridker, 2001). However, unlike other systemic inflammatory conditions such as rheumatoid arthritis, levels of CRP in atherosclerosis are characteristically not elevated above the conventional normal range, and a correlation between CRP level and coronary events was only demonstrated after development of a highly sensitive assay for CRP (hs-

CRP) that was capable of measuring levels below the lower limit of detection of conventional assays. Similar, though less compelling correlations with clinical events have also been published for other markers of inflammation including soluble ICAM-1 (Ridker et al., 1998a), VCAM-1 (de Lemos et al., 2000; Peter et al., 1999), P-selectin (Ridker et al., 2001) and interleukin-6 - the primary driver of CRP production (Ridker et al., 2000b). Finally, a recent study has confirmed the importance of local inflammation in the pathogenesis of unstable atherosclerosis, showing widespread activation of inflammatory cells across the coronary vascular bed in patients with unstable angina, regardless of the location of the culprit stenosis (Buffon et al., 2002).

1.2.7 The balance of atherosclerosis

Atherosclerosis is a dynamic process where the balance between the destructive influence of inflammatory cells and the reactive, stabilising effects of VSMCs determines outcome. This balance can be tipped towards plaque rupture by factors such as an atherogenic lipoprotein profile, high levels of lipid oxidation, local free radical generation, and genetic variability in expression and activity of certain central inflammatory molecules. For example, an association between plaque progression and a polymorphism in the stromelysin-1 gene promoter has been described (Ye et al., 1996). It is also possible that infectious organisms might be involved in atherosclerosis, either as plaque initiators or as having some role in causing plaque rupture. This fiercely debated question has still to be resolved but *chlamydia pneumoniae* remains the most plausible candidate pathogen. It is found in plaques, localising at high concentrations within macrophages, but is rarely seen in normal arteries (Kol et al., 1998). Although these data imply a pathological association between the presence of chlamydia infection and atherosclerosis, neither a causative role nor a convincing association between serum markers of infection and ischaemic heart disease has been established. Animal work has shown that healthy rabbits that have been nasally inoculated with chlamydia develop extensive atherosclerosis (Muhlestein et al., 1998). However, in humans the situation appears to be somewhat different. Two large prospective studies and an extensive meta-analysis of previous data have failed to show any association between serum markers of infection with chlamydia and incidence of, or mortality from ischaemic heart disease (Danesh et al., 2000; Wald et al., 2000). The results of these two studies have effectively excluded a strong association, but allow the possibility of a weaker link, and several trials of anti-chlamydial antibiotics for the prevention of ischaemic heart disease are currently in progress.

The balance of atherosclerosis can be tipped towards plaque stability by a reduction in plaque inflammation, or by an increase in VSMC-driven repair. Lipid reduction, by whatever means, reduces clinical events. Evidence that this may be due to a plaque stabilising effect comes from animal studies which showed that statins reduced inflammatory cell number while increasing the VSMC content of plaques (Shiomi et al.,

1995; Williams et al., 1998), changes that would be expected to enhance stability. More importantly, however, evidence from human clinical studies also points to a plaque stabilising effect of statins. Angiographic trials have shown that statins produce only a small, haemodynamically insignificant reduction in progression of established stenoses (MAAS Investigators, 1994; MAAS Investigators, 1994; Pitt et al., 1995; Jukema et al., 1995). They also reduce new lesion formation, and, importantly, the number of new vessel occlusions. Occlusions arise after rupture of a plaque, leading to an occlusive thrombus in the context of a well-collateralised myocardial circulation. This seems to imply that statins are stabilising plaques by reducing rupture rate. This conclusion is supported by the results of all the large primary and secondary prevention studies, which have demonstrated that statins produce major reductions in events due to plaque rupture, such as myocardial infarction and stroke (Shepherd et al., 1995; Sacks et al., 1996; LIPID Study Group, 1998; 4S Study, 1994; Downs et al., 1998). Since statins have only a modest effect on plaque size, but cause profound reductions in number of clinical events, these studies highlight the inadequacy of angiography for the prediction of clinical events, and suggest that statins have beneficial effects on plaque inflammation in addition to, or as a result of, their lipid lowering effects. Importantly, this notion is supported by the observation that the reduction in clinical events due to statin therapy is accompanied by a parallel decrease in CRP levels that is unlikely to be due to effects of statins on non-atherosclerotic inflammation (Ridker et al., 1998b; Jialal et al., 2001). In addition, in the first study of its kind, it has recently been shown that statins reduce inflammation and apoptosis, and increase collagen content in human carotid artery atherosclerosis (Crisby et al., 2001).

Statin drugs may help stabilise plaques in a number of different ways. It is known that they can exert direct effects on endothelial cell function, inflammatory cell number and activity, VSMC proliferation, platelet aggregation and thrombus formation (Treasure et al., 1995; Katznelson et al., 1998; Negre-Aminou et al., 1997; Rosenson et al., 1998; Lacoste et al., 1995). Evidence that non-lipid lowering effects may be important *in-vivo* comes from animal studies in which pravastatin caused beneficial changes in plaque composition (but not size), even when lipids were maintained at pre-treatment levels

(Williams et al., 1998). Additionally, in mice, simvastatin has direct anti-inflammatory effects that are as potent as those of indomethacin (Sparrow et al., 2001). Recently, a newly recognised effect of statins as immune modulators has been described, whereby major histocompatibility complex class II mediated T-cell activation is reduced by a variety of statins (Kwak et al., 2000). These observations point to potentially important effects of statins that are poorly understood and have yet to be fully defined.

1.3 CAROTID ARTERY ATHEROSCLEROSIS

Carotid artery atherosclerosis has a number of distinct features that distinguish it from other forms of the disease. It has been shown in clinical trials that carotid artery plaques at high risk of rupture are characterised by the presence of high-grade internal carotid artery stenosis. As the degree of stenosis increases, so does the risk of an embolic event (i.e. Transient Ischaemic Attack – TIA) (ECST Group, 1998; Barnett et al., 1998).

However, as at other arterial sites, the degree of inflammation is also crucial in determining the risk of rupture of carotid plaques. Pathological studies have found that the fibrous cap in symptomatic patients is thinner, and more infiltrated with macrophages and T-cells than caps associated with asymptomatic plaques (Svindland et al., 1988; Jander et al., 1998; Feeley et al., 1991; Golledge et al., 2000). Others have demonstrated increased levels of macrophage-derived proteolytic enzymes in ruptured carotid plaques (Galis et al., 1994; Sukhova et al., 1999).

Carotid plaque rupture can have different outcomes. Either there can be distal embolisation of platelet-rich thrombus with sustained, but reduced, blood flow, or otherwise, if the thrombus load is greater, complete occlusion of the artery may occur. Both situations can result in reduced cerebral perfusion and either TIA or stroke, depending on additional factors such as collateral blood supply, local thrombolysis and extent of cerebral artery atherosclerosis.

Consideration will now be given to the current practice of atherosclerosis imaging, and, based on the underlying pathobiology of the disease, to the potential role of new imaging modalities in detecting the atherosclerotic plaque at risk of rupture – the vulnerable plaque.

1.4 IMAGING THE ATHEROSCLEROTIC PLAQUE

The idea of direct visualisation of atherosclerotic plaques is a worthwhile research and clinical goal for at least three reasons. Firstly, it might allow a better understanding of the natural history of atherosclerosis. Secondly, it might permit investigators to predict those plaques at risk of rupture. Thirdly, monitoring of atherosclerotic plaques with a reliable and reproducible technique might allow one to assess longitudinally the effects of plaque modifying drugs. This discussion will focus on the imaging of atherosclerosis in general, with specific examples being given of interesting applications in individual vascular beds. Imaging techniques can be divided according to whether or not they are invasive of the vasculature.

1.4.1 Invasive imaging

1.4.1.1 X-ray contrast angiography

For the past 40 years, x-ray contrast angiography has been the universally accepted, standard modality for imaging of the vascular tree. The procedure is performed by introducing a catheter under x-ray guidance into the artery of interest and injecting radio-opaque contrast dye into the lumen. The presence of atherosclerotic disease is judged indirectly, according to whether the lumen is regular and smooth, by the rate of contrast flow, and by whether contrast completely fills the distal artery. Whilst angiography is an excellent technique for the high-resolution definition of the site and severity of arterial stenoses, it does have a number of important drawbacks.

Angiography is invasive and it requires the use of ionizing radiation. Both of these factors mean that it has a finite complication rate, and as such, it tends to be used in symptomatic individuals only. This precludes the prospect of its being used for serial monitoring of asymptomatic patients at high-risk of atherosclerosis. Angiography also gives no information whatsoever about the vessel wall, because the wall is not directly imaged. This means that no knowledge is gleaned about the inflammatory state or

composition of the plaque and thus no guide to the likelihood of plaque rupture. Finally, diffuse atherosclerotic disease may narrow the entire arterial lumen, and as a result angiography may underestimate the degree of local stenosis. It is well known that some plaques can be displaced outwards from the wall as a result of vessel remodelling, giving the angiographic impression of a normal arterial lumen despite significant atheromatous disease (Glagov et al., 1987). This has been demonstrated particularly in carotid atherosclerosis (Saito et al., 2002).

1.4.1.2 Intravascular ultrasound

This is a catheter-based method of assessing the arterial wall using sound waves. It is becoming widely used as an adjunct to percutaneous coronary intervention, where it can aid in the selection of the most appropriate transcatheter therapy (Fayad et al., 2001a; Vallabhajosula et al., 1997). The technique does allow the skilled operator to distinguish various elements of the atherosclerotic plaque, such as lipid core, fibrous cap and thrombus on the basis of their differing echogenicity. However, it is of little use in the evaluation of asymptomatic individuals who are not already undergoing percutaneous investigation.

1.4.1.3 Intravascular angioscopy

Rather than the indirect appreciation of the vessel wall and plaque that can be gained from intravascular ultrasound, angioscopy allows the direct visualisation of both elements (Fayad et al., 2001b; Vallabhajosula et al., 1997). Surface colour, the presence of thrombus and macroscopic features of plaque instability (such as fissuring and ulceration) can all be appreciated. Once again, however, this procedure is limited by its invasiveness and its current role is as a research tool. Additionally, one is only able to visualise the inner vessel surface, with no information obtained about the different layers that comprise the vessel wall.

1.4.1.4 Thermography

This experimental technique relies on the fact that atherosclerotic plaques exhibit a range of temperatures. A study that examined carotid endarterectomy specimens demonstrated temperature heterogeneity over the surface of the plaque, with the hotter areas being more densely infiltrated with macrophages. Following on from this observation, a catheter-based technique was developed to examine coronary arteries *in vivo*. It was shown that coronary artery plaques in patients presenting with acute coronary syndromes had higher temperatures than those with symptoms of stable angina (Verheye et al., 2002; Naghavi et al., 2001; Stefanadis et al., 2001; Stefanadis et al., 2000; Stefanadis et al., 1999), and moreover, that temperatures within plaques could be reduced with statin therapy (Stefanadis et al., 2002). Thermography might be combined with IVUS to yield both anatomical and functional information from the same plaque.

1.4.2 Non-invasive imaging

1.4.2.1 Surface ultrasound

Accurate measurement of carotid wall thickness and some examination of plaque morphology can be carried out with surface B-mode ultrasound studies. The echogenicity of the plaque reflects its underlying composition, with a hypoechoic appearance on ultrasound being associated with the presence of lipids and haemorrhage, whereas a hyperechoic image suggests an underlying fibrous or calcified plaque. Both the NASCET and ACAS trials have shown that the degree of stenosis and its haemodynamic consequences are predictive of subsequent stroke (Barnett et al., 1998; Warlow et al., 1996). High resolution B-mode ultrasound has become the first line investigation for evaluating suspected carotid artery disease. Measurements of the intima-media thickness have been shown to correlate with the extent of coronary atherosclerosis (O'Leary et al., 1999). However, as with other ultrasound techniques, this method is highly operator-dependent and has low reproducibility.

1.4.2.2 Electron beam computed tomography

This technique uses a beam of electrons to produce an image with an acquisition time of only 100 milliseconds. Its primary role is to assess the amount of calcium in the arteries under evaluation (known as the calcium score). The utility of this measure lies in the fact that high calcium scores are predictive of advanced atherosclerosis in patients judged at intermediate risk of disease, but this technique cannot be said to assess any aspect of the plaque except its calcium content. Furthermore, there is insufficient good evidence to suggest that changes in coronary calcification correspond to changes in cardiovascular risk (Schmermund et al., 2001; Callister et al., 1998; O'Rourke et al., 2000). Finally, although both the presence of an elevated serum CRP level and a high coronary calcium score are independently predictive of cardiac events and cardiac death, it was shown recently that there is no association between the two (Redberg et al., 2000), which suggests that both markers are measuring different aspects of the same process.

1.4.2.3 Nuclear scintigraphy

Many radiotracers, targeted against molecules and cells involved in atherosclerosis, have been evaluated as potential candidates for imaging atherosclerosis. Targets have included lipoproteins, macrophages, vascular smooth muscle cells and endothelial cell adhesion molecules (Vallabhajosula et al., 1997; Fayad et al., 2001a; Naghavi et al., 2001; Rumberger, 2001; Chen et al., 2002). They have met with limited success however, because although they all accumulated to some extent in atherosclerosis, the signal to noise ratios were poor as a result of slow blood tracer clearance (Loscalzo et al., 1992). Some nuclear agents do appear more suited to imaging atherosclerosis, such as antibodies to the platelet glycoprotein 2b3a receptor (Mitchel et al., 2000), which have a better clearance rate from blood. Unfortunately, however, there has yet to emerge a single radiotracer that is ideal for not only imaging atheroma but also providing prognostic information about the risk of plaque rupture.

1.4.2.4 Magnetic resonance imaging

High-resolution magnetic resonance (HRMR) has emerged as the leading non-invasive imaging modality for atherosclerotic plaque characterisation. It differentiates plaque components on the basis of several biophysical and biochemical parameters, including physical state, chemical composition and concentration, water content, molecular motion, or diffusion. HRMR has the huge advantage that it does not involve ionizing radiation, and studies can therefore be repeated to monitor the progression and regression of disease.

High-resolution MR relies on the same underlying principles as other MR techniques. The patient is subjected to a high strength local magnetic field, usually 1.5 Tesla but increasingly greater, which aligns the protons in the body in the direction of the field. A radiofrequency pulse then excites these protons, and receiver coils detect the radiofrequencies emitted as they relax. Detected signals are influenced by the relaxation times (called T1 and T2), proton density, motion and flow, molecular diffusion, magnetization transfer and changes in susceptibility. Three additional magnetic fields (gradient fields) are applied during MRI; one selects the slice and two encode spatial information. The timing of the excitation pulses and the successive magnetic field gradients determine the image contrast.

MR images can be "weighted" to the T1, T2, or proton density values through manipulation of the MR parameters (i.e. repetition time and echo time). In a T1-weighted (T1W) image, tissues with low T1 values will be displayed as hyperintense picture elements or pixels (high signal intensity) and, conversely, high T1 values will be displayed as hypointense pixels (low signal intensity). In a T2-weighted (T2W) image, tissues with high T2 values will be portrayed as hyperintense pixels, and those with low T2 values as hypointense pixels. Thus, a T1W and a T2W image of the same anatomy can appear quite different because an MR image is not a photograph, but a computerized map of radio signals emitted by the tissue under study. Finally, in a proton density-weighted (PDW) image the differences in contrast are proportional to the density of water and fat

within which the protons are incorporated. PDW images are also referred to as intermediate-weighted images because the contrast in the image is a combination of mild T1 and T2 contrast.

1.4.2.4.1 Plaque characterisation with MR

Much of the experimental work that has validated the technique of high-resolution plaque MR has been performed by Fayad and his group. They have shown that the physical components of the atherosclerotic plaque can be distinguished from one another on the basis of their MR relaxation times (Fayad et al., 2000a). The differing characteristics are described below in Table 1.1 [adapted from (Fayad et al., 2001b)].

	Relative MR Signal Intensity*		
	T1W	PDW	T2W
Calcium	Hypointense	Very hypointense	Very hypointense
Lipid	Very hyperintense	Hyperintense	Hypointense
Fibrous	Isointense to slightly hyperintense	Isointense to slightly hyperintense	Isointense to slightly hyperintense
Thrombus	Variable	Variable	Variable

Table 1.1
*Relative to that of immediately adjacent muscle tissue.

In studies of atherosclerosis in rabbits, MR images have been shown to correlate well with pathology (Worthley et al., 2000). Furthermore, other investigators have tracked

both progression and regression of atheroma in the abdominal aorta (Worthley et al., 2000; McConnell et al., 1999; Helft et al., 2001). Regression of atheroma was induced both by withdrawal of a high fat diet and by the use of statin therapy. Plaque complications such as thrombus have been detected and characterised using MR (Corti et al., 2002). MR technology is now sufficiently advanced to allow the imaging of abdominal atherosclerosis in animals as small as Apo-E knockout mice (Fayad et al., 1998). Using a magnetic field strength of 9.4 Tesla, Fayad was able to generate an in-plane resolution of between 50 – 97 μ m, with a slice thickness of 500 μ m. There was excellent correlation between MR images and aortic plaque histology.

1.4.2.4.2 Atherosclerosis imaging with MR in humans

Advances in both hardware and software have allowed rapid development of *in vivo* MR imaging of atherosclerosis in humans. In most cases, a dedicated carotid phased-array coil is used for this purpose (Hayes et al., 1996). Imaging has been carried out in the carotid arteries (Yuan et al., 2001; Yuan et al., 1998) where plaque volume was accurately determined by high-resolution MR scanning. Different plaque components can be accurately documented (Hatsukami et al., 2000) and plaque progression can be monitored with serial imaging (Corti et al., 2001; Zhao et al., 2001). Recently, even new blood vessel formation within advanced plaque has been imaged successfully using a combination of non-contrast and gadolinium-enhanced MR (Yuan et al., 2002a). In addition, reliable documentation of the state of the fibrous cap has been demonstrated (Yuan et al., 2002b). Prospective studies will be required to determine whether the appearance of a disrupted cap on a high-resolution MR study is predictive of future carotid territory ischaemic events.

Other vascular beds have been imaged using MR, including peripheral arteries, where vessel remodelling after balloon angioplasty was accurately documented (Couliden et al., 2000). Imaging of the coronary arteries with MR presents a special challenge for investigators; their deep location, small calibre and susceptibility to respiratory and cardiac motion artifacts mean that the most useful images have been obtained using an

MR coil embedded in a transoesophageal probe, although some investigators are having increasing success using a surface coil (Fayad et al., 2000b; Quick et al., 2002; Fayad et al., 2001a). Aortic atheroma has been visualised using MR with a torso coil (Fayad et al., 2000c), the results correlating well with transoesophageal images. It must be recalled, however, that MR imaging can only give information concerning the anatomy of the plaque. It cannot demonstrate inflammation – the most important determinant of plaque rupture.

1.5 INTRODUCTION TO POSITRON EMISSION TOMOGRAPHY

An introduction to the background, physics and chemistry of positron emission tomography (PET) relevant to this work will be provided here. There will be some expansion on image analysis and quantification in the chapters dealing with PET imaging of human carotid atherosclerosis (Chapter 5), and experimental atherosclerosis (Chapter 6).

It has been recognised since the 1930s that cancer cells use more glucose than healthy cells, with requirements being greatest in the fastest growing tumours (Warburg, 1930; Warburg, 1956). This is the basis for PET using 2-[¹⁸F]fluoro-2-deoxy-D-glucose (FDG). PET is an imaging modality that allows the quantification (and visualisation) of regional physiology, biochemistry and pharmacology. It is the most sensitive and specific means available for imaging molecular pathways and interactions *in vivo*. By providing such functional information, it is an excellent accompaniment to the anatomical information that can be derived from computed tomography (CT) and magnetic resonance imaging.

PET involves the administration of a positron-emitting radiotracer, followed by the detection, using a PET scanner, of gamma photon pairs that result from positron-electron annihilations within the subject (Figure 1.1). Tomographic image reconstruction techniques, similar to those used in CT, are then employed to produce a three dimensional image of the distribution of the PET tracer in the subject. Analyses can be performed on the image data to derive quantitative information, for example metabolic rate for glucose, blood flow, oxygen extraction or receptor binding potential, depending on the tracer and the region under investigation.

1.5.1 Positron emission

All radioisotopes used in PET decay, at least in part, by positron emission. Figure 1.1 is a schematic diagram representing a positron-emitting radioisotope. Positrons are positively charged electrons. They are emitted from the nucleus of certain radioisotopes that are unstable because of an excessive number of protons relative to neutrons and hence have a positive charge. Positron emission stabilizes the nucleus by removing the positive charge through the conversion of a proton into a neutron. In doing this, one element is converted into another, the latter having an atomic number one less than the former. For radioisotopes used in PET, the element formed from positron decay is stable (i.e., not radioactive). A positron emitted from a decaying nucleus travels a short distance (~0.6mm for ¹⁸Fluorine (¹⁸F)), losing energy through scattering collisions with electrons, before eventually annihilating with an electron. In this annihilation, the mass of the two particles is converted to energy (governed by Einstein's formula, $E=MC^2$), in the form of two 511 keV gamma photons, emitted at (almost) 180° to each other. The vast majority of these photons escape from the body and are recorded by the rings of detectors contained within the PET scanner. The distance that the positron travels in tissue before annihilating with an electron is short but important; it is this distance that is one of the factors that determines the maximum resolution of PET scanning. In addition, the two gamma rays are not emitted at exactly 180 degrees to each other, due to the non-zero momentum of the electron-positron system at annihilation: this factor also contributes to the theoretical limit of spatial resolution of PET. In practice, however, it is the finite detector size, scanner sensitivity and the need to smooth the dataset to limit noise that constrain resolution in most clinical settings.

1.5.2 PET scanner

A PET scanner consists of a cylindrical arrangement of rings of scintillation detectors. These are capable of detecting the annihilation photons emitted from electron-positron annihilations. Coincidence electronics are used to pair up detected photons; typically, two events detected in opposing arcs of the ring within 12nsecs of each other are deemed a

valid event. In this case, the positron decay is assumed to have occurred somewhere along a line joining the two detectors. The cylindrical configuration of detectors collects data sufficient for tomographic reconstruction of a quantitative 3-D image of the distribution of the tracer in the subject under study: this is known as an emission scan. Emission scans may be performed in two modes : 2-D or 3-D. In 2-D mode, annular rings made of lead or tungsten, known as septa, separate the detector rings from each other. This means that photons from decay events are rejected when they have originated outside the field of view, and also if they don't travel perpendicular to the axis of the scanner, which would otherwise degrade the signal to noise ratio.

The sensitivity of the PET scanner can be increased by a factor of up to five times by operating in 3-D mode. In this mode, the septa are withdrawn, allowing the acquisition of decay events between detectors in different planes of the scanner. However, this is done at the expense of a large increase in the amount of scatter, and the detection of other background events, especially from activity outside the field of view. In addition, the computing power required to process data acquired in 3-D mode is much greater than for 2-D mode.

1.5.3 Data corrections

In PET, in order to obtain a quantitative image, corrections must be applied to the data gathered during the emission study. Corrections are applied for attenuation of the photons due to scattering that occurs en route to the pair of detectors; this is known as attenuation correction. The correction factor is obtained by calculating the ratio between two additional scans - a blank scan and a transmission scan. The blank scan is performed when the scanner is empty, and the transmission scan is done using a radioactive rod source (Germanium 68) which rotates around the patient once inside the scanner, but before the administration of FDG. In this project, in Chapter 5, the transmission scan image was used to provide a crude 'CT-like' image of the patient's neck, in order to ensure that the carotid area was adequately covered by the field of view.

The emission dataset is also corrected for detector dead time (when the detector is processing a decay, there is a finite time before it can register a further decay – this is known as the dead time), random decays (events produced by pairing up of gamma photons from separate annihilations purely due to the chance that they occurred within 12 nsecs of each other) and scatter (photon pairs Compton-scattered by collisions with electrons in the patient and also the detectors). Finally, corrections are applied to the PET data for both sensitivity and normalisation, making all imaging planes and lines of response equally sensitive, and cross-calibrating the image planes to a well counter to generate images in kilobecquerels per millilitre (kBq/ml).

1.5.4 PET tracers

As positron emitters do not exist in nature, they must be manufactured in a dedicated particle accelerator known as a cyclotron. Because of the short half lives of most positron emitters, this facility needs to be close to the PET scanner itself – the exception being ^{18}F , which has a relatively long half life (109.8 minutes). The majority of radiotracers used in PET are based upon the atoms carbon, nitrogen and oxygen as these are biologically important elements; therefore radioactive versions of these can be used to study important biological processes *in vivo*. The fourth key positron emitter is Fluorine-18. ^{18}F can be introduced into the glucose structure, in the place of a hydroxyl moiety at the C-2 position in the carbon ring, to produce fluorodeoxyglucose (FDG). FDG is a glucose analogue, and was used as the tracer for imaging atherosclerosis in this project.

1.5.5 Metabolic pathway of FDG

The fate of FDG once injected into the body is shown in Figure 1.2. It is taken up by metabolically active cells throughout the body in a similar way to glucose, and is therefore widely distributed. Its normal distribution in healthy tissues includes the brain, heart, kidneys and urinary tract. FDG is transported into cells via the facilitative glucose transporter protein system in the same way as glucose itself. There are at least nine of these structurally related molecules, which are known as GLUT 1–5, GLUT 7 and GLUT

10-12 (Brown, 2000). No tissue has been discovered where the GLUT 6 gene is expressed (Kayano et al., 1990; Brown, 2000; Burant et al., 1991). In addition, a tiny fraction of FDG enters the cell by passive diffusion, with the small remainder entering through a sodium-dependent glucose transporter.

Once inside the cell, both glucose and FDG undergo the first step in the glycolytic pathway, being phosphorylated by the hexokinase enzyme to glucose-6-phosphate and FDG-6-phosphate respectively. After this reaction, however, the two molecules have different fates. Glucose is further metabolised down the glycolytic pathway. However, for stoichiometric reasons, FDG-6-phosphate is unable to proceed further down this pathway. Additionally, it is a polar molecule, which prevents it from crossing the cell membrane and leaving the cell. FDG-6-phosphate can be dephosphorylated, by glucose-6-phosphatase, but this enzyme is found at low concentrations in most cells. FDG thus becomes trapped in the cell in quantities that reflect the glucose usage of that cell (Gallagher et al., 1978).

1.5.6 Quantification of cellular FDG accumulation

One of the strengths of PET is the ability to perform quantitative studies. In its most basic form, relative quantification means that average values of tracer uptake can be compared in different areas of interest in the region under study. At the other end of the spectrum, absolute quantification allows the determination of physiological parameters in absolute units for the tissue of interest (e.g. blood flow, oxygen extraction, metabolic rate for glucose etc). Both forms of analysis are discussed in general terms below.

1.5.6.1 Qualitative image analysis

This is the commonest form of analysis in clinical PET studies. It involves simple visual inspection and interpretation of PET images, without an attempt at any form of numerical quantification. It is widely used in oncological PET to diagnose metastatic disease. The

accuracy of this method can be improved upon by careful co-registration with another imaging modality such as CT or MR. This technique is known as image fusion.

1.5.6.2 Quantative image analysis

1.5.6.2.1 Time-activity curves

This method involves simple comparisons of mean tracer uptake over time in different regions of interest. For example, in brain studies, a region in the area of interest (e.g. tumour) might be compared with a control region comprising presumed normal brain tissue. This is known as a tissue time-activity curve (TAC). Significantly, there is no requirement for an input function such as blood FDG activity with this approach to quantification. Using the time-activity curve approach, one can crudely compare PET studies performed under similar conditions with one another by examining the shape of their respective time-activity curves.

1.5.6.2.2 Standard uptake value

The TAC method can be improved upon to allow numerical comparison between patients by normalizing the uptake of tracer. The most common example of such normalization is the standard uptake value (SUV), commonly used in oncology PET to differentiate benign and malignant tumours on the basis of differing degrees of FDG uptake. The tracer uptake is normalized for patient mass and administered radioactivity (see equation below). The calculation of an SUV allows a reliable measure of glucose metabolism to be made from a single image without the need for blood sampling.

$$\text{SUV} = \frac{\text{Tracer Uptake in ROI (MBq/ml)}}{\text{Activity administered (MBq) / Patient mass (Kg)}}$$

There are, however, a number of limitations with the SUV technique. Firstly, SUVs are only accurate if the uptake of tracer has reached steady state at the time of measurement. This is not always the case, because some tissues will continue to accumulate FDG for a number of hours after its administration. Therefore, in order to compare patients, PET data must always be acquired at the same time after injection. A second problem arises in diabetic patients, especially those that are obese, where high serum glucose levels can compete with FDG for entry in the cells (Wahl et al., 1992). A correction that reflects the blood glucose level should therefore be applied to the data before comparisons between patients can be made.

1.5.6.3 Absolute quantification

1.5.6.3.1 Full kinetic modelling

Full kinetic modelling is the holy grail of PET quantification. As shown in Figure 1.2, FDG is not fully metabolised, and its behaviour can be characterised by a three-compartment model with four rate constants (k_1 - k_4). In many tissues, the concentration of the enzyme glucose-6-phosphatase is low, and k_4 therefore approximates zero and FDG thus behaves like a tissue-bound tracer. Given this assumption, a single plateau PET image in conjunction with knowledge of k_1 , k_2 and k_3 and a dynamic arterial blood curve (input function) can be used to quantify FDG uptake in the region of interest. If the value of the rate constants is not known, it can be determined by acquiring a dynamic sequence of PET and blood data, and mathematically fitting these data to the compartment model. Finally, in order to convert FDG uptake into glucose uptake for the tissue of interest, a correction factor known as the ‘lumped constant’ must be applied to the data. This is equal to the ratio of the rate of FDG phosphorylation to the rate of glucose phosphorylation under steady state conditions (Schmidt et al., 1996).

1.5.6.3.2 Patlak plot

An alternative approach to full kinetic modelling is a graphical technique known as a Patlak Plot. This method was developed to address the case where a tracer is irreversibly trapped in tissue. In reality, very few tracers truly become permanently trapped, as there is almost always a path out of the tissue. However, a tracer is considered irreversibly trapped if there is no significant efflux during the time period of the PET scan. For such cases, the Patlak Plot was developed (Albert Gjedde first proposed this approach in 1981 (Gjedde, 1981), but Patlak's seminal 1983 paper in which he formally developed this method caused his name to be associated with it (Patlak et al., 1983)).

Construction of a Patlak plot involves plotting an ordinate and an abscissa using various combinations of the input function and image data at each of the observed time points of the PET study. The beauty of the Patlak plot is that it becomes linear at those time-points when the free tracer compartment is at steady state.

The mathematical derivation of the Patlak method is shown below, where C_T is the concentration of FDG in a tissue region-of-interest, C_f is the concentration of free FDG in a tissue ROI, C_b is the concentration of bound FDG in a tissue ROI, C_p is the concentration of FDG in the plasma (derived from arterial blood sampling), k_1 - k_3 are rate constants as shown in Figure 1.3 and t is the time elapsed since injection of FDG.

The rate of change of free FDG in the tissue ROI is governed by the outward flux and the inward flux as below:

$$\text{Equation 1 : } dC_f / dt = k_1 \cdot C_p - (k_2 + k_3) \cdot C_f$$

The rate of change of bound FDG in the tissue ROI is governed by the flux inwards (assuming k_4 equals zero):

$$\text{Equation 2 : } dC_b / dt = k_3 \cdot C_f$$

The concentration of tissue FDG is the sum of free and bound FDG:

Equation 3 : $C_T = C_f + C_b$

Substituting for C_b by rearranging Equation 2:

Equation 4 : $C_T = C_f + k_3 \cdot \int_0^t C_f$

At steady state: $dC_f / dt = 0$ (assuming that the concentration of free FDG at steady state does not change with time) :

From Equation 1 $\Rightarrow k_1 \cdot C_p = (k_2 + k_3) \cdot C_f$

Substituting into Equation 3:

$$C_T = \frac{k_1}{(k_2 + k_3)} \cdot C_p + \frac{k_1 \cdot k_3}{(k_2 + k_3)} \cdot \int_0^t C_p$$

Divide by C_p :

$$(C_T/C_P) = \frac{k_1 \cdot k_3}{(k_2 + k_3)} \cdot \frac{\int_0^t C_p}{C_p} + \frac{k_1}{(k_2 + k_3)}$$

$$y = m x + c$$

Thus if (C_T/C_P) is plotted against $\int_0^t C_p / C_p$, then a line with a gradient equal to $(k_1 \cdot k_3) / (k_2 + k_3)$ is obtained, with an intercept of $(k_1) / (k_2 + k_3)$. If the gradient term is multiplied by the plasma glucose concentration, and divided by the ‘lumped constant’, the answer will be the metabolic rate for glucose (MRGlc) of the region of interest (Patlak et al., 1983). The intercept term is the volume of distribution of FDG.

In a later publication, Patlak showed that some assumptions in his earlier work could be relaxed (Patlak et al., 1985). He stated that the tracer need not be trapped "forever", but that the net influx must be positive for an appreciable duration of time, i.e. the tracer can be transiently irreversibly bound.

Patlak analysis is employed in Chapter 5 to analyse FDG uptake in dynamic PET studies of carotid artery atherosclerosis.

1.5.7 Partial volume effect

A key limitation to all forms of quantification in PET within small regions of interest is the partial volume effect. This is a consequence of the inherent resolution of PET. Whenever objects with dimensions less than approximately twice the spatial resolution of PET are studied, the apparent activity in a hyperintense object is decreased, whilst that in a hypointense object is increased. For objects with a diameter equal to the spatial resolution, the apparent activity in a hyperintense object may be less than 50% of the true value (Mazziotta et al., 1981; Marsden, 1999). As with quantification of FDG uptake, once again, this topic is discussed more fully in Chapter 5.

1.6 PROJECT DESIGN

The primary hypothesis behind this work was that FDG-PET would be able to image and quantify inflammation within human atherosclerotic plaques, and further that unstable plaques might be highlighted by virtue of their higher metabolic activity in comparison to stable plaques.

There are several lines of evidence backing up this hypothesis. Firstly, unstable plaques, prone to fibrous cap rupture and clinical events, have a high macrophage to vascular smooth muscle cell ratio (Davies, 1996). Macrophages from unstable plaques are highly activated, producing MMPs and inflammatory cytokines, and ingesting oxidised lipid through scavenger receptors. A study using a sensitive thermistor (Casscells et al., 1996) demonstrated increased temperatures within excised human carotid plaques compared to surrounding tissue, which was interpreted as reflecting the high metabolic activity of plaque inflammatory cells.

Secondly, it has been shown that macrophages, contained within tumour stromal tissue, avidly accumulate FDG, and may be responsible for up to 30% of the total tumour FDG uptake (Kubota et al., 1992; Kubota et al., 1994). Additionally, in an experimental model of subcutaneous inflammation in rats, macrophages were responsible for taking up the largest proportion of FDG of all cells within the lesions (Yamada et al., 1995).

Thirdly, there are several reports of the use of FDG-PET imaging of atherosclerosis in animal models, which have been published in abstract form (Vallabhajosula et al., 1996; Badimon et al., 1999). The methods used in these reports differ significantly from those devised for this project, but nevertheless are supportive of the principle hypothesis.

Therefore, firstly, it was determined whether a monocyte cell line might be capable of accumulating tritiated deoxyglucose (HDG) - an *in vitro* analogue of FDG - in cell culture conditions. Having established that this was the case, other experiments were devised to change the metabolic activity of the monocytes, to see if these differences

would be reflected by changes in HDG uptake. Similar experiments were then performed with freshly isolated human macrophages in culture. The results are described in Chapter 3.

Having established that macrophages would accumulate HDG, and that changes in activation were reflected by changes in HDG uptake, it was investigated whether human carotid atheroma removed from symptomatic patients might accumulate FDG, and furthermore, whether the degree of accumulation might correlate with the macrophage content of the plaques imaged. Autoradiographic studies were carried out to confirm the findings. Results from this group of experiments are shown in Chapter 4.

The strategy outlined above, firstly using isolated macrophages and then carotid plaques yielded promising results, and suggested that it might be profitable to proceed to FDG-PET imaging of carotid artery disease in symptomatic patients, the results of which are presented in Chapter 5.

Finally, in pilot experiments, a rabbit model of atherosclerosis was established to investigate two related questions: firstly whether a small animal PET scanner might detect atheroma, and secondly whether FDG-PET could image and perhaps quantify atherosclerosis progression and its subsequent regression, and these results are presented in Chapter 6.

1.7 REFERENCES

1. 4S Study (1994). Randomised trial of cholesterol lowering in 4444 patients with coronary heart disease: the Scandinavian Simvastatin Survival Study (4S) [see comments]. Lancet, 344, 1383-1389.
2. Albert, C. M., Ma, J., Rifai, N., Stampfer, M. J., & Ridker, P. M. (2002). Prospective Study of C-Reactive Protein, Homocysteine, and Plasma Lipid Levels as Predictors of Sudden Cardiac Death. Circulation, 105, 2595-2599.
3. Amento, E. P., Ehsani, N., Palmer, H., & Libby, P. (1991). Cytokines and growth factors positively and negatively regulate interstitial collagen gene expression in human vascular smooth muscle cells. Arterioscler.Thromb., 11, 1223-1230.
4. Anggard, E. (1994). Nitric oxide: mediator, murderer, and medicine [see comments]. Lancet, 343, 1199-1206.
5. Aniteschkow, N. Uber die veränderung der Kaninchenaorta bei experimenteller cholesterinsteatose. Pathol.Anat.Allg.Pathol. 56, 379-404. 1913.
Ref Type: Journal (Full)
6. Badimon, J. J., Zyang, Z. Y., Machac, J., Helft, G., Worthley, S. G., Tang, C. Y., Osende, J. I., Lipszyc, H., Buschbaum, M. S., & Fuster, V. (1999). Non-Invasive imaging of atherosclerotic plaque macrophage in a rabbit model with F-18 FDG PET: A histopathological correlation. J.Nucl.Med., 40, 88P-88P.
7. Barnett, H. J., Taylor, D. W., Eliasziw, M., Fox, A. J., Ferguson, G. G., Haynes, R. B., Rankin, R. N., Clagett, G. P., Hachinski, V. C., Sackett, D. L., Thorpe, K. E., & Meldrum, H. E. (1998). Benefit of carotid endarterectomy in patients with symptomatic moderate or severe stenosis. North American Symptomatic Carotid Endarterectomy Trial Collaborators. N.Engl.J.Med., 339, 1415-1425.
8. Bennett, M. R., Littlewood, T. D., Schwartz, S. M., & Weissberg, P. L. (1997). Increased sensitivity of human vascular smooth muscle cells from atherosclerotic plaques to p53-mediated apoptosis. Circ.Res., 81, 591-599.
9. Bennett, M. R., Macdonald, K., Chan, S. W., Boyle, J. J., & Weissberg, P. L. (1998). Cooperative interactions between RB and p53 regulate cell proliferation, cell senescence, and apoptosis in human vascular smooth muscle cells from atherosclerotic plaques. Circ.Res., 82, 704-712.
10. Berliner, J. A., Navab, M., Fogelman, A. M., Frank, J. S., Demer, L. L., Edwards, P. A., Watson, A. D., & Lusis, A. J. (1995). Atherosclerosis: basic mechanisms. Oxidation, inflammation, and genetics. Circulation, 91, 2488-2496.
11. Bhagat, K. & Vallance, P. (1996). Nitric oxide 9 years on. J.R.Soc.Med., 89, 667-673.
12. Bini, A., Fenoglio, J. J., Jr., Mesa-Tejada, R., Kudryk, B., & Kaplan, K. L. (1989). Identification and distribution of fibrinogen, fibrin, and fibrin(ogen) degradation products in atherosclerosis. Use of monoclonal antibodies. Arteriosclerosis, 9, 109-121.
13. Boring, L., Gosling, J., Cleary, M., & Charo, I. F. (1998). Decreased lesion formation in CCR2^{-/-} mice reveals a role for chemokines in the initiation of atherosclerosis. Nature, 394, 894-897.

14. Boyle, J. J. (1997). Association of coronary plaque rupture and atherosclerotic inflammation. J.Pathol., 181, 93-99.
15. Boyle, J. J., Bennett, M. R., proudfoot, D., Bowyer, D., & Weissberg, P. L. Human monocyte/macrophages induce human smooth muscle cell apoptosis in culture. J.Pathol. 184, A13-A13. 2000.
Ref Type: Abstract
16. Brown, G. K. (2000). Glucose transporters: structure, function and consequences of deficiency. J.Inherit.Metab Dis., 23, 237-246.
17. Buffon, A., Biasucci, L. M., Liuzzo, G., D'Onofrio, G., Crea, F., & Maseri, A. (2002). Widespread coronary inflammation in unstable angina. N.Engl.J.Med., 347, 5-12.
18. Burant, C. F., Sivitz, W. I., Fukumoto, H., Kayano, T., Nagamatsu, S., Seino, S., Pessin, J. E., & Bell, G. I. (1991). Mammalian glucose transporters: structure and molecular regulation. Recent Prog.Horm.Res., 47, 349-387.
19. Calabresi, L., Franceschini, G., Sirtori, C. R., De Palma, A., Saresella, M., Ferrante, P., & Taramelli, D. (1997). Inhibition of VCAM-1 expression in endothelial cells by reconstituted high density lipoproteins. Biochem.Biophys.Res.Commun., 238, 61-65.
20. Callister, T. Q., Raggi, P., Cooil, B., Lippolis, N. J., & Russo, D. J. (1998). Effect of HMG-CoA reductase inhibitors on coronary artery disease as assessed by electron-beam computed tomography. N.Engl.J.Med., 339, 1972-1978.
21. Cardona-Sanclemente, L. E. & Born, G. V. (1995). Effect of inhibition of nitric oxide synthesis on the uptake of LDL and fibrinogen by arterial walls and other organs of the rat. Br.J.Pharmacol., 114, 1490-1494.
22. Casscells, W., Hathorn, B., David, M., Krabach, T., Vaughn, W. K., McAllister, H. A., Bearman, G., & Willerson, J. T. (1996). Thermal detection of cellular infiltrates in living atherosclerotic plaques: possible implications for plaque rupture and thrombosis. Lancet, 347, 1447-1451.
23. Chen, J., Tung, C. H., Mahmood, U., Ntziachristos, V., Gyurko, R., Fishman, M. C., Huang, P. L., & Weissleder, R. (2002). In Vivo Imaging of Proteolytic Activity in Atherosclerosis. Circulation, 105, 2766-2771.
24. Cooper, R., Cutler, J., Desvigne-Nickens, P., Fortmann, S. P., Friedman, L., Havlik, R., Hogelin, G., Marler, J., McGovern, P., Morosco, G., Mosca, L., Pearson, T., Stamler, J., Stryer, D., & Thom, T. (2000). Trends and disparities in coronary heart disease, stroke, and other cardiovascular diseases in the United States: findings of the national conference on cardiovascular disease prevention. Circulation, 102, 3137-3147.
25. Corti, R., Fayad, Z. A., Fuster, V., Worthley, S. G., Helft, G., Chesebro, J., Mercuri, M., & Badimon, J. J. (2001). Effects of lipid-lowering by simvastatin on human atherosclerotic lesions: a longitudinal study by high-resolution, noninvasive magnetic resonance imaging. Circulation, 104, 249-252.
26. Corti, R., Osende, J. I., Fayad, Z. A., Fallon, J. T., Fuster, V., Mizsei, G., Dickstein, E., Drayer, B., & Badimon, J. J. (2002). In vivo noninvasive detection and age definition of arterial thrombus by MRI. J.Am.Coll.Cardiol., 39, 1366-1373.

27. Coulden, R. A., Moss, H., Graves, M. J., Lomas, D. J., Appleton, D. S., & Weissberg, P. L. (2000). High resolution magnetic resonance imaging of atherosclerosis and the response to balloon angioplasty. Heart, 83, 188-191.
28. Crisby, M., Nordin-Fredriksson, G., Shah, P. K., Yano, J., Zhu, J., & Nilsson, J. (2001). Pravastatin Treatment Increases Collagen Content and Decreases Lipid Content, Inflammation, Metalloproteinases, and Cell Death in Human Carotid Plaques : Implications for Plaque Stabilization. Circulation, 103, 926-933.
29. Danesh, J., Whincup, P., Walker, M., Lennon, L., Thomson, A., Appleby, P., Wong, Y., Bernardes-Silva, M., & Ward, M. (2000). Chlamydia pneumoniae IgG titres and coronary heart disease: prospective study and meta-analysis [see comments]. BMJ, 321, 208-213.
30. Davies, M. J. (1995). Acute coronary thrombosis--the role of plaque disruption and its initiation and prevention. Eur.Heart J., 16 Suppl L, 3-7.
31. Davies, M. J. (1996). Stability and instability: two faces of coronary atherosclerosis. The Paul Dudley White Lecture 1995. Circulation, 94, 2013-2020.
32. de Boer, O. J., van der Wal, A. C., & Becker, A. E. (2000). Atherosclerosis, inflammation, and infection. J.Pathol., 190, 237-243.
33. de Lemos, J. A., Hennekens, C. H., & Ridker, P. M. (2000). Plasma concentration of soluble vascular cell adhesion molecule-1 and subsequent cardiovascular risk. J.Am.Coll.Cardiol., 36, 423-426.
34. Downs, J. R., Clearfield, M., Weis, S., Whitney, E., Shapiro, D. R., Beere, P. A., Langendorfer, A., Stein, E. A., Kruyer, W., & Gotto, A. M., Jr. (1998). Primary prevention of acute coronary events with lovastatin in men and women with average cholesterol levels: results of AFCAPS/TexCAPS. Air Force/Texas Coronary Atherosclerosis Prevention Study [see comments]. JAMA, 279, 1615-1622.
35. ECST Group (1998). Randomised trial of endarterectomy for recently symptomatic carotid stenosis: final results of the MRC European Carotid Surgery Trial (ECST). Lancet, 351, 1379-1387.
36. Farb, A., Burke, A. P., Tang, A. L., Liang, T. Y., Mannan, P., Smialek, J., & Virmani, R. (1996). Coronary plaque erosion without rupture into a lipid core. A frequent cause of coronary thrombosis in sudden coronary death. Circulation, 93, 1354-1363.
37. Farzaneh-Far, A., Rudd, J., & Weissberg, P. L. (2001). Inflammatory mechanisms. Br.Med.Bull., 59, 55-68.
38. Fayad, Z. A., Fallon, J. T., Shinnar, M., Wehrli, S., Dansky, H. M., Poon, M., Badimon, J. J., Charlton, S. A., Fisher, E. A., Breslow, J. L., & Fuster, V. (1998). Noninvasive In vivo high-resolution magnetic resonance imaging of atherosclerotic lesions in genetically engineered mice. Circulation, 98, 1541-1547.
39. Fayad, Z. A. & Fuster, V. (2000a). Characterization of atherosclerotic plaques by magnetic resonance imaging. Ann.N.Y.Acad.Sci., 902, 173-186.
40. Fayad, Z. A. & Fuster, V. (2001a). Clinical imaging of the high-risk or vulnerable atherosclerotic plaque. Circ.Res., 89, 305-316.

41. Fayad, Z. A. & Fuster, V. (2001b). Clinical imaging of the high-risk or vulnerable atherosclerotic plaque. *Circ.Res.*, 89, 305-316.
42. Fayad, Z. A., Fuster, V., Fallon, J. T., Jayasundera, T., Worthley, S. G., Helft, G., Aguinaldo, J. G., Badimon, J. J., & Sharma, S. K. (2000b). Noninvasive in vivo human coronary artery lumen and wall imaging using black-blood magnetic resonance imaging. *Circulation*, 102, 506-510.
43. Fayad, Z. A., Nahar, T., Fallon, J. T., Goldman, M., Aguinaldo, J. G., Badimon, J. J., Shinnar, M., Chesebro, J. H., & Fuster, V. (2000c). In vivo magnetic resonance evaluation of atherosclerotic plaques in the human thoracic aorta: a comparison with transesophageal echocardiography. *Circulation*, 101, 2503-2509.
44. Feeley, T. M., Leen, E. J., Colgan, M. P., Moore, D. J., Hourihane, D. O., & Shanik, G. D. (1991). Histologic characteristics of carotid artery plaque. *J.Vasc.Surg.*, 13, 719-724.
45. Galis, Z. S., Sukhova, G. K., Lark, M. W., & Libby, P. (1994). Increased expression of matrix metalloproteinases and matrix degrading activity in vulnerable regions of human atherosclerotic plaques. *J.Clin.Invest*, 94, 2493-2503.
46. Gallagher, B. M., Fowler, J. S., Gutterson, N. I., MacGregor, R. R., Wan, C. N., & Wolf, A. P. (1978). Metabolic trapping as a principle of oradiopharmaceutical design: some factors responsible for the biodistribution of [¹⁸F] 2-deoxy-2-fluoro-D- glucose. *J.Nucl Med.*, 19, 1154-1161.
47. Gauthier, T. W., Scalia, R., Murohara, T., Guo, J. P., & Lefer, A. M. (1995). Nitric oxide protects against leukocyte-endothelium interactions in the early stages of hypercholesterolemia. *Arterioscler.Thromb.Vasc.Biol.*, 15, 1652-1659.
48. Geng, Y. J., Henderson, L. E., Levesque, E. B., Muszynski, M., & Libby, P. (1997). Fas is expressed in human atherosclerotic intima and promotes apoptosis of cytokine-primed human vascular smooth muscle cells. *Arterioscler.Thromb.Vasc.Biol.*, 17, 2200-2208.
49. Geng, Y. J., Wu, Q., Muszynski, M., Hansson, G. K., & Libby, P. (1996). Apoptosis of vascular smooth muscle cells induced by in vitro stimulation with interferon-gamma, tumor necrosis factor-alpha, and interleukin-1 beta. *Arterioscler.Thromb.Vasc.Biol.*, 16, 19-27.
50. Gimbrone, M. A., Jr. (1999). Vascular endothelium, hemodynamic forces, and atherogenesis [comment]. *Am.J.Pathol.*, 155, 1-5.
51. Gjedde, A. (1981). High- and low-affinity transport of D-glucose from blood to brain. *J.Neurochem.*, 36, 1463-1471.
52. Glagov, S., Weisenberg, E., Zarins, C. K., Stankunavicius, R., & Kolettis, G. J. (1987). Compensatory enlargement of human atherosclerotic coronary arteries. *N.Engl.J.Med.*, 316, 1371-1375.
53. Golledge, J., Greenhalgh, R. M., & Davies, A. H. (2000). The symptomatic carotid plaque. *Stroke*, 31, 774-781.
54. Gosling, J., Slaymaker, S., Gu, L., Tseng, S., Zlot, C. H., Young, S. G., Rollins, B. J., & Charo, I. F. (1999). MCP-1 deficiency reduces susceptibility to atherosclerosis in mice that overexpress human apolipoprotein B. *J.Clin.Invest*, 103, 773-778.
55. Hatsukami, T. S., Ross, R., Polissar, N. L., & Yuan, C. (2000). Visualization of fibrous cap thickness and rupture in human atherosclerotic carotid plaque in vivo with high-resolution magnetic resonance imaging. *Circulation*, 102, 959-964.

56. Hayes, C. E., Mathis, C. M., & Yuan, C. (1996). Surface coil phased arrays for high-resolution imaging of the carotid arteries. *J.Magn Reson.Imaging*, 6, 109-112.
57. Heitzer, T., Just, H., & Munzel, T. (1996). Antioxidant vitamin C improves endothelial dysfunction in chronic smokers [see comments]. *Circulation*, 94, 6-9.
58. Helft, G., Worthley, S. G., Fuster, V., Zaman, A. G., Schechter, C., Osende, J. I., Rodriguez, O. J., Fayad, Z. A., Fallon, J. T., & Badimon, J. J. (2001). Atherosclerotic aortic component quantification by noninvasive magnetic resonance imaging: an in vivo study in rabbits. *J.Am.Coll.Cardiol.*, 37, 1149-1154.
59. Hobbs, A. J., Higgs, A., & Moncada, S. (1999). Inhibition of nitric oxide synthase as a potential therapeutic target. *Annu.Rev.Pharmacol.Toxicol.*, 39, 191-220.
60. Jander, S., Sitzer, M., Schumann, R., Schroeter, M., Siebler, M., Steinmetz, H., & Stoll, G. (1998). Inflammation in high-grade carotid stenosis: a possible role for macrophages and T cells in plaque destabilization. *Stroke*, 29, 1625-1630.
61. Jialal, I., Stein, D., Balis, D., Grundy, S. M., Adams-Huet, B., & Devaraj, S. (2001). Effect of hydroxymethyl glutaryl coenzyme a reductase inhibitor therapy on high sensitive c-reactive protein levels. *Circulation*, 103, 1933-1935.
62. Jukema, J. W., Bruschke, A. V., van Boven, A. J., Reiber, J. H., Bal, E. T., Zwinderman, A. H., Jansen, H., Boerma, G. J., van Rappard, F. M., & Lie, K. I. (1995). Effects of lipid lowering by pravastatin on progression and regression of coronary artery disease in symptomatic men with normal to moderately elevated serum cholesterol levels. The Regression Growth Evaluation Statin Study (REGRESS). *Circulation*, 91, 2528-2540.
63. Kaartinen, M., Penttila, A., & Kovanen, P. T. (1994). Accumulation of activated mast cells in the shoulder region of human coronary atheroma, the predilection site of atheromatous rupture. *Circulation*, 90, 1669-1678.
64. Kaartinen, M., van der Wal, A. C., van der Loos, C. M., Piek, J. J., Koch, K. T., Becker, A. E., & Kovanen, P. T. (1998). Mast cell infiltration in acute coronary syndromes: implications for plaque rupture. *J.Am.Coll.Cardiol.*, 32, 606-612.
65. Katznelson, S., Wang, X. M., Chia, D., Ozawa, M., Zhong, H. P., Hirata, M., Terasaki, P. I., & Kobashigawa, J. A. (1998). The inhibitory effects of pravastatin on natural killer cell activity in vivo and on cytotoxic T lymphocyte activity in vitro. *J.Heart Lung Transplant.*, 17, 335-340.
66. Kayano, T., Burant, C. F., Fukumoto, H., Gould, G. W., Fan, Y. S., Eddy, R. L., Byers, M. G., Shows, T. B., Seino, S., & Bell, G. I. (1990). Human facilitative glucose transporters. Isolation, functional characterization, and gene localization of cDNAs encoding an isoform (GLUT5) expressed in small intestine, kidney, muscle, and adipose tissue and an unusual glucose transporter pseudogene-like sequence (GLUT6). *J.Biol.Chem.*, 265, 13276-13282.
67. Knopp, R. H. (1999). Review Articles: Drug Therapy: Drug Treatment of Lipid Disorders. *N.Engl.J.Med.*, 341, 498-511.
68. Kol, A., Sukhova, G. K., Lichtman, A. H., & Libby, P. (1998). Chlamydial heat shock protein 60 localizes in human atheroma and regulates macrophage tumor necrosis factor-alpha and matrix metalloproteinase expression. *Circulation*, 98, 300-307.
69. Kubota, R., Kubota, K., Yamada, S., Tada, M., Ido, T., & Tamahashi, N. (1994). Microautoradiographic study for the differentiation of intratumoral macrophages, granulation

- tissues and cancer cells by the dynamics of fluorine-18-fluorodeoxyglucose uptake. J.Nucl.Med., 35, 104-112.
70. Kubota, R., Yamada, S., Kubota, K., Ishiwata, K., Tamahashi, N., & Ido, T. (1992). Intratumoral distribution of fluorine-18-fluorodeoxyglucose in vivo: high accumulation in macrophages and granulation tissues studied by microautoradiography. J.Nucl.Med., 33, 1972-1980.
 71. Kwak, B., Mulhaupt, F., Myit, S., & Mach, F. (2000). Statins as a newly recognized type of immunomodulator [In Process Citation]. Nat.Med., 6, 1399-1402.
 72. Lacoste, L., Lam, J. Y., Hung, J., Letchacovski, G., Solymoss, C. B., & Waters, D. (1995). Hyperlipidemia and coronary disease. Correction of the increased thrombogenic potential with cholesterol reduction [see comments]. Circulation, 92, 3172-3177.
 73. Li, H. & Forstermann, U. (2000). Nitric oxide in the pathogenesis of vascular disease. J.Pathol., 190, 244-254.
 74. Liaw, L., Almeida, M., Hart, C. E., Schwartz, S. M., & Giachelli, C. M. (1994). Osteopontin promotes vascular cell adhesion and spreading and is chemotactic for smooth muscle cells in vitro. Circ.Res., 74, 214-224.
 75. Libby, P. (1995). Molecular bases of the acute coronary syndromes. Circulation, 91, 2844-2850.
 76. Libby, P., Sukhova, G., Lee, R. T., & Galis, Z. S. (1995). Cytokines regulate vascular functions related to stability of the atherosclerotic plaque. J.Cardiovasc.Pharmacol., 25 Suppl 2, S9-12.
 77. LIPID Study Group (1998). Prevention of cardiovascular events and death with pravastatin in patients with coronary heart disease and a broad range of initial cholesterol levels. The Long-Term Intervention with Pravastatin in Ischaemic Disease (LIPID) Study Group [see comments]. N.Engl.J.Med., 339, 1349-1357.
 78. Loscalzo, J. & Rocco, T. P. (1992). Imaging arterial thrombi. An elusive goal. Circulation, 85, 382-385.
 79. MAAS Investigators (1994). Effect of simvastatin on coronary atheroma: the Multicentre Anti-Atheroma Study (MAAS) [published erratum appears in Lancet 1994 Sep 10;344(8924):762] [see comments]. Lancet, 344, 633-638.
 80. Marsden, P. K. (1999). Principles and Methods. In Atlas of Clinical Positron Emission Tomography (pp. 3-48). Oxford: Arnold.
 81. Mazziotta, J. C., Phelps, M. E., Plummer, D., & Kuhl, D. E. (1981). Quantitation in positron emission computed tomography: 5. Physical-- anatomical effects. J.Comput.Assist.Tomogr., 5, 734-743.
 82. McConnell, M. V., Aikawa, M., Maier, S. E., Ganz, P., Libby, P., & Lee, R. T. (1999). MRI of rabbit atherosclerosis in response to dietary cholesterol lowering. Arterioscler.Thromb.Vasc.Biol., 19, 1956-1959.
 83. McGovern, P. G., Pankow, J. S., Shahar, E., Doliszny, K. M., Folsom, A. R., Blackburn, H., & Luepker, R. V. (1996). Recent trends in acute coronary heart disease--mortality, morbidity, medical care, and risk factors. The Minnesota Heart Survey Investigators. N.Engl.J.Med., 334, 884-890.

84. McNamara, C. A., Sarembock, I. J., Bachhuber, B. G., Stouffer, G. A., Ragosta, M., Barry, W., Gimple, L. W., Powers, E. R., & Owens, G. K. (1996). Thrombin and vascular smooth muscle cell proliferation: implications for atherosclerosis and restenosis. Semin.Thromb.Hemost., 22, 139-144.
85. Mitchel, J., Waters, D., Lai, T., White, M., Alberghini, T., Salloum, A., Knibbs, D., Li, D., & Heller, G. V. (2000). Identification of coronary thrombus with a IIb/IIIa platelet inhibitor radiopharmaceutical, technetium-99m DMP-444: A canine model. Circulation, 101, 1643-1646.
86. Muhlestein, J. B., Anderson, J. L., Hammond, E. H., Zhao, L., Trehan, S., Schwobe, E. P., & Carlquist, J. F. (1998). Infection with Chlamydia pneumoniae accelerates the development of atherosclerosis and treatment with azithromycin prevents it in a rabbit model. Circulation, 97, 633-636.
87. Naghavi, M., Madjid, M., Khan, M. R., Mohammadi, R. M., Willerson, J. T., & Casscells, S. W. (2001). New developments in the detection of vulnerable plaque. Curr.Atheroscler.Rep., 3, 125-135.
88. Nakashima, Y., Plump, A. S., Raines, E. W., Breslow, J. L., & Ross, R. (1994). ApoE-deficient mice develop lesions of all phases of atherosclerosis throughout the arterial tree. Arterioscler.Thromb., 14, 133-140.
89. Negre-Aminou, P., van Vliet, A. K., van Erck, M., van Thiel, G. C., van Leeuwen, R. E., & Cohen, L. H. (1997). Inhibition of proliferation of human smooth muscle cells by various HMG-CoA reductase inhibitors; comparison with other human cell types. Biochim.Biophys.Acta, 1345, 259-268.
90. NHLBI (1998). NHLBI Fact Book Fiscal Year 1997. Bethesda, MD.
91. O'Leary, D. H., Polak, J. F., Kronmal, R. A., Manolio, T. A., Burke, G. L., & Wolfson, S. K., Jr. (1999). Carotid-artery intima and media thickness as a risk factor for myocardial infarction and stroke in older adults. Cardiovascular Health Study Collaborative Research Group. N.Engl.J.Med., 340, 14-22.
92. O'Rourke, R. A., Brundage, B. H., Froelicher, V. F., Greenland, P., Grundy, S. M., Hachamovitch, R., Pohost, G. M., Shaw, L. J., Weintraub, W. S., Winters, W. L., Jr., Forrester, J. S., Douglas, P. S., Faxon, D. P., Fisher, J. D., Gregoratos, G., Hochman, J. S., Hutter, A. M., Jr., Kaul, S., & Wolk, M. J. (2000). American College of Cardiology/American Heart Association Expert Consensus document on electron-beam computed tomography for the diagnosis and prognosis of coronary artery disease. Circulation, 102, 126-140.
93. Office of National Statistics (1997). Deaths: selected causes (International Classification) and sex, 1971 onwards (England & Wales). Health Statistics Quarterly, 04.
94. Palmer, R. M., Ferrige, A. G., & Moncada, S. (1987). Nitric oxide release accounts for the biological activity of endothelium-derived relaxing factor. Nature, 327, 524-526.
95. Panza, J. A., Garcia, C. E., Kilcoyne, C. M., Quyyumi, A. A., & Cannon, R. O., III (1995). Impaired endothelium-dependent vasodilation in patients with essential hypertension. Evidence that nitric oxide abnormality is not localized to a single signal transduction pathway. Circulation, 91, 1732-1738.
96. Patlak, C. S. & Blasberg, R. G. (1985). Graphical evaluation of blood-to-brain transfer constants from multiple- time uptake data. Generalizations. J.Cereb.Blood Flow Metab, 5, 584-590.

97. Patlak, C. S., Blasberg, R. G., & Fenstermacher, J. D. (1983). Graphical evaluation of blood-to-brain transfer constants from multiple- time uptake data. J.Cereb.Blood Flow Metab, 3, 1-7.
98. Peter, K., Weirich, U., Nordt, T. K., Ruef, J., & Bode, C. (1999). Soluble vascular cell adhesion molecule-1 (VCAM-1) as potential marker of atherosclerosis. Thromb.Haemost., 82 Suppl 1, 38-43.
99. Pitt, B., Mancini, G. B., Ellis, S. G., Rosman, H. S., Park, J. S., & McGovern, M. E. (1995). Pravastatin limitation of atherosclerosis in the coronary arteries (PLAC I): reduction in atherosclerosis progression and clinical events. PLAC I investigation. J.Am.Coll.Cardiol., 26, 1133-1139.
100. Quick, H. H., Debatin, J. F., & Ladd, M. E. (2002). MR imaging of the vessel wall. Eur.Radiol., 12, 889-900.
101. Radomski, M. W., Palmer, R. M., & Moncada, S. (1987). The anti-aggregating properties of vascular endothelium: interactions between prostacyclin and nitric oxide. Br.J.Pharmacol., 92, 639-646.
102. Redberg, R. F., Rifai, N., Gee, L., & Ridker, P. M. (2000). Lack of association of C-reactive protein and coronary calcium by electron beam computed tomography in postmenopausal women: implications for coronary artery disease screening. J.Am.Coll.Cardiol., 36, 39-43.
103. Resnick, N., Yahav, H., Khachigian, L. M., Collins, T., Anderson, K. R., Dewey, F. C., & Gimbrone, M. A., Jr. (1997). Endothelial gene regulation by laminar shear stress. Adv.Exp.Med.Biol., 430, 155-164.
104. Ridker, P. M. (2001). High-sensitivity c-reactive protein : potential adjunct for global risk assessment in the primary prevention of cardiovascular disease. Circulation, 103, 1813-1818.
105. Ridker, P. M., Buring, J. E., & Rifai, N. (2001). Soluble P-selectin and the risk of future cardiovascular events. Circulation, 103, 491-495.
106. Ridker, P. M., Cushman, M., Stampfer, M. J., Tracy, R. P., & Hennekens, C. H. (1997). Inflammation, aspirin, and the risk of cardiovascular disease in apparently healthy men [published erratum appears in N Engl J Med 1997 Jul 31;337(5):356] [see comments]. N.Engl.J.Med., 336, 973-979.
107. Ridker, P. M., Hennekens, C. H., Buring, J. E., & Rifai, N. (2000a). C-reactive protein and other markers of inflammation in the prediction of cardiovascular disease in women. N.Engl.J.Med., 342, 836-843.
108. Ridker, P. M., Hennekens, C. H., Roitman-Johnson, B., Stampfer, M. J., & Allen, J. (1998a). Plasma concentration of soluble intercellular adhesion molecule 1 and risks of future myocardial infarction in apparently healthy men [see comments]. Lancet, 351, 88-92.
109. Ridker, P. M., Rifai, N., Pfeffer, M. A., Sacks, F. M., Moye, L. A., Goldman, S., Flaker, G. C., & Braunwald, E. (1998b). Inflammation, pravastatin, and the risk of coronary events after myocardial infarction in patients with average cholesterol levels. Cholesterol and Recurrent Events (CARE) Investigators. Circulation, 98, 839-844.
110. Ridker, P. M., Rifai, N., Stampfer, M. J., & Hennekens, C. H. (2000b). Plasma concentration of interleukin-6 and the risk of future myocardial infarction among apparently healthy men. Circulation, 101, 1767-1772.

111. Rokitansky, K. (1855). The Organs of Circulation : A Manual of Pathological Anatomy. (Vols. 4) Philadelphia: Blanchard and Lea.
112. Rosenson, R. S. & Tangney, C. C. (1998). Antiatherothrombotic properties of statins: implications for cardiovascular event reduction [see comments]. JAMA, 279, 1643-1650.
113. Ross, R. (1986). The pathogenesis of atherosclerosis--an update. N.Engl.J.Med., 314, 488-500.
114. Ross, R. (1993). The pathogenesis of atherosclerosis: a perspective for the 1990s. Nature, 362, 801-809.
115. Ross, R. (1999). Atherosclerosis--an inflammatory disease. N.Engl.J.Med., 340, 115-126.
116. Ross, R. & Glomset, J. A. (1973). Atherosclerosis and the arterial smooth muscle cell: Proliferation of smooth muscle is a key event in the genesis of the lesions of atherosclerosis. Science, 180, 1332-1339.
117. Ross, R., Wight, T. N., Strandness, E., & Thiele, B. (1984). Human atherosclerosis. I. Cell constitution and characteristics of advanced lesions of the superficial femoral artery. Am.J.Pathol., 114, 79-93.
118. Rumberger, J. A. (2001). Tomographic (plaque) imaging: state of the art. Am.J.Cardiol., 88, 66E-69E.
119. Sacks, F. M., Pfeffer, M. A., Moye, L. A., Rouleau, J. L., Rutherford, J. D., Cole, T. G., Brown, L., Warnica, J. W., Arnold, J. M., Wun, C. C., Davis, B. R., & Braunwald, E. (1996). The effect of pravastatin on coronary events after myocardial infarction in patients with average cholesterol levels. Cholesterol and Recurrent Events Trial investigators [see comments]. N.Engl.J.Med., 335, 1001-1009.
120. Sacks, F. M. & Ridker, P. M. (1999). Lipid lowering and beyond: results from the CARE study on lipoproteins and inflammation. Cholesterol and Recurrent Events. Herz, 24, 51-56.
121. Saito, D., Oka, T., Kajiyama, A., Ohnishi, N., & Shiraki, T. (2002). Factors predicting compensatory vascular remodelling of the carotid artery affected by atherosclerosis. Heart, 87, 136-139.
122. Schmermund, A. & Erbel, R. (2001). Unstable coronary plaque and its relation to coronary calcium. Circulation, 104, 1682-1687.
123. Schmidt, K. C., Lucignani, G., & Sokoloff, L. (1996). Fluorine-18-fluorodeoxyglucose PET to determine regional cerebral glucose utilization: a re-examination. J.Nucl Med., 37, 394-399.
124. Shanahan, C. M., Cary, N. R., Metcalfe, J. C., & Weissberg, P. L. (1994). High expression of genes for calcification-regulating proteins in human atherosclerotic plaques. J.Clin.Invest., 93, 2393-2402.
125. Shanahan, C. M. & Weissberg, P. L. (1998). Smooth muscle cell heterogeneity: patterns of gene expression in vascular smooth muscle cells in vitro and in vivo. Arterioscler.Thromb.Vasc.Biol., 18, 333-338.
126. Shepherd, J., Cobbe, S. M., Ford, I., Isles, C. G., Lorimer, A. R., MacFarlane, P. W., McKillop, J. H., & Packard, C. J. (1995). Prevention of coronary heart disease with pravastatin in men with hypercholesterolemia. West of Scotland Coronary Prevention Study Group [see comments]. N.Engl.J.Med., 333, 1301-1307.

127. Shiomi, M., Ito, T., Tsukada, T., Yata, T., Watanabe, Y., Tsujita, Y., Fukami, M., Fukushige, J., Hosokawa, T., & Tamura, A. (1995). Reduction of serum cholesterol levels alters lesional composition of atherosclerotic plaques. Effect of pravastatin sodium on atherosclerosis in mature WHHL rabbits. *Arterioscler.Thromb.Vasc.Biol.*, 15, 1938-1944.
128. Sparrow, C. P., Burton, C. A., Hernandez, M., Mundt, S., Hassing, H., Patel, S., Rosa, R., Hermanowski-Vosatka, A., Wang, P. R., Zhang, D., Peterson, L., Detmers, P. A., Chao, Y. S., & Wright, S. D. (2001). Simvastatin has anti-inflammatory and antiatherosclerotic activities independent of plasma cholesterol lowering. *Arterioscler.Thromb.Vasc.Biol.*, 21, 115-121.
129. Stefanadis, C., Diamantopoulos, L., Dernellis, J., Economou, E., Tsiamis, E., Toutouzas, K., Vlachopoulos, C., & Toutouzas, P. (2000). Heat production of atherosclerotic plaques and inflammation assessed by the acute phase proteins in acute coronary syndromes. *J.Mol.Cell Cardiol.*, 32, 43-52.
130. Stefanadis, C., Diamantopoulos, L., Vlachopoulos, C., Tsiamis, E., Dernellis, J., Toutouzas, K., Stefanadi, E., & Toutouzas, P. (1999). Thermal heterogeneity within human atherosclerotic coronary arteries detected in vivo: A new method of detection by application of a special thermography catheter. *Circulation*, 99, 1965-1971.
131. Stefanadis, C., Toutouzas, K., Tsiamis, E., Stratos, C., Vavuranakis, M., Kallikazaros, I., Panagiotakos, D., & Toutouzas, P. (2001). Increased local temperature in human coronary atherosclerotic plaques: an independent predictor of clinical outcome in patients undergoing a percutaneous coronary intervention. *J.Am.Coll.Cardiol.*, 37, 1277-1283.
132. Stefanadis, C., Toutouzas, K., Vavuranakis, M., Tsiamis, E., Tousoulis, D., Panagiotakos, D. B., Vaina, S., Pitsavos, C., & Toutouzas, P. (2002). Statin treatment is associated with reduced thermal heterogeneity in human atherosclerotic plaques. *Eur.Heart J.*, 23, 1664-1669.
133. Stroes, E. S., Koomans, H. A., de Bruin, T. W., & Rabelink, T. J. (1995). Vascular function in the forearm of hypercholesterolaemic patients off and on lipid-lowering medication. *Lancet*, 346, 467-471.
134. Sukhova, G. K., Schonbeck, U., Rabkin, E., Schoen, F. J., Poole, A. R., Billingham, R. C., & Libby, P. (1999). Evidence for increased collagenolysis by interstitial collagenases-1 and -3 in vulnerable human atheromatous plaques. *Circulation*, 99, 2503-2509.
135. Svindland, A. & Torvik, A. (1988). Atherosclerotic carotid disease in asymptomatic individuals: An histological study of 53 cases. *Acta Neurol.Scand.*, 78, 506-517.
136. Tontonoz, P., Nagy, L., Alvarez, J. G., Thomazy, V. A., & Evans, R. M. (1998). PPARgamma promotes monocyte/macrophage differentiation and uptake of oxidized LDL. *Cell*, 93, 241-252.
137. Topper, J. N., Cai, J., Falb, D., & Gimbrone, M. A., Jr. (1996). Identification of vascular endothelial genes differentially responsive to fluid mechanical stimuli: cyclooxygenase-2, manganese superoxide dismutase, and endothelial cell nitric oxide synthase are selectively up-regulated by steady laminar shear stress. *Proc.Natl.Acad.Sci.U.S.A.*, 93, 10417-10422.
138. Treasure, C. B., Klein, J. L., Weintraub, W. S., Talley, J. D., Stillabower, M. E., Kosinski, A. S., Zhang, J., Bocuzzi, S. J., Cedarholm, J. C., & Alexander, R. W. (1995). Beneficial effects of cholesterol-lowering therapy on the coronary endothelium in patients with coronary artery disease [see comments]. *N.Engl.J.Med.*, 332, 481-487.
139. Tsao, P. S., Buitrago, R., Chan, J. R., & Cooke, J. P. (1996). Fluid flow inhibits endothelial adhesiveness. Nitric oxide and transcriptional regulation of VCAM-1. *Circulation*, 94, 1682-1689.

140. Tsao, P. S., Wang, B., Buitrago, R., Shyy, J. Y., & Cooke, J. P. (1997). Nitric oxide regulates monocyte chemotactic protein-1. Circulation, *96*, 934-940.
141. Vallabhajosula, S. & Fuster, V. (1997). Atherosclerosis: imaging techniques and the evolving role of nuclear medicine. J.Nucl.Med., *38*, 1788-1796.
142. Vallabhajosula, S., Machac, J., Knesaurek, K., Telsey, J., Lipszyc, H., Bastidas, D. A., Zhao, Q. H., & Buschbaum, M. S. (1996). Imaging atherosclerosis macrophage density by positron emission tomography using F-18-Fluorodeoxyglucose (FDG). J.Nucl.Med., *37*, 38P.
143. van der Wal, A. C., Becker, A. E., van der Loos, C. M., & Das, P. K. (1994). Site of intimal rupture or erosion of thrombosed coronary atherosclerotic plaques is characterized by an inflammatory process irrespective of the dominant plaque morphology. Circulation, *89*, 36-44.
144. Verheye, S., De Meyer, G. R., Van Langenhove, G., Knaapen, M. W., & Kockx, M. M. (2002). In vivo temperature heterogeneity of atherosclerotic plaques is determined by plaque composition. Circulation, *105*, 1596-1601.
145. Virchow (1858). Cellular Pathology. London: John Churchill.
146. Wahl, R. L., Henry, C. A., & Ethier, S. P. (1992). Serum glucose: effects on tumor and normal tissue accumulation of 2-[F- 18]-fluoro-2-deoxy-D-glucose in rodents with mammary carcinoma. Radiology, *183*, 643-647.
147. Wald, N. J., Law, M. R., Morris, J. K., Zhou, X., Wong, Y., & Ward, M. E. (2000). Chlamydia pneumoniae infection and mortality from ischaemic heart disease: large prospective study [see comments]. BMJ, *321*, 204-207.
148. Warburg, O. (1930). The Metabolism of Tumours. In (pp. 129-169). London: Constable.
149. Warburg, O. (1956). On the origin of cancer cells. Science, *123*, 309-314.
150. Warlow, C. P., Dennis, M. S., van Gijn, J., Hankey, G., Sandercock, P. A. G., Bamford, J., & Wardlaw, J. (1996). Stroke: A practical guide to management. Oxford, UK: Blackwell Scientific.
151. Warner, S. J., Friedman, G. B., & Libby, P. (1989). Immune interferon inhibits proliferation and induces 2'-5'- oligoadenylate synthetase gene expression in human vascular smooth muscle cells. J.Clin.Invest, *83*, 1174-1182.
152. Wilcox, J. N., Smith, K. M., Williams, L. T., Schwartz, S. M., & Gordon, D. (1988). Platelet-derived growth factor mRNA detection in human atherosclerotic plaques by in situ hybridization. J.Clin.Invest, *82*, 1134-1143.
153. Williams, J. K., Sukhova, G. K., Herrington, D. M., & Libby, P. (1998). Pravastatin has cholesterol-lowering independent effects on the artery wall of atherosclerotic monkeys. J.Am.Coll.Cardiol., *31*, 684-691.
154. Williams, S. B., Cusco, J. A., Roddy, M. A., Johnstone, M. T., & Creager, M. A. (1996). Impaired nitric oxide-mediated vasodilation in patients with non- insulin-dependent diabetes mellitus. J.Am.Coll.Cardiol., *27*, 567-574.
155. Wilson, P. W., Castelli, W. P., & Kannel, W. B. (1987). Coronary risk prediction in adults (the Framingham Heart Study). Am.J.Cardiol., *59*, 91G-94G.

156. Wong, N. D., Wilson, P. W., & Kannel, W. B. (1991). Serum cholesterol as a prognostic factor after myocardial infarction: the Framingham Study. Ann.Intern.Med., 115, 687-693.
157. Worthley, S. G., Helft, G., Fuster, V., Zaman, A. G., Fayad, Z. A., Fallon, J. T., & Badimon, J. J. (2000). Serial in vivo MRI documents arterial remodeling in experimental atherosclerosis. Circulation, 101, 586-589.
158. Xia, P., Vadas, M. A., Rye, K. A., Barter, P. J., & Gamble, J. R. (1999). High density lipoproteins (HDL) interrupt the sphingosine kinase signaling pathway. A possible mechanism for protection against atherosclerosis by HDL. J.Biol.Chem., 274, 33143-33147.
159. Yamada, S., Kubota, K., Kubota, R., Ido, T., & Tamahashi, N. (1995). High accumulation of fluorine-18-fluorodeoxyglucose in turpentine- induced inflammatory tissue. J.Nucl.Med., 36, 1301-1306.
160. Ye, S., Eriksson, P., Hamsten, A., Kurkinen, M., Humphries, S. E., & Henney, A. M. (1996). Progression of coronary atherosclerosis is associated with a common genetic variant of the human stromelysin-1 promoter which results in reduced gene expression. J.Biol.Chem., 271, 13055-13060.
161. Yuan, C., Beach, K. W., Smith, L. H., Jr., & Hatsukami, T. S. (1998). Measurement of atherosclerotic carotid plaque size in vivo using high resolution magnetic resonance imaging. Circulation, 98, 2666-2671.
162. Yuan, C., Kerwin, W. S., Ferguson, M. S., Polissar, N., Zhang, S., Cai, J., & Hatsukami, T. S. (2002a). Contrast-enhanced high resolution MRI for atherosclerotic carotid artery tissue characterization. J.Magn Reson.Imaging, 15, 62-67.
163. Yuan, C., Mitsumori, L. M., Beach, K. W., & Maravilla, K. R. (2001). Carotid atherosclerotic plaque: noninvasive MR characterization and identification of vulnerable lesions. Radiology, 221, 285-299.
164. Yuan, C., Zhang, S. X., Polissar, N. L., Echelard, D., Ortiz, G., Davis, J. W., Ellington, E., Ferguson, M. S., & Hatsukami, T. S. (2002b). Identification of fibrous cap rupture with magnetic resonance imaging is highly associated with recent transient ischemic attack or stroke. Circulation, 105, 181-185.
165. Yusuf, S., Sleight, P., Pogue, J., Bosch, J., Davies, R., & Dagenais, G. (2000). Effects of an angiotensin-converting-enzyme inhibitor, ramipril, on cardiovascular events in high-risk patients. The Heart Outcomes Prevention Evaluation Study Investigators [see comments] [published errata appear in N Engl J Med 2000 Mar 9;342(10):748 and 2000 May 4;342(18):1376]. N.Engl.J.Med., 342, 145-153.
166. Zaman, A. G., Helft, G., Worthley, S. G., & Badimon, J. J. (2000). The role of plaque rupture and thrombosis in coronary artery disease [In Process Citation]. Atherosclerosis, 149, 251-266.
167. Zhao, X. Q., Yuan, C., Hatsukami, T. S., Frechette, E. H., Kang, X. J., Maravilla, K. R., & Brown, B. G. (2001). Effects of prolonged intensive lipid-lowering therapy on the characteristics of carotid atherosclerotic plaques in vivo by MRI: a case-control study. Arterioscler.Thromb.Vasc.Biol., 21, 1623-1629.

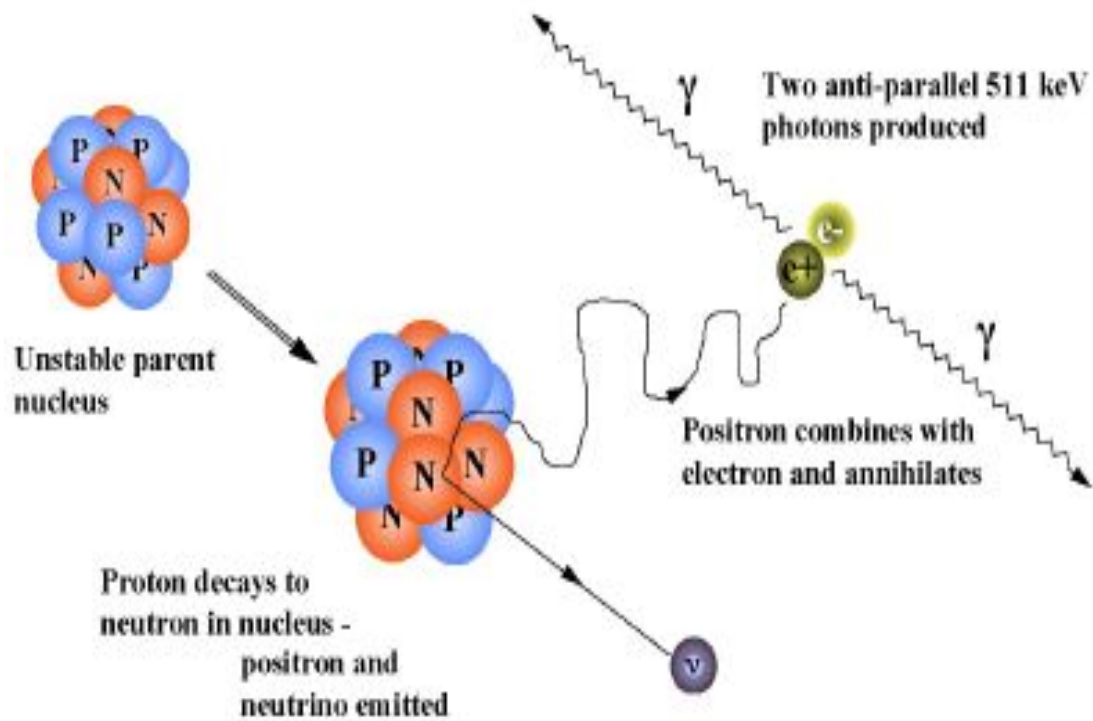


Figure 1.1 The process of positron emission
 p=proton, n=neutron, v=neutrino, e=electron

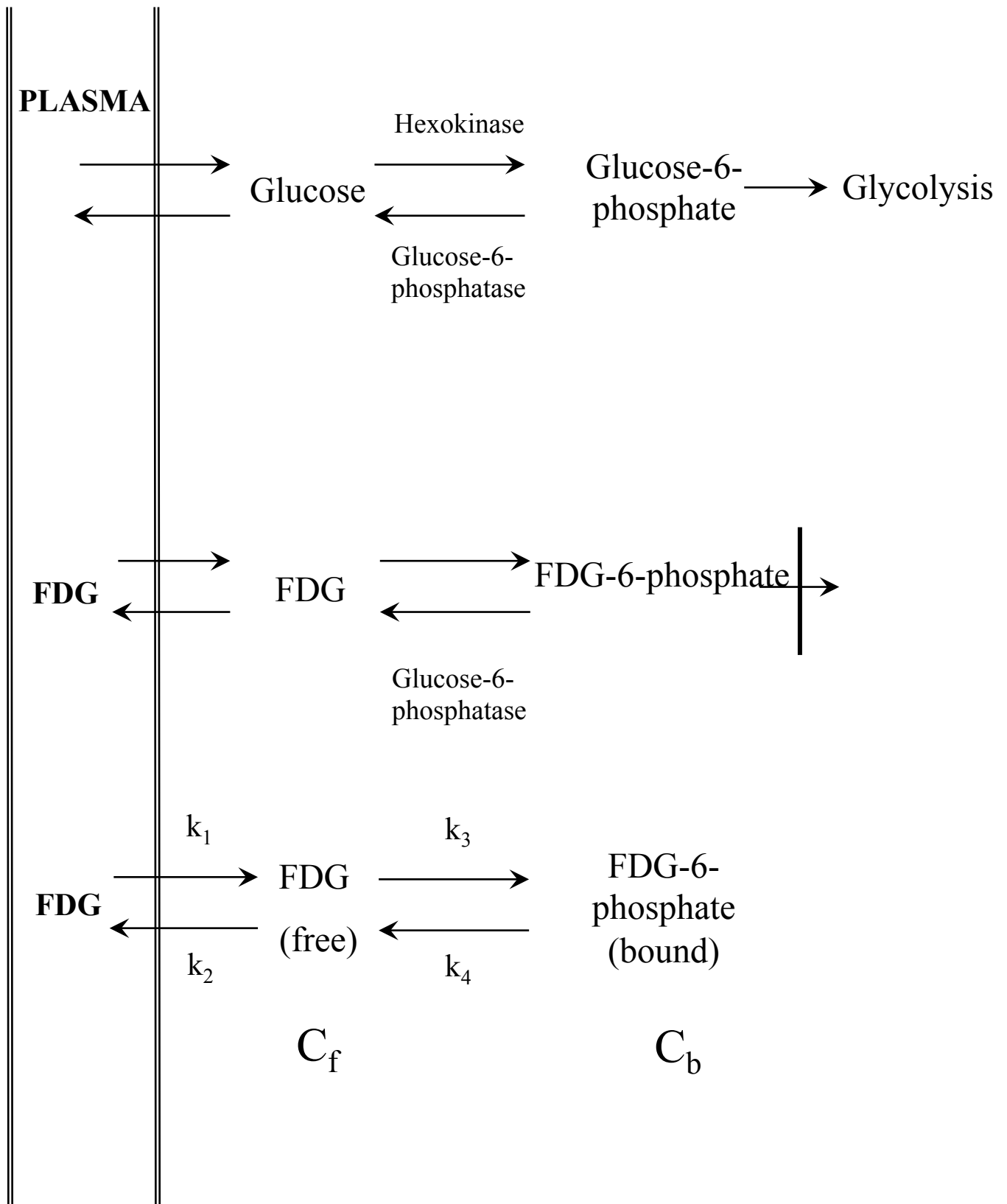


Figure 1.2 The metabolic pathway of FDG

Full explanation is given in Sections 1.5.5 and 1.5.6.3.1

Chapter 2

CHAPTER 2

MATERIALS AND METHODS

2.1 MATERIALS

2.1.1 General laboratory reagents

2-[¹⁸ F]fluoro-2-deoxy-D-glucose	Cyclotron, WBIC
2-Deoxy-D-[1- ³ H]glucose	Amersham
Acetone	BDH
Amphotericin B	Sigma
Bovine serum albumin	Sigma
Dimethylsulphoxide	Sigma
Ethylene diamine tetra-acetic acid	Sigma
Fluorescent mount medium	Dako
Foetal calf serum	Sigma
Histopaque-1077	Sigma
Hoerscht nuclear stain	Sigma
Hydrogen peroxide	Sigma
Interferon- γ	Sigma
Iodoacetic acid	Sigma
L-glutamine	Sigma
Lipopolysaccharide E Coli Serotype 026:86 (TCA extract)	Sigma
Lipoprotein-deficient serum	Sigma
Liquid scintillation fluid (Ultima Gold XR)	Packard
Low density lipoprotein, oxidised and native	Sigma
Medium 199	Sigma
Methanol	BDH
Niopam 300	Merck
Paraformaldehyde	BDH
Penicillin	Sigma

Phorbol myristate acetate	Sigma
Phosphate-buffered saline tablets	Oxoid
Polysucrose/sodium diatrizoate (Ficoll-Hypaque)	Sigma
Soluene 350	Packard
Streptomycin	Sigma
Trypan blue	Sigma
Tumour Necrosis Factor-Alpha	Sigma
Xylene	BDH

2.1.2 Materials for imaging experiments

Alphaxalone/alphadolone (Saffan)	Schering-Plough
Cholesterol-enriched (0.2%) rabbit diet	SDS
Fiducial markers	Intermark
Fogarty balloon embolectomy catheters	Baxter
Iopamidol	Merck
Isoflurane	Rhodia Organique
New Zealand White rabbits (female)	Charles River
Pentobarbitone (Euthatal)	Rhone Merieux
Papaverine	Rhone Merieux
Standard rabbit diet	SDS
Sutures (ethilon/vicryl)	NHS supplies

2.2 GENERAL STOCK SOLUTIONS

Phosphate-buffered saline

10 PBS tablets in 1L H₂O

Ethylenediamine tetra-acetic acid

For 0.5M solution, 93.05g Na₂EDTA.2H₂O dissolved in 350ml H₂O (dissolved in fume cupboard); pH adjusted to 8.0; made up to 500ml in H₂O.

Blocking buffer for immunocytochemistry

3% (w/v) Bovine serum albumin made up in PBS

Destain solution for immunohistochemistry

250ml methanol, 4ml 1M HCl, made up to 500ml in H₂O.

Scott's blueing solution

10g MgSO₄, 1g NaHCO₃ in 500ml H₂O.

Tris-buffered saline

For 10x stock solution: 87.66g NaCl, 12.11g Tris base in 800ml H₂O; pH adjusted to 8.0, made up to 1l in H₂O.

2.3 EXPERIMENTAL METHODS

Except for methods relating to histological analysis of tissue, which are described below, the methods used for the work in each individual chapter will be described there. This is because there are only a few methods that are common to more than one chapter.

2.3.1 Histology protocols

Tissues were paraffin-embedded, sectioned and mounted on slides by Mrs N Figg in the University of Cambridge Department of Cardiovascular Medicine

2.3.1.1 Anti-smooth muscle cell immunochemistry for animal studies

Slides were deparaffinised in xylene (twice for 10 minutes), then hydrated by passing through graded alcohols (100%, 90% and 70% ethanol for 3 minutes each) into distilled water (5 minutes). They were then heated in a microwave with citrate buffer pH6 twice for 5 minutes. After cooling by placing under running tap water for 10 minutes, slides were equilibrated in PBS for 5 minutes. To abolish endogenous peroxidase activity, slides were incubated for 10 minutes in 0.3 % (v/v) hydrogen peroxide in methanol, and were then washed for 5 minutes in running water and twice for 5 minutes in PBS. The slides were then blocked by incubation with 5% horse serum in PBS for 30 minutes at room temperature. The blocking buffer was drained off and a solution of primary antibody was applied for 1 hour (Alpha smooth muscle

actin clone 1A4, M0851, Dako, UK). The antibody was used at a concentration of 1:50 (v/v) in 5% horse serum in PBS. This antibody is a murine monoclonal antibody. The slides were then washed twice for 5 minutes in PBS, and secondary antibody solution (biotinylated rabbit anti-mouse antibody [Vector], 1/400 [v/v] in PBS) was applied for 30 minutes. After a further 2 washes in PBS, sections were incubated in Avidin-Biotin Complex (Vector) for 30 minutes, and washed twice more with PBS. Diaminobenzidine (Sigma) was then applied for 1-5 minutes, the progress of the reaction being assessed through the microscope. The slides were washed in running tap water for 5 minutes and counterstained with Harris's Haematoxylin (Sigma) for 5 minutes, washed again in water for 5 minutes and dehydrated by reversing the rehydration regime described above. Coverslips were then applied.

2.3.1.2 Anti-macrophage immunochemistry for animal studies

Slides were deparaffinised in xylene (twice for 10 minutes), then hydrated by passing through graded alcohols (100%, 90% and 70% ethanol for 3 minutes each) into distilled water (5 minutes). They were then heated in a microwave with citrate buffer (pH6) twice for 10 minutes. They were cooled for 20 minutes under running tap water and then washed in milli-Q water for a further 5 minutes. They were washed next in tris-buffered saline (TBS) for 5 minutes (pH 7.4-7.6). To abolish endogenous peroxidase activity, slides were incubated for 15 minutes in 3% (v/v) hydrogen peroxide in TBS at room temperature, and were then washed twice for 5 minutes in TBS. The slides were then blocked by incubation with horse serum diluted 1:5 in TBS for 30 minutes at room temperature. The excess serum was wiped away, and the slides were incubated with the primary antibody (RAM 11, M0633, Dako, UK) diluted 1:50 (v/v) in TBS for 30 minutes. They were then washed twice in TBS for 5 minutes, and incubated with biotinylated secondary goat anti-mouse antibody for 30 minutes (Dako Duet Kit K0492), and washed again in TBS twice for 5 minutes. The slides were then incubated for 30 minutes with ABCComplex/HRP (Dako Duet Kit), and washed twice for 5 minutes in TBS. They were then incubated with DAB working solution (Vector SK4100), the progress of the reaction being monitored under a microscope. Finally they were washed in milli-Q water for 5 minutes and then counterstained with haematoxylin for 20 seconds and washed in tap water for 5 minutes. They were then

dehydrated through graded alcohols, cleared in xylene and mounted in DPX. Coverslips were then applied.

2.3.1.3 Anti-macrophage and smooth muscle cell immunochemistry for human studies

Slides were deparaffinised in xylene (twice for 10 minutes), then hydrated by passing through graded alcohols (100%, 90% and 70% ethanol for 3 minutes each) into distilled water (5 minutes). They were then heated in a microwave with citrate buffer (pH6) twice for 5 minutes. After cooling by placing under running tap water for 10 minutes, slides were equilibrated in PBS for 5 minutes. To abolish endogenous peroxidase activity, slides were incubated for 10 minutes in 0.3 % (v/v) hydrogen peroxide in methanol, and were then washed for 5 minutes in running water and twice for 5 minutes in PBS. Slides were then incubated in normal serum for 10 minutes. The serum was then drained from the sections and they were incubated in Dako mouse anti-human CD68 antibody (M0876 clone PG-M1) at a concentration of 1:100 (v/v) for 1 hour. After washing 3 times for 5 minutes in PBS, secondary antibody was applied for 30 minutes and again the slides were washed 3 times for 5 minutes each in PBS. Slides were incubated with Avidin-Biotin Complex (Vector) for 30 minutes and finally washed 3 times for 5 minutes each with PBS. DAB chromogen with Nickel enhancement (Vector) was applied for 5 minutes, after which the sections were well rinsed in running tap water. They were incubated with 0.01% avidin for 10 minutes, washed 3 times for 5 minutes in PBS, and then incubated with 0.001% biotin for 10 minutes. After another 3 x 5 minute washes with PBS, mouse anti-human smooth muscle antibody (Dako M0851 clone 1A4) was applied at a concentration of 1:50 (v/v) for 30 minutes. Slides were then washed again in PBS, 3 times for 5 minutes, and incubated with Dako envision Polymer secondary antibody (catalogue number 4006) for 30 minutes, following which they were washed again for 5 minutes in PBS 3 times. NovaRed chromogen (Vector SK4800) was applied for 5 minutes, and the slides were counterstained with Carazzi's haematoxylin for 1 minute. They were washed again in water for 5 minutes and dehydrated by reversing the rehydration regime described above. Coverslips were then applied.

2.3.2 Haematoxylin and eosin staining

Sections were deparaffinised in xylene (twice for 10 minutes), then hydrated by passing through graded alcohols (100%, 90% and 70% methanol for 5 minutes each) into distilled water (5 minutes). Slides were immersed in Harris's Haematoxylin solution (Sigma) for 5 minutes, then placed in destain solution for 15 seconds. The slides were then immersed in Scott's solution for 5 minutes, followed by immersion in Eosin (Sigma) for 3 minutes. They were rinsed briefly in distilled water and then rapidly dehydrated by reversing the rehydration regime above. Finally, coverslips were applied.

2.4 STATISTICAL ANALYSIS

Decisions concerning the statistical methods used in this work were taken after discussion with Dr Chris Palmer and Mrs Barbara Arch, statisticians at the Centre for Applied Medical Statistics, University of Cambridge.

Results are expressed as mean \pm standard error of the mean (SEM) with 95% confidence intervals in brackets where appropriate (95% CI). Error bars on graphs represent SEM. Statistical significance at the 5% level is expressed graphically by the symbol '*'.

The unpaired two-tailed t-test was used to compare uptake of HDG in monocytes and macrophages under different conditions in Chapter 3.

Pearson's r-test was used to investigate correlations between FDG uptake and cell type in the *in-vitro* work described in Chapter 4. P values were generated from Pearson's r-test using hypothesis testing (Altman, 1991).

The paired two-tailed t-test was used to compare FDG accumulation in symptomatic and asymptomatic plaques in the human studies described in Chapter 5.

Paired and unpaired two-tailed t-tests were used as appropriate in Chapter 6 to compare cholesterol levels and aortic FDG uptake between different groups of animals.

2.5 REFERENCES

1. Altman, D. G. (1991). Practical Statistics For Medical Research. London: Chapman and Hall.

Chapter 3

CHAPTER 3

THE CHARACTERISTICS OF HDG UPTAKE IN A MONOCYTE CELL LINE (THP-1) AND IN HUMAN MACROPHAGES IN CULTURE

3.1 INTRODUCTION

The primary objective of the research described in this chapter was to test the hypothesis that tritiated deoxyglucose (HDG) - an *in-vitro* analogue of fluorodeoxyglucose (d'Argy et al., 1988) (Kubota et al., 1992)- would accumulate in proportion to cellular metabolic activity. The hypothesis was examined in two populations of cells; an immortalised monocyte cell line (THP-1), and freshly isolated human monocytes that were allowed to differentiate into macrophages in culture. These cell populations were chosen because their metabolic activity can be easily manipulated to ascertain if HDG uptake varies. These experiments form a basis for the work undertaken in the following chapters, which address the measurement of FDG uptake into freshly resected human atherosclerotic plaque *in vitro*, human carotid plaque *in vivo*, and experimental atherosclerosis in a rabbit model.

As highlighted in Chapter 1, monocytes (which differentiate into macrophages once they have left the bloodstream and entered the plaque) play a crucial role in plaque rupture. Plaques containing a high proportion of activated macrophages in relation to vascular smooth muscle cells have the greatest risk of rupture. This is because macrophages within plaque are responsible for the production of toxic cytokines and matrix metalloproteinases, and the induction of smooth muscle cell apoptosis (Davies, 1996) which both lead to fibrous cap weakening. As a first step towards imaging atherosclerosis, it was postulated that this high metabolic activity seen in plaque macrophages might be reflected in measurable accumulation of HDG in cultured cells.

Inflammatory cells, such as macrophages and neutrophils, like tumour cells, predominantly metabolise glucose. When stimulated, they can increase the expression

of transporter proteins that facilitate the movement of glucose into the cell (Gamelli et al., 1996) to support the greater energy required in the activated state (Hagi et al., 2000; Chakrabarti et al., 1994; Fukuzumi et al., 1996). Macrophages mainly express glucose transporter protein 1 (GLUT 1), the levels of which are increased substantially after stimulation with lipopolysaccharide (LPS), either alone or in combination with TNF- α (Fukuzumi et al., 1996; Gamelli et al., 1996), to allow increased glucose entry into the cells. Also present on human macrophages is GLUT 3, which is expressed at higher levels on the cell surface after the respiratory burst (Ahmed et al., 1997). Human macrophages do not, however, express the insulin-sensitive GLUT 4 transporter subtype (Daneman et al., 1992; Estrada et al., 1994), whose mRNA is increased after insulin challenge.

In this chapter, the uptake of HDG in two similar cell populations was examined. Initially, the immortalised monocyte THP-1 cell line was used, because it provided a plentiful source of monocytes without the need for lengthy and expensive extraction of monocytes from either buffy coats or peripheral blood. This cell line was originally derived from a 1 year old patient with acute monocytic leukaemia (Tsuchiya et al., 1980). The cells are morphologically and functionally similar to non-immortalised human monocytes, in that they express Fc and c3b receptors, contain lysosomes and are capable of phagocytosis (Tsuchiya et al., 1980). The cells can be differentiated in culture to a macrophage-like phenotype by treatment with the protein kinase C activator phorbol myristate acetate (PMA), resulting in a loss of proliferation, adherence to cultureware, phagocytosis of latex beads and expression of the surface markers CD14 and CD11b. (Schwende et al., 1996a; Asseffa et al., 1993a; Akuzawa et al., 2000a).

Subsequently, the uptake of HDG in human macrophages was evaluated. These cells were isolated as monocytes from buffy coats, and then differentiated to macrophages over the course of seven days in culture (Boyle et al., 2001; Gordon et al., 1995).

Finally, both THP-1 cells and macrophages were treated with cellular activators, and the effect of these interventions on HDG uptake was assessed.

3.2 METHODS

3.2.1 General cell culture techniques

Human peripheral blood-derived monocytes and macrophages were grown in Medium 199 (M199), supplemented with 100IU/ml penicillin, 100µg/ml streptomycin, 250µg/ml amphotericin B and 4mmol/l L-glutamine. THP-1 cells were grown under identical conditions, except they did not receive amphotericin supplements. Culture medium for all cells was enriched with 20% foetal calf serum (FCS). Cells were maintained in 5% CO₂ at 37°C in a humidified incubator. All manipulations of live cells were performed in a Class II laminar flow hood. Cells were counted using a haemocytometer (Neubater). All cells contained within four grids were counted, and the density of the cell suspension was determined from the formula:

$$\text{Number of cells / ml} = \frac{(\text{Total cell number in 4 grids})}{4 \times 10^4}$$

Cell viability was assessed using trypan blue incubation as follows - cells were stained in filter-sterilised 0.2% trypan blue in PBS for 5 minutes, washed in PBS and then counted on a haemocytometer. Cell viability was calculated as the number of cells that excluded trypan blue as a proportion of the total cell number.

3.2.2 Culture of THP-1 cells

THP-1 cells were purchased from the European Collection of Cell Cultures. Cells were grown in suspension, in Corning T75 tissue culture flasks containing 50 mls medium. The medium was changed and the cells were split every 3 days. Cells were maintained in culture at a density of approximately 5×10^5 cells/ml.

3.2.3 Isolation of peripheral blood-derived mononuclear cells

Fresh buffy coats, rich in leukocytes, were obtained from the National Blood Transfusion Service. Human peripheral blood mononuclear cells were isolated from them using established methods (Boyle et al., 2001; Geng et al., 1992a). Aliquots of 35 mls of buffy coat were spun through 15mls of polysucrose/sodium diatrizoate mixture in a Sorvall centrifuge at 2500 rpm for 35 minutes. The interface between plasma and hypaque was removed. Microscopic examination of this layer confirmed that it consisted of human peripheral blood mononuclear cells (PBMC), mainly monocytes and lymphocytes, with some platelets and red cells. The PBMCs were washed in 110%PBS / 0.5mM EDTA during two further 5 minute centrifuge spins at 1400 rpm to remove platelet and red cell contamination.

3.2.4 Purification of monocyte fraction

The purification method used relies on the fact that monocytes adhere more quickly and more firmly to plastic culture wells than lymphocytes. PBMCs were counted, and 1ml aliquots containing 2×10^6 cells were pipetted into plastic 24-well tissue culture plates (Lab-Tek) and incubated at 37°C for 45 minutes. The wells were then washed twice with M199 to remove the non-adherent lymphocytes. Finally, 1 ml M199 was added to each well and the cells were cultured for 7 days. This time period allows the monocytes to differentiate into macrophages (Boyle et al., 2001). The cells obtained after the purification steps were shown to be highly pure monocytes by immunocytochemistry (see below), with a viability of approximately 95% by trypan blue assay.

3.2.5 Immunocytochemical characterisation of monocytes

PBMCs were isolated from buffy coats as in Section 3.2.3. The cells were seeded in 8-well plates (Lab-Tek) at a density of 0.2×10^7 cells per well in 0.2 mls M199. Monocytes were purified from PBMCs as in Section 3.2.4. After 24 hours in culture, each well was washed twice with PBS for 5 minutes. A 200 μ L aliquot of chilled acetone (4°C) was added to each well for 10 minutes as a cellular fixative. The wells were then washed again with PBS twice for 5 minutes. Blocking buffer was added for 60 minutes to block non-specific antibody binding.

Cells were then incubated in darkness with primary antibody for 60 minutes (FITC-labelled mouse IgG2a kappa anti-human CD14 monocyte (Dako)), diluted in blocking buffer at 1:10 (v/v). Appropriate negative control antibody was used at the same concentration (FITC-labelled mouse IgG2a (Dako)). After one hour the wells were washed three times with PBS for 5 minutes. Hoerscht (50µg/ml) was then added to each well as a nuclear counterstain, 100µL per well. The plastic dividers between the wells were removed, fluorescent mount medium was added, and coverslips applied (BDH). The coverslips were sealed with nail varnish (Estee Lauder). Plates were stored in darkness at 4°C overnight, and then examined using fluorescence microscopy the following day.

3.2.6 Analysis of HDG uptake over time in THP-1 cells

Approximately one million THP-1 cells in a volume of 900µL M199 were placed into eppendorf tubes (1.5 ml). 1 microcurie of HDG in 100µL M199 was added to each tube and the eppendorfs were incubated at 37°C. To assess the degree of HDG uptake at different times, eppendorfs were batched into groups of three, and iodoacetic acid (10µL of 1mM solution) was added to halt HDG uptake to one set of tubes after 10 minutes, another after 30 minutes, another after 60 minutes and finally the last set of three tubes was halted after 120 minutes. Iodoacetic acid is a potent glycolytic pathway inhibitor which acts on the enzyme glyceraldehyde-3-phosphate dehydrogenase (Rego et al., 1999). It has been shown to inhibit HDG uptake via the glucose transporter proteins (Waki et al., 1997). As controls, one eppendorf in each group was treated with iodoacetic acid at time = 0. Eppendorfs were then centrifuged in a benchtop centrifuge (MSE) at 13000rpm for 5 minutes to pellet the cells. 500µL of supernatant was removed from each eppendorf, added to 3mls of liquid scintillation fluid, and counted in a Packard Tricarb liquid scintillation counter.

The cell pellet was washed three times with PBS and resuspended in 1 ml volume. It was then dissolved overnight in Soluene 350 at room temperature (this solvent is a mixture of toluene and ammonium hydroxide that dissolves cell membranes, allowing efficient mixing of dissolved cells and scintillation fluid to ensure accurate counting).

After 12 hours, 3mls of liquid scintillation fluid was added to the dissolved cell suspension, the mixture placed in scintillation vials and counted in the scintillation counter.

3.2.7 Analysis of HDG uptake over time in human macrophages

A similar protocol was used to that described for THP-1 cells above. The main differences occur because macrophages in culture are adherent to plastic cultureware. Therefore, after incubation with HDG has been completed, cells have to be removed from the plastic wells with a dilute EDTA washing step.

Human monocytes were isolated and purified as described in Sections 3.2.3 and 3.2.4. They were seeded in 24-well plates at a density of approximately 1×10^6 cells per well. The cells were cultured for 7 days to allow differentiation to macrophages (Boyle et al., 2001). Then, HDG (1 μ Ci) was added to each well at time = 0. The experiment was performed with n = 3 for each timepoint. Uptake of HDG was halted by the addition of 10 μ L iodoacetic acid per well at predetermined timepoints. 500 μ L of fluid was then pipetted from each well, added to 3mls of liquid scintillation fluid, and counted in a Packard Tricarb liquid scintillation counter. Adherent macrophages were removed from the wells by vigorous pipetting with ice-cold 110% PBS / 0.5mM EDTA solution, and transferred to eppendorfs. Inspection of the 24 well plates with a phase contrast microscope confirmed that adherent cells had been removed. The cells were then counted, pelleted, washed with PBS and dissolved overnight in Soluene 350, in an identical manner to the THP-1 cells. After 12 hours, 3mls of liquid scintillation fluid was added to the cell suspension, the mixture placed in scintillation vials and counted in the scintillation counter.

3.2.8 Analysis of HDG uptake in THP-1 cells after stimulation with PMA

One million cells were incubated with 0.1 μ L PMA (1mg/ml) in eppendorf tubes. Controls were treated with PBS. After 18 hours of incubation, HDG uptake was assessed by adding 1 μ Ci HDG per tube, and incubating at 37°C for one hour. HDG accumulation was halted after this time by the addition of 10 μ L iodoacetic acid per

tube. Cells were then spun down, washed and scintillation counted as in Section 3.2.6. Experiments were performed in triplicate.

3.2.9 Analysis of HDG uptake in human macrophages after activation with various agonists

Human monocytes were isolated and purified as described in Sections 3.2.3 and 3.2.4. They were cultured in 24-well plates at a density of approximately 1×10^6 cells per well. The cells were cultured for 7 days to allow differentiation to macrophages (Boyle et al., 2001). Cellular agonists were then added, at different concentrations and times, as described in the Results section (3.3.7). After agonist treatment, HDG uptake at 60 minutes was assessed by adding $1\mu\text{Ci}$ HDG per well, stopping uptake after 60 minutes with $10\mu\text{L}$ iodoacetic acid and then removing adherent macrophages by vigorous pipetting with 110% PBS / 0.5mM EDTA. Cells were subsequently dissolved and scintillation counted as in Section 3.2.7. Each agonist experiment was performed in triplicate.

3.3 RESULTS

3.3.1 Visual morphology of THP-1 cells in culture

Figures 3.1 and 3.2 show THP-1 cells photographed in culture. The cells in Figure 3.1 are unstimulated, whereas those in Figure 3.2 have been differentiated towards a macrophage-like phenotype by stimulation for 48 hours with the phorbol ester, PMA. The cells have changed from having a rounded shape in Figure 3.1, to a spindle-like appearance in Figure 3.2, which is characteristic of macrophages in culture. Also seen is the emergence of dendritic processes from some macrophages in Figure 3.2..

3.3.2 Visual morphology of monocyte/macrophage cells in culture

Figures 3.3 and 3.4 chart the morphological changes that occur as monocytes differentiate into macrophages over time in culture. Figure 3.3 shows the appearance of freshly isolated monocytes, photographed on Day 1. Figure 3.4 shows the same cells after 5 days in culture on glass. On Day 1, the cells are rounded monocytes, similar to the THP-1 cells before differentiation. After 5 days, some of the cells have taken on an altered appearance and adopted the spindle shapes and cytoplasmic processes characteristic of macrophages.

3.3.3 Immunocytochemical characterisation of monocytes

Cells isolated from buffy coats were stained with a FITC-labelled primary antibody against CD14, a monocyte lineage marker. Nuclear counterstaining was performed by means of Hoerscht staining. Over 95% cells examined expressed CD14 (Figure 3.5), indicating a relatively pure fraction of monocytes that would differentiate into macrophages.

3.3.4 Analysis of HDG uptake over time in THP-1 cells

The results are shown in Figure 3.6. The results from 3 experiments are combined, with each timepoint measured in triplicate, therefore, $n = 9$ for each timepoint. The lower line shows cells that have been pre-treated with iodoacetic acid (IAA), which switches off the glycolytic pathway, meaning that the cells take up very little HDG and can act as a negative control. The cellular uptake of HDG is expressed as percentage uptake per million cells, divided by the activity remaining in the supernatant from those cells, i.e.:

Decays per minute (DPM) per million cells / DPM in supernatant per million cells

This method of expressing HDG uptake is analogous to the method of quantitative regional analysis of PET data. For example in Chapter 5, tissue/plasma FDG uptake ratios are employed to calculate the degree of FDG uptake into the vessel wall.

The graph shows an increase in cellular HDG concentration over time. After 60 minutes, HDG uptake was 0.47% (± 0.05) in the THP-1 cells, compared to 0.16% (± 0.01) in the control group, $p=0.003$. By 120 minutes, the gap had widened, with an uptake of 1.13% (± 0.17) versus 0.23% (± 0.03) respectively, $p=0.005$.

3.3.5 Effect of PMA stimulation on HDG uptake in THP-1 cells

The results are shown in Figure 3.7. It can be seen that the treatment of THP-1 cells with PMA causes a statistically significant increase in HDG uptake after one hour, compared to undifferentiated control cells treated with PBS (1.14% (± 0.04) vs 0.31% (± 0.03)), $p=0.005$.

3.3.6 Analysis of HDG uptake over time in macrophages

The results are shown in Figure 3.8. The uptake of HDG was examined in Day 7 macrophages and in control cells that had been incubated with IAA. It can be seen that HDG accumulates within macrophages in a time-dependent manner similar to that seen in THP-1 cells. There were significant differences between macrophages and

controls after 60 minutes (5.04% (\pm 0.47) vs 0.32% (\pm 0.03)), **p=0.001** and 90 minutes (7.25% (\pm 0.92) vs 0.34% (\pm 0.03)), **p=0.002**.

3.3.7 Effect of various cytokine and non-cytokine activators on macrophage HDG uptake

In order to investigate the effects of macrophage activation on deoxyglucose uptake, cells were exposed to various activating agents : interferon gamma (IFN), tumour necrosis factor alpha (TNF- α), bacterial lipopolysaccharide (LPS) and low-density lipoprotein (LDL).

IFN is produced by activated T-cells, and is present in atherosclerotic plaques (Amento et al., 1991; Geng et al., 1996). It has a variety of actions on macrophages, acting as a priming agent, but also reducing expression of scavenger receptors and secretion of platelet-derived growth factor (Kosaka et al., 1992; Geng et al., 1992b). These effects of IFN on macrophages in culture suggest a crucial role in the control of macrophage behaviour in atherosclerotic plaques.

Inflammatory cells, including macrophages, produce TNF- α (Kume et al., 2000; Kaartinen et al., 1998). It is a potent cytokine that is toxic to VSMCs, resulting in their apoptosis (Geng et al., 1996; Sukhova et al., 1999), thereby leading to weakening of the fibrous cap. It can also act in an autocrine fashion, activating those cells which release it (Fan et al., 1991a; Hori et al., 1987a).

Lipopolysaccharide is a glycolipid component of gram-negative bacterial cell walls. It binds to the macrophage surface receptor CD14, causing upregulation of the transcription of inflammation-related genes, such as those encoding TNF- α (Kielian et al., 1995; Chow et al., 1995; Decker, 1998).

Low density lipoprotein is found in atherosclerotic plaques, frequently in an oxidised state, where it accumulates within resident macrophages and leads to their transformation into foam cells (Kume et al., 2000; Hamilton et al., 1999; Ross, 1999; De Vries et al., 1998). In culture, the cellular responses induced in macrophages by LDL have been shown to depend on its concentration, degree of oxidation and the

length of its exposure to the cells (Hamilton et al., 1999; Han et al., 1999; De Vries et al., 1998; Geng et al., 1992a).

3.3.7.1 Effect of treatment with IFN and TNF- α on macrophage HDG uptake

Experiment 1 : Control wells received PBS

IFN 50ng/ml alone for 24 hours then TNF- α 50ng/ml for 30 mins prior to addition of HDG

IFN 50ng/ml alone for 24 hours prior to addition of HDG

TNF- α 50ng/ml alone for 30 mins prior to addition of HDG

IFN was added at a concentration of 50ng/ml, this concentration being based on work by others (Geng et al., 1992a; Geng et al., 1996). TNF- α was used at the same concentration, again based upon work by both Geng (Geng et al., 1996) and others (Fan et al., 1991b; Hori et al., 1987b), who showed that this concentration was sufficient to enhance the cytolytic activity of macrophages in culture.

Cellular HDG uptake under the various conditions was as follows : Control wells 0.12% (\pm 0.02), IFN and TNF- α 0.16% (\pm 0.01), IFN alone 0.10% (\pm 0.02), TNF- α alone 0.13% (\pm 0.01). These results are shown in graphical form in Figure 3.9.

After pre-treatment of macrophages with IFN alone for 24 hours, there is a significant increase in HDG accumulation, compared with control, when they are subsequently treated with TNF- α for 30 minutes, **p=0.02**. This fits with the known priming effect of IFN on macrophages. Incubation with IFN allows greater response to subsequent exposure to activating agents like TNF- α , when compared to the effect of TNF- α alone, as seen here.

The fact that treatment with IFN alone for 24 hours reduced subsequent HDG uptake compared with control is in broad agreement with Geng, who showed that IFN treatment for 3 days caused a marked reduction in scavenger receptor-mediated uptake of LDL, by decreasing the number of cell membrane receptors (Geng et al., 1992b).

3.3.7.2 Effect of native and oxidised LDL on HDG uptake by macrophages

In this experiment, to exclude the possibility that there was lipoprotein contamination in the foetal calf serum present in the growth milieu, cells were incubated in serum-free medium 60 minutes before the addition of HDG. After 30 minutes incubation with HDG alone, the following reagents were added to the macrophages:

Experiment 2 : Native LDL 50µg/ml

Oxidised LDL 25µg/ml

Oxidised LDL 50µg/ml

Control wells received PBS

HDG uptake was halted 30 minutes after the addition of the reagents.

Cellular HDG uptake under the various conditions was as follows: Native LDL 0.039% (\pm 0.007), oxidised LDL 25µg/ml 0.07% (\pm 0.014), oxidised LDL 50µg/ml 0.05% (\pm 0.005), control wells 0.051% (\pm 0.01). The results are shown graphically in Figure 3.10.

Compared with control cells, oxidised LDL 25µg/ml significantly increased HDG uptake, **p=0.04**. There was no significant effect on HDG uptake of either a higher concentration of oxidised LDL, or of native (unoxidised) LDL. This result is similar to that seen by De Vries, who used a microphysiometer to directly measure metabolic activity within macrophages (De Vries et al., 1998). This group noted a maximal excitatory effect upon macrophages with a dose of 35µg/ml oxidised LDL, with little effect seen with higher doses of oxidised LDL, or by the use of unoxidised LDL.

3.3.7.3 Effect of serum withdrawal, and the effect of IFN and LPS in combination, on HDG uptake in macrophages

Experiment 3 : 0% serum 24 hours prior to addition of HDG

20% serum 24 hours prior to addition of HDG

IFN 50ng/ml and LPS 5µg/ml 24 hours prior to addition of HDG

Finally, the effect of serum withdrawal was examined. This has the effect of inducing metabolic quiescence in many cell types (Tanner et al., 1998).

Results under the various conditions were as follows : HDG uptake in cells cultured in serum-starved conditions 0.032% (± 0.004), in 20% serum 0.047% (± 0.007), IFN and LPS 0.05% (± 0.005). The results are shown graphically in Figure 3.11.

It was demonstrated that reducing serum levels in culture medium non-significantly reduced uptake of HDG, compared with 20% serum (the standard concentration employed in macrophage culture) whilst the synergistic effect on macrophage activation of IFN plus LPS was evidenced by the large increase in HDG uptake compared to the 0% serum control, **p=0.03**.

3.4 DISCUSSION

In this chapter, it has been shown that two populations of cells, namely THP-1 monocyte line cells and buffy coat-derived macrophages, will accumulate HDG in culture over time. In addition, by changing the degree of activation of the cells one can produce detectable changes in HDG uptake.

The accumulation of HDG over time is not surprising, since it is a glucose analogue and both types of cells use glucose as their principle source of energy. Once inside the cell HDG is not fully metabolised and becomes trapped. The consistent levels of uptake at each timepoint, the increasing levels of uptake with time, and the significant reduction in uptake by pre-treatment with iodoacetic acid indicate that the uptake mechanism is unlikely to be non-specific.

In THP-1 cells, pre-treatment for 18 hours with 1 µg of the phorbol ester PMA caused a 4-fold increase in HDG uptake. PMA differentiates THP-1 cells towards macrophages (Schwende et al., 1996b). This is an energy intensive process, with the cells undergoing many morphological and transcriptional changes (Akuzawa et al., 2000b; Asseffa et al., 1993b) including surface adhesion and the ability to perform phagocytosis. Hence, it might be expected that energy requirements would increase during this process.

It has also been demonstrated that stimulation of macrophages with various activators including oxidised LDL, and the combination of IFN and both LPS and TNF- α caused significant increases in HDG uptake in the cells. These results are similar to those obtained by others using LPS (Orlinska et al., 1993; Gamelli et al., 1996). Fukuzumi examined the uptake of HDG into murine peritoneal macrophages and found that the combination of LPS and IFN increased uptake by a factor of two to three times, mainly by upregulating the expression of GLUT 1 mRNA (Fukuzumi et al., 1996). Spolarics also noted a rapid-onset doubling in glucose usage in macrophage-rich tissues in rats challenged with systemic LPS (Spolarics et al., 1995). It might therefore be expected that both TNF- α (Gamelli et al., 1996; Meszaros et al., 1987) and oxidised LDL (Hamilton et al., 1999; De Vries et al., 1998) have much the

same effect as LPS on glucose usage (and hence HDG uptake) in macrophages. TNF- α , in particular, is capable of exerting strong metabolic effects in macrophage-rich tissues, and increased secretion of TNF- α may be one mechanism by which the body can respond to the demands of sepsis and endotoxemia. Of course, this mechanism appears to be detrimental within atherosclerotic plaque, where release of TNF- α by macrophages is central to plaque rupture (Ross, 1999).

As well as in isolated cell culture, there is evidence that tissue-based macrophages in inflammatory conditions are capable of accumulating deoxyglucose. Within the inflammatory stromal tissue associated with malignant deposits, macrophages avidly take up FDG, and can be responsible for up to 30% of the total FDG uptake of tumour masses (Kubota et al., 1992; Kubota et al., 1995; Kubota et al., 1994).

Additionally, in an experimental model of subcutaneous inflammation in rats, Yamada showed that macrophages took up the largest proportion of FDG of all cells found within the lesions (Yamada et al., 1995). In a similar rodent model, this time of bacterial abscess formation, macrophages were shown to accumulate more FDG than neutrophils, with virtually no contribution to FDG uptake coming from fibroblasts (Kaim et al., 2002). This experimental uptake of FDG by metabolically active macrophages may explain the high levels of FDG uptake seen in humans with other inflammatory conditions, in which macrophages are known to play a part in pathogenesis, such as during abscess formation (Strauss, 1996), sarcoidosis (Lewis et al., 1994; Brudin et al., 1994) and tuberculosis (Strauss, 1996).

Having demonstrated that variations in macrophage activity can result in changes in HDG accumulation, in the next chapter the role of FDG uptake in freshly excised atheroma was evaluated, to determine whether these findings in cultured cells are replicated in living atherosclerotic plaque.

3.5 REFERENCES

1. Ahmed, N., Kansara, M., & Berridge, M. V. (1997). Acute regulation of glucose transport in a monocyte-macrophage cell line: Glut-3 affinity for glucose is enhanced during the respiratory burst. *Biochem.J.*, 327 (Pt 2), 369-375.
2. Akuzawa, N., Kurabayashi, M., Ohyama, Y., Arai, M., & Nagai, R. (2000a). Zinc finger transcription factor Egr-1 activates Flt-1 gene expression in THP-1 cells on induction for macrophage differentiation. *Arterioscler.Thromb.Vasc.Biol.*, 20, 377-384.
3. Akuzawa, N., Kurabayashi, M., Ohyama, Y., Arai, M., & Nagai, R. (2000b). Zinc finger transcription factor Egr-1 activates Flt-1 gene expression in THP-1 cells on induction for macrophage differentiation. *Arterioscler.Thromb.Vasc.Biol.*, 20, 377-384.
4. Amento, E. P., Ehsani, N., Palmer, H., & Libby, P. (1991). Cytokines and growth factors positively and negatively regulate interstitial collagen gene expression in human vascular smooth muscle cells. *Arterioscler.Thromb.*, 11, 1223-1230.
5. Asseffa, A., Dickson, L. A., Mohla, S., & Bremner, T. A. (1993a). Phorbol myristate acetate-differentiated THP-1 cells display increased levels of MHC class I and class II mRNA and interferon-gamma-inducible tumoricidal activity. *Oncol.Res.*, 5, 11-18.
6. Asseffa, A., Dickson, L. A., Mohla, S., & Bremner, T. A. (1993b). Phorbol myristate acetate-differentiated THP-1 cells display increased levels of MHC class I and class II mRNA and interferon-gamma-inducible tumoricidal activity. *Oncol.Res.*, 5, 11-18.
7. Boyle, J. J., Bowyer, D. E., Weissberg, P. L., & Bennett, M. R. (2001). Human blood-derived macrophages induce apoptosis in human plaque- derived vascular smooth muscle cells by Fas-ligand/Fas interactions. *Arterioscler.Thromb.Vasc.Biol.*, 21, 1402-1407.
8. Brudin, L. H., Valind, S. O., Rhodes, C. G., Pantin, C. F., Sweatman, M., Jones, T., & Hughes, J. M. (1994). Fluorine-18 deoxyglucose uptake in sarcoidosis measured with positron emission tomography. *Eur.J.Nucl Med.*, 21, 297-305.
9. Chakrabarti, R., Jung, C. Y., Lee, T. P., Liu, H., & Mookerjee, B. K. (1994). Changes in glucose transport and transporter isoforms during the activation of human peripheral blood lymphocytes by phytohemagglutinin. *J.Immunol.*, 152, 2660-2668.
10. Chow, C. W., Grinstein, S., & Rotstein, O. D. (1995). Signaling events in monocytes and macrophages. *New Horiz.*, 3, 342-351.
11. d'Argy, R., Paul, R., Frankenberg, L., Stalnacke, C. G., Lundqvist, H., Kangas, L., Halldin, C., Nagren, K., Roeda, D., Haaparanta, M., & . (1988). Comparative double-tracer whole-body autoradiography: uptake of ¹¹C-, ¹⁸F- and ³H-labeled compounds in rat tumors. *Int.J.Rad.Appl.Instrum.B*, 15, 577-585.
12. Daneman, D., Zinman, B., Elliott, M. E., Bilan, P. J., & Klip, A. (1992). Insulin-stimulated glucose transport in circulating mononuclear cells from nondiabetic and IDDM subjects. *Diabetes*, 41, 227-234.
13. Davies, M. J. (1996). Stability and instability: two faces of coronary atherosclerosis. The Paul Dudley White Lecture 1995. *Circulation*, 94, 2013-2020.
14. De Vries, H. E., Ronken, E., Reinders, J. H., Buchner, B., Van Berkel, T. J., & Kuiper, J. (1998). Acute effects of oxidized low density lipoprotein on metabolic responses in macrophages. *FASEB J.*, 12, 111-118.

15. Decker, K. (1998). The response of liver macrophages to inflammatory stimulation. *Keio J.Med.*, 47, 1-9.
16. Estrada, D. E., Elliott, E., Zinman, B., Poon, I., Liu, Z., Klip, A., & Daneman, D. (1994). Regulation of glucose transport and expression of GLUT3 transporters in human circulating mononuclear cells: studies in cells from insulin- dependent diabetic and nondiabetic individuals. *Metabolism*, 43, 591-598.
17. Fan, S., Fehr, H. G., & Adams, D. (1991a). Activation of macrophages for ADCC in vitro: effects of IL-4, TNF, interferons-alpha/beta, interferon-gamma, and GM-CSF. *Cell Immunol.*, 135, 78-87.
18. Fan, S., Fehr, H. G., & Adams, D. (1991b). Activation of macrophages for ADCC in vitro: effects of IL-4, TNF, interferons-alpha/beta, interferon-gamma, and GM-CSF. *Cell Immunol.*, 135, 78-87.
19. Fukuzumi, M., Shinomiya, H., Shimizu, Y., Ohishi, K., & Utsumi, S. (1996). Endotoxin-induced enhancement of glucose influx into murine peritoneal macrophages via GLUT1. *Infect.Immun.*, 64, 108-112.
20. Gamelli, R. L., Liu, H., He, L. K., & Hofmann, C. A. (1996). Augmentations of glucose uptake and glucose transporter-1 in macrophages following thermal injury and sepsis in mice. *J.Leukoc.Biol.*, 59, 639-647.
21. Geng, Y. J. & Hansson, G. K. (1992a). Interferon-gamma inhibits scavenger receptor expression and foam cell formation in human monocyte-derived macrophages. *J.Clin.Invest*, 89, 1322-1330.
22. Geng, Y. J. & Hansson, G. K. (1992b). Interferon-gamma inhibits scavenger receptor expression and foam cell formation in human monocyte-derived macrophages. *J.Clin.Invest*, 89, 1322-1330.
23. Geng, Y. J., Wu, Q., Muszynski, M., Hansson, G. K., & Libby, P. (1996). Apoptosis of vascular smooth muscle cells induced by in vitro stimulation with interferon-gamma, tumor necrosis factor-alpha, and interleukin-1 beta. *Arterioscler.Thromb.Vasc.Biol.*, 16, 19-27.
24. Gordon, S., Clarke, S., Greaves, D., & Doyle, A. (1995). Molecular immunobiology of macrophages: recent progress. *Curr.Opin.Immunol.*, 7, 24-33.
25. Hagi, A., Hayashi, H., Kishi, K., Wang, L., & Ebina, Y. (2000). Activation of G-protein coupled fMLP or PAF receptor directly triggers glucose transporter type 1 (GLUT1) translocation in Chinese hamster ovary (CHO) cells stably expressing fMLP or PAF receptor. *J.Med.Invest*, 47, 19-28.
26. Hamilton, J. A., Myers, D., Jessup, W., Cochrane, F., Byrne, R., Whitty, G., & Moss, S. (1999). Oxidized LDL can induce macrophage survival, DNA synthesis, and enhanced proliferative response to CSF-1 and GM-CSF. *Arterioscler.Thromb.Vasc.Biol.*, 19, 98-105.
27. Han, C. Y. & Pak, Y. K. (1999). Oxidation-dependent effects of oxidized LDL: proliferation or cell death. *Exp.Mol.Med.*, 31, 165-173.
28. Hori, K., Ehrke, M. J., Mace, K., Maccubbin, D., Doyle, M. J., Otsuka, Y., & Mihich, E. (1987a). Effect of recombinant human tumor necrosis factor on the induction of murine macrophage tumoricidal activity. *Cancer Res.*, 47, 2793-2798.
29. Hori, K., Ehrke, M. J., Mace, K., Maccubbin, D., Doyle, M. J., Otsuka, Y., & Mihich, E. (1987b). Effect of recombinant human tumor necrosis factor on the induction of murine macrophage tumoricidal activity. *Cancer Res.*, 47, 2793-2798.
30. Kaartinen, M., van der Wal, A. C., van der Loos, C. M., Piek, J. J., Koch, K. T., Becker, A. E., & Kovanen, P. T. (1998). Mast cell infiltration in acute coronary syndromes: implications for plaque rupture. *J.Am.Coll.Cardiol.*, 32, 606-612.

31. Kaim, A. H., Weber, B., Kurrer, M. O., Gottschalk, J., Von Schulthess, G. K., & Buck, A. (2002). Autoradiographic quantification of ¹⁸F-FDG uptake in experimental soft-tissue abscesses in rats. *Radiology*, 223, 446-451.
32. Kielian, T. L. & Blecha, F. (1995). CD14 and other recognition molecules for lipopolysaccharide: a review. *Immunopharmacology*, 29, 187-205.
33. Kosaka, C., Masuda, J., Shimokado, K., Zen, K., Yokota, T., Sasaguri, T., & Ogata, J. (1992). Interferon-gamma suppresses PDGF production from THP-1 cells and blood monocyte-derived macrophages. *Atherosclerosis*, 97, 75-87.
34. Kubota, R., Kubota, K., Yamada, S., Tada, M., Ido, T., & Tamahashi, N. (1994). Microautoradiographic study for the differentiation of intratumoral macrophages, granulation tissues and cancer cells by the dynamics of fluorine-18-fluorodeoxyglucose uptake. *J.Nucl.Med.*, 35, 104-112.
35. Kubota, R., Kubota, K., Yamada, S., Tada, M., Takahashi, T., Iwata, R., & Tamahashi, N. (1995). Methionine uptake by tumor tissue: a microautoradiographic comparison with FDG. *J.Nucl Med.*, 36, 484-492.
36. Kubota, R., Yamada, S., Kubota, K., Ishiwata, K., Tamahashi, N., & Ido, T. (1992). Intratumoral distribution of fluorine-18-fluorodeoxyglucose in vivo: high accumulation in macrophages and granulation tissues studied by microautoradiography. *J.Nucl.Med.*, 33, 1972-1980.
37. Kume, N., Moriwaki, H., Kataoka, H., Minami, M., Murase, T., Sawamura, T., Masaki, T., & Kita, T. (2000). Inducible expression of LOX-1, a novel receptor for oxidized LDL, in macrophages and vascular smooth muscle cells. *Ann.N.Y.Acad.Sci.*, 902, 323-327.
38. Lewis, P. J. & Salama, A. (1994). Uptake of fluorine-18-fluorodeoxyglucose in sarcoidosis. *J.Nucl Med.*, 35, 1647-1649.
39. Meszaros, K., Lang, C. H., Bagby, G. J., & Spitzer, J. J. (1987). Tumor necrosis factor increases in vivo glucose utilization of macrophage-rich tissues. *Biochem.Biophys.Res.Comm.*, 149, 1-6.
40. Orłinska, U. & Newton, R. C. (1993). Role of glucose in interleukin-1 beta production by lipopolysaccharide-activated human monocytes. *J.Cell Physiol*, 157, 201-208.
41. Rego, A. C., Areias, F. M., Santos, M. S., & Oliveira, C. R. (1999). Distinct glycolysis inhibitors determine retinal cell sensitivity to glutamate-mediated injury. *Neurochem.Res.*, 24, 351-358.
42. Ross, R. (1999). Atherosclerosis--an inflammatory disease. *N.Engl.J.Med.*, 340, 115-126.
43. Schwende, H., Fitzke, E., Ambs, P., & Dieter, P. (1996b). Differences in the state of differentiation of THP-1 cells induced by phorbol ester and 1,25-dihydroxyvitamin D₃. *J.Leukoc.Biol.*, 59, 555-561.
44. Schwende, H., Fitzke, E., Ambs, P., & Dieter, P. (1996a). Differences in the state of differentiation of THP-1 cells induced by phorbol ester and 1,25-dihydroxyvitamin D₃. *J.Leukoc.Biol.*, 59, 555-561.
45. Spolarics, Z. & Spitzer, J. J. (1995). Acute endotoxin tolerance is accompanied by stimulated glucose use in macrophage rich tissues. *Biochem.Biophys.Res.Comm.*, 211, 340-346.
46. Strauss, L. G. (1996). Fluorine-18 deoxyglucose and false-positive results: a major problem in the diagnostics of oncological patients. *Eur.J.Nucl Med.*, 23, 1409-1415.

47. Sukhova, G. K., Schonbeck, U., Rabkin, E., Schoen, F. J., Poole, A. R., Billingham, R. C., & Libby, P. (1999). Evidence for increased collagenolysis by interstitial collagenases-1 and -3 in vulnerable human atheromatous plaques. *Circulation*, 99, 2503-2509.
48. Tanner, F. C., Yang, Z. Y., Duckers, E., Gordon, D., Nabel, G. J., & Nabel, E. G. (1998). Expression of cyclin-dependent kinase inhibitors in vascular disease. *Circ.Res.*, 82, 396-403.
49. Tsuchiya, S., Yamabe, M., Yamaguchi, Y., Kobayashi, Y., Konno, T., & Tada, K. (1980). Establishment and characterization of a human acute monocytic leukemia cell line (THP-1). *Int.J.Cancer*, 26, 171-176.
50. Waki, A., Fujibayashi, Y., Sadato, N., Tsuchida, T., Ishii, Y., Yokoyama, A., & Yonekura, Y. (1997). Effects of antitumor agents on 3H-2-deoxyglucose uptake in tumor cells and their relationship with the main targets of the antitumor agents. *Ann.Nucl.Med.*, 11, 183-188.
51. Yamada, S., Kubota, K., Kubota, R., Ido, T., & Tamahashi, N. (1995). High accumulation of fluorine-18-fluorodeoxyglucose in turpentine- induced inflammatory tissue. *J.Nucl.Med.*, 36, 1301-1306.

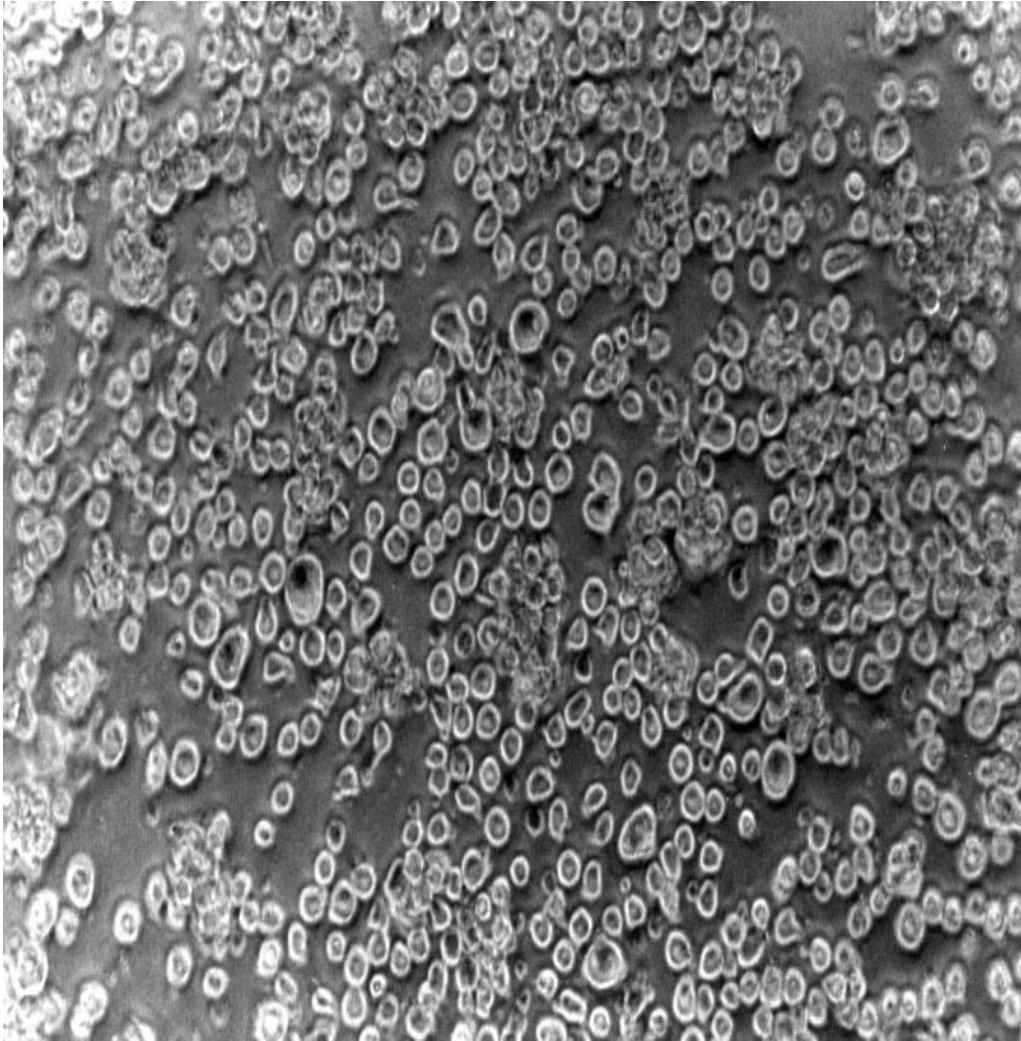


Figure 3.1 THP-1 cells in culture - unstimulated

Unstimulated THP-1 cells, magnification x20.

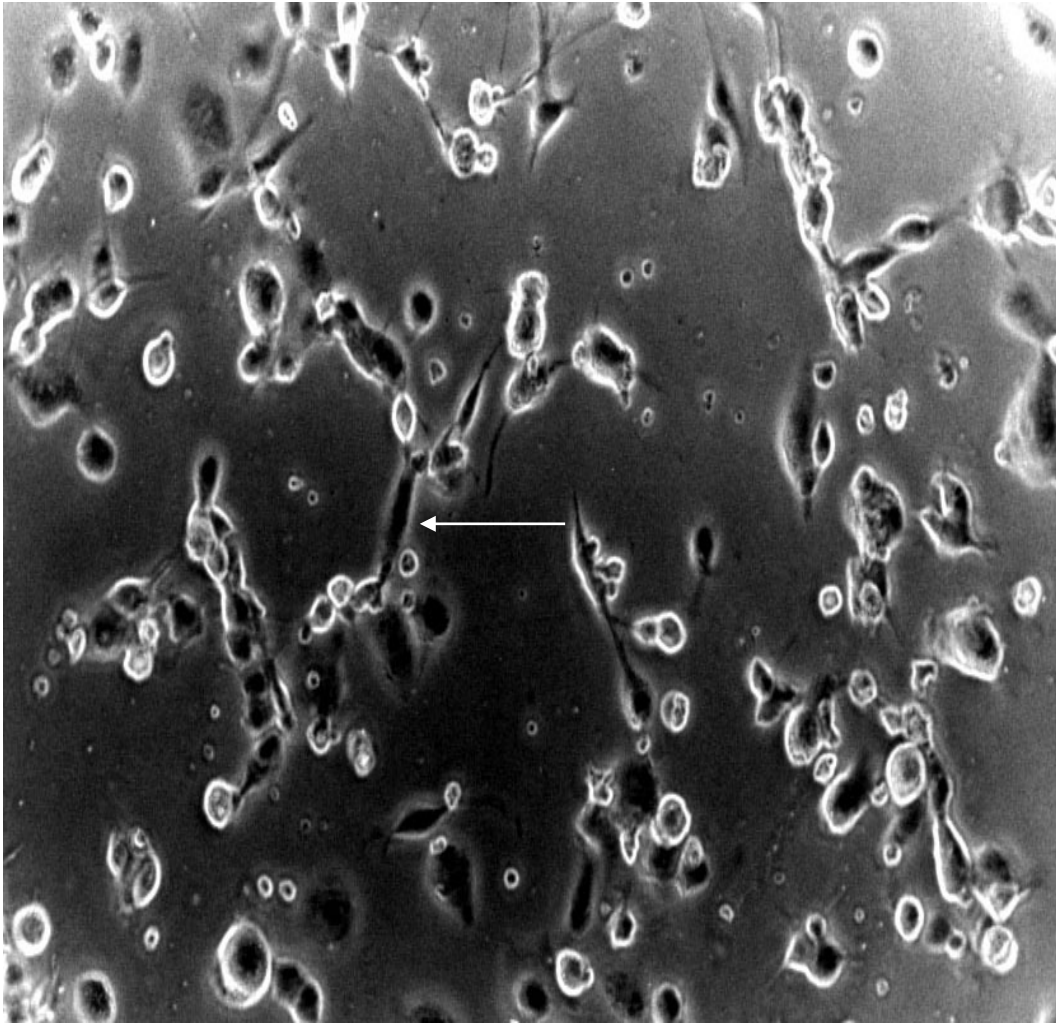


Figure 3.2 THP-1 cells in culture - stimulated

THP-1 cells, stimulated for 48 hours with PMA, magnification x40. The white arrow is pointing towards a dendritic process emerging from a cell.

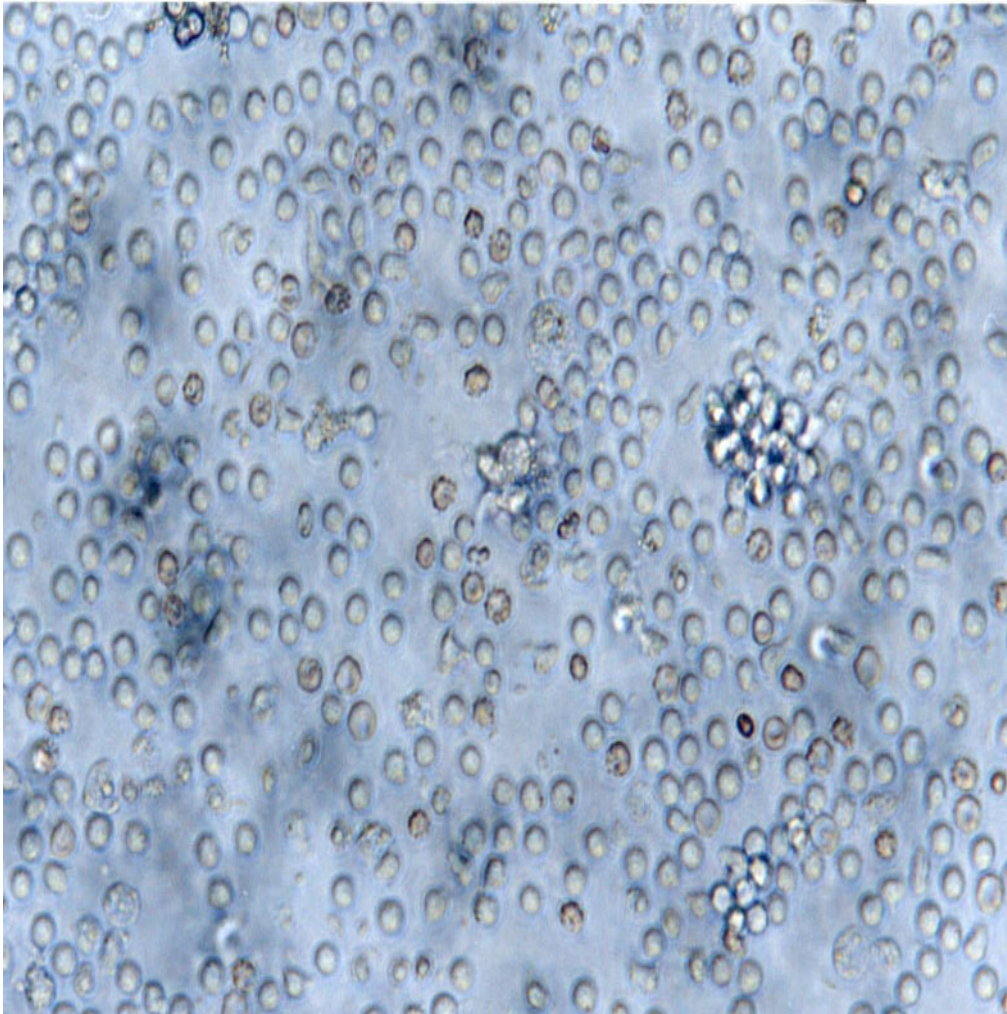


Figure 3.3 Monocytes in culture

Freshly isolated monocytes, day 1 of culture on glass, magnification x20.

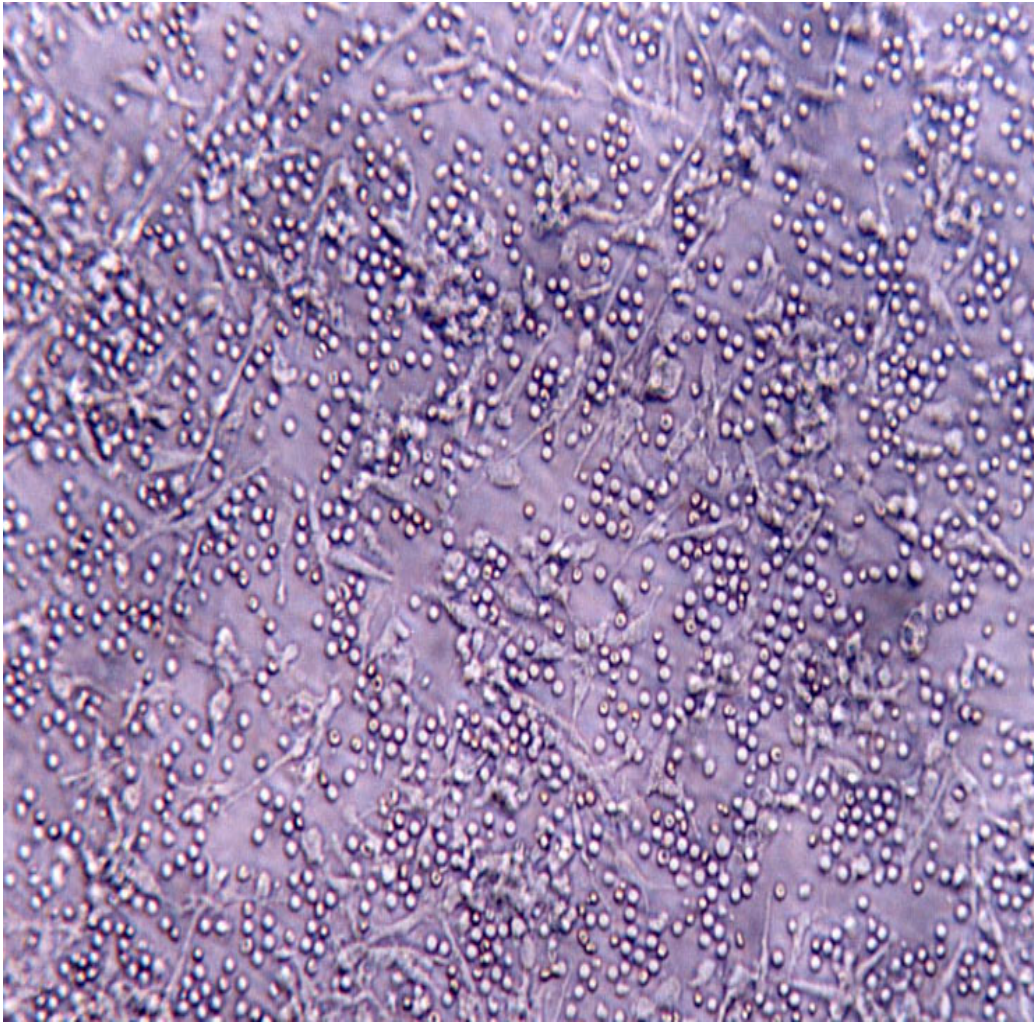


Figure 3.4 Macrophages in culture

Day 7 macrophages in culture on glass,
magnification x10.

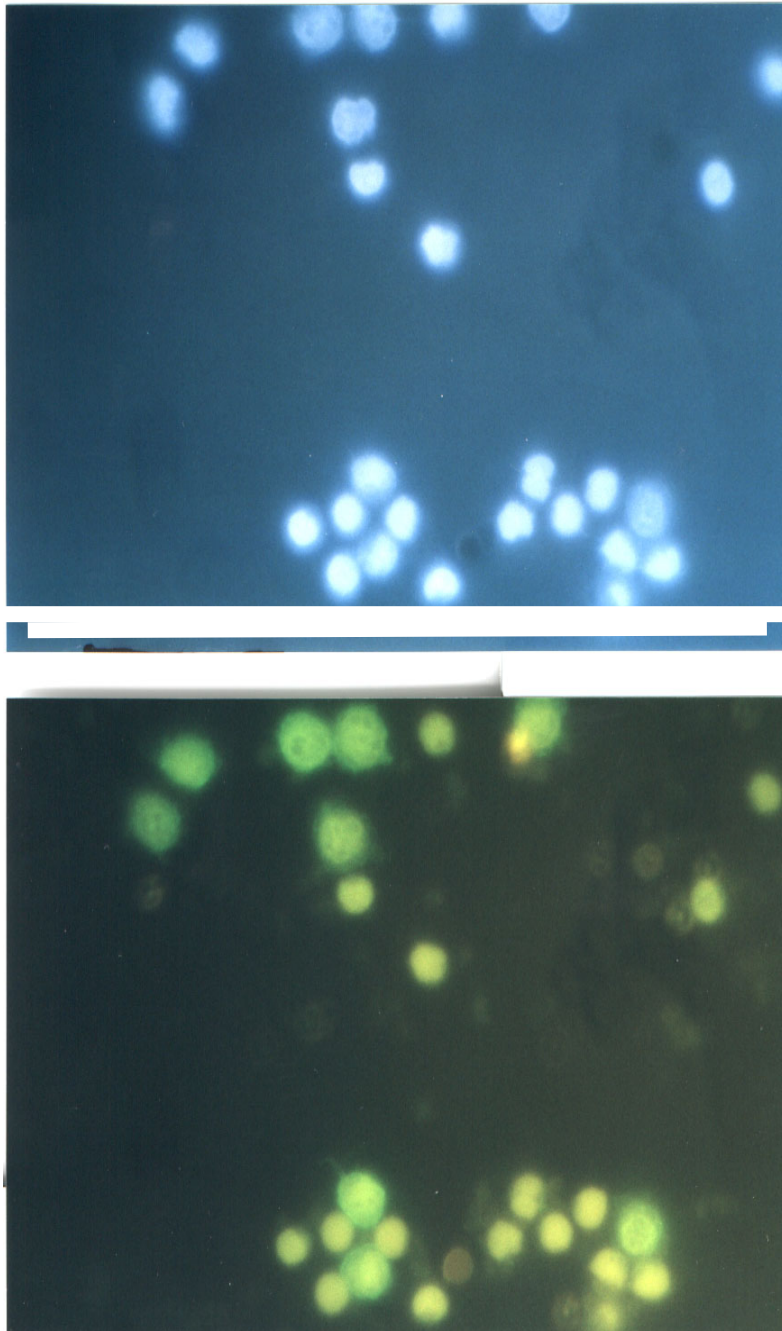


Figure 3.5 CD14 immunocytochemistry

Top panel shows CD14 FITC labelling of freshly isolated cells. Cells in the bottom panel are stained with nuclear counterstain (Hoerscht). Over 95% of cells express the monocyte marker CD14. Magnification x40.

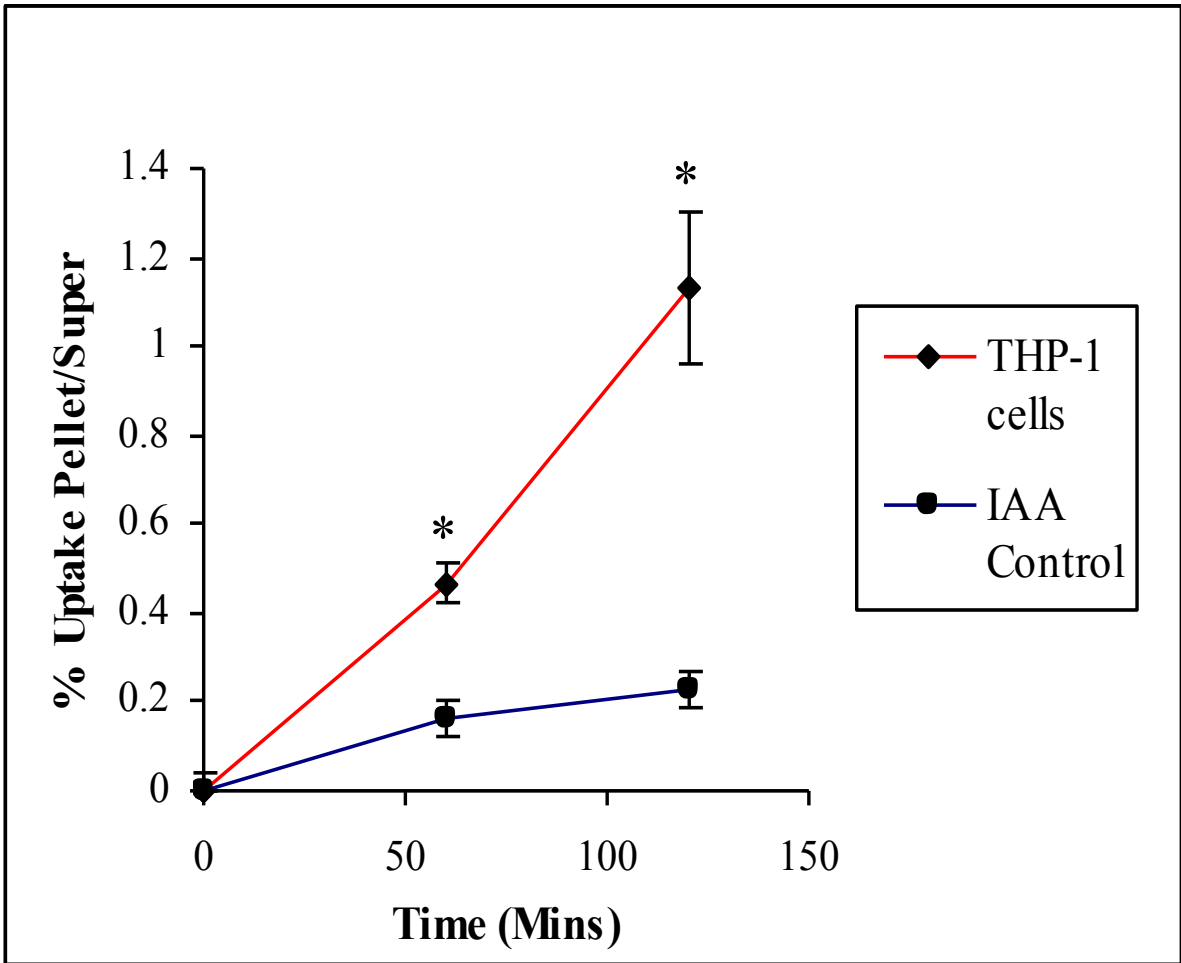


Fig 3.6 The uptake of HDG in THP-1 cells over time

The graph demonstrates that HDG accumulates within THP-1 cells over time to a greater extent than it does within cells pre-treated with IAA, $p=0.003$ at 60 minutes and $p=0.005$ at 120 minutes.

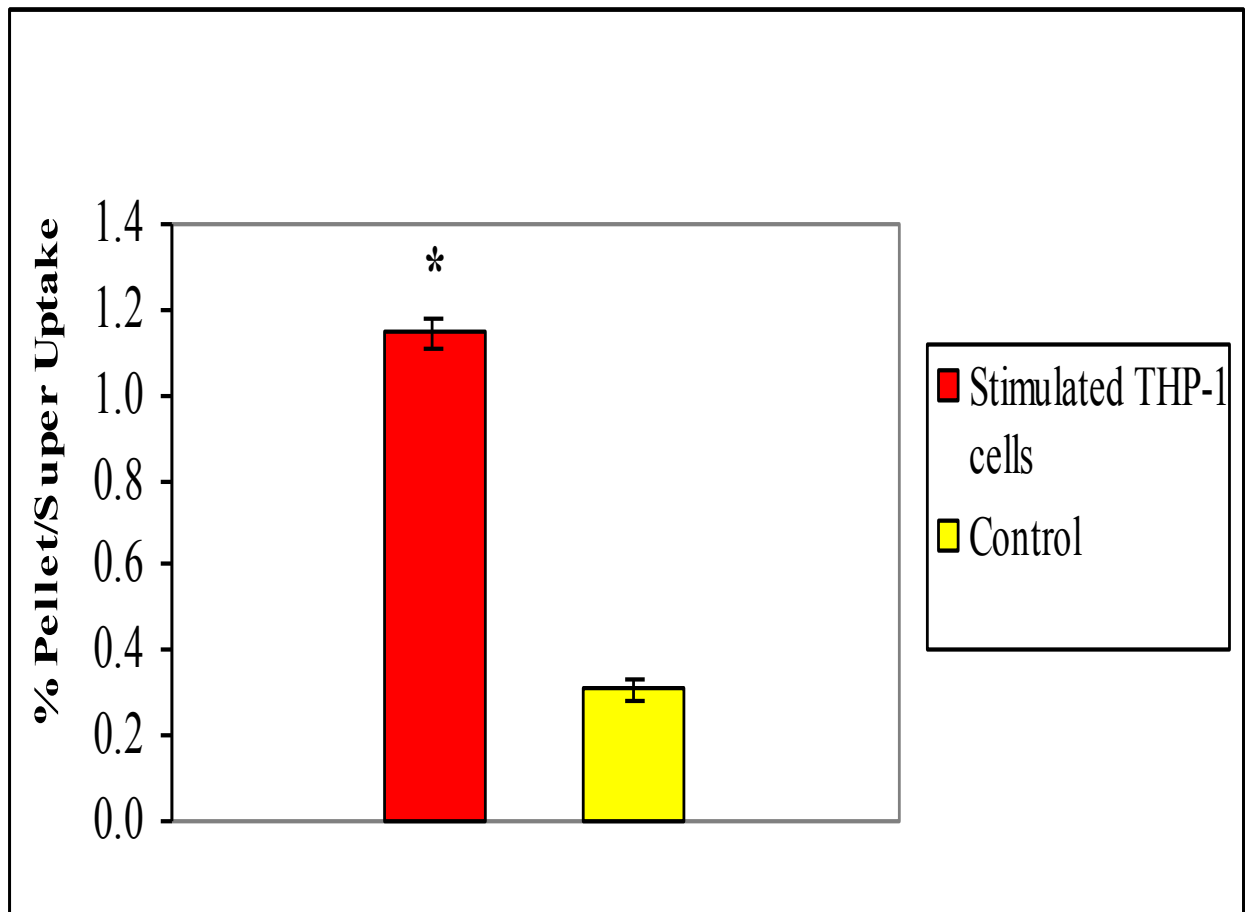


Figure 3.7 HDG uptake in THP-1 cells after PMA stimulation

HDG accumulates within PMA-stimulated cells to a greater extent than in unstimulated control cells, $p=0.005$.

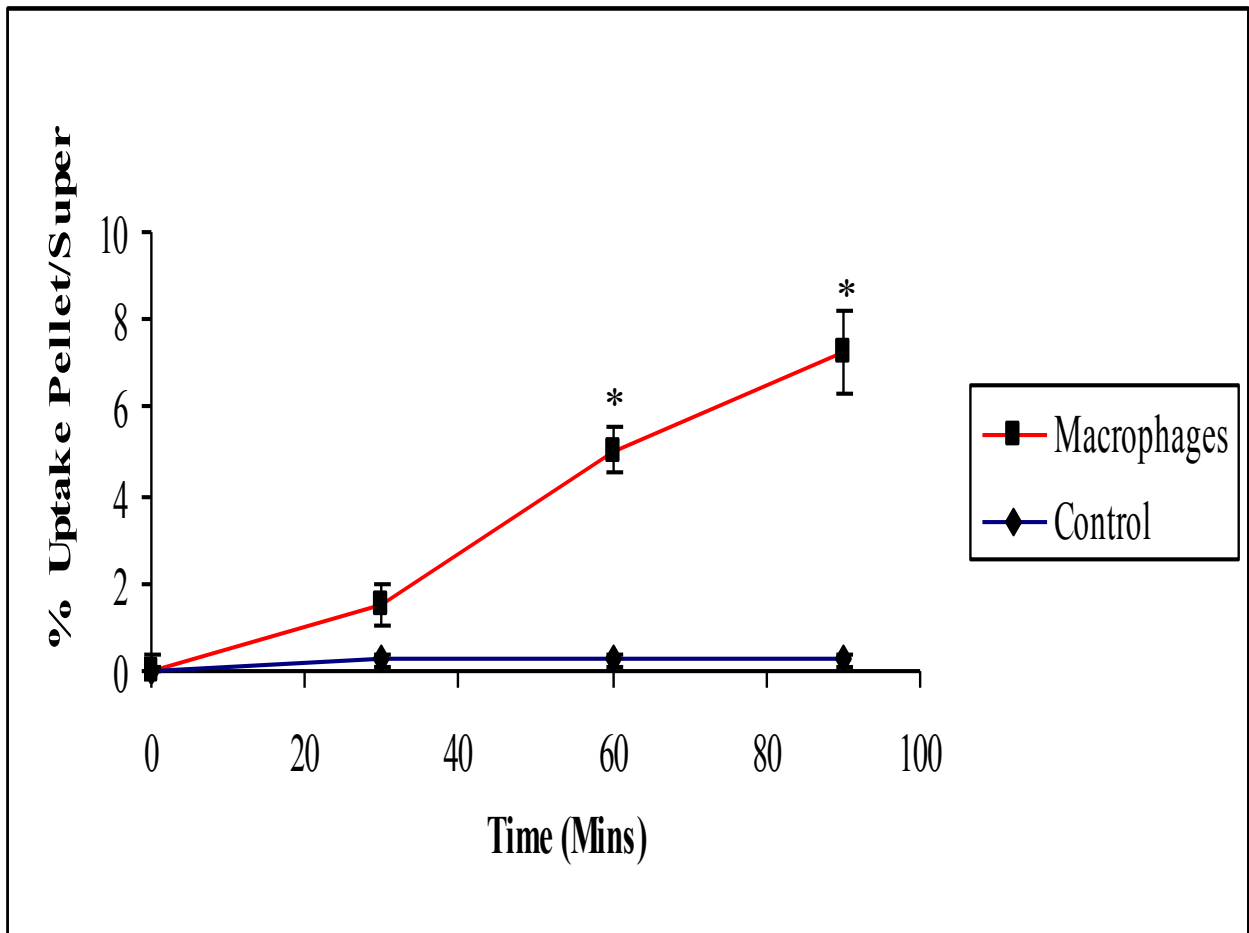


Figure 3.8 HDG uptake in human macrophages over time

The graph demonstrates that HDG accumulates within untreated macrophages over time to a greater extent than it does in control macrophages pre-treated with IAA. $p=0.001$ and 0.002 at 60 and 90 minutes respectively.

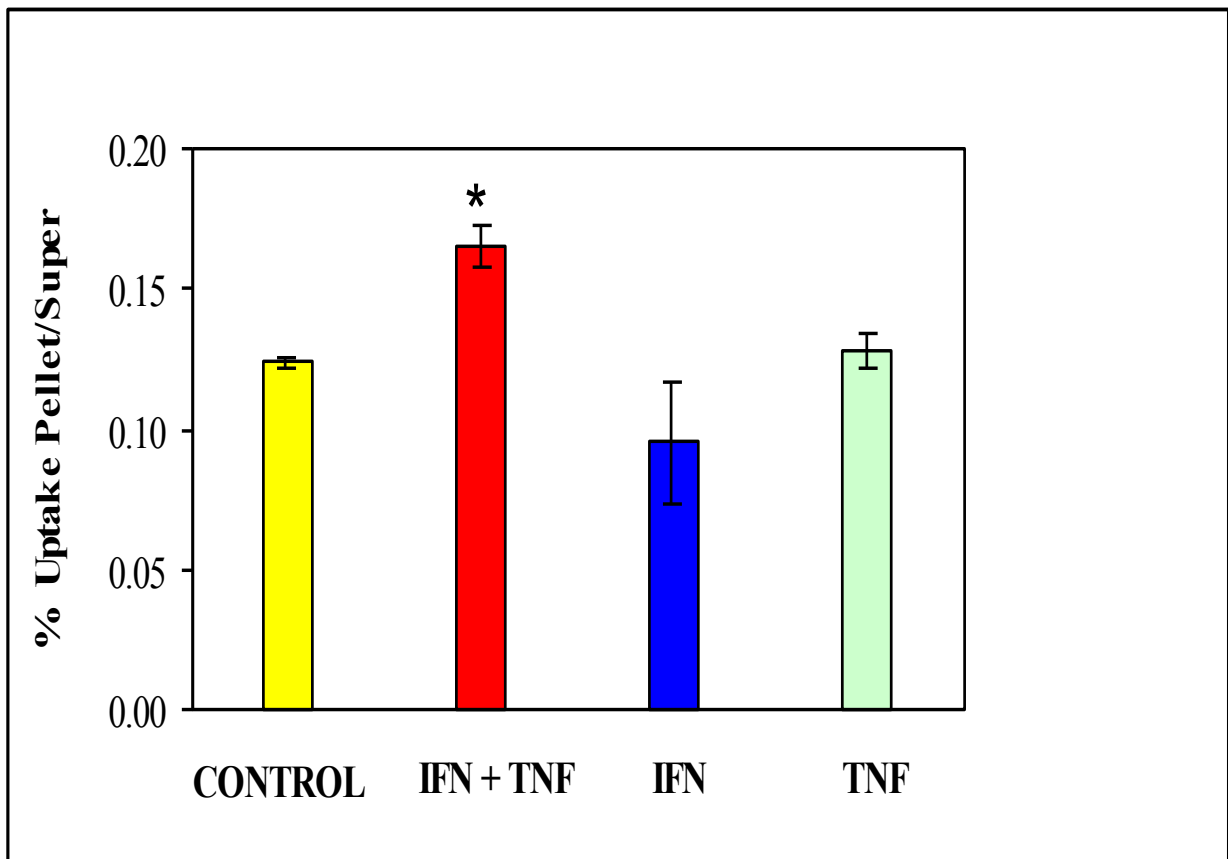


Fig 3.9 The effect of agonists on HDG uptake in human macrophages (1)

Full explanation is given in Section 3.3.7.1. $p=0.02$ compared to control.

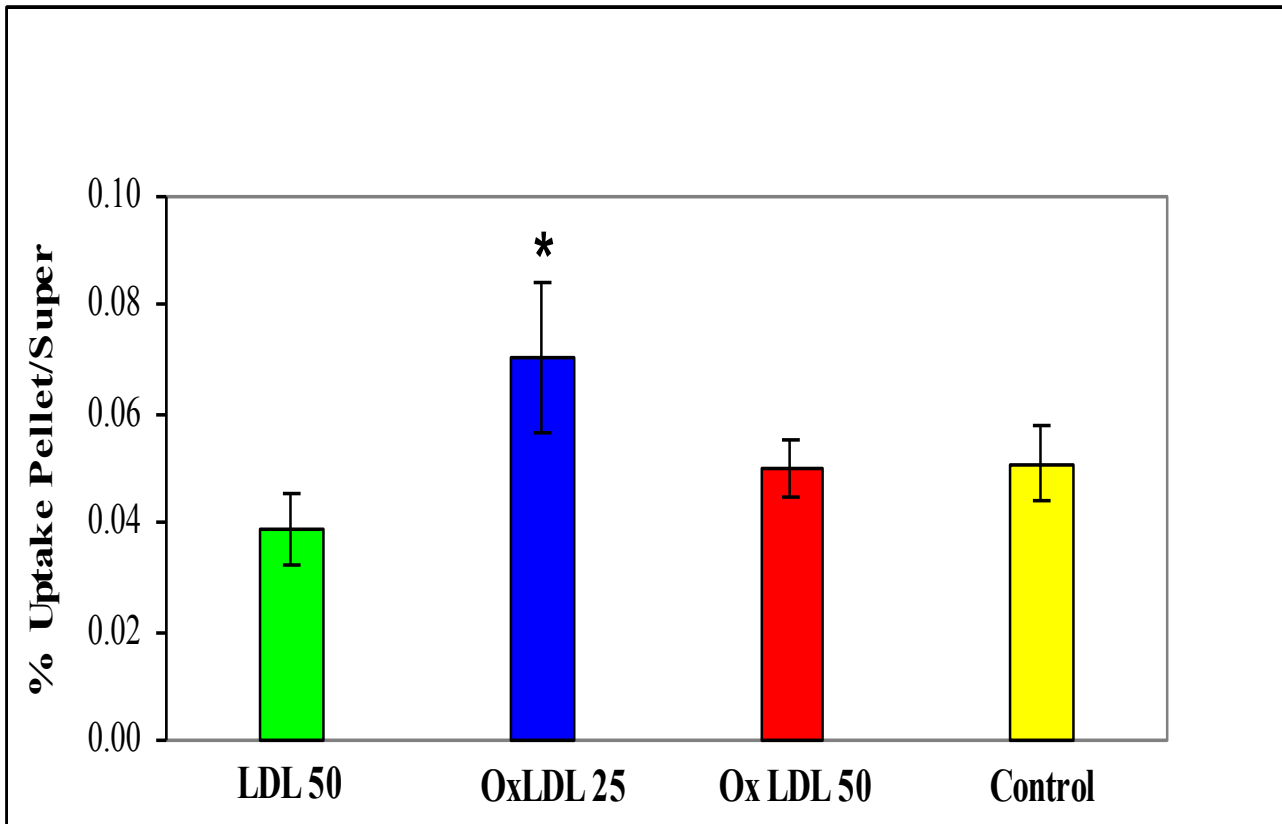


Fig 3.10 The effect of agonists on HDG uptake in human macrophages (2)

Full explanation is given in Section 3.3.7.2. $p=0.04$ compared to control.

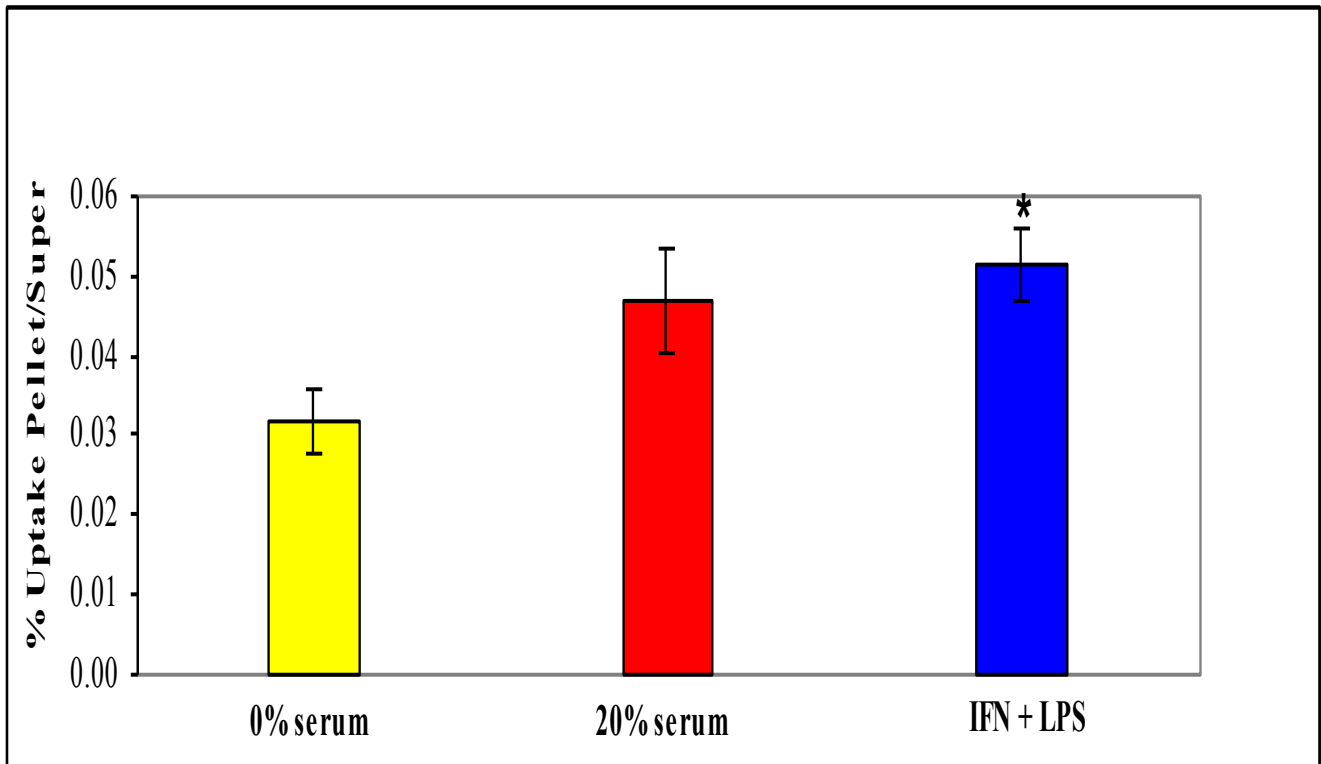


Fig 3.11 The effect of agonists on HDG uptake in human macrophages (3)

Full explanation is given in Section 3.3.7.3. $p=0.03$ compared to 0% serum control.

Chapter 4

CHAPTER 4

THE UPTAKE OF FDG IN ATHEROSCLEROSIS *IN VITRO*

4.1 INTRODUCTION

The aim of the work described in this chapter was to assess of the degree of uptake of FDG into symptomatic carotid atherosclerotic plaque. The plaques had been removed at endarterectomy because of carotid territory vascular symptoms. The experiments described here are a progression from those presented in the previous chapter, where it was demonstrated that macrophages in culture would accumulate HDG in proportion to their metabolic activity. It was felt important to determine whether macrophages would take up FDG, more so than surrounding cells, when they were present within the milieu of a symptomatic atherosclerotic plaque.

It is now accepted that the presence of macrophage inflammatory cells in the fibrous cap region of plaques is a strong determinant of subsequent plaque rupture (Ross, 1999). As a result, the hypothesis tested here was that this inflammatory activity might be visualised and quantified within plaques using the autoradiographic technique of phosphor imaging. A second aim was to attempt to correlate the extent of any FDG uptake seen in plaque with the cellular composition of the tissue. Lastly, tritiated autoradiography of the plaque was used to try to determine the cell type (or types) responsible for any deoxyglucose uptake.

4.2 METHODS

4.2.1 Phosphor imaging technique

Phosphor imaging is an autoradiographic technique that allows the visualisation and measurement of radioactivity within tissue samples. By placing exposed tissue in close proximity to a phosphor screen, a latent image of the tissue radioactivity becomes stored on the screen. The phosphor screen is covered with a thin layer of BaFBr:Eu²⁺ phosphor crystals on one side. These crystals absorb the energy emitted by FDG trapped in the tissue sample, and subsequently re-emit it as blue light in proportion to the energy deposited, when excited by a red laser contained within the screen reading device (Johnston et al., 1990).

Phosphor imaging screens have a higher sensitivity to energy photons than conventional x-ray film, meaning that brief exposure times are sufficient. This makes phosphor imaging ideal for use with short-lived positron emitting nuclides such as ¹¹C and ¹⁸F (with half-lives of 20.3 minutes and 109.7 minutes, respectively). The use of traditional x-ray film autoradiography with such nuclides is unfeasible, because its lower sensitivity means that exposure times stretching to many half-lives would be required to create an image, by which time much of the activity stored in the tissue would have decayed away.

The phosphor screen used in this work has a spatial resolution of approximately 500µm (with ¹⁸F) and can detect radioactivity concentrations as low as 0.04 Bq/mm². The screen was read at a resolution of 600 dots per inch (42 µm pixel size). As this is much lower than the spatial resolution of the screen with ¹⁸F, it was assumed that the screen reader has a negligible influence on the overall spatial resolution. The reported linear dynamic range for the phosphor screen is five orders of magnitude, with a ± 5% standard deviation over the dynamic range.

4.2.2 Phosphor imaging of carotid atherosclerosis

Carotid endarterectomy samples were obtained from patients undergoing surgery for symptomatic internal carotid artery disease of at least 70% stenosis. All had experienced a carotid territory TIA within three months of operation, and all gave full informed consent to the study.

Plaques were collected from the operating theatre at Addenbrookes hospital, and immediately sectioned transversely into slices of approximately 5mm thickness. Each section was incubated with 0.037MBq FDG in 1ml M199 for one hour at 37°C. This FDG dose was derived from typical plasma radioactivity levels seen during a whole-body FDG-PET scan. Calculations showed that 0.037MBq per ml applied to the tissue sections *in vitro* was broadly equivalent to the plasma concentration of FDG fifteen minutes after injection of 370MBq FDG in a whole-body PET scan.

After incubation for sixty minutes, FDG uptake into the carotid sections was halted by the addition of 10µl of 1mM iodoacetic acid, followed by three 5 minute washes with PBS to remove free FDG. The carotid sections were then placed onto glass slides (BDH), covered with clingfilm, apposed to a 43cm x 12.5cm high-resolution phosphor imaging screen (Packard Instrument Company, Connecticut, U.S.A.) and finally encased in an x-ray cassette for three hours. After this time, the screen was read in the scanning carousel (Packard Instrument Company, Connecticut, U.S.A.), and the resulting images were analysed using the OptiQuant software package (Packard Instrument Company, Connecticut, U.S.A.), by drawing regions of interest (ROI) of uniform size around the plaque phosphor images.

To allow measurement of accumulated radioactivity in the tissue samples to be derived from the ROI data, a standard curve was constructed using serial dilutions of a known volume and activity of FDG. Aliquots containing 2µL were diluted serially by a factor of two and pipetted onto blotting paper, producing a series of blots of the same volume, each having half the radioactivity of the previous. The blotting paper was positioned next to the exposed tissue sections before apposing to the phosphor plate.

4.2.3 Plaque histological characterisation

Following phosphor imaging, after allowing for a period of decay of FDG, the tissue sections were fixed in 4% paraformaldehyde for 12 hours at 4°C. Specimens were then paraffin-embedded, sectioned to 5µm thickness and stained with haematoxylin and eosin as in Section 2.3.2 of Chapter 2. Immunohistochemistry was performed using monoclonal antibodies against markers for macrophages and vascular smooth muscle cells using the method described in Section 2.3.1.3 of Chapter 2. Histological images were digitised on a Nikon digital microscope, and image analysis was performed using Photoshop software version 5 (Adobe). A colour threshold method was employed to estimate the area of CD68 and SMA positive staining on each section as a percentage of its total area (Lehr et al., 1999).

4.2.4 Correlation between plaque FDG uptake and cellular composition

Comparisons were made between the FDG uptake in each section of plaque, derived from phosphor imaging data and expressed in units of Bq/mm², and its macrophage and smooth muscle cell content, derived from immunohistochemical staining and expressed as area of plaque containing each cell type as a percentage of total plaque area. The statistical methods employed are described in Section 2.4 of Chapter 2.

4.2.5 Tritiated deoxyglucose autoradiography of carotid atherosclerosis

In a separate autoradiographic study, carotid plaques from an identical group of symptomatic patients were incubated whole with 50µCi tritiated deoxyglucose (HDG) in 5mls M199 for 60 minutes at 37°C. Subsequently, paraffin sections of 5µm thickness were coated with autoradiographic emulsion (LM-1, Amersham, UK), exposed for 6 weeks, developed (D19, Kodak), and counterstained with haematoxylin and eosin as in Section 2.3.2 of Chapter 2. Control slides were prepared without radioactivity.

4.3 RESULTS

4.3.1 Phosphor imaging of carotid atherosclerosis

Phosphor imaging was carried out on plaques removed from seven patients. An example of phosphor imaging of two sections from a single plaque is shown in Figure 4.1, along with single stained immunohistochemistry for both macrophages and smooth muscle cells on the same plaque. Red areas in the phosphor images reflect high levels of FDG uptake, whilst areas in blue have accumulated FDG to a lesser extent.

It can be seen in the plaque section on the left hand side of the figure that high levels of FDG uptake in central areas (shown in red) co-localise with an area rich in macrophages. Conversely, in the plaque section shown on the right hand side of the figure, there is a low degree of FDG uptake (shown in blue). Examination of the corresponding histology shows that this piece of plaque that is made up largely of smooth muscle cells and contains very few macrophages.

The results of a statistical analysis designed to detect correlations between plaque cell composition and FDG uptake are presented below.

4.3.2 Correlation between plaque FDG uptake and cellular composition

FDG uptake and cellular composition in seven carotid endarterectomy samples, sectioned into a total of 41 slices, were assessed using a weighted statistical technique described in Section 2.4 of Chapter 2. The results are presented in the two tables below. Table 4.1 shows data concerning FDG uptake and plaque macrophage percentage area. Table 4.2 shows data relating FDG uptake and plaque vascular smooth muscle cell percentage area.

In both tables, n = the number of slices generated from each carotid specimen, r = correlation coefficient for each carotid experiment, slope = gradient of the correlation

curve for each carotid experiment, SE of slope = standard error of the gradient of each correlation graph.

Carotid number	n	r	Slope	SE of slope
1	9	0.94	0.04	0.01
2	5	0.60	0.21	0.16
3	7	-0.43	-0.03	0.03
4	5	0.01	0.00	0.15
5	4	0.13	0.03	0.14
6	5	0.70	0.09	0.05
7	6	0.55	0.05	0.04

Table 4.1

The overall weighted correlation coefficient for FDG uptake and macrophage % area was $r = 0.56$, with 95% CI: (-0.33,0.92), $p = 0.19$.

Carotid number	n	r	Slope	SE of slope
1	9	-0.57	-0.17	0.09
2	5	-0.31	-0.02	0.04
3	7	0.74	0.09	0.04
4	5	-0.18	-0.08	0.36
5	4	-0.64	-0.03	0.26
6	5	0.62	0.07	0.03
7	6	-0.15	-0.06	0.05

Table 4.2

The overall weighted correlation coefficient for FDG uptake and VSMC area % was $r = -0.12$ with 95% CI:(-0.80,0.70), $p = 0.80$.

It can be therefore be concluded from these data that there was no statistically significant positive or negative correlation between plaque FDG uptake, and either macrophage or smooth muscle cell content, as assessed by FDG phosphor imaging and quantitative immunohistochemistry.

There was a non-significant positive correlation between macrophage content and FDG uptake, with $r = 0.56$ and $p = 0.19$, which reflects the variability of results between different carotid samples.

4.3.3 Tritiated deoxyglucose autoradiography of carotid atherosclerosis

Carotid plaque autoradiography with tritiated deoxyglucose was performed on six plaque specimens, in an attempt to pin down the cell type responsible for the FDG uptake into plaques that had been noted in the phosphor imaging experiments presented above.

However, three of these six plaques were heavily calcified, meaning that the cutting of sections from the exposed tissue was impossible; further analysis of these plaques was not feasible. Therefore, images shown here were obtained from the three plaques in which autoradiography was successful. In addition, two further carotid endarterectomy specimens were used as negative controls (not exposed to tritium, but fixed, coated with autoradiographic emulsion, developed and stained with H and E). This was done firstly to ensure that the autoradiographic process itself did not cause the development of silver grains in the tissue, and secondly that non-specific reactions within the plaques could not precipitate silver in the absence of radioactivity.

In all plaques studied, silver grains were present in the macrophage-rich areas, especially at the lipid core/fibrous cap border of the lesions, implying accumulation of HDG in those areas. There was little uptake seen in other areas of the plaques.

Figure 4.2 shows a representative example of carotid atheroma tritiated autoradiography with HDG uptake seen in the fibrous cap/lipid core region. Figure 4.3 shows autoradiographic images in the top row, and the same images viewed under dark field microscopic conditions in the bottom row. The use of dark field microscopy

helps to improve the visualisation of the silver grains, which become more striking under these conditions. Figure 4.4 confirms, at higher magnification, the development of silver grains within macrophages near the lipid core area of the plaque. Control sections, prepared without radioactivity, (Figure 4.5) showed no development of silver grains.

4.4 DISCUSSION

In this chapter, freshly excised carotid atheroma, taken from patients with recent symptoms and hence by definition unstable, was incubated with FDG under conditions designed to mimic those encountered during clinical PET scans.

Results showed that these tissue sections, composed largely of surgically removed arterial intima, were capable of accumulating FDG, and moreover, they did this in a heterogeneous manner both within and between adjacent sections of the same plaque. There was a trend towards a positive association between the degree of FDG uptake and the macrophage content of the tissue, expressed as a percentage of total area, but this did not reach statistical significance. There did not seem to be any discernable relationship between percentage content of vascular smooth muscle cells and FDG accumulation by symptomatic atheroma.

Following on from these observations, tritiated autoradiography revealed a strong co-localisation between plaque areas containing large numbers of macrophages and HDG uptake, which was consistent across all plaques studied. This relationship might account for the heterogeneous uptake of FDG into the plaque sections, because it is well known that macrophage content can vary widely within different areas of the same plaque (Boyle, 1997; Jander et al., 1998; Stary et al., 1995). How can the differences between the autoradiography results and the immunohistochemical-based studies be accounted for?

One possible explanation lies with the choice of antigen targeted by immunohistochemistry. CD68 antigen is expressed on the macrophage cell surface as well as the cytoplasm (Pulford et al., 1990). This means that as well as labelling viable cells, CD68 also stains dead macrophages that clearly cannot accumulate FDG. There are often large numbers of these non-viable cells found within the lipid core of the plaque. This means that with the method used for calculating macrophage area based on area of CD68 staining, there was probably often an overestimate of the number of viable macrophages in a particular plaque section, causing any relationship between FDG uptake and true macrophage content to be diluted.

A second factor is that, even with perfect immunohistochemical quantification of macrophages contained within a plaque, all the plaques analysed in this work were taken from recently symptomatic patients, and therefore by definition were unstable and contained large numbers of macrophages. In order to determine more easily whether a relationship truly exists between FDG uptake and cellular composition of the plaque, specimens containing a range of macrophage numbers from few to many would need to be analysed. The source of plaques in this work meant that this was not possible. It may be that animal studies of experimental atherosclerosis might be able to fulfil this need by providing plaques in various stages of development containing a broader range of inflammatory cells.

In order to improve the tritiated autoradiography technique, it was intended to perform immunocytochemistry against CD68 on adjacent sections of plaques. This was attempted several times, but there were technical difficulties because of the inability of the CD68 antibody to penetrate the autoradiographic emulsion and it proved impossible. Instead, the autoradiography sections were analysed by a local atherosclerosis expert histopathologist (Dr Martin Goddard, Papworth hospital), who confirmed that the silver grains were co-localised to macrophages on the H and E sections. Nevertheless, it will be important in future work to make provision for the compatibility of the autoradiographic emulsion and the antibody to allow staining of adjacent sections to be accomplished.

Biologically, the conclusion that macrophages are responsible for the majority of FDG uptake within plaque makes sense, and sits well with the cell work presented in Chapter 3, which showed that macrophage HDG uptake could be modified by changing the activation state of the cells. In addition, later work, to be described in the following chapter, shows that unstable symptomatic plaques are responsible for greater FDG uptake than stable asymptomatic lesions, which also fits with what has been demonstrated here.

If future studies support this work, namely that macrophages are the main source of metabolic activity within the atherosclerotic plaque, it might be profitable to use a more macrophage-specific positron-emitting compound than FDG, such as (¹¹C) 1-(2-chlorophenyl)-N-methyl-N-(1-methylpropyl)-1-isoquinolonecarboxamide (PK11195)

to repeat studies of this type. This is a ligand that binds with high affinity to the peripheral benzodiazepine receptor (Langer et al., 1988). These receptors, which have now been cloned (Weizman et al., 1993), are found at high concentrations within activated glial cells in the brain. Receptors are also found in monocytes, and at high densities in macrophages, especially when the cells are activated (Rocca et al., 1993). The receptors are expressed on mitochondrial membranes, and thus binding is not possible after cell death. This approach should enable better identification and quantification of viable macrophages within plaque specimens.

The results from this chapter paved the way for *in-vivo* FDG-PET studies of human atherosclerosis, which are described in Chapter 5.

4.5 REFERENCES

1. Boyle, J. J. (1997). Association of coronary plaque rupture and atherosclerotic inflammation. *J.Pathol.*, 181, 93-99.
2. Jander, S., Sitzer, M., Schumann, R., Schroeter, M., Siebler, M., Steinmetz, H., & Stoll, G. (1998). Inflammation in high-grade carotid stenosis: a possible role for macrophages and T cells in plaque destabilization. *Stroke*, 29, 1625-1630.
3. Johnston, R. F., Pickett, S. C., & Barker, D. L. (1990). Autoradiography using storage phosphor technology. *Electrophoresis*, 11, 355-360.
4. Langer, S. Z. & Arbilla, S. (1988). Limitations of the benzodiazepine receptor nomenclature: a proposal for a pharmacological classification as omega receptor subtypes. *Fundam.Clin.Pharmacol.*, 2, 159-170.
5. Lehr, H. A., van der Loos, C. M., Teeling, P., & Gown, A. M. (1999). Complete chromogen separation and analysis in double immunohistochemical stains using Photoshop-based image analysis. *J.Histochem.Cytochem.*, 47, 119-126.
6. Pulford, K. A., Sipos, A., Cordell, J. L., Stross, W. P., & Mason, D. Y. (1990). Distribution of the CD68 macrophage/myeloid associated antigen. *Int.Immunol.*, 2, 973-980.
7. Rocca, P., Bellone, G., Benna, P., Bergamasco, B., Ravizza, L., & Ferrero, P. (1993). Peripheral-type benzodiazepine receptors and diazepam binding inhibitor- like immunoreactivity distribution in human peripheral blood mononuclear cells. *Immunopharmacology*, 25, 163-178.
8. Ross, R. (1999). Atherosclerosis--an inflammatory disease. *N.Engl.J.Med.*, 340, 115-126.
9. Stary, H. C., Chandler, A. B., Dinsmore, R. E., Fuster, V., Glagov, S., Insull, W., Jr., Rosenfeld, M. E., Schwartz, C. J., Wagner, W. D., & Wissler, R. W. (1995). A definition of advanced types of atherosclerotic lesions and a histological classification of atherosclerosis. A report from the Committee on Vascular Lesions of the Council on Arteriosclerosis, American Heart Association. *Arterioscler.Thromb.Vasc.Biol.*, 15, 1512-1531.
10. Weizman, R. & Gavish, M. (1993). Molecular cellular and behavioral aspects of peripheral-type benzodiazepine receptors. *Clin.Neuropharmacol.*, 16, 401-417.

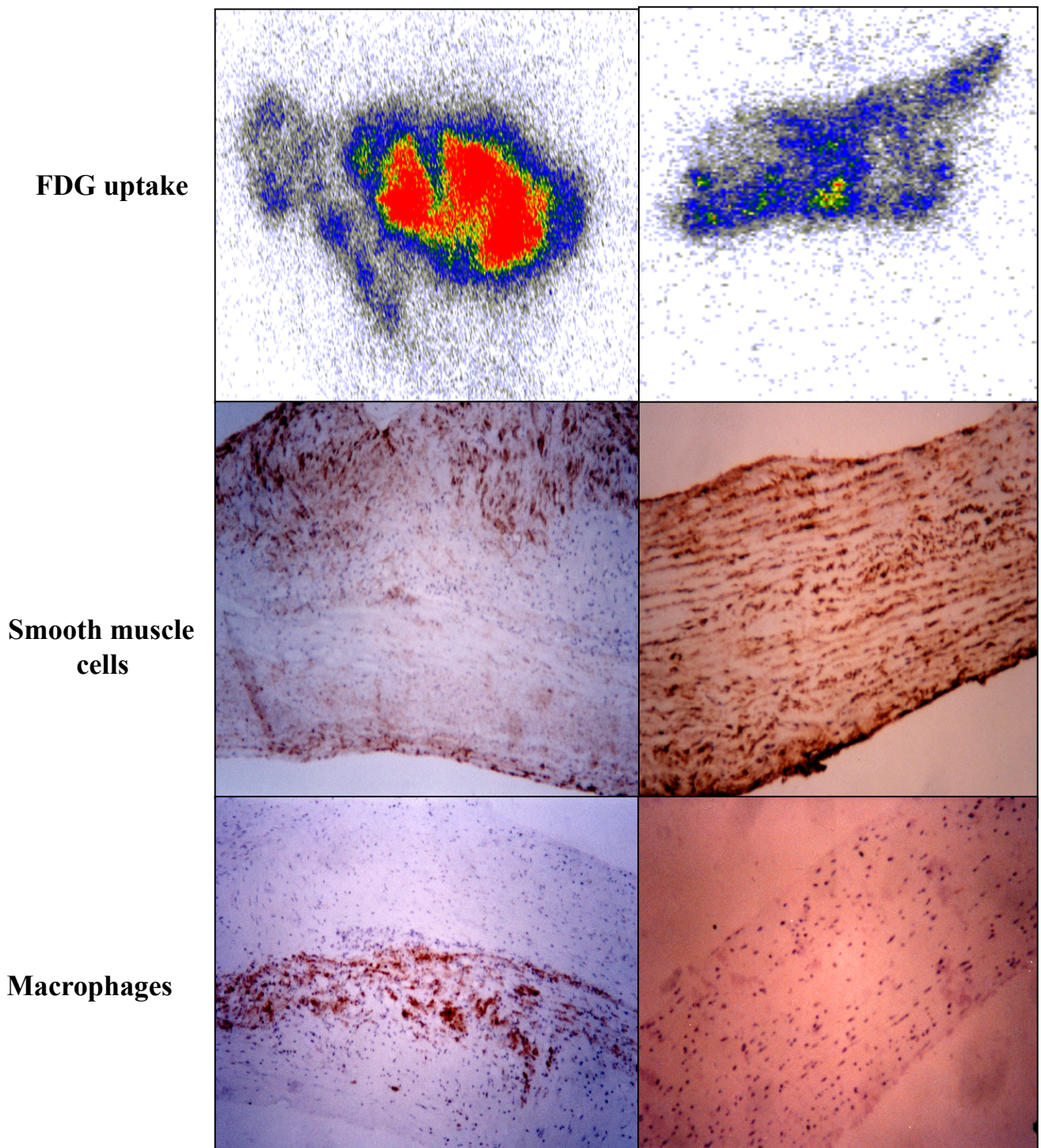


Figure 4.1 Plaque FDG phosphor imaging

Comparison of FDG uptake by phosphor imaging within two sections of plaque (top row), with corresponding histology for vascular smooth muscle cells and macrophages (middle and bottom rows respectively), magnification x20.

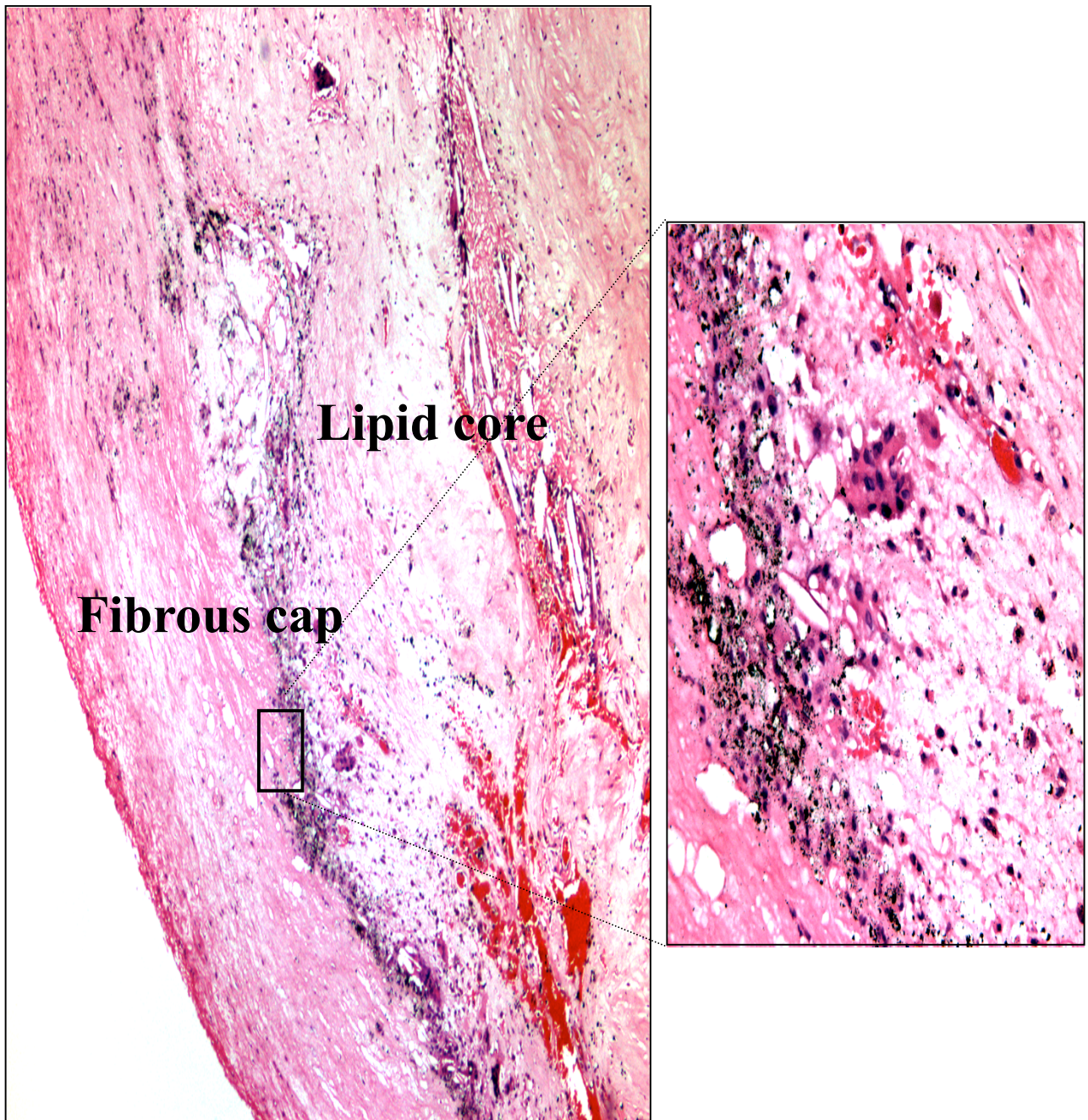


Figure 4.2 Plaque HDG autoradiography (1)

A section of plaque is shown at magnifications x10 and x20, counterstained with H and E. The black dots are silver grains, and their presence implies HDG uptake. This is noted especially at the fibrous cap/lipid core junction

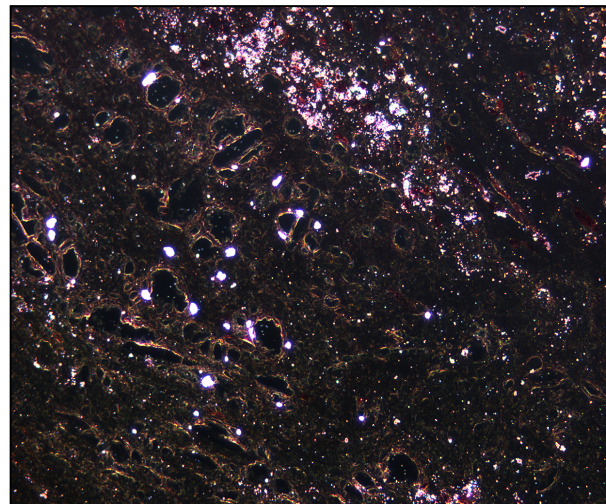
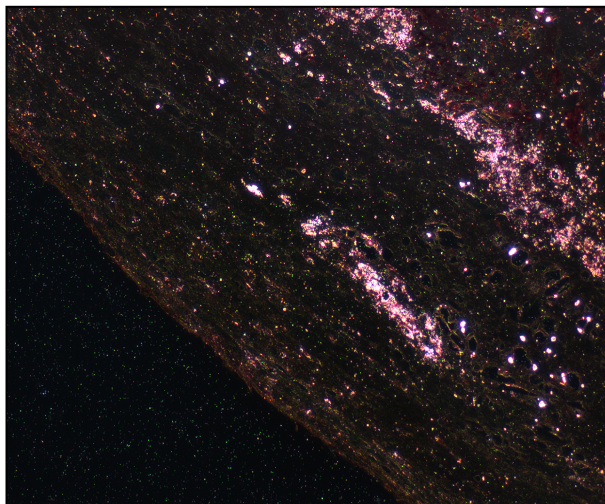
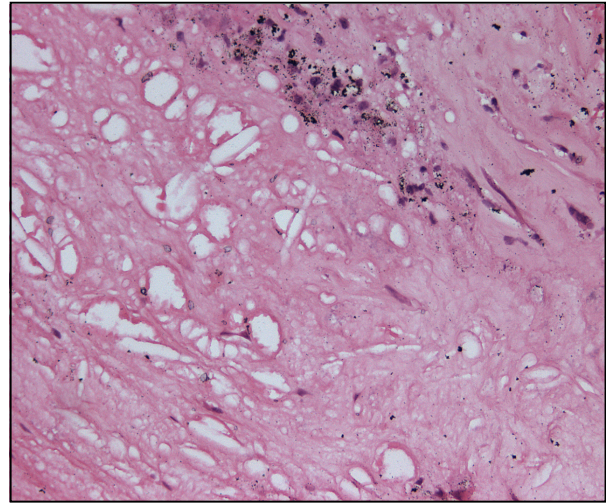
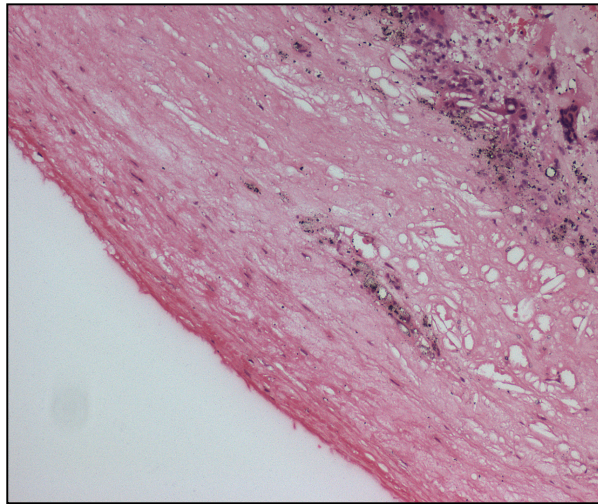


Figure 4.3 Plaque HDG autoradiography (2)

The top row shows HDG plaque autoradiography, whilst on the bottom row are the same sections viewed under dark field conditions in order to improve the visibility of the silver grains. Magnification x10 for the left hand images, x20 for the right hand images.

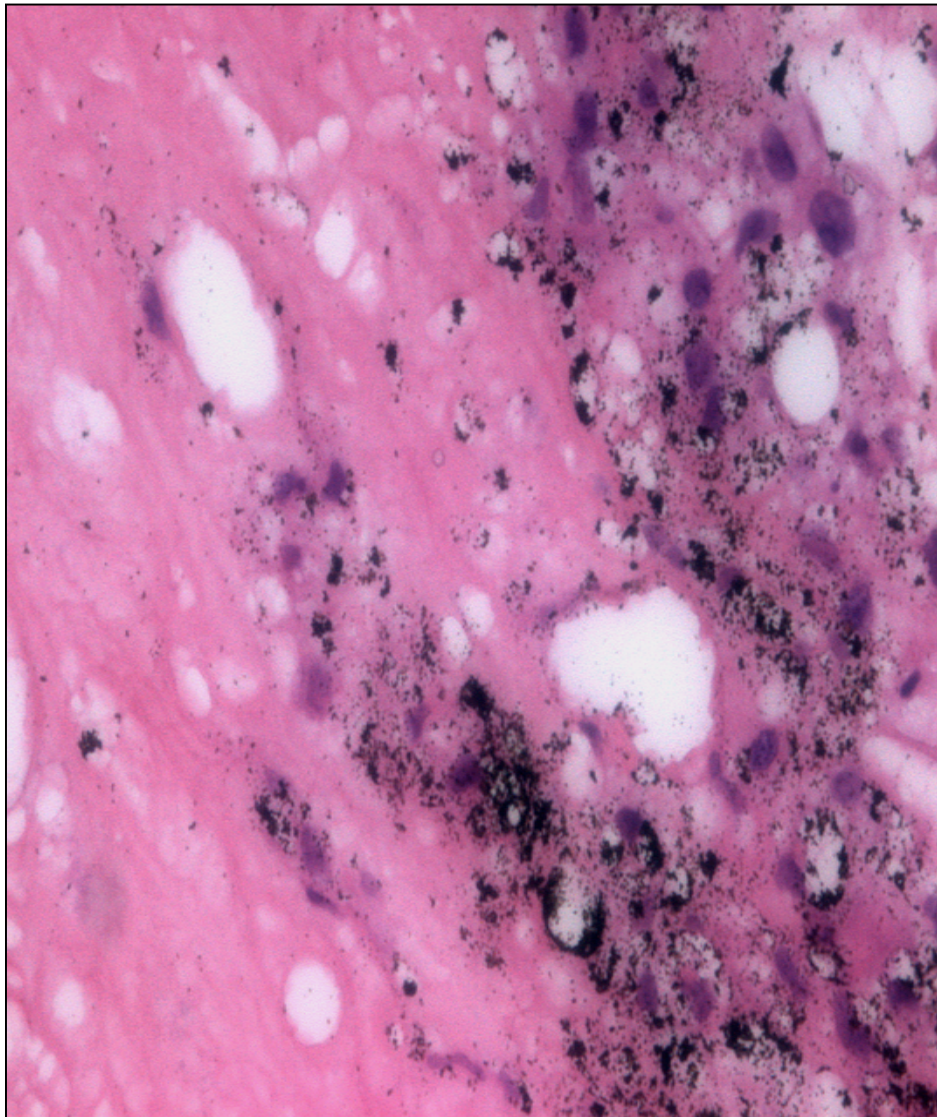


Figure 4.4 Plaque HDG autoradiography (3)

High power autoradiographic image showing cellular localisation of silver grains within macrophages. Magnification x40.

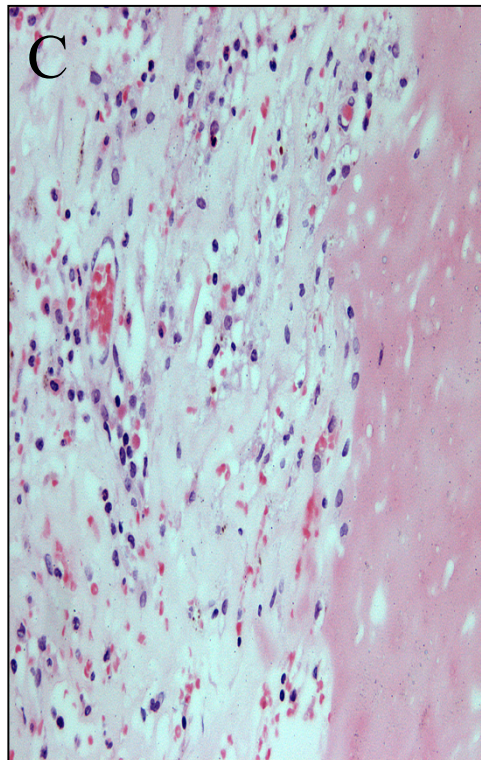
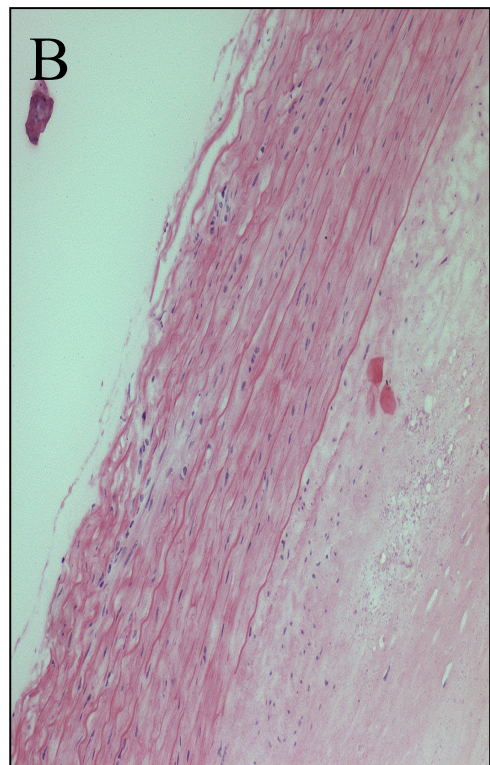
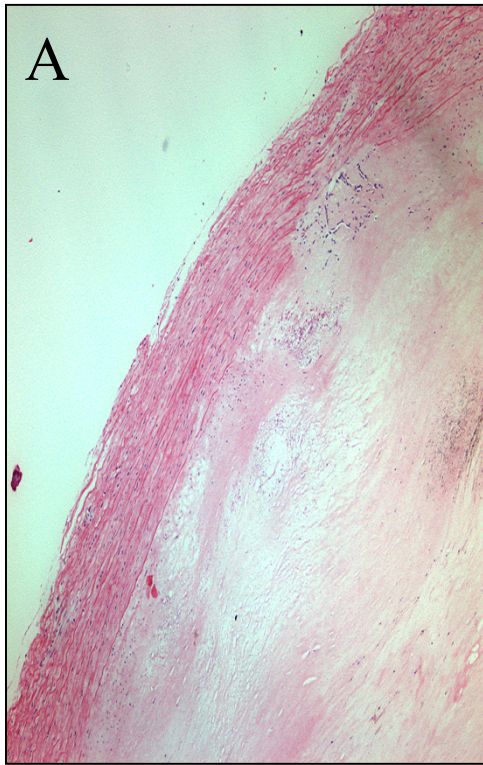


Figure 4.5 Plaque HDG autoradiography (4)

Control images of plaque prepared without radioactivity, shown at low (x10), medium (x20) and high (x40) magnification (A,B and C respectively). There are no silver grains present.

Chapter 5

CHAPTER 5

THE UPTAKE OF FDG IN HUMAN ATHEROSCLEROSIS

5.1 INTRODUCTION

Having demonstrated in Chapters 3 and 4 that deoxyglucose accumulates in macrophages in culture and in atherosclerotic plaque, the hypothesis that FDG-PET might be of use to visualise and quantify inflammatory cell activity within atheroma in patients with carotid artery disease was tested.

There is a need to quantify plaque inflammation, firstly to predict risk of plaque rupture and secondly to monitor the effects of atheroma-modifying therapies. This is crucial since recent experimental and clinical studies strongly suggest that HMG Co-A reductase inhibitors promote plaque stability by decreasing plaque macrophage content and activity without substantially reducing plaque size and therefore angiographic appearance (Williams et al., 1998; Stefanadis et al., 2002; Crisby et al., 2001), making angiography a poor tool for monitoring purposes.

FDG-PET has been used successfully by others to image inflammation *in vivo* in a variety of inflammatory conditions, including polymyalgia rheumatica, Takayasu arteritis, inflammatory bowel disease and asthma (Skehan et al., 1999; Taylor et al., 1996; Blockmans et al., 1999; Hara et al., 1999). However, none of these studies has been able to determine which cell type was responsible for the accumulation of FDG within the tissue studied.

As far as atherosclerosis is concerned, there have been several reports of FDG uptake noted in blood vessels of patients undergoing whole body FDG-PET imaging for staging of malignant disease (Yun et al., 2001; Machac et al., 2001). These studies have shown a correlation between the degree of FDG uptake and the presence of vascular risk factors. However, neither report examined histological correlations or used any form of anatomical co-registration with the PET images. More direct

evidence that FDG might be taken up in atherosclerosis has come from work in cholesterol-fed rabbits, where the degree of FDG uptake in lesions correlated with their macrophage density (Lederman et al., 2001; Badimon et al., 1999).

As noted in the Chapter 1, symptomatic carotid plaques causing transient ischaemic attack are characterised by the presence of thin fibrous caps, large volume lipid cores and low smooth muscle cell to macrophage ratios (Svindland et al., 1988; Jander et al., 1998; Feeley et al., 1991; Golledge et al., 2000; Galis et al., 1994; Sukhova et al., 1999). Consistent with this, several investigators have found increased temperatures within atherosclerotic plaques (Casscells et al., 1996; Stefanadis et al., 2002; Stefanadis et al., 1999; Stefanadis et al., 2000); this has been ascribed to inflammation within the lesions, with symptomatic unstable plaques being hotter than stable ones.

In patients who sustain a TIA, the risk of stroke is greatest in the three months following the event (Warlow et al., 1996a), implying a period during which the culprit plaque is unstable. This risk is greatly reduced by carotid endarterectomy (Warlow et al., 1996b; ECST Group, 1998). There is therefore a window of opportunity, between symptoms and surgery, for imaging unstable atheroma.

5.2 METHODS

Three preliminary one hour 2-D dynamic PET studies were performed as pilot studies ('Pilot 2-D dynamic imaging protocol'). Unfortunately, in all cases, high FDG blood signal was problematic, giving rise to a low plaque-to-background contrast. In addition, there was neck movement both during and between the PET and CT scans which made anatomical co-registration very difficult.

In order to improve matters, the PET protocol was amended ('Late imaging protocol'). Scanning mode was changed to 3-D in order to improve sensitivity, but at the expense of increased scatter. A stiff cervical collar was employed to minimise patient movement between the PET and CT scans. A higher dose of FDG was administered, and images were acquired later than previously, at 90 and 180 minutes after tracer injection, in order to try to enhance plaque-to-blood contrast. In addition, fiducial markers were employed to improve anatomical co-registration of the two scans.

In parallel experiments, two 3-D dynamic PET studies were performed, with stiff collar, arterial blood sampling and fiducial markers, in a quest to obtain kinetic data and perform Patlak analysis.

Subsequently, in order to image plaque with high resolution, some patients having PET scans also underwent high-resolution MR scanning of the carotid arteries. By using this dual approach to carotid imaging, it was hoped to be able to combine detailed plaque anatomy (from HRMR) with functional metabolic information (from FDG-PET) within a single image.

5.2.1 Patient recruitment

Patients were recruited from the Addenbrookes Neurovascular clinic, a rapid access clinic for patients with suspected TIA. All had experienced a recent carotid-territory TIA with an internal carotid artery stenosis of at least 70%, confirmed angiographically prior to the PET study. Patients were excluded if they had either

carotid artery occlusion or diabetes. The study protocol was approved by the local ethics committee and the UK Administration of Radioactive Substances Advisory Committee. All patients gave written informed consent.

5.2.2 Computed tomography protocol

Using a GE Hispeed Advantage CT scanner (GE Medical Systems, Milwaukee, U.S.A.), helical contrast CT angiograms were acquired from skull base to 3 cm below the level of the carotid bifurcation. CT was performed immediately after PET imaging. The contrast agent used was iopamidol (Niopam).

5.2.3 PET protocols

All PET imaging was carried out using a GE Advance PET scanner (GE Medical Systems, Milwaukee, U.S.A.), with the subject in a fasting state to avoid insulin-induced hypoglycaemia (which may increase FDG uptake in brain and muscle tissue (Torizuka et al., 1997)). PET images were reconstructed using the PROMIS algorithm (Kinahan et al., 1989), with corrections applied for attenuation, dead time, scatter and random coincidences.

5.2.3.1 Pilot 2-D dynamic imaging protocol

185 MBq of FDG were injected at the start of the study. PET images were acquired in 2-D mode, as 5x1, 5x2 and 9x5 minute frames with venous blood sampling taking place throughout the study.

5.2.3.2 Late imaging protocol

370 MBq FDG were administered intravenously over 60 seconds. PET images (as 4x 5 minute frames) were acquired in 3-D mode, approximately 90 and 180 minutes after FDG administration. A stiff cervical collar was worn to minimise patient movement, being put into position, along with fiducial markers, shortly before the start of image acquisition.

5.2.3.3 3-D dynamic imaging protocol

This protocol required the insertion of an arterial line under local anaesthesia prior to imaging to enable measurement of arterial activity. 185 MBq FDG was administered intravenously over 60 seconds, and PET data were acquired in 3-D mode continuously as 5x1 minute, 5x2 minute and 21x5 minute frames. A cervical collar and fiducial markers were positioned at the start of imaging.

5.2.4 Image co-registration

Rigid body co-registration with CT images was performed manually, using a combination of four fiducial markers (Intermark, Bromley, UK) and internal anatomical landmarks (spinal cord and muscles of the jaw and neck). This resulted in co-registration typically to within 1mm in each dimension around the stenosis. The fiducial markers, comprising a vanadium-48 disc (2mm diameter) within a CT-visible hydrogel annulus, were placed bilaterally on the temporomandibular joints, on the point of the chin, with the fourth marker just to the left of the central chin marker, to facilitate subsequent left/right orientation during image reconstruction and analysis. Automated rigid body co-registration was attempted, but was difficult because of occasional different degrees of neck flexion between the PET and CT studies. It was for this reason that the manual system was chosen for these studies. The software package 'MPI tool' (Max Planck Institut, Cologne, Germany) was used to display both the CT and PET images and apply translational and rotational offsets to co-register the images. The program 'XV image' (John Bradley – University of Philadelphia) was used to convert Raster File images to Tagged Image File Format files that could be printed as hard copies.

5.2.5 Quantification of plaque FDG concentration in late imaging studies

To estimate plaque FDG concentration in the late imaging studies, three-dimensional volumes of interest (VOI) were drawn around the area of stenosis on the contrast CT scan using the Analyze software package (Robb et al., 1991). These regions were then placed onto the co-registered PET images to produce mean FDG concentration values (kBq/ml) for the early and late timepoints. The mean VOI size was 148 mm³ (range

100-305mm³). Plasma FDG concentration up to the scan time was measured to generate the input function. The use of venous blood to generate input function data has been shown to be equivalent to arterial blood approximately 30 minutes post-FDG injection (Ratib et al., 1982; Phelps et al., 1979). Therefore, with imaging times much later than this, it was assumed that venous blood sampling would be adequate for quantification of the late imaging studies.

A semi-quantative method was used to derive information about FDG uptake into the VOI. Ideally, as explained in Chapter 1, one would quantify FDG metabolism in terms of FDG metabolic rate and relate this to metabolic rate for glucose (MRGlc) by multiplying by the lumped constant. However, this would require knowledge of the rate constants (k1-k4), which are not yet defined for atherosclerotic plaque. Hence, it was decided to express FDG uptake in terms of the net FDG accumulation rate (see below for derivation). This parameter is more accurate than quoting SUV, as it uses the integral of the measured input function, whereas SUV only approximates the integral of the input function from the injected FDG dose and body mass.

The estimated net FDG accumulation rate was determined by dividing the mean decay-corrected plaque FDG concentration in the VOI by the integral of the decay-corrected input function. It is expressed in units of sec⁻¹.

$$\text{Net FDG accumulation rate (sec}^{-1}\text{)} = \frac{\text{Decay-corrected plaque FDG concentration (kBq/ml)}}{\text{Integral of the decay-corrected input function (kBqsec/ml)}}$$

In three patients who presented with unilateral carotid artery disease, where there was no contralateral asymptomatic stenosis around which to draw VOI's, a direct vessel wall-to-plasma FDG uptake ratio was calculated to assess tracer uptake into the angiographically normal artery. To determine this value, a VOI was drawn around the asymptomatic carotid bifurcation on the CT scan, and then placed onto the co-registered PET scan. The Analyze software package was then employed to obtain the FDG concentration value (kBq/ml) within the VOI. This figure was then divided by

the plasma FDG activity at the mid-frame time (kBq/ml) to derive the vessel wall-to-plasma FDG uptake ratio. This approach was chosen because a vessel wall-to-plasma ratio of 1.0 indicated that the FDG signal was purely due to FDG in blood, i.e. no FDG uptake into the vessel wall. This would not have been so clearly demonstrated using net FDG accumulation rate.

5.2.6 Quantification of plaque FDG concentration in 3-D dynamic studies

To express FDG uptake in the dynamic studies performed, Patlak plots were constructed, as described in Chapter 1. The fundamental assumption in this model is that the tracer is essentially trapped in the bound tissue compartment so that k_4 approximates zero (See Figure 1.2 in Chapter 1). As in the late imaging protocol, volumes of interest were drawn using the software package ‘Analyze’ to derive numerical data for the construction of Patlak plots. The input function was obtained from arterial sampling during the study

5.2.7 High-resolution magnetic resonance (HRMR) protocol

Images were acquired using a dedicated phased-array KNEEPA neck MR coil, on a GE systems 1.5 Tesla scanner. The coil was positioned over the carotid bifurcations after scout images had been acquired. An axial gated blood suppressed fast spin echo sequence was employed to acquire proton density weighted images (Echo Time (TE) = 38.4msec, echo train length (ETL) = 24, bandwidth = 31.2kHz, FOV=10x10cm, slice thickness = 3.0/0.0, gating = 2 x RR, matrix = 256x256, number of excitations (NEX) = 2, frequency direction = R/L, to cover 1cm inferior to the bifurcation and 4cm superior, i.e. total coverage of 5cm at 3mm thickness, i.e. 17 slices). This protocol resulted in an in-plane resolution of 0.39 x 0.39 mm.

T2 weighted images were acquired as above, but with TE = 100.4, and fat suppression and STIR images were also taken by appropriate selection from the MR setup menus.

Image co-registration of HRMR to FDG-PET studies was performed using the following sequence : The PET data were co-registered to the corresponding CT images by applying shifts (rotations and offsets) to the CT images where necessary,

using the software package 'MPI Tool'. Following PET and CT co-registration, the next step was to co-register the CT and the MR data, once again using MPI Tool, and applying shifts to the MR images only. Therefore, finally, the PET and MR scans could be co-registered by the summation of the two sets of shifts. This co-registration technique ensured a better accuracy than directly co-registering the PET and MR scans due to the limited extent of the MR studies in the 'z' direction and the relative lack of anatomical detail in PET.

5.2.8 Plaque histological characterisation

Following surgery, carotid endarterectomy samples were fixed, blocked and sectioned to 5 μ m thickness. Slides were stained with haematoxylin and eosin, and immunohistochemistry was performed against macrophages and vascular smooth muscle cells according to Sections 2.3.2 and 2.3.1.3 in Chapter 2.

5.3 RESULTS

5.3.1 Patient characteristics

Thirteen symptomatic patients were recruited for FDG/CT imaging with the late imaging PET protocol. Of these, useful data was acquired in 10 subjects. Of the three studies that did not yield useful data, one patient did not proceed to carotid endarterectomy because his TIA was felt to be due to a cardiac embolus, a further patient had a tissue FDG injection, and the third patient did not complete the scanning protocol because of claustrophobia; the procedure was halted after a few minutes.

Two patients underwent the 3-D dynamic PET protocol. Of these, only one yielded a dataset that could be used for Patlak analysis. The other patient did not complete the imaging protocol because of claustrophobia.

Seven patients underwent high-resolution MR scanning in addition to FDG-PET and CT imaging.

5.3.2 Late imaging protocol

The baseline characteristics of the 10 symptomatic patients imaged with the late protocol, along with those from the one satisfactory dynamic imaging subject are shown in Table 5.1. The median time between symptoms and PET study was 4 months, and between PET and carotid endarterectomy was 39 days.

In all 10 patients, co-registered late PET images acquired around three hours revealed FDG accumulation at the site of the symptomatic plaque, enhanced above surrounding tissue (Figure 5.1). Figure 5.2 shows an example of late FDG uptake in an asymptomatic plaque. Figure 5.3 shows late FDG uptake in the coronal and sagittal views, demonstrating unilateral uptake of FDG in this patient.

Normal physiological FDG uptake can be seen in these studies, for example in brain, salivary glands (Jabour et al., 1993) and laryngeal muscles (Kostakoglu et al., 1996). Some of this uptake is visible in these figures and it emphasises the importance of accurate anatomical co-registration to ensure that FDG uptake is anatomically correctly localised.

Seven of the ten patients had contralateral asymptomatic stenoses ranging from 35%-75% measured angiographically. A comparison was made between the late net FDG accumulation rate in symptomatic plaques and contralateral asymptomatic plaques. In all cases, symptomatic lesions had higher FDG accumulation rates than asymptomatic lesions; the mean late symptomatic net accumulation rate was $8.23 \times 10^{-5} \pm 0.58 \times 10^{-5} \text{ sec}^{-1}$, 95% CI:($6.91-9.55 \times 10^{-5}$), the mean late asymptomatic net accumulation rate was $6.33 \times 10^{-5} \pm 0.82 \times 10^{-5} \text{ sec}^{-1}$, 95% CI:($4.33-8.34 \times 10^{-5}$), with a mean difference between symptomatic and asymptomatic lesions of $1.90 \times 10^{-5} \pm 0.47 \times 10^{-5} \text{ sec}^{-1}$, 95% CI:($0.75-3.05 \times 10^{-5}$) (**p=0.008**). Table 5.2 lists the net FDG accumulation rates for all symptomatic and asymptomatic plaques at both the early and late time points.

The corresponding early values were as follows : mean early symptomatic net accumulation rate was $11.27 \times 10^{-5} \pm 0.87 \text{ sec}^{-1}$, 95% CI:($9.31-13.22 \times 10^{-5} \text{ sec}^{-1}$). The mean early asymptomatic net accumulation rate was $10.34 \times 10^{-5} \pm 0.92 \text{ sec}^{-1}$, 95% CI:($8.08-12.60 \times 10^{-5} \text{ sec}^{-1}$), with a mean difference between symptomatic and asymptomatic of $1.14 \times 10^{-5} \pm 0.74 \times 10^{-5} \text{ sec}^{-1}$, 95% CI:($-0.67-2.95$). The p value for the difference between symptomatic and asymptomatic plaques at the earlier time point was not significant (**p=0.175**). The mean early and late mid frame times were 101.8 (± 4.6) and 186.4 (± 5.9) minutes respectively.

Three patients had angiographically normal arteries on the asymptomatic side, with no significant uptake of FDG into those vessels; neither the early nor the late FDG concentration in a VOI around the carotid bifurcation differed significantly from that measured in plasma (mean early wall-to-plasma FDG concentration ratio = 0.9 ± 0.1 , mean late wall-to-plasma FDG concentration ratio = 1.2 ± 0.2).

Histological examination of the excised symptomatic plaques from all patients who had undergone imaging revealed heavy macrophage infiltration. Examples are shown in Figures 5.4 (Patient 1) and 5.5 (Patient 9).

5.3.3 Dynamic imaging PET protocol

Dynamic imaging studies were performed in five subjects; three of these were part of preliminary pilot work and were performed in 2-D mode. Images from one of these studies are shown in Figure 5.6.

Two further 3-D dynamic scans were performed, but only one study yielded useful data and this is shown in Figure 5.7. The patient was a 79 year old male who presented with a short history of left sided hemiparesis. He had several major vascular risk factors, and carotid angiography revealed a significant right internal carotid artery stenosis measuring 79%, there was disease on the left side amounting to a 29% stenosis.

FDG-PET, CT and co-registered images from both carotid regions are shown in Fig 5.7. The PET images were derived from the final frames of the study, one hour after FDG administration. FDG uptake is seen bilaterally in the carotid artery wall (arrowed), starting from well below the carotid bifurcation and extending upwards into the internal carotid artery, consistent with the extent of atherosclerotic disease noted angiographically.

Patlak plots of the carotid stenosis regions on both sides were constructed using the arterial input function and 'Analyze' data from VOI's drawn around the regions of stenosis.

Plots are presented in Figures 5.8 and 5.9. Figure 5.8 shows the plot for the symptomatic stenosis in the right carotid artery. It is plotted from a mid-frame time of 8 minutes to the end of the scan. Similarly, Figure 5.9 is the plot derived from data gathered for the left-sided asymptomatic stenosis. Both graphs have linear regression lines plotted on the same axes. Of note is the gradient of the linear plot (shown in bold on each plot). For the symptomatic lesion, the gradient is 0.82, compared to 0.67 for

the asymptomatic side. Recalling that the gradient of a Patlak plot is directly proportional to the metabolic rate of glucose usage in the region of interest (MRGlc) (Chapter 1 Section 1.5.6.3.2), it appeared that, in this patient, the MRGlc was greater in the symptomatic lesion than in the contralateral asymptomatic stenosis.

5.3.4 FDG-PET/HRMR imaging

Co-registered FDG-PET and HRMR images were acquired in seven patients. Representative FDG-PET with co-registered HRMR images are shown in Figures 5.10, 5.11, 5.12 and 5.13. Full explanations of the images and arrows are given in the figure legends.

5.4 DISCUSSION

Anecdotal reports of ‘hot spots’ in blood vessels of patients at high risk of atherosclerosis undergoing whole body FDG-PET studies for oncological indications, along with a single study in cholesterol-fed rabbits (Lederman et al., 2001), have suggested that FDG may accumulate in atherosclerotic plaques *in vivo*.

By combining PET and CT imaging, with the addition of HRMR in some cases, it has been demonstrated in this chapter that FDG accumulates in human carotid artery atherosclerotic plaques, with significantly higher uptake in symptomatic than in asymptomatic lesions 3 hours after injection (23% greater).

At earlier timepoints, the differences in FDG accumulation between symptomatic and asymptomatic lesions were not significant; this fact justifies the decision to modify the original protocol to extend data acquisition out to three hours. Net FDG accumulation rates were on average lower in the late frames; this is likely to be due to the fact that k_4 is becoming more significant later on in the study.

The Patlak plots in Figures 5.8 and 5.9, albeit in a single subject, showed a steeper positive gradient (thus implied higher metabolic activity) in symptomatic than asymptomatic plaque. Furthermore, it has already been demonstrated in Chapter 4, at least *in vitro*, that the majority of deoxyglucose accumulates in macrophage-rich areas of plaques, perhaps explaining the results shown in this chapter: namely that inflammation is present to a greater degree in symptomatic than asymptomatic plaques.

These results suggest that FDG-PET may be capable of imaging and potentially quantifying plaque inflammation. This raises the possibility that FDG-PET could be used to predict risk of future plaque rupture, and perhaps therefore to target carotid surgery to high-risk stenoses regardless of angiographic appearance. More importantly perhaps, this approach might be used to monitor effectiveness of systemic atheroma-modifying treatments, since it is likely that any measurable effects of treatment on inflammation in carotid atheroma will reflect similar changes in other vascular beds, including the coronary arteries (Hulthe et al., 1997).

Before this potential can be realised, further studies are required to determine the precise relationship between FDG uptake, plaque macrophage activity and risk of plaque rupture. Histological and experimental data point to a close correlation between macrophage infiltration and plaque rupture. Furthermore, animal data suggest that statins stabilise plaques by attenuating plaque inflammation, thereby reducing clinical events. However, the implication from this work, that measured differences in plaque FDG uptake do indeed reflect differences in plaque macrophage content or activity (the two are not necessarily equivalent) needs to be confirmed. However, such confirmation would require measurements of FDG uptake in a number of plaques containing a spectrum of macrophage infiltration, ranging from large fibrotic plaques with little macrophage infiltration to small intensely inflamed plaques. Since it was possible only to obtain clinical specimens from patients undergoing carotid surgery for symptomatic, severely stenotic disease (the criteria for surgical intervention), there was access only to plaques that, by definition, were unstable and were, not surprisingly therefore, heavily infiltrated with macrophages. In other words, plaques were only available from one end of the disease spectrum. Thus, in this population, very large numbers of specimens would be required to obtain a statistically meaningful correlation between FDG uptake and macrophage number, particularly when one considers the inherent inaccuracies in trying to quantify macrophage content histologically. Therefore, the only way to address this important issue is by employing an animal model of atherosclerosis, in which plaque size and inflammation can be independently manipulated. A preliminary study using such a model was undertaken, and the results are presented and discussed in the Chapter 6.

Although PET has limited spatial resolution ($\sim 5\text{mm}$ FWHM for GE Advance), it has been shown here that image co-registration with CT and/or MR can localise the FDG signal to individual atherosclerotic lesions. However, because CT angiography cannot accurately measure plaque volume (because remodelling can accommodate large plaques with little impact on lumen diameter) it was not possible, in this study, to apply a segmentation-based approach to partial volume correction to these data. It will be important in subsequent studies that partial volume error is minimised as much as possible by obtaining high-resolution MR in all subjects. The MR scans could then be segmented into stenosis, blood and background (soft tissue), then blurred to the

resolution of PET (5 x 5 x 6mm) (Meltzer et al., 1999). This will provide an estimate of the components that are contributing to FDG uptake in the stenosis region. Using the input function data, and a partial volume-free estimate of the background from the images in a uniform region away from the blood vessel, an estimate for the tracer concentration in pure stenosis could be calculated. However, this approach assumes a homogeneous tracer uptake in the plaque, which may not be accurate according to the phosphor imaging data presented in Chapter 4, so the situation becomes extremely complex. Even without full partial volume correction, the work in this chapter provides valuable additional information about plaque inflammatory state above that which is achievable by conventional imaging with either angiography, ultrasound, CT or MR.

Future work will help to explore the potential uses and pitfalls of this imaging technique and will include FDG-PET imaging of a group of symptomatic TIA patients both before and after the administration of plaque stabilising drugs, most probably statins. The hypothesis here is that there would be quantifiable differences in FDG signal before and after statin therapy, thereby making the technique useful for monitoring the effect of these disease-modifying drugs. This hypothesis has recently been supported by a study which found that the significant temperature difference between atherosclerotic and healthy artery walls was ameliorated by atorvastatin treatment, achieved by a substantial reduction in macrophage number within the atherosclerotic plaques studied, suggesting a direct anti-inflammatory role for statins (Stefanadis et al., 2002). Additionally, the use of radiotracers that are more macrophage-specific than FDG, such as ¹¹C-PK11195 (Myers et al., 1991), will be evaluated with the hope of improving the plaque/background ratio. This might eventually permit imaging of atherosclerosis in arteries where background uptake of FDG would be prohibitively high, such as those in the cerebral and coronary circulation.

In summary, this chapter provides the first direct evidence that human atherosclerotic plaque inflammation can be assessed non-invasively by FDG-PET, and paves the way for a new approach to atheroma imaging that reflects the cellular pathology of the disease process rather than its anatomical consequences.

5.5 REFERENCES

1. Badimon, J. J., Zyang, Z. Y., Machac, J., Helft, G., Worthley, S. G., Tang, C. Y., Osende, J. I., Lipszyc, H., Buschbaum, M. S., & Fuster, V. (1999). Non-Invasive imaging of atherosclerotic

- plaque macrophage in a rabbit model with F-18 FDG PET: A histopathological correlation. *J.Nucl.Med.*, 40, 88P.
2. Blockmans, D., Maes, A., Stroobants, S., Nuyts, J., Bormans, G., Knockaert, D., Bobbaers, H., & Mortelmans, L. (1999). New arguments for a vasculitic nature of polymyalgia rheumatica using positron emission tomography. *Rheumatology*, 38, 444-447.
 3. Casscells, W., Hathorn, B., David, M., Krabach, T., Vaughn, W. K., McAllister, H. A., Bearman, G., & Willerson, J. T. (1996). Thermal detection of cellular infiltrates in living atherosclerotic plaques: possible implications for plaque rupture and thrombosis. *Lancet*, 347, 1447-1451.
 4. Crisby, M., Nordin-Fredriksson, G., Shah, P. K., Yano, J., Zhu, J., & Nilsson, J. (2001). Pravastatin Treatment Increases Collagen Content and Decreases Lipid Content, Inflammation, Metalloproteinases, and Cell Death in Human Carotid Plaques : Implications for Plaque Stabilization. *Circulation*, 103, 926-933.
 5. ECST Group (1998). Randomised trial of endarterectomy for recently symptomatic carotid stenosis: final results of the MRC European Carotid Surgery Trial (ECST). *Lancet*, 351, 1379-1387.
 6. Feeley, T. M., Leen, E. J., Colgan, M. P., Moore, D. J., Hourihane, D. O., & Shanik, G. D. (1991). Histologic characteristics of carotid artery plaque. *J.Vasc.Surg.*, 13, 719-724.
 7. Galis, Z. S., Sukhova, G. K., Lark, M. W., & Libby, P. (1994). Increased expression of matrix metalloproteinases and matrix degrading activity in vulnerable regions of human atherosclerotic plaques. *J.Clin.Invest*, 94, 2493-2503.
 8. Golledge, J., Greenhalgh, R. M., & Davies, A. H. (2000). The symptomatic carotid plaque. *Stroke*, 31, 774-781.
 9. Hara, M., Goodman, P. C., & Leder, R. A. (1999). FDG-PET finding in early-phase Takayasu arteritis. *J.Comput.Assist.Tomogr.*, 23, 16-18.
 10. Hulthe, J., Wikstrand, J., Emanuelsson, H., Wiklund, O., de Feyter, P. J., & Wendelhag, I. (1997). Atherosclerotic changes in the carotid artery bulb as measured by B- mode ultrasound are associated with the extent of coronary atherosclerosis. *Stroke*, 28, 1189-1194.
 11. Jabour, B. A., Choi, Y., Hoh, C. K., Rege, S. D., Soong, J. C., Lufkin, R. B., Hanafee, W. N., Maddahi, J., Chaiken, L., Bailet, J., & . (1993). Extracranial head and neck: PET imaging with 2-[F-18]fluoro-2-deoxy-D- glucose and MR imaging correlation. *Radiology*, 186, 27-35.
 12. Jander, S., Sitzer, M., Schumann, R., Schroeter, M., Siebler, M., Steinmetz, H., & Stoll, G. (1998). Inflammation in high-grade carotid stenosis: a possible role for macrophages and T cells in plaque destabilization. *Stroke*, 29, 1625-1630.
 13. Kinahan, P. E. & Rogers, J. G. (1989). Analytic 3D image reconstruction using all detected events. *IEEE Trans Nucl Sci*, 36, 964-968.
 14. Kostakoglu, L., Wong, J. C., Barrington, S. F., Cronin, B. F., Dynes, A. M., & Maisey, M. N. (1996). Speech-related visualization of laryngeal muscles with fluorine-18-FDG. *J.Nucl Med.*, 37, 1771-1773.
 15. Lederman, R. J., Raylman, R. R., Fisher, S. J., Kison, P. V., San, H., Nabel, E. G., & Wahl, R. L. (2001). Detection of atherosclerosis using a novel positron-sensitive probe and 18-fluorodeoxyglucose (FDG). *Nucl Med.Commun.*, 22, 747-753.
 16. Machac, J., Zhang, Z., Nunez, R., Chen, W., Macapinlac, H., & Larson, S. (2001). 18F Fluorodeoxyglucose uptake in human thoracic aortas assessed in vivo by positron emission tomography. *J.Nucl.Med.* 54P.

17. Meltzer, C. C., Kinahan, P. E., Greer, P. J., Nichols, T. E., Comtat, C., Cantwell, M. N., Lin, M. P., & Price, J. C. (1999). Comparative evaluation of MR-based partial-volume correction schemes for PET. *J.Nucl Med.*, 40, 2053-2065.
18. Myers, R., Manjil, L. G., Cullen, B. M., Price, G. W., Frackowiak, R. S., & Cremer, J. E. (1991). Macrophage and astrocyte populations in relation to [3H]PK 11195 binding in rat cerebral cortex following a local ischaemic lesion. *J.Cereb.Blood Flow Metab*, 11, 314-322.
19. Phelps, M. E., Huang, S. C., Hoffman, E. J., Selin, C., Sokoloff, L., & Kuhl, D. E. (1979). Tomographic measurement of local cerebral glucose metabolic rate in humans with (F-18)2-fluoro-2-deoxy-D-glucose: validation of method. *Ann.Neurol.*, 6, 371-388.
20. Ratib, O., Phelps, M. E., Huang, S. C., Henze, E., Selin, C. E., & Schelbert, H. R. (1982). Positron tomography with deoxyglucose for estimating local myocardial glucose metabolism. *J.Nucl Med.*, 23, 577-586.
21. Robb, R. A. & Hanson, D. P. (1991). A software system for interactive and quantitative visualization of multidimensional biomedical images. *Australas.Phys.Eng Sci.Med.*, 14, 9-30.
22. Skehan, S. J., Issenman, R., Mernagh, J., Nahmias, C., & Jacobson, K. (1999). 18F-fluorodeoxyglucose positron tomography in diagnosis of paediatric inflammatory bowel disease. *Lancet*, 354, 836-837.
23. Stefanadis, C., Diamantopoulos, L., Dernellis, J., Economou, E., Tsiamis, E., Toutouzas, K., Vlachopoulos, C., & Toutouzas, P. (2000). Heat production of atherosclerotic plaques and inflammation assessed by the acute phase proteins in acute coronary syndromes. *J.Mol.Cell Cardiol.*, 32, 43-52.
24. Stefanadis, C., Diamantopoulos, L., Vlachopoulos, C., Tsiamis, E., Dernellis, J., Toutouzas, K., Stefanadi, E., & Toutouzas, P. (1999). Thermal heterogeneity within human atherosclerotic coronary arteries detected in vivo: A new method of detection by application of a special thermography catheter. *Circulation*, 99, 1965-1971.
25. Stefanadis, C., Toutouzas, K., Vavuranakis, M., Tsiamis, E., Tousoulis, D., Panagiotakos, D. B., Vaina, S., Pitsavos, C., & Toutouzas, P. (2002). Statin treatment is associated with reduced thermal heterogeneity in human atherosclerotic plaques. *Eur.Heart J.*, 23, 1664-1669.
26. Sukhova, G. K., Schonbeck, U., Rabkin, E., Schoen, F. J., Poole, A. R., Billingham, R. C., & Libby, P. (1999). Evidence for increased collagenolysis by interstitial collagenases-1 and -3 in vulnerable human atheromatous plaques. *Circulation*, 99, 2503-2509.
27. Svindland, A. & Torvik, A. (1988). Atherosclerotic carotid disease in asymptomatic individuals: An histological study of 53 cases. *Acta Neurol.Scand.*, 78, 506-517.
28. Taylor, I. K., Hill, A. A., Hayes, M., Rhodes, C. G., O'Shaughnessy, K. M., O'Connor, B. J., Jones, H. A., Hughes, J. M., Jones, T., Pride, N. B., & Fuller, R. W. (1996). Imaging allergen-invoked airway inflammation in atopic asthma with [18F]-fluorodeoxyglucose and positron emission tomography. *Lancet*, 347, 937-940.
29. Torizuka, T., Fisher, S. J., & Wahl, R. L. (1997). Insulin-induced hypoglycemia decreases uptake of 2-[F-18]fluoro-2-deoxy- D-glucose into experimental mammary carcinoma. *Radiology*, 203, 169-172.
30. Warlow, C. P., Dennis, M. S., van Gijn, J., Hankey, G., Sandercock, P. A. G., Bamford, J., & Wardlaw, J. (1996a). *Stroke: A practical guide to management*. Oxford, UK: Blackwell Scientific.
31. Warlow, C. P., Dennis, M. S., van Gijn, J., Hankey, G., Sandercock, P. A. G., Bamford, J., & Wardlaw, J. (1996b). *Stroke: A practical guide to management*. Oxford, UK: Blackwell Scientific.

32. Williams, J. K., Sukhova, G. K., Herrington, D. M., & Libby, P. (1998). Pravastatin has cholesterol-lowering independent effects on the artery wall of atherosclerotic monkeys. *J.Am.Coll.Cardiol.*, 31, 684-691.
33. Yun, M., Cotter, A., Kim, W., Eldeiry, L., & Newberg, A. (2001). 18FDG Uptake in the large arteries: correlation with the risk factors of atherosclerosis. *J.Nucl.Med.* 2P.

Patient	ID	Sex	Age	Symptoms	Symptoms to PET (Months)
Dynamic	010252	M	79	L hemiparesis	4
1	000250	M	66	R amaurosis x 2	2
2	000320	M	71	Aphasia x 3	4
3	000361	F	48	R hemiparesis	8
4	000396	M	68	L amaurosis x 2	6
5	000435	M	52	L hemiparesis x 6	4
6	000495	M	63	L hemiparesis x 2	4
7	010067	F	69	L hemisensory	2
8	010183	M	71	R hemiparesis	2
9	010494	F	72	R hemiparesis	5
10	010498	M	76	L amaurosis	3
		Female (%)	Mean age	-	
		30	65.6		

Table 5.1 Characteristics of patients undergoing late and FDG-PET dynamic imaging.

Patient	ID	Symptomatic	Symptomatic	Asymptomatic	Asymptomatic
		early	late	early	late
1	000250	13.66	5.88	13.04	3.44
2	000320	11.69	8.05	-	-
3	000361	10.18	7.59	10.18	4.95
4	000396	11.06	8.44	9.41	7.71
5	000435	10.74	8.38	5.65	4.74
6	000495	5.37	5.77	-	-
7	010067	13.29	10.87	12.57	9.91
8	010183	12.28	8.65	11.21	6.49
9	010494	9.16	7.24	10.33	7.10
10	010498	15.23	11.47	-	-
MEAN		11.27	8.23	10.34	6.33
S.E.		0.87	0.58	0.92	0.82
95% C.I.		9.31 – 13.22	6.91 – 9.55	8.08 – 12.60	4.33 – 8.34

Table 5.2 Early and late net FDG accumulation rate for late protocol FDG-PET patients (expressed as $\times 10^{-5} \text{ sec}^{-1}$). Dashes represent contralateral arteries without stenosis.

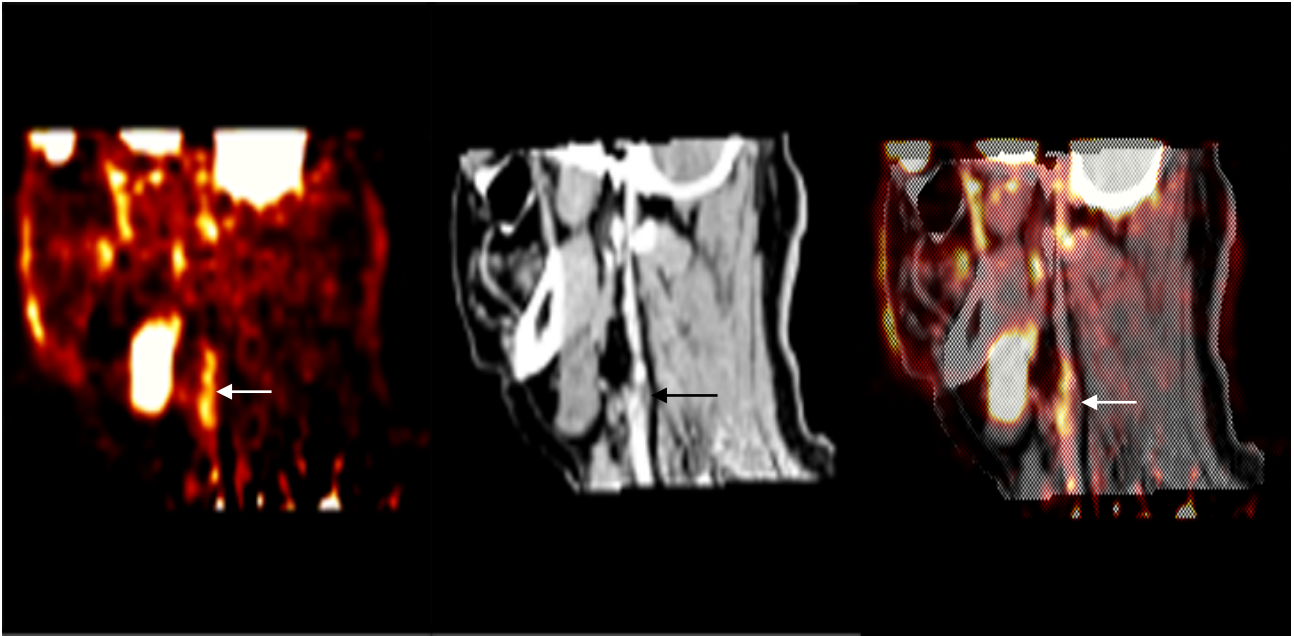


Figure 5.1 PET imaging of symptomatic carotid atherosclerosis

The images (from left to right) show PET, contrast CT and co-registered PET/CT images in the sagittal plane, from a 63 year old male who had experienced two episodes of left-sided hemiparesis. Angiography demonstrated 80% stenosis of the proximal right internal carotid artery; this was confirmed on the CT image (black arrow). The white arrows show FDG uptake at the level of the plaque in the carotid artery. As expected, there was high FDG uptake in the brain, jaw muscles and facial soft tissues.

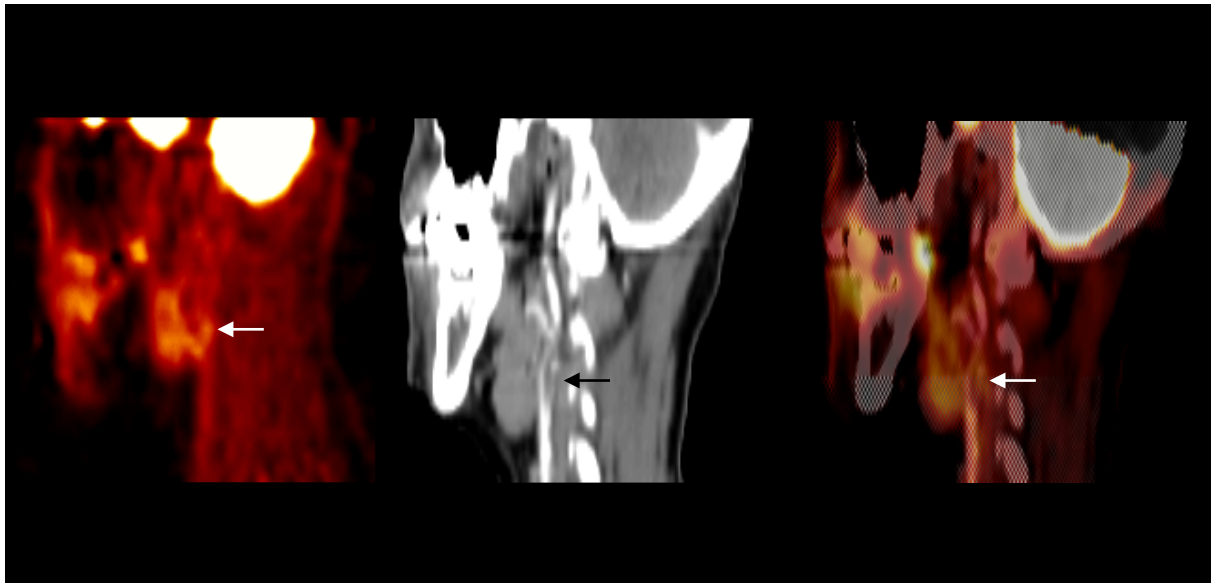


Figure 5.2 PET imaging of asymptomatic carotid atherosclerosis

The images (from left to right) demonstrate a low level of FDG uptake in an asymptomatic 65% carotid stenosis. The black arrow highlights the stenosis on the CT angiogram, and the white arrows demonstrate minimal FDG accumulation at this site on the FDG-PET and co-registered PET/CT images.

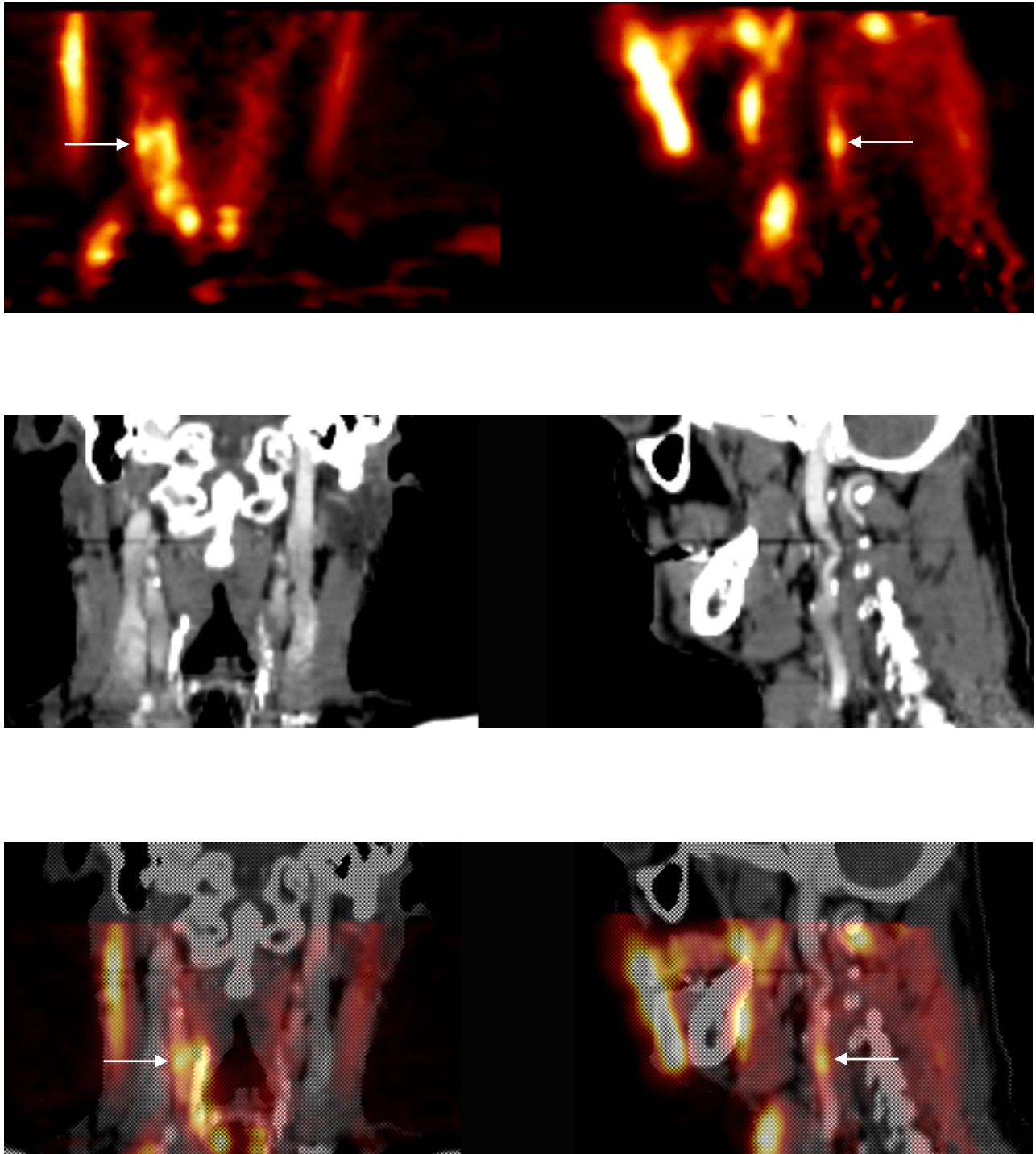


Figure 5.3 Unilateral carotid FDG uptake.

From top to bottom, FDG-PET, CT and co-registered PET/CT images, coronal views on the left, sagittal views on the right. The white arrows indicate FDG uptake at the site of carotid atheroma in the right internal carotid artery. Note there is no uptake above background on the left side

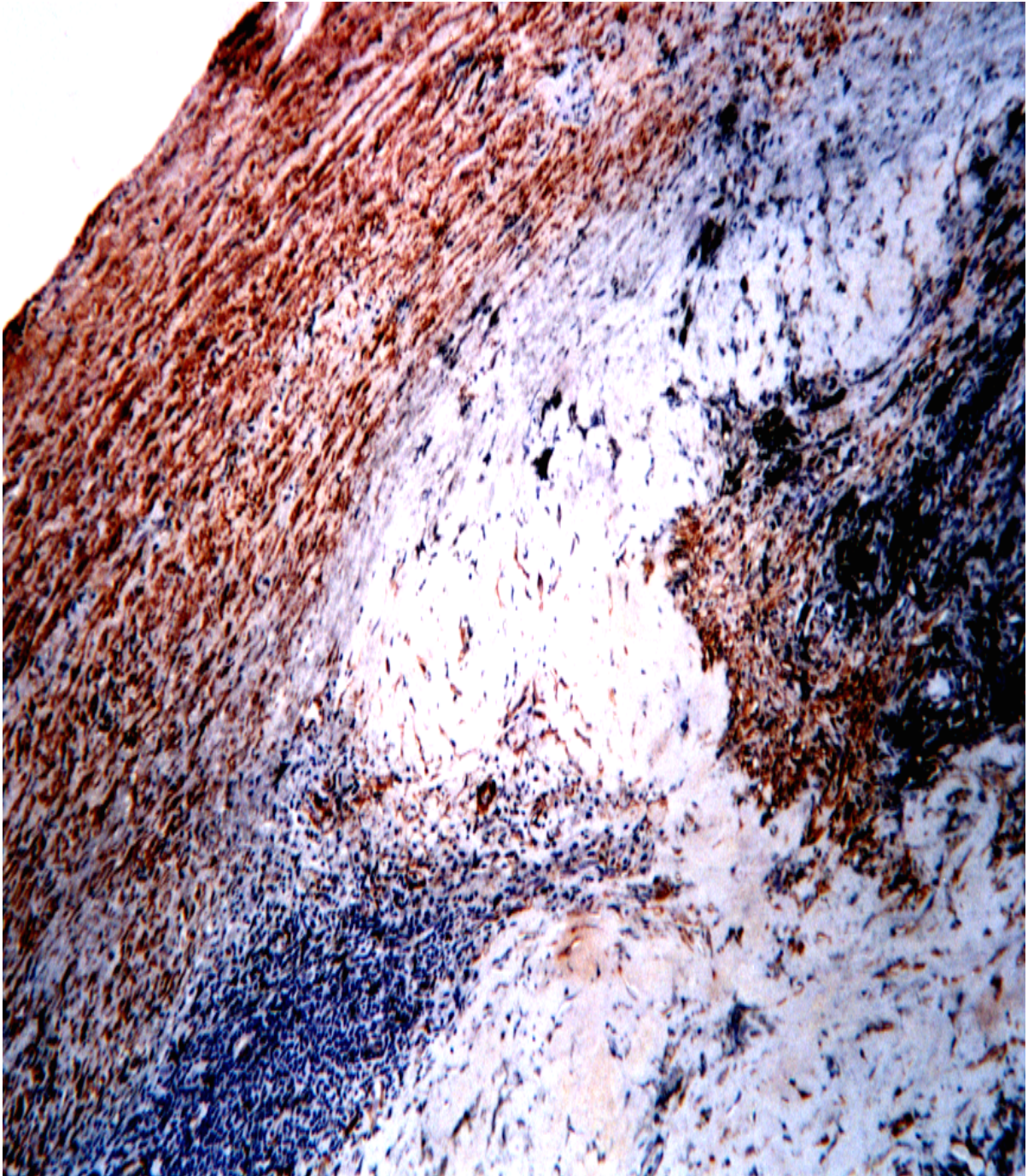


Figure 5.4 Carotid plaque histology.

Double immunohistochemistry demonstrating black stained macrophages beneath a brown coloured smooth muscle cell-rich fibrous cap (From Patient 1). Magnification x40.

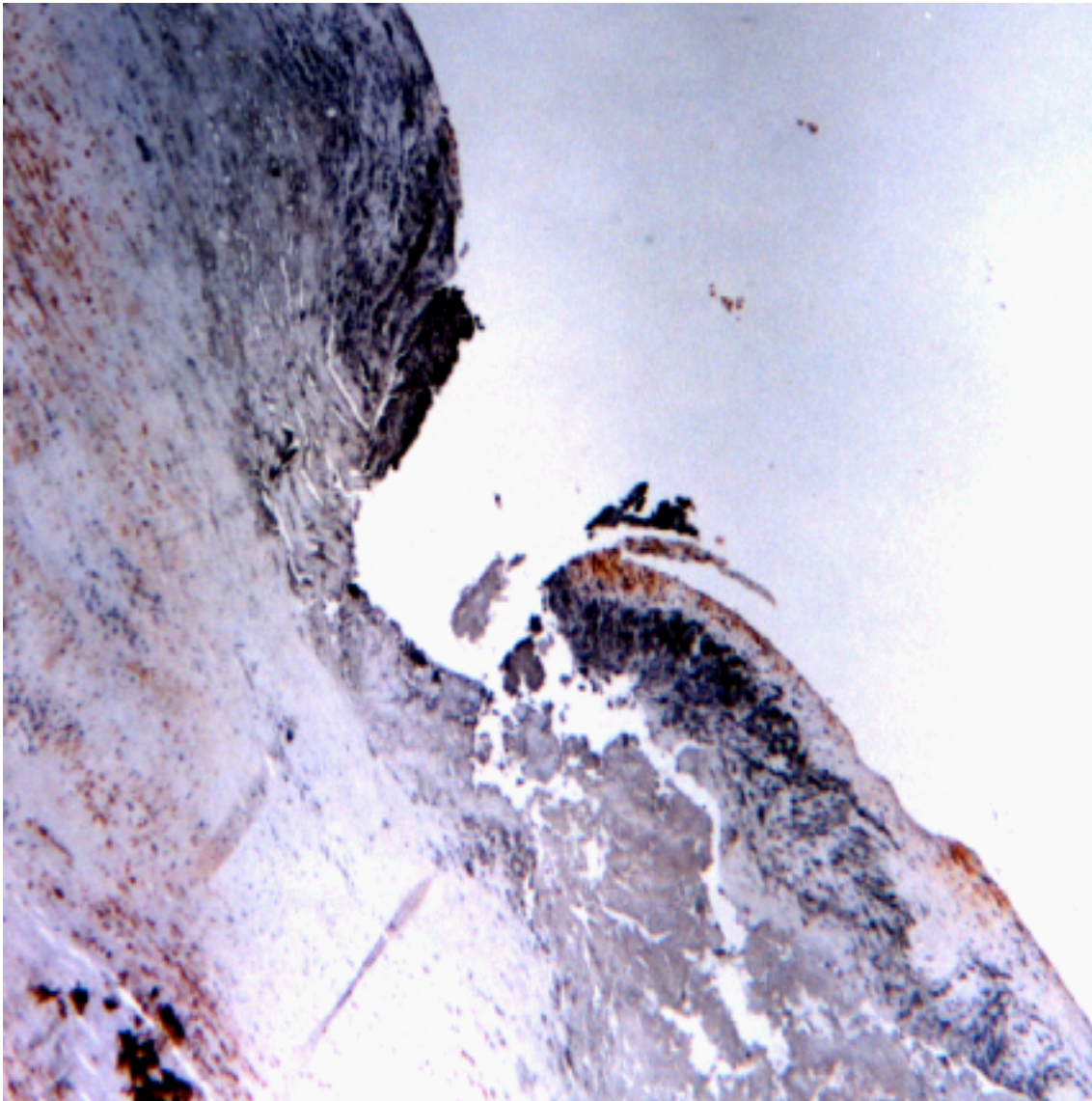


Figure 5.5 Histology of ruptured carotid plaque

Double immunohistochemistry against smooth muscle cells and macrophages. Macrophages, stained black, are present below the ruptured fibrous cap (From Patient 9). Magnification x40.

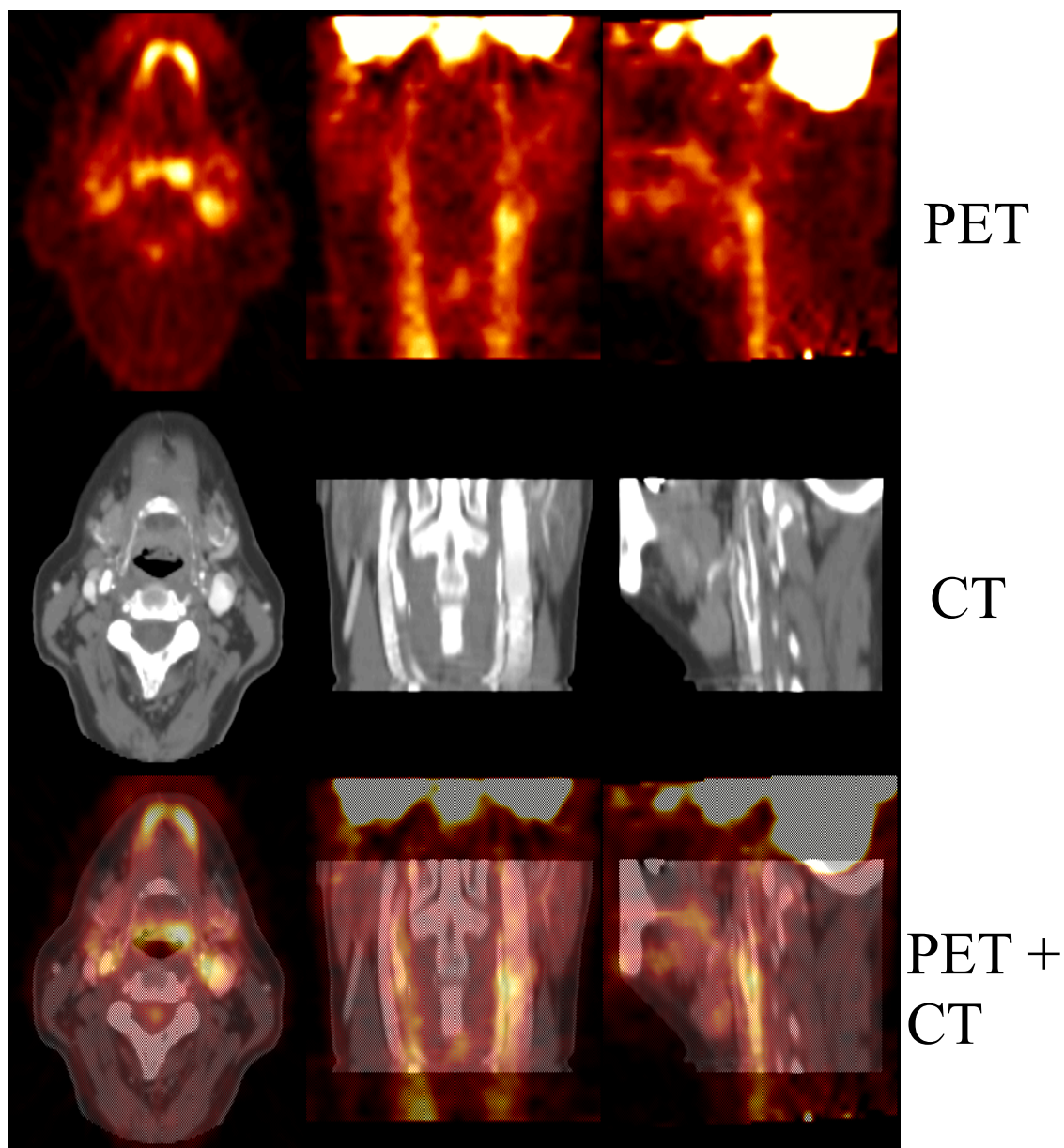


Figure 5.6 Pilot 2-D dynamic FDG-PET images

This figure shows high blood pool FDG activity in the PET images, acquired 45 minutes after FDG injection. From top to bottom, PET, CT and co-registered PET/CT images. Transverse, coronal and sagittal views from left to right.

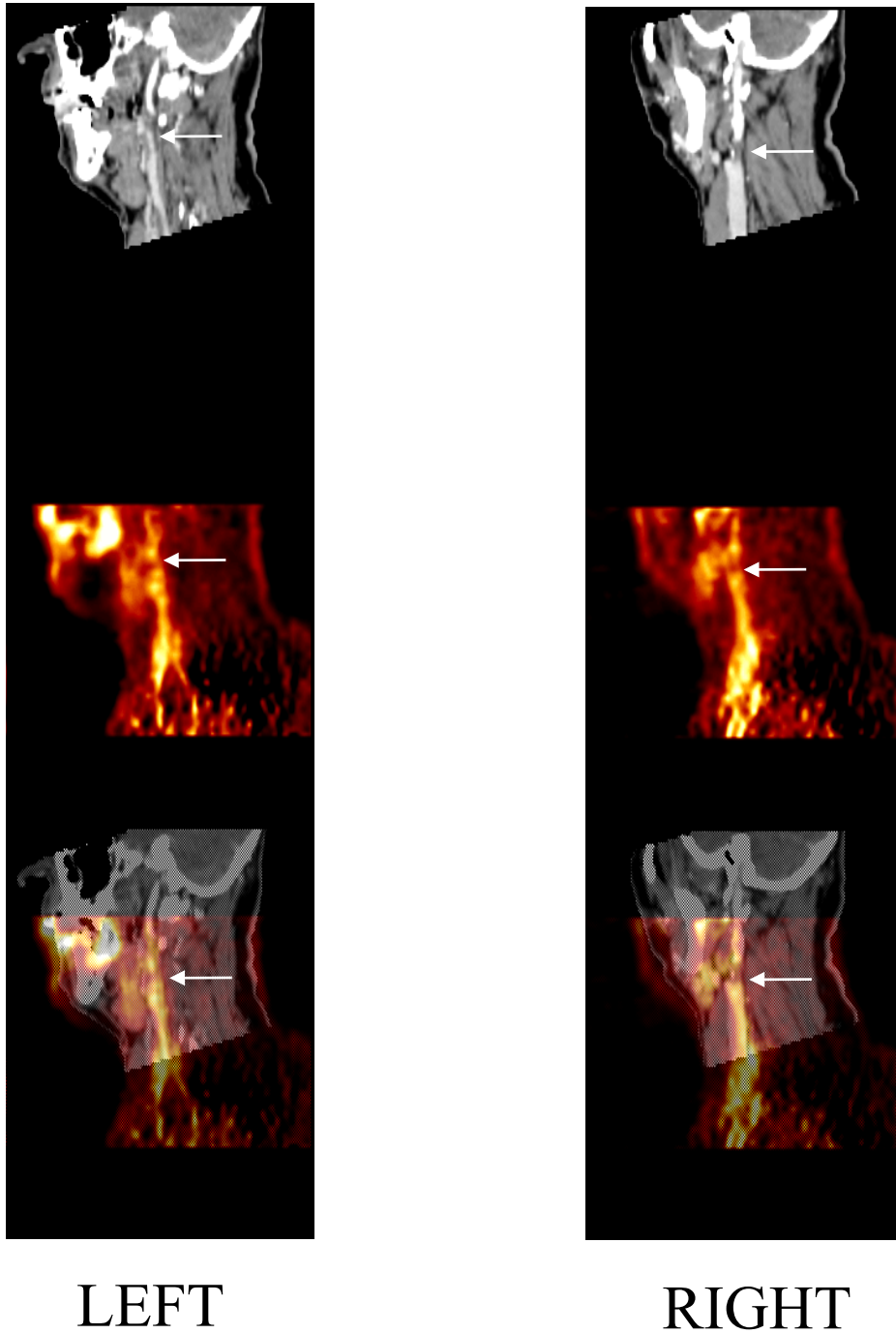


Figure 5.7 3-D dynamic carotid FDG-PET imaging

This figure shows bilateral FDG uptake in the carotid region, seen in these sagittal views. The white arrows indicate the sites of stenosis. Patlak plots were constructed from these data.

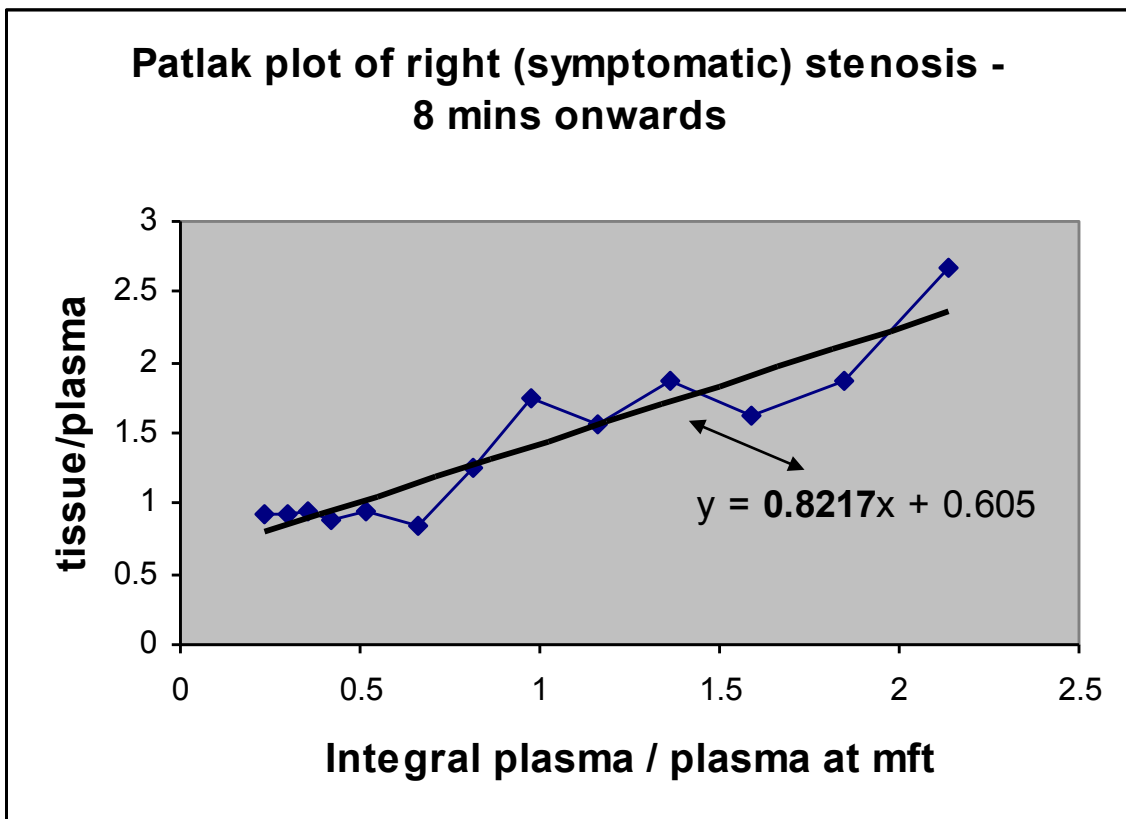


Figure 5.8 Patlak plot – symptomatic lesion

This figure is a Patlak plot of the region around the symptomatic stenosis of the patient shown in Figure 5.7. The gradient of the linear regression line of this plot is 0.82.

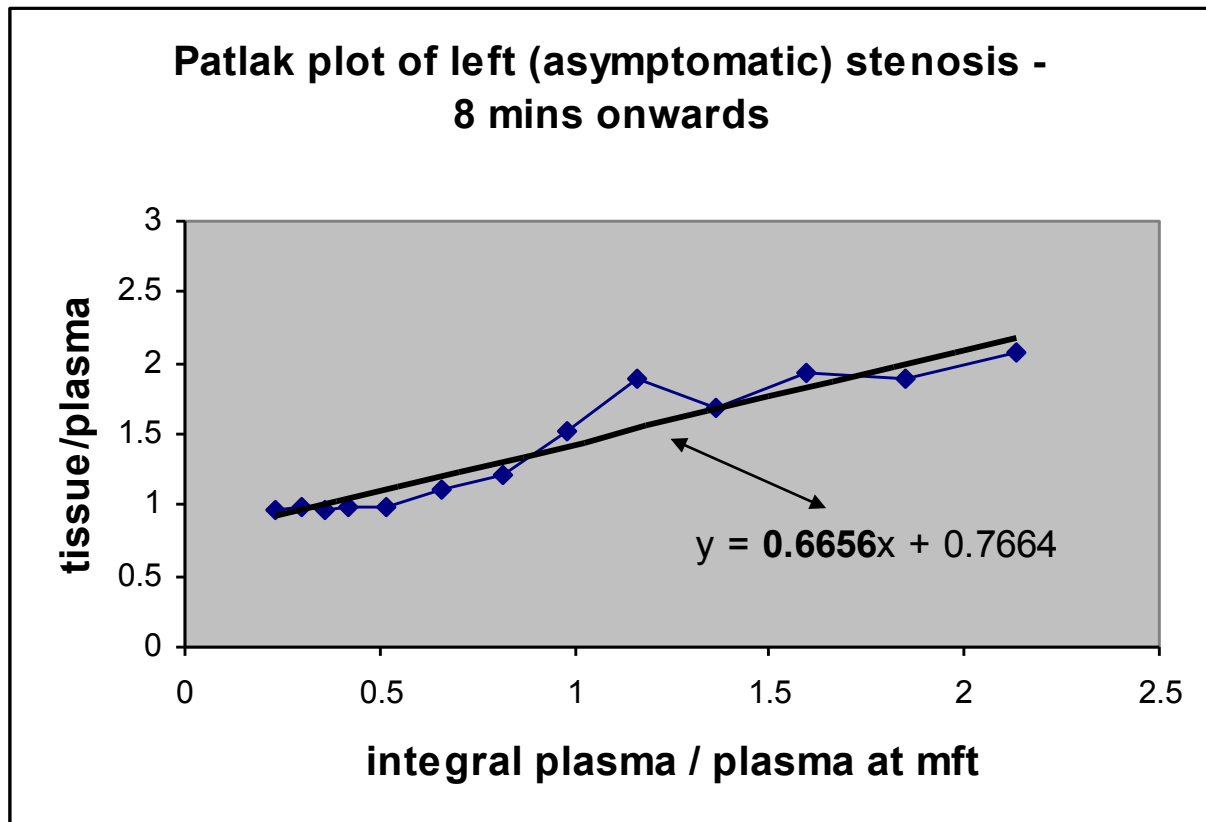


Figure 5.9 Patlak plot – asymptomatic lesion

This figure is a Patlak plot of the region around the asymptomatic stenosis of the patient shown in Figure 5.7. The gradient of the linear regression line of this plot is 0.67.



Figure 5.10 HRMR carotid plaque imaging

This figure shows a HRMR scan at the level of the carotid arteries, with a left sided symptomatic plaque visible as a high signal lesion, arrowed in red.

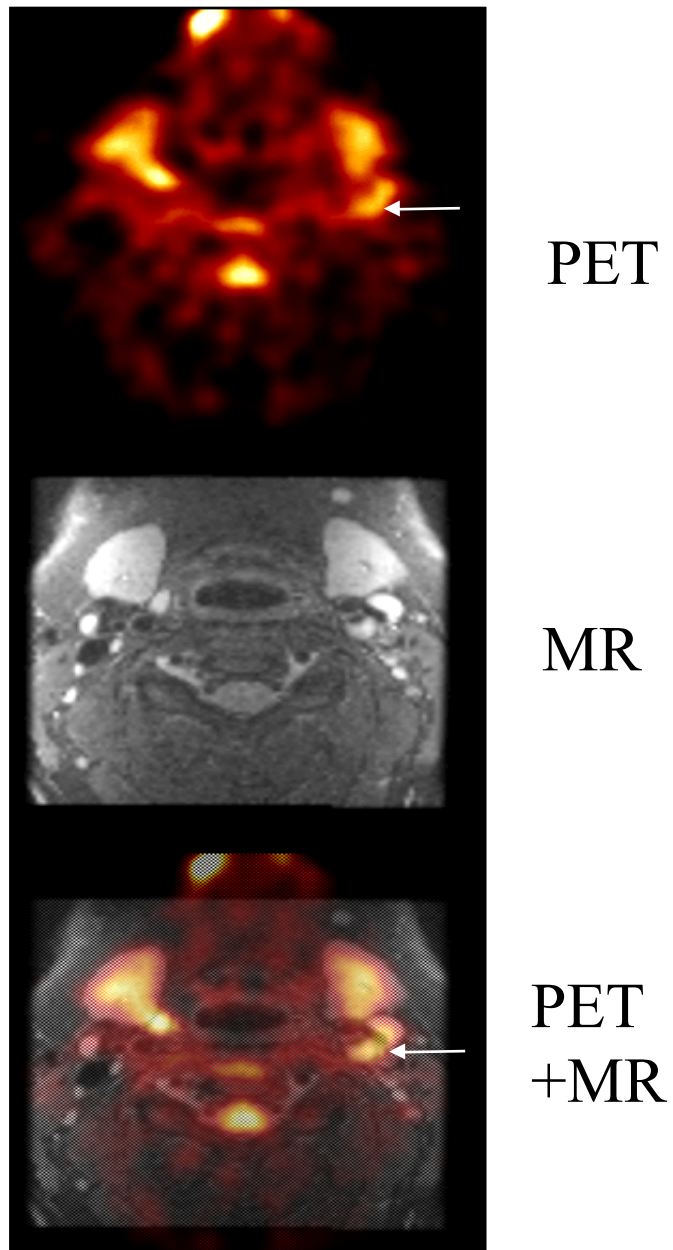


Figure 5.11 HRMR/FDG-PET carotid plaque imaging

This figure shows images from the same patient as in Figure 5.10. From top to bottom are PET, MR and co-registered PET/MR images. Note the high FDG accumulation at the site of the lesion on the PET scan (white arrows).



Figure 5.12 HRMR carotid plaque imaging

This figure shows a HRMR scan at the level of the carotid arteries. The left sided lesion is symptomatic, and has a smoothly thickened wall. On the asymptomatic right side, the wall is eccentrically thickened by plaque, with an area of high signal on the medial side of the vessel (arrowed in red).

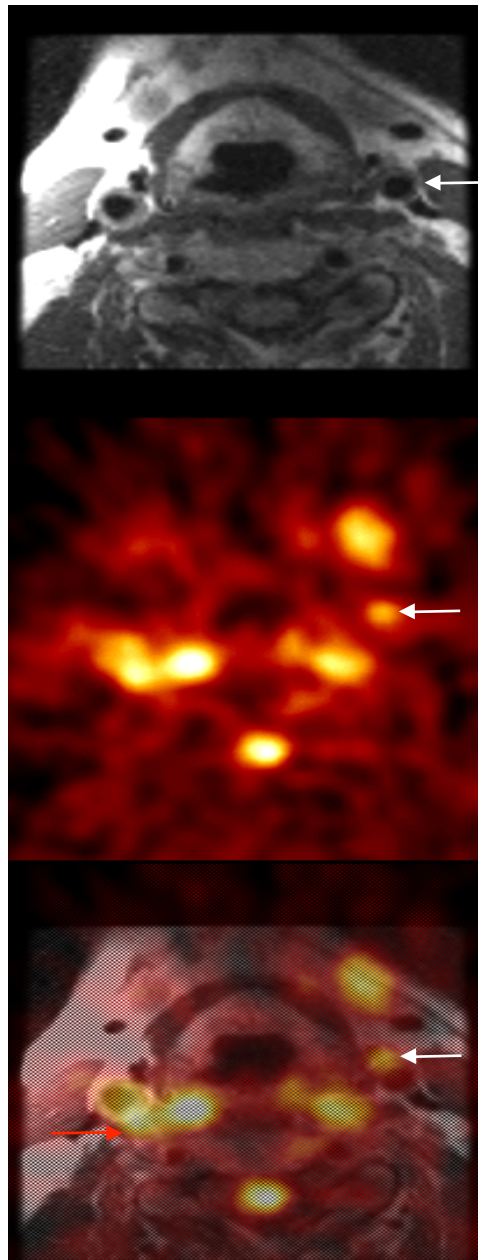


Figure 5.13 HRMR/HDG-PET carotid plaque imaging

This figure shows images from the same patient as Figure 5.12. The symptomatic left sided lesion has accumulated FDG (white arrows), whilst the asymptomatic lesion on the right (red arrow) has also taken up FDG to a similar extent, suggesting high inflammatory activity in this plaque also.

Chapter 6

CHAPTER 6

THE UPTAKE OF FDG IN AN EXPERIMENTAL MODEL OF ATHEROSCLEROSIS

6.1 INTRODUCTION

The work described in this chapter was prompted by the results described in Chapter 5, which showed that FDG accumulation occurs in atherosclerotic plaque above background levels, and furthermore that FDG accumulates to a greater extent in symptomatic plaques than asymptomatic plaques. Some of the questions raised by the results in Chapter 5, such as the relationship between FDG signal and plaque macrophage content and activity, the feasibility of serial imaging and the manipulation of plaque macrophage content cannot easily be addressed in studies of human subjects.

Therefore it was decided to establish an experimental animal model of atherosclerosis, and to use the recently developed microPET small animal scanner to image the lesions generated. The questions addressed by this group of experiments were fourfold.

Firstly, was it possible to establish an animal model of atherosclerosis to generate targeted lesions in the aorta?

Secondly, was it feasible to perform serial imaging of these lesions using the microPET scanner and FDG?

Thirdly, could any FDG uptake be quantified?

The final intention was to gain pilot data on the feasibility of manipulating the macrophage content of lesions, over an extended time period, by altering dietary lipid intake of the animals.

6.1.1 Background to the model of atherosclerosis

The New Zealand white rabbit (NZWR) balloon injury model of atherosclerosis was used. This model, described in detail below, has been extensively validated by others (Verheye et al., 2002; Meding et al., 2002; McConnell et al., 1999; Johnstone et al., 2001; Galis et al., 1995; Aikawa et al., 1998; Abela et al., 1995) and reliably generates lesions that resemble human atherosclerotic plaques, having a recognisable fibrous cap covering a macrophage-rich lipid core. Plaques produced in this way have been reported (McConnell et al., 1999) to be more similar to human lesions than those derived from the other, less widely used rabbit model of atheroma (this uses Watanabe rabbits, which have a genetic defect in the region coding for the LDL receptor, and which spontaneously develop aortic atherosclerotic plaques as a result).

In addition, after a lesion has been generated by the NZWR model, a reduction in the cholesterol content of the diet of the animal will result in amelioration of both macrophage proteolytic capability and the inflammatory cell content of the lesion; in other words dietary intervention can stabilize the lesions (Aikawa et al., 1998; Verheye et al., 2002).

A balloon injury to the aortic endothelium in combination with a high cholesterol diet was employed as an alternative to high cholesterol diet alone. This is because the endothelial denudation it creates tends to accelerate lesion formation, produces lesions more uniform in size and distribution, and generates plaques with a smooth muscle cell-rich cap overlying a layer of lipid laden macrophages (Aikawa et al., 1998; Galis et al., 1995). It was for this reason, and because the balloon injury model allows the lesions to be targeted in the aorta for later PET imaging, that the NZWR model of atherosclerosis was chosen. Accurate targeting was necessary because there was no means of acquiring anatomical co-registration scans in this early work.

6.1.2 MicroPET system

Animal models of human disease are widely used in research for elucidating pathological mechanisms and for assessing the therapeutic potential of treatments on a disease process. Radiotracer techniques such as autoradiography are commonly

employed in these studies, but their use requires the sacrifice of several animals at the end of a single experiment, meaning that longitudinal studies necessarily involve the use of large numbers of animals.

PET is the technique of choice for providing *in-vivo*, non-invasive functional imaging in animal models of disease. It may not have a spatial resolution approaching that of autoradiography, but with PET there is no requirement for animal sacrifice after each experiment, allowing longitudinal observations in a single animal. In addition, much information can still be obtained about disease pathogenesis and the kinetics of injected tracers even at a resolution of ~ 2 mm. Clinical PET scanners do not have sufficient resolution for small animal applications; therefore, a dedicated, high resolution small animal PET scanner is required to undertake these studies, and such a machine became available in Cambridge in late 2001.

The scanner used was the microPET system, 4-ring primate version (P4) (Concorde Microsystems, Knoxville, TN, USA). Detailed evaluation and validation of this machine has been published elsewhere (Chatziioannou et al., 1999; Tornai et al., 1999). MicroPET allows serial PET imaging to be performed in a variety of animal models ranging in size from mouse to non-human primate. The scanner specifications are shown in Table 6.1.

An important point to note is that the scanner resolution is significantly superior to that of the GE Advance clinical PET scanner used for the carotid atherosclerosis studies in Chapter 5 (~ 1.85 mm vs ~ 5 mm, respectively, at the centre of the field of view). The main reason for this is that the detector dimensions are 2×2 mm *en face* rather than 8×4 mm in the Advance scanner. In addition, the resolution loss due to photon non-collimetry is reduced with the smaller ring diameter (26cm vs 93cm). Finally, replacing the bismuth germanate scintillation detectors in the Advance with lutetium oxyorthosilicate in the microPET system results in a faster scintillation decay time and more than five times the light output. A consequence of this is a significantly improved count rate performance and the ability to use a shorter coincidence time window (6nsecs in the microPET vs 12nsecs in the Advance). This shorter time window reduces the sensitivity of the scanner to random coincidences, which is

especially important as the scanner has no septa and therefore operates exclusively in 3D mode.

Employing an identical animal model of atherosclerosis to the one used here, a fiberoptic positron detection probe has already been used successfully to investigate atheroma *ex-vivo* (Lederman et al., 2001). The probe was able to distinguish diseased artery from normal segments on the basis of differing degrees of FDG accumulation. The authors of this study also noted a positive correlation between FDG signal and the intima-media ratio of the aortic wall. Others have reported work, in abstract form, (Badimon et al., 1999; Vallabhajosula et al., 1996), in which clinical PET scanners were used to image animal models of atherosclerosis. Both these studies revealed FDG accumulation at the site of previous balloon injury. However, neither used scanners with the spatial resolution that microPET affords, and additionally, serial PET imaging after manipulation of lipid levels was not undertaken.

6.2 METHODS

The experimental plan is shown in Table 6.2

Firstly, to provide control images, FDG-PET imaging was performed in two animals before balloon injury. Secondly, FDG uptake was assessed in eight animals, four months after a combination of balloon injury and high cholesterol diet (Atheroma progression imaging). Then, the animals were split into two groups - one group remained on a high cholesterol diet, and the second group was switched to a normal diet. Finally, all animals were imaged again, 75 days after this split, and a comparison was made between PET images obtained from the two dietary groups (Atheroma regression imaging). In addition, histological characterisation of the lesions in the aorta was carried out after the final imaging session.

6.2.1 Rabbit housing and diet

All animal work was covered by appropriate Home Office licences. Nine female, 10-week old New Zealand white rabbits were purchased from Charles River (UK), and housed, one animal per cage, in a dedicated animal facility. The animals were fed 200g per day of standard rabbit diet during an induction period from Day 1 until Day 48, when they were all switched to a 50:50 mixture of standard diet and 0.2% cholesterol enriched diet. By Day 59, all rabbits had been fully established on 200g of 0.2% cholesterol enriched diet. This was continued for a total of 128 days. Surgery was undertaken on Day 65. At Day 187, half of the animals were randomly switched back to 200g daily of standard rabbit diet, while the other half remained on the high cholesterol diet. On Day 290, 103 days after the dietary split, all of the animals were sacrificed.

6.2.2 Lipid measurements

Total cholesterol was measured in plasma samples taken from the marginal ear vein using a commercially available enzymatic assay kit (Cholesterol C-Test, Wako, UK).

Serum was obtained from whole blood by centrifuging at 8000rpm for 10 minutes. The reaction was assayed at 492nm, with each sample analysed in triplicate.

6.2.3 Anaesthesia

General anaesthesia was used during surgery and PET imaging. Induction was achieved using intravenous alphaxalone/alphadalone (Saffan, Schering-Plough, 0.2ml/kg) diluted in saline to a volume of 5mls, and anaesthesia was maintained with a mixture of oxygen (0.5L/min), nitrous oxide (0.8-1L/min) and isoflurane (2.5-4%) delivered by secured facemask. There was no need for endotracheal intubation during any of the surgical or imaging sessions. Rectal temperature was constantly monitored with the animal placed on a padded warming blanket throughout the procedure. Towards the end of the procedures, reducing the inspired concentration of isoflurane lightened anaesthesia. Animals were monitored closely until they had made a full recovery following anaesthesia. There were no anaesthetic-related adverse outcomes.

6.2.4 Aortic balloon injury

Under general anaesthesia, the right groin was shaved and the leg abducted to expose the femoral triangle. An incision was made in the right groin and the femoral vessels were isolated and freed from connective tissue using scalpel, scissors and forceps. Special care was taken to separate the femoral artery from the femoral nerve, which often ran close together in the inguinal canal. The vein was identified easily because of its dark colouration. Once isolated, the distal end of the artery was tied off using an Ethilon suture (4/0), and then cut. To facilitate cannulation of the artery, papaverine 2% (3mls) was dripped slowly onto the exposed vessels to cause vasodilatation over the course of a minute. A clip was applied proximal to the tied off artery, exposing a length of artery measuring 2 to 3 cm. Iridectomy scissors were used to create an arteriotomy as distally as possible. A Fogarty balloon catheter (4F size) was then introduced into the artery to a distance of 30cm, measured using the 10cm markings on the catheter. Having tested and primed the balloon with 1.5mls air, 0.2mls were withdrawn, and the catheter was then pulled back to the aortic bifurcation with the balloon inflated. This resulted in an injury to the aorta of about 20cm in length. The balloon was then deflated and withdrawn from the artery. A bulldog clip was applied

around the arteriotomy site and tied off with Ethilon (4/0). Haemostasis was secured, and the fascia and skin were closed with Vicryl sutures (4/0).

6.2.5 FDG-PET imaging protocols

Imaging was performed using the University of Cambridge microPET scanner. Rabbits were imaged under general anaesthesia. An average dose of 129 MBq FDG was administered intravenously over 20 seconds via the marginal ear vein. The energy and coincidence windows for both the control imaging and first set of plaque imaging PET studies were 250-750 keV and 10 nsecs respectively.

Further work indicated that narrowing of both of these parameters would improve data quality by cutting down scatter and random events, without significant sacrifice of true events. Thus the final series of PET images were acquired using energy and coincidence windows at 350-650 keV and 6 nsecs respectively.

Blood sampling during PET scans was not performed because of the difficulties inherent in taking repeated aliquots of blood from the animals' marginal ear veins. These are fragile vessels which tend to thrombose if a cannula is left in place for longer than five minutes. This will be addressed in future experiments by using the central artery of the ear to obtain samples. Therefore an approximation of the input function was derived from the ventricular cavity of the control images as explained in Section 6.2.7.

6.2.5.1 Control imaging (Day 29)

The heart was centred in the field of view (FOV) of the scanner using the laser guide lights. Images were acquired over ninety minutes as 10x1, 5x2 and 14x5 minute frames in a single bed position.

6.2.5.2 Atheroma Progression imaging (Day 170)

The descending aorta was placed at the centre of the FOV. Three frames of 35 seconds duration in three consecutive bed positions were acquired immediately

following injection of FDG in order to provide a ‘blood image’ of a length of aorta that would be crucial for delineating the aorta in late FDG images. There was a 2cm overlap between each of the three bed positions. This was followed by 8x1, 10x2, 12x5 minute frames with the descending aorta in the centre of the FOV. Finally two bed positions adjacent to this were used to obtain images, as 3x5 minute frames at each position, above and below the initial FOV.

6.2.5.3 Atheroma Regression imaging (Day 262)

The protocol for atheroma progression imaging described in Section 6.2.5.2 was used.

6.2.6 Data corrections

In order to generate fully quantifiable emission data, a whole series of data corrections must be applied to the data : normalisation, sensitivity, dead time, decay, scatter, randoms and attenuation. The software supplied with the microPet scanner only provides correction for random events (decay is also a trivial correction). Consequently, the Cambridge microPet group has been developing methods to achieve the other corrections. Normalisation correction was applied to these data, but the attenuation, dead time and sensitivity methods developed recently have only become available since the data in this chapter were acquired (scatter correction is still under development). Hence, it was not possible to achieve quantified images (KBq/ml) in these early experiments.

Once acquired, image frames were reconstructed using an in-house version of the 3-D PROMIS algorithm (Kinahan et al., 1989) with correction applied for normalisation. Image frames were then imported into the ‘Analyze’ software package (Robb et al., 1991).

6.2.7 Assessment of plaque FDG concentration

Regions of interest were drawn around the aorta on the initial early ‘blood’ images, which were formed through the concatenation of three 35 second frames at three overlapping bed positions, encapsulating 18cm of the aorta. This ROI was then

applied to the dynamic data set and FDG intensity during all frames of the study was determined. This value represents FDG uptake by the combination of aortic atheroma, vessel wall and also FDG in the bloodstream within the lumen of the vessel. In order to estimate the FDG signal purely due to uptake in atheroma at each timepoint of the scan, blood FDG uptake was subtracted using the following method.

The control PET images were used to generate a blood curve (input function), in a similar way to that used in cardiac PET studies. Six frames, representing the final 30 minutes of the study were averaged, and regions were drawn within the ventricular cavity, on three slices, well away from myocardial muscle. The assumption made is that any FDG signal from this cavity is due entirely to blood (this is obviously an approximation because of scatter and partial volume effects from the myocardial tissue). These ROI were then applied to the entire dynamic control image set, to generate an approximate blood curve input function for all timepoints. Blood curves were generated from both of the control studies and then averaged to give a mean input function curve.

Once the input function curve had been derived, it was then possible to scale the early part (≈ 10 mins) of each aortic FDG uptake curve to this blood curve, making the assumption that early FDG activity within the aortic region would be coming almost entirely from blood within the lumen. The final step was to subtract the blood curve from the scaled aortic FDG uptake curve, leaving a pure aortic FDG uptake value for each timepoint of the scan. All values were decay corrected and the mean ROI size was $650\text{mm}^3 (\pm 25.8)$.

This analysis was carried out using the PET data for each animal from two studies : atheroma progression (Day 170) and atheroma regression (Day 262). The data from all animals were averaged, to allow comparisons of FDG aortic accumulation in both dietary groups.

6.2.8 Perfusion fixation

The animals were sacrificed by a rapid intravenous injection of 4mls of sodium pentobarbitone (Euthatal). After sacrifice, the chest was opened by cutting through the

ribs on either side of the sternum. Once the heart had been exposed, the pericardium was incised and stripped away. The left ventricle was cannulated, the cannula being secured using forceps, and the animals were then perfused for 30 minutes with warmed PBS, followed by 30 minutes with 4% paraformaldehyde solution. Ten seconds after the start of perfusion, the right atrium was incised to allow displaced blood to escape the circulation. In order to achieve adequate perfusion pressure, the saline and fixative solutions were raised to a height of 1.5 metres above the animal. This arrangement provided an intra-aortic pressure of approximately 80mmHg.

After perfusion, the aorta, from arch to iliac bifurcation, was removed and fixed in 4% paraformaldehyde for a further 48 hours. Renal arteries were also taken to allow orientation of the aorta with the PET images. The aortas were photographed whole, and transverse sections were cut from each aortic specimen in the region that had undergone balloon injury. Sections were cut 5µm thick and mounted on BDH Superfrost Plus slides. These were stained using haematoxylin and eosin using the protocol described in Section 2.3.2 of Chapter 2, and immunocytochemistry was carried out against vascular smooth muscle cells (Chapter 2, Section 2.3.1.1) and macrophages (Chapter 2, Section 2.3.1.2).

6.3 RESULTS

Surgery was carried out successfully in all nine animals, without immediate complications. However, one animal had to be sacrificed 15 days post-operatively because of a 20% loss of body weight (a Home Office criterion for immediate sacrifice). After examination by the veterinary surgeon, the cause of this weight loss was thought to be pneumonia. After euthanasia, examination of the surgical site of the animal showed no evidence of haemorrhage, infection or wound breakdown.

6.3.1 Lipid profiles

The mean (\pm SEM) total cholesterol before starting the high cholesterol diet for the whole group of 8 remaining animals was 66.0mg/dl (\pm 5.8), range 33.5-84.4 mg/dl. After 128 days on a 0.2% enriched cholesterol diet, the mean total cholesterol of the group had increased significantly to 1008.3mg/dl (\pm 157.4), range 146.9-1686.0 mg/dl, **p = 0.0006**.

The eight rabbits were then split into two groups of four animals. One group continued on the high cholesterol diet ('High group' i.e. animals numbered 5,7,8,9) while the other group returned to a normal diet ('Low group' i.e. animals numbered 1,2,3,4) for the remainder of the experiment. Mean total cholesterol in the four animals randomised to normal diet had dropped significantly after 103 days [from 1150.4mg/dl (\pm 210.6) to 226.2mg/dl (\pm 102.1), **p = 0.0085**], and, as expected, it remained elevated in those animals randomised to continue on high cholesterol diet [from 866.2mg/dl (\pm 240.3) to 939.7mg/dl (\pm 337.0), **p = 0.7**].

However, at the end of the experiment, 103 days after the groups split, mean total cholesterol levels did not differ significantly between the two dietary groups [939.7mg/dl (\pm 337.0) vs 226.2mg/dl (\pm 102.1), **p = 0.089**], mainly as a result of one non-responder to high cholesterol diet in 'High group' (animal number 7), and one animal in the 'Low group' whose serum cholesterol over the 103 days remained elevated (animal number 2) despite being on a normal diet (See Figure 6.1 and Tables 6.3 and 6.4).

6.3.2 Aortic histology

Examples of aortic histopathology are shown in Figure 6.2, taken from animal 9. The upper left panel shows sections that have been stained with haematoxylin and eosin to illustrate the three layers of the arterial wall. The upper right and lower panels show the same arterial section that has had immunochemistry performed against smooth muscle cells and macrophages respectively. The typical position of these cell types within the plaque is illustrated.

6.3.3 Control FDG-PET imaging

Control FDG-PET images were acquired in two animals after one month of standard rabbit diet. Early, late and composite images are shown in three planes in Figure 6.3. The heart was placed at the centre of the field of view with the region of the ascending and descending aorta also covered. The top row of images were generated from the summation of five one minute frames taken early after FDG injection. The late images in the middle row were generated from the summation of four five minute frames, the first being taken 60 minutes after FDG administration. The composite row contains images that are the result of fusion of early and late frames. In the early images, activity can just be seen within the ventricular cavity of the heart. The descending aorta is out of plane in these slices and is not seen.

In the late images there is the predicted uniform uptake of FDG in myocardial tissue, but no accumulation above background seen in either the ascending or descending aorta (traced out by white arrows), confirming what was found in the human studies in Chapter 5, namely that FDG uptake into normal vessel wall is at background tissue levels. Blood in the ventricular cavity was used to generate input function data for quantification of FDG uptake in the later atheroma progression and regression FDG-PET images.

6.3.4 Atheroma Progression FDG-PET Imaging

Imaging was carried out successfully in all eight animals, 170 days after the start of the experiment.

Figure 6.4 shows representative FDG-PET images in three planes from animal 2. The images on the top row were acquired during the first minute after tracer injection, and are therefore a good marker for activity contained within the bloodstream. Images in the middle row are the average of three five minute frames acquired one hour after FDG injection. The bottom row shows composites of the one minute and one hour images, where the later images have been overlaid onto the early ones, confirming that the FDG uptake seen in the late frames is situated within the aorta. The sections displayed in Figure 6.4 are at the level of the descending aorta, in the middle of the area targeted by the balloon injury procedure.

FDG within the bloodstream in the descending aorta is well seen in the coronal and sagittal early images (yellow arrows). In the middle row, one hour after injection, activity from the blood pool has been lost, but there remains FDG uptake in the descending aorta (blue arrows). On the bottom row, the composite images confirm that this activity at one hour is within the aorta, because its position coincides exactly with the aortic blood activity in the early images. Figure 6.5 shows a close-up of a coronal 90 minute image from the same animal, again demonstrating FDG uptake in the aortic region (blue arrows).

The averaged aortic FDG uptake curves over time, derived from all eight animals, are shown in Fig 6.6. Activity in the bloodstream has been subtracted as described in Section 6.2.7, leaving only FDG activity derived from aortic tissue.

It can be seen that FDG accumulates in the aorta with time, plateauing at around 70 minutes after FDG injection. It should be noted that all animals were on high cholesterol diet at this stage. The black curve is derived from the average aortic FDG activity in all eight animals. The red curve is the average of the four animals destined for low cholesterol diet, the blue curve is the average of the four animals destined for continued high cholesterol feeding.

It can be seen that there are slight differences between FDG uptake in the two groups (red and blue curves), with the red group having generally higher FDG uptake values. This finding might be explained by the fact that this group, destined for subsequent low cholesterol diet, actually had higher average cholesterol values at the time of this

scan (see Fig 6.1, red line), even though all animals were receiving identical diets at the time of imaging ($1150.4 \pm 210.6\text{mg/dl}$ versus $866.2 \pm 240.3\text{mg/dl}$).

6.3.5 Atheroma Regression FDG-PET Imaging

Imaging was carried out successfully in all eight animals at day 262. Illustrative data from three animals are shown below:

Animal 2 : This animal was switched to low cholesterol diet at 170 days. The atheroma progression images from this animal are shown in Figures 6.4 and 6.5, and discussed above, illustrating FDG uptake in the aorta.

The atheroma regression FDG-PET images in the same animal are shown in Figures 6.7 and 6.8. Figure 6.7 shows the averaged early frames of the study, with three bed positions appended together and is essentially a blood image that delineates the aorta. Figure 6.8 is a late FDG-PET image of the aorta taken at 90 minutes after FDG injection, obtained over three bed positions, averaged together and appended. It can be seen that there is little FDG uptake in the aorta. Therefore, the uptake clearly seen in the progression images (Figures 6.4 and 6.5) is considerably reduced after the change to a low cholesterol diet, despite the fact that the cholesterol did not fall as far as the other rabbits in this group.

Aortic microscopy of this animal is demonstrated in Figure 6.9 and shows that there is little difference in macrophage content at either level sampled. Both sections show the presence of moderate numbers of macrophages.

Animal 5 : In this animal, with continued high cholesterol feeding throughout the experiment, substantial diffuse FDG uptake in the aorta is demonstrated after 90 minutes, shown by the arrows in Figure 6.10. In the histology sections, shown in Figure 6.11, it can be seen that at both levels of the aorta sampled there are large volume, macrophage-rich lesions, consistent with the high levels of uptake of FDG.

Animal 8 : In this animal, once again from the continued high cholesterol feeding group, there is significant FDG uptake seen in aorta in the late PET image (Fig 6.12). The histology image (Figure 6.13) shows bulky, macrophage filled lesions at both levels sampled.

In Figure 6.14, mean aortic FDG uptake curves are shown, derived from data from all animals at the time of the second PET scan. There are clear differences in FDG uptake between the two dietary groups at 67.5 minutes after FDG injection, but these differences do not quite reach statistical significance (647.5 vs 1880.1; **p=0.084**). This timepoint was chosen because it was felt that FDG flux would have reached steady state by this stage after injection. This result may be explained by the mean cholesterol measurements in the two groups, as shown in Figure 6.1, which at the time of the second PET scan are not statistically significantly different from each other.

To explore this possibility further, at the end of the experiment, a correlation coefficient between serum cholesterol levels and FDG uptake in all animals was calculated. There was a significant positive correlation noted, with **r=0.71**, **p=0.11**. If animal 7 was excluded from the calculation, because it did not respond well to the high cholesterol diet, then the correlation between cholesterol level and FDG uptake became stronger, with **r=0.86**, **p=0.07**.

6.4 DISCUSSION

It has been shown in this chapter that a model for generating aortic atherosclerotic lesions has been successfully established. Both the serum lipid levels generated by cholesterol feeding, and their reduction after its withdrawal in the low cholesterol group agree closely with the work of others, who also noted plaques that were morphologically similar to those produced here, in terms of size, inflammatory cell content, lack of complications and anatomical position within the aorta (Verheye et al., 2002; Aikawa et al., 1998; Johnstone et al., 2001; McConnell et al., 1999).

Nevertheless, the NZWR model is not perfect as a model of human atherosclerosis. It did not produce complicated plaques, such as those with fibrous cap rupture, thrombosis or haemorrhage, that are frequently encountered in man. Although these outcomes can be achieved with pharmacological manipulation shortly before imaging (Johnstone et al., 2001; Abela et al., 1995), the effects are not reliably reproducible and this approach was not employed in this study. Non-responders to high cholesterol diet, and slow responders to its subsequent withdrawal are fairly frequently seen with this model (Kolodgie et al., 1996), and were therefore not unexpected in this work. It will be important to control for this in future studies.

A second caveat is that the atherosclerotic plaques produced by this model are generated over several months, rather than the decades it takes for the development of a human plaque. This probably results from the extreme degree of hypercholesterolaemia in the rabbits, which greatly exceeds that encountered in man.

There are therefore important differences in the natural history of plaques produced by this model and those found in man, but the NZWR method remains one of the most useful and widely used experimental models of this disease.

The accumulation of FDG was successfully imaged within these plaques, and at a higher resolution than previous groups (Vallabhajosula et al., 1996). It has also been shown that quantitative changes in FDG uptake within atherosclerotic lesions can be detected after manipulating serum lipid levels using dietary interventions known to

stabilize plaques. Although, because of non-responders in both the small groups of animals, the lipid levels in the two groups did not differ significantly at the end of the experiment, quantitative differences between animals in both groups were still noted when the averaged FDG aortic uptake values were examined. In the four rabbits that continued high cholesterol feeding throughout the experiment, average FDG uptake around an hour after FDG injection was higher at the final imaging session (Fig 6.14), than in the four animals that switched to low cholesterol diet halfway through the experiment, although the differences fell short of statistical significance. There was also a strong, but once again non-significant positive correlation between serum cholesterol values and aortic FDG uptake at the end of the experiment.

The lack of key data corrections (attenuation, dead time and scatter) meant that absolute quantification of FDG accumulation was impossible in this data series. Although limited graphical quantification and comparison between groups of animals was possible using estimated input function data, it will be desirable in subsequent work to try to achieve these corrections and also to perform plasma sampling during imaging sessions. A recent software upgrade provided by the manufacturers, and in-house software and methodological work means that it will now be feasible to perform attenuation, sensitivity and dead time corrections on future studies. An in-house Monte Carlo-based scatter correction technique is still under development.

Based on work reported in Chapters 3, 4 and 5, it seems likely that the majority of FDG taken up into plaques in NZWR is sequestered by macrophages within the plaque. A reduction in both macrophage number and function in this model (as measured by matrix metalloproteinase production) occurs after several months of cholesterol-free diet (this varies between three and 16 months in published papers) (Aikawa et al., 1998; Verheye et al., 2002; McConnell et al., 1999), but a more potent and rapid effect is seen with the administration of statins (Bustos et al., 1998; Aikawa et al., 2001), which virtually abolish macrophage infiltration into the plaque after only four weeks treatment. It is probable, therefore, that such a change in the macrophage content of lesions (Shiomi et al., 1999) might have a greater effect on reducing FDG uptake than dietary changes alone in future longitudinal imaging studies. Once these issues have been resolved, future projects using this model will investigate whether

potent statin drugs are able to reduce inflammation within atherosclerotic plaques, and furthermore whether this can be visualised and quantified using FDG-PET.

Additionally, other more macrophage-specific markers, such as [¹¹C] PK11195, will be employed, for tandem imaging with FDG, in the hope of mapping out both macrophage content and activity within the same atherosclerotic plaque. Finally, the testing of novel anti-atheroma drugs may also be feasible, with the need for fewer animals than exists today with current approaches to the evaluation of such compounds.

6.5 REFERENCES

1. Abela, G. S., Picon, P. D., Friedl, S. E., Gebara, O. C., Miyamoto, A., Federman, M., Tofler, G. H., & Muller, J. E. (1995). Triggering of plaque disruption and arterial thrombosis in an atherosclerotic rabbit model. *Circulation*, 91, 776-784.
2. Aikawa, M., Rabkin, E., Okada, Y., Voglic, S. J., Clinton, S. K., Brinckerhoff, C. E., Sukhova, G. K., & Libby, P. (1998). Lipid lowering by diet reduces matrix metalloproteinase activity and increases collagen content of rabbit atheroma: a potential mechanism of lesion stabilization [see comments]. *Circulation*, 97, 2433-2444.
3. Aikawa, M., Rabkin, E., Sugiyama, S., Voglic, S. J., Fukumoto, Y., Furukawa, Y., Shiomi, M., Schoen, F. J., & Libby, P. (2001). An HMG-CoA Reductase Inhibitor, Cerivastatin, Suppresses Growth of Macrophages Expressing Matrix Metalloproteinases and Tissue Factor In Vivo and In Vitro. *Circulation*, 103, 276-283.
4. Badimon, J. J., Zyang, Z. Y., Machac, J., Helft, G., Worthley, S. G., Tang, C. Y., Osende, J. I., Lipszyc, H., Buschbaum, M. S., & Fuster, V. (1999). Non-Invasive imaging of atherosclerotic plaque macrophage in a rabbit model with F-18 FDG PET: A histopathological correlation. *J.Nucl.Med.*, 40, 88P-88P.
5. Bustos, C., Hernandez-Presa, M. A., Ortego, M., Tunon, J., Ortega, L., Perez, F., Diaz, C., Hernandez, G., & Egido, J. (1998). HMG-CoA reductase inhibition by atorvastatin reduces neointimal inflammation in a rabbit model of atherosclerosis. *J.Am.Coll.Cardiol.*, 32, 2057-2064.
6. Chatziioannou, A. F., Cherry, S. R., Shao, Y., Silverman, R. W., Meadors, K., Farquhar, T. H., Pedarsani, M., & Phelps, M. E. (1999). Performance evaluation of microPET: a high-resolution lutetium oxyorthosilicate PET scanner for animal imaging [see comments]. *J.Nucl.Med.*, 40, 1164-1175.
7. Galis, Z. S., Sukhova, G. K., Kranzhofer, R., Clark, S., & Libby, P. (1995). Macrophage foam cells from experimental atheroma constitutively produce matrix-degrading proteinases. *Proc.Natl.Acad.Sci.U.S.A.*, 92, 402-406.
8. Johnstone, M. T., Botnar, R. M., Perez, A. S., Stewart, R., Quist, W. C., Hamilton, J. A., & Manning, W. J. (2001). In vivo magnetic resonance imaging of experimental thrombosis in a rabbit model. *Arterioscler.Thromb.Vasc.Biol.*, 21, 1556-1560.
9. Kinahan, P. E. & Rogers, J. G. (1989). Analytic 3D image reconstruction using all detected events. *IEEE Trans Nucl Sci*, 36, 964-968.
10. Kolodgie, F. D., Katocs, A. S., Jr., Largis, E. E., Wrenn, S. M., Cornhill, J. F., Herderick, E. E., Lee, S. J., & Virmani, R. (1996). Hypercholesterolemia in the rabbit induced by feeding graded amounts of low-level cholesterol. Methodological considerations regarding individual variability in response to dietary cholesterol and development of lesion type. *Arterioscler.Thromb.Vasc.Biol.*, 16, 1454-1464.
11. Lederman, R. J., Raylman, R. R., Fisher, S. J., Kison, P. V., San, H., Nabel, E. G., & Wahl, R. L. (2001). Detection of atherosclerosis using a novel positron-sensitive probe and 18-fluorodeoxyglucose (FDG). *Nucl Med.Commun.*, 22, 747-753.
12. McConnell, M. V., Aikawa, M., Maier, S. E., Ganz, P., Libby, P., & Lee, R. T. (1999). MRI of rabbit atherosclerosis in response to dietary cholesterol lowering. *Arterioscler.Thromb.Vasc.Biol.*, 19, 1956-1959.

13. Meding, J., Dinkelborg, L. M., Grieshaber, M. K., & Semmler, W. (2002). Targeting of endothelin receptors for molecular imaging of atherosclerosis in rabbits. *J.Nucl Med.*, 43, 400-405.
14. Robb, R. A. & Hanson, D. P. (1991). A software system for interactive and quantitative visualization of multidimensional biomedical images. *Australas.Phys.Eng Sci.Med.*, 14, 9-30.
15. Shiomi, M. & Ito, T. (1999). Effect of cerivastatin sodium, a new inhibitor of HMG-CoA reductase, on plasma lipid levels, progression of atherosclerosis, and the lesional composition in the plaques of WHHL rabbits. *Br.J.Pharmacol.*, 126, 961-968.
16. Tornai, M. P., Jaszczak, R. J., Turkington, T. G., & Coleman, R. E. (1999). Small-animal PET: advent of a new era of PET research [editorial; comment]. *J.Nucl.Med.*, 40, 1176-1179.
17. Vallabhajosula, S., Machac, J., Knesaurek, K., Telsey, J., Lipszyc, H., Bastidas, D. A., Zhao, Q. H., & Buschbaum, M. S. (1996). Imaging atherosclerosis macrophage density by positron emission tomography using F-18-Fluorodeoxyglucose (FDG). *J.Nucl.Med.*, 37, 38P.
18. Verheye, S., De Meyer, G. R., Van Langenhove, G., Knaapen, M. W., & Kockx, M. M. (2002). In vivo temperature heterogeneity of atherosclerotic plaques is determined by plaque composition. *Circulation*, 105, 1596-1601.

Specifications	microPET[®] P4
Detector Diameter	26.0cm
Animal Port	22cm
No. of Blocks per Ring	42
No. of Detector Blocks	168
Total No. of LSO Elements	10,752
Timing Window	Variable at 2, 6, 10, 14 or 18 nsec
Energy Window	Variable from 0keV - 810keV
Absolute System Sensitivity	~650cps/ μ Ci
Resolution at Center of FOV	~1.85mm
Reconstruction	SSRB, FORE

Table 6.1 Technical specifications of the Concorde microPet P4 model, taken from Concorde Microsystems website.

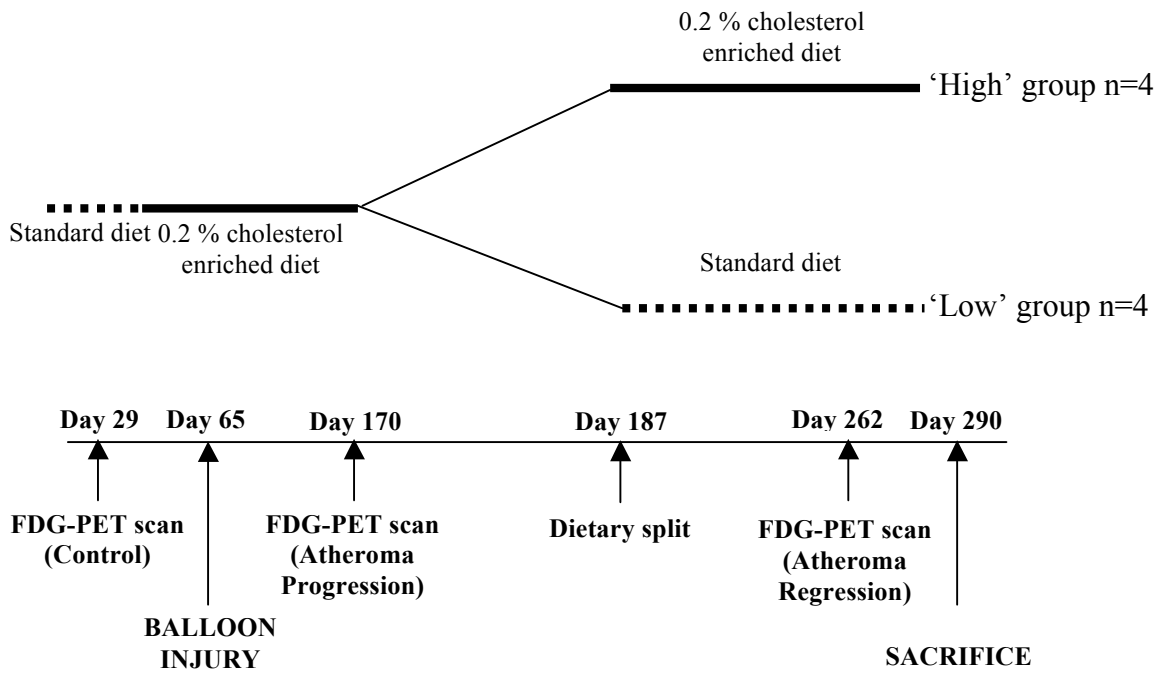


Table 6.2 The timeline of the experiments described in this chapter is shown above.

	Before feeding (n=8)	At Split whole group (n=8)	At Split high group (n=4)	At Split low group (n=4)	Final high group (n=4)	Final low group (n=4)
Mean total cholesterol ± SEM (mg/dl)	66.0 ± 5.8	1008.3 ± 157.4	866.2 ± 240.3	1150.4 ± 210.6	939.7 ± 337.0	226.2 ± 102.1
Range (mg/dl)	33.5-84.4	146.9-1686.0	146.9-1152.3	773.4-1686.0	92.8-1740.1	92.8-525.9

Table 6.3 Mean total cholesterol profiles of NZWR. All animals received a high cholesterol diet for 128 days. At this timepoint, the group was split into two groups of four animals. One continued with the high cholesterol diet. The other four animals received standard diet without supplemental cholesterol. The experiment was terminated 103 days after splitting the groups.

	Baseline	PET scan 1 and diet split	PET scan 2 and cull
Animal 1	73.0	1283.8	92.8
Animal 2	84.4	1686.0	525.9
Animal 3	59.0	858.5	100.5
Animal 4	72.7	773.4	185.6
Animal 5	55.4	1082.8	1005.4
Animal 7	79.9	146.9	92.8
Animal 8	33.5	1082.8	920.3
Animal 9	70.0	1152.4	1740.1

Table 6.4 Cholesterol profiles of individual NZWR. All animals received a high cholesterol diet from baseline until the dietary split after 128 days. At this timepoint, the group was separated into two groups of four animals. Animals 5 to 9 continued with the high cholesterol diet. Animals 1 to 4 received standard diet without supplemental cholesterol. It can be seen that animal 7, which received high cholesterol feeding throughout the experiment, did not respond as well as the other animals to the diet. Conversely, the cholesterol levels in animal 2 did not fall as far as the others in its group once it was switched from high cholesterol diet to low cholesterol diet. Cholesterol values are expressed in mg/dl.

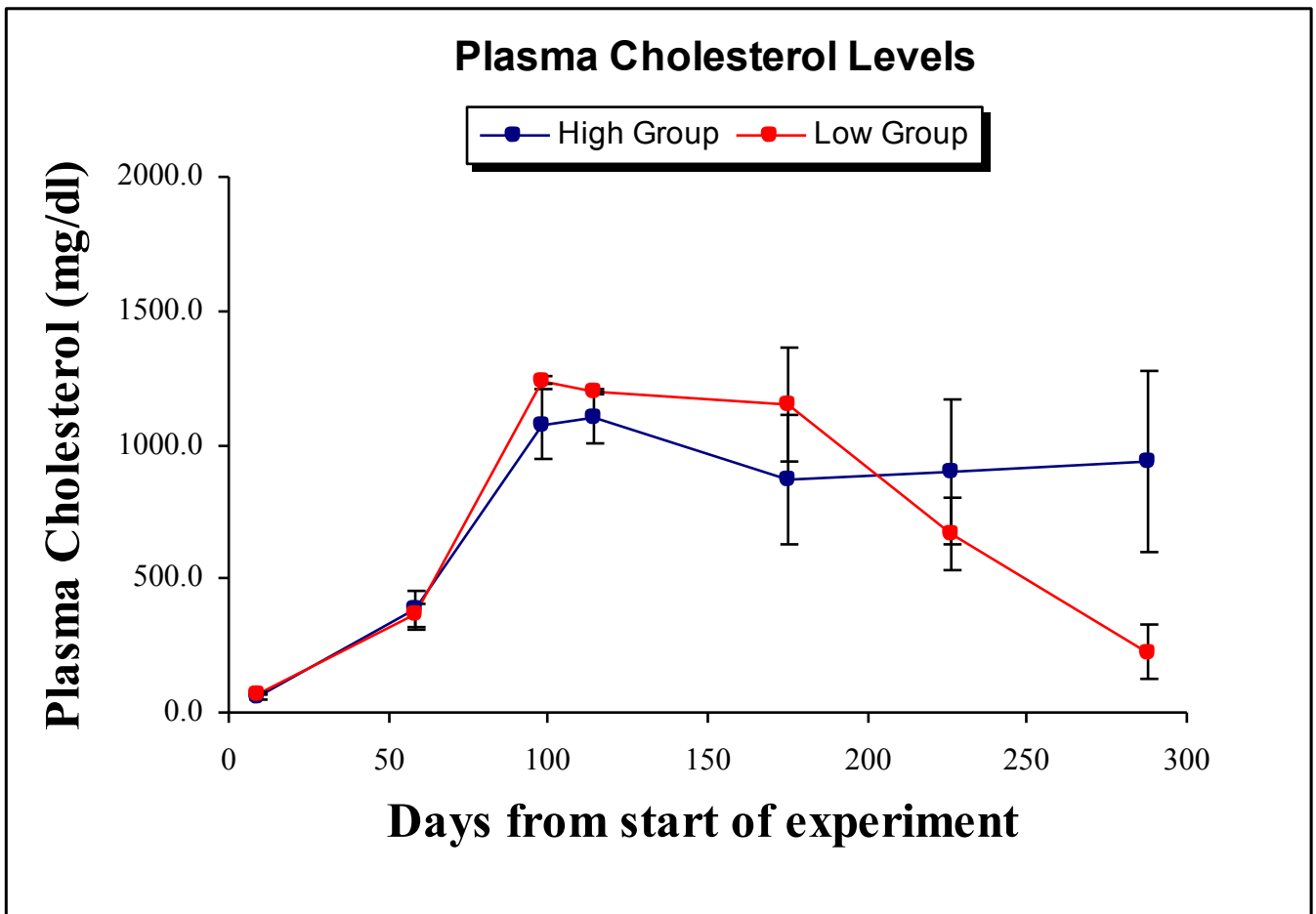


Figure 6.1 Plasma cholesterol concentrations over time

All animals received 0.2% cholesterol enriched diet until day 187 when they were split into two groups. Those illustrated by the blue graph continued on the high lipid diet, whereas those shown on the pink graph reverted to standard rabbit diet.

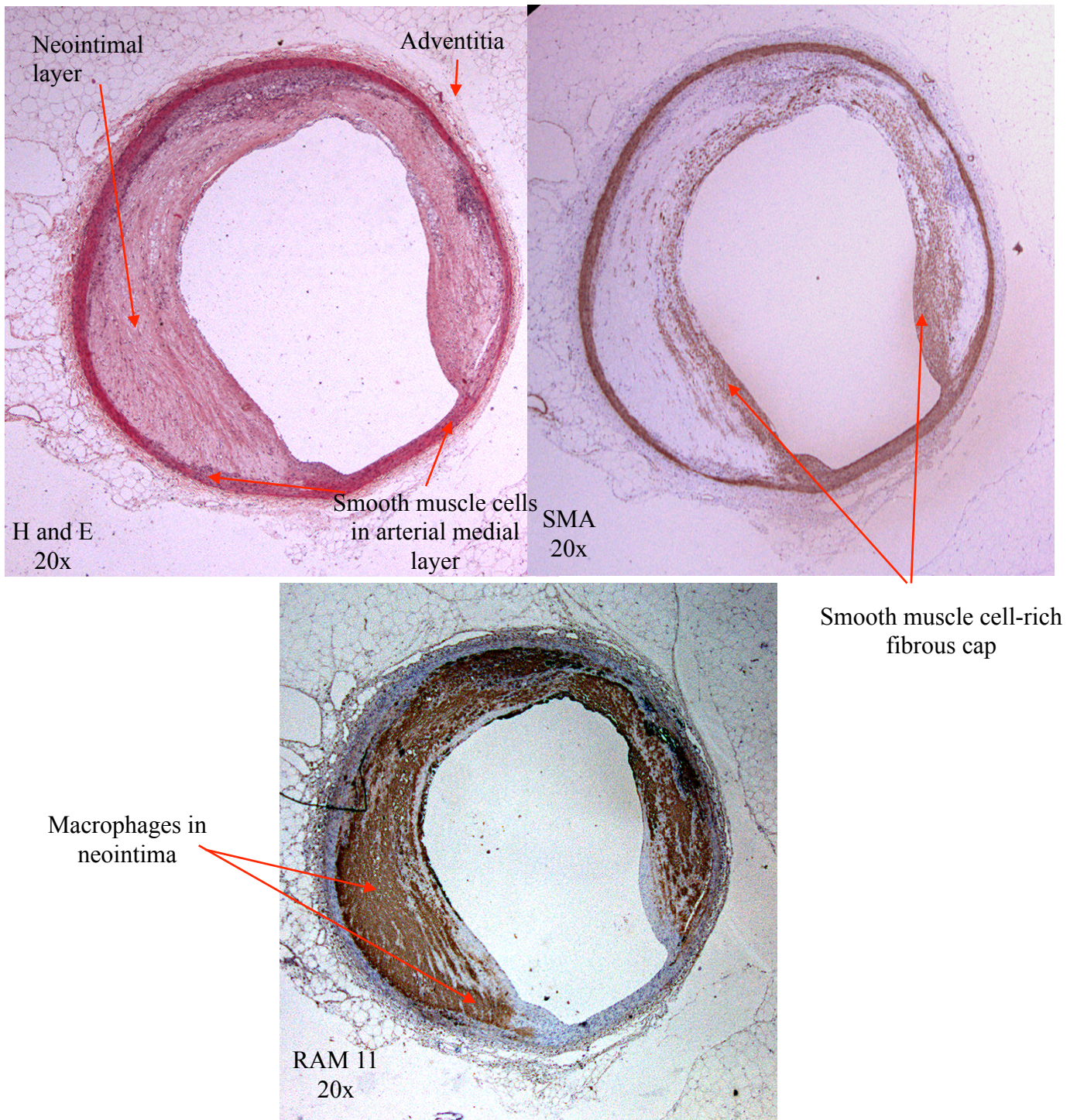
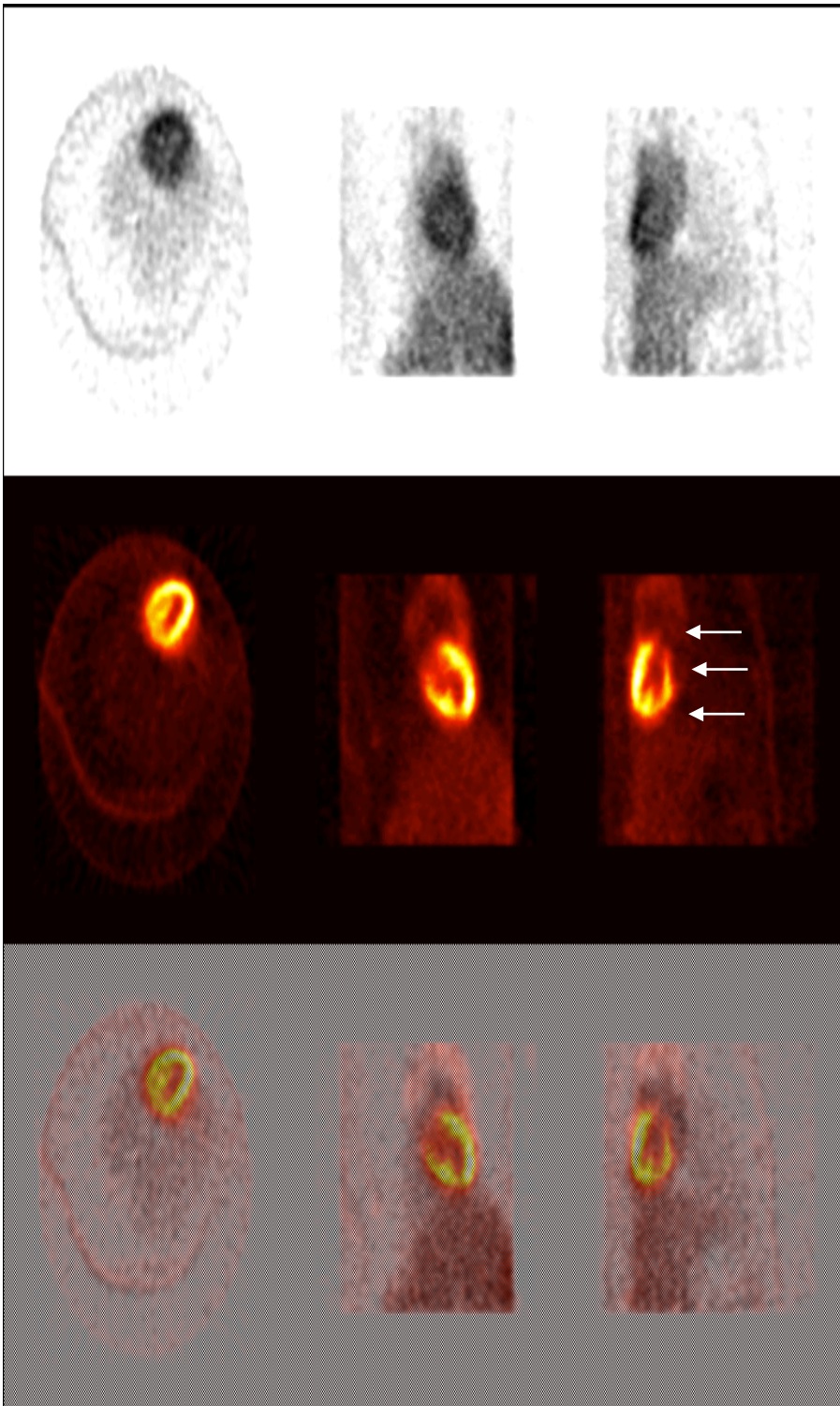


Figure 6.2 *H and E, SMA and RAM 11 stained sections of aorta showing a typical plaque generated by the NZWR model*

The sections are taken from animal 9, which received a high cholesterol diet throughout the experiment.



Early

Late

Composite

Figure 6.3 FDG-PET imaging of control NZWR

Early, late and composite early/late images are shown from top to bottom. From left to right are transaxial, coronal and sagittal planes. There is significant FDG uptake in the myocardial tissue. There is no accumulation of FDG in the descending aorta, whose course is traced out by the white arrows.

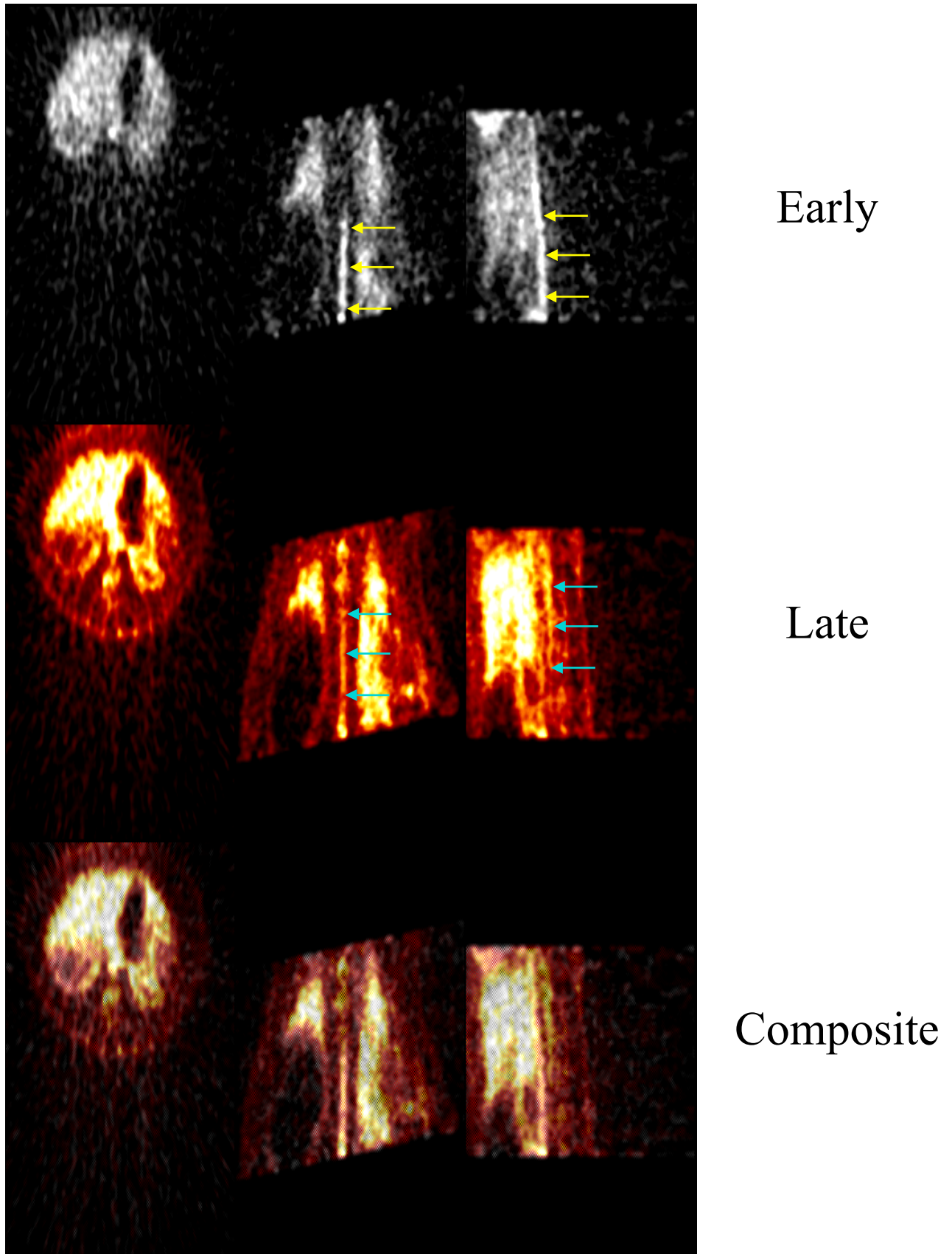


Figure 6.4 FDG-PET imaging of NZWR atherosclerosis during high lipid diet (1)

Early, late and composite early/late images are shown of animal 2, taken 170 days after the start of the experiment. From left to right are transaxial, coronal and sagittal planes. Yellow arrows indicate blood activity in the early images. Blue arrows show late FDG uptake into aortic atherosclerosis. See text for further explanation.

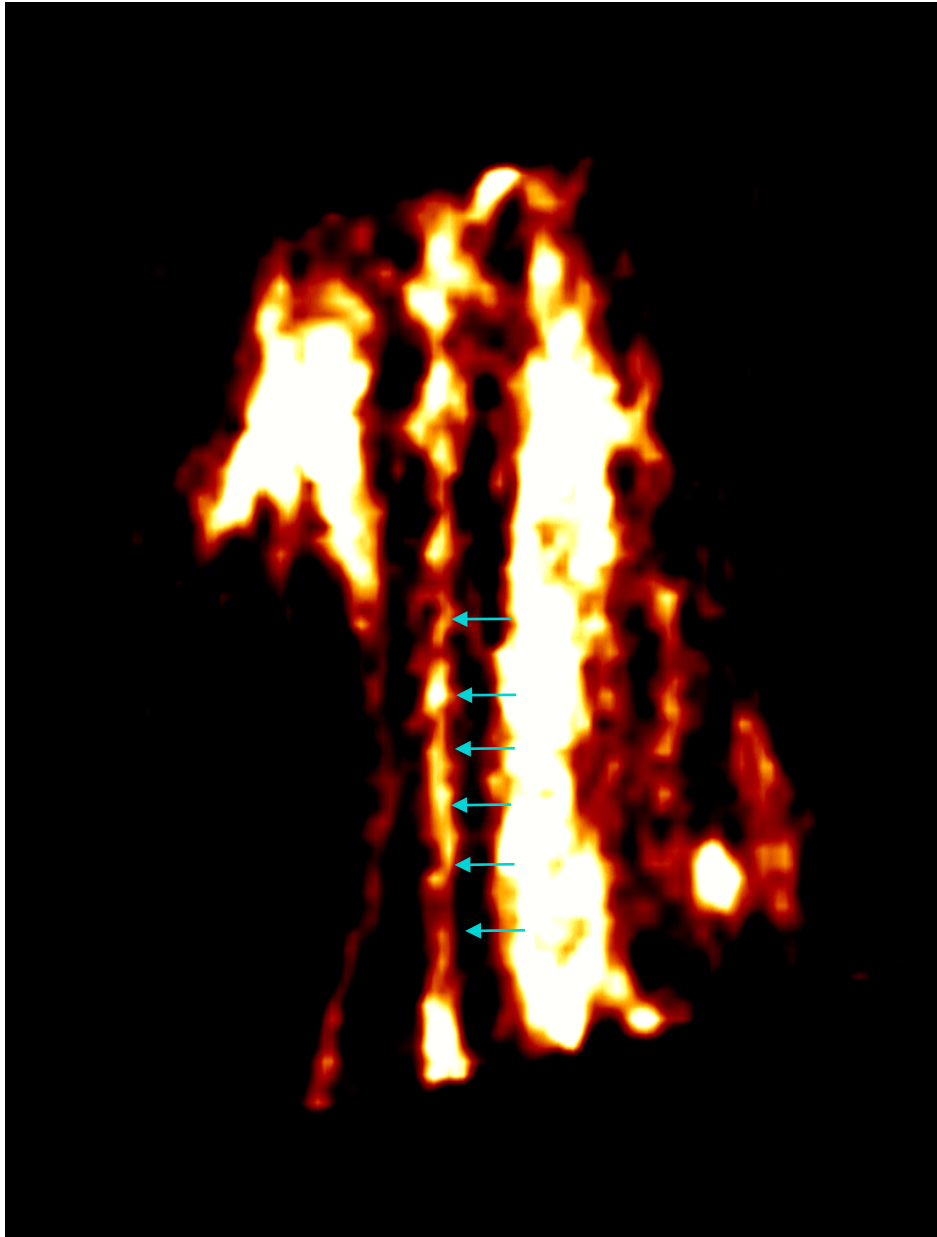


Figure 6.5 FDG-PET imaging of NZWR atherosclerosis during high lipid diet (2)

Coronal image taken 90 minutes after FDG injection, derived from animal 2. Blue arrows show late FDG uptake into aortic atherosclerosis.

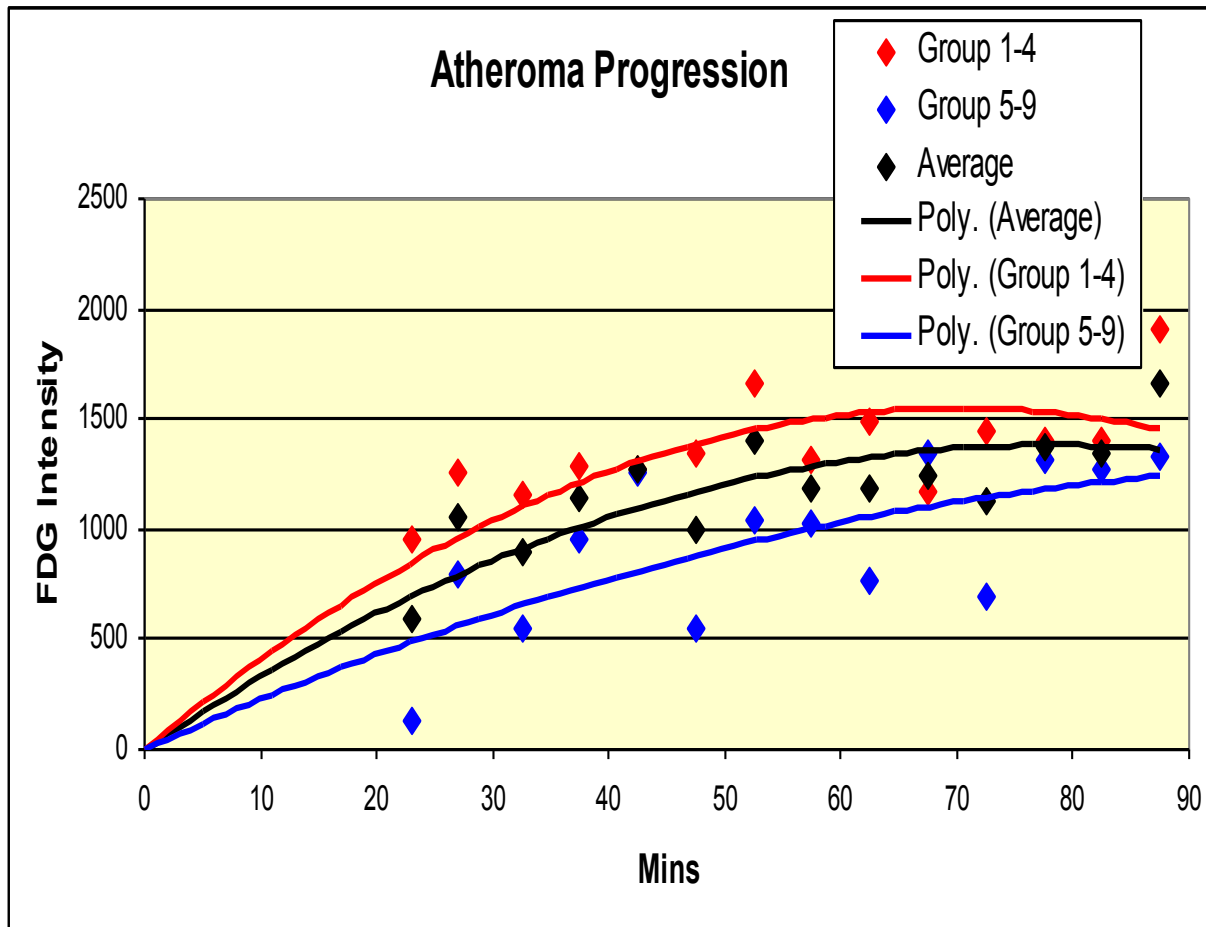


Figure 6.6 Graphical representation of average aortic FDG uptake, after subtraction of FDG signal within the bloodstream.

The average aortic FDG uptake of the whole group is shown in black, those animals destined for low cholesterol diet (1 to 4) are shown in red, and those destined to continue high cholesterol feeding (5-9) are shown in blue. It can be seen that FDG accumulates within the aorta over time, and plateaus at around 70 minutes after injection. Those animals in the red group had a higher serum cholesterol than those in the blue group. The lines are polynomial curves, fitted to the data points.

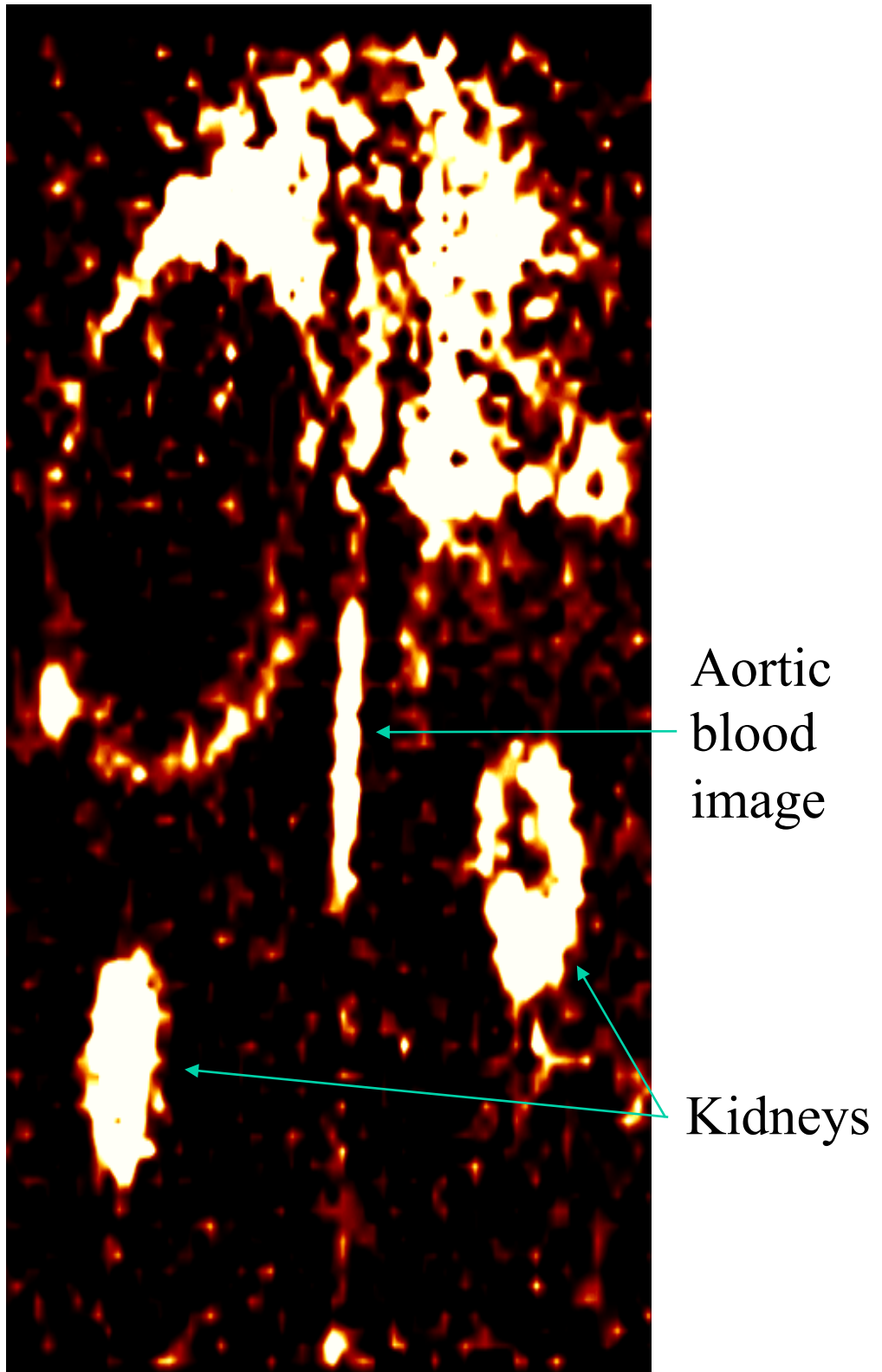
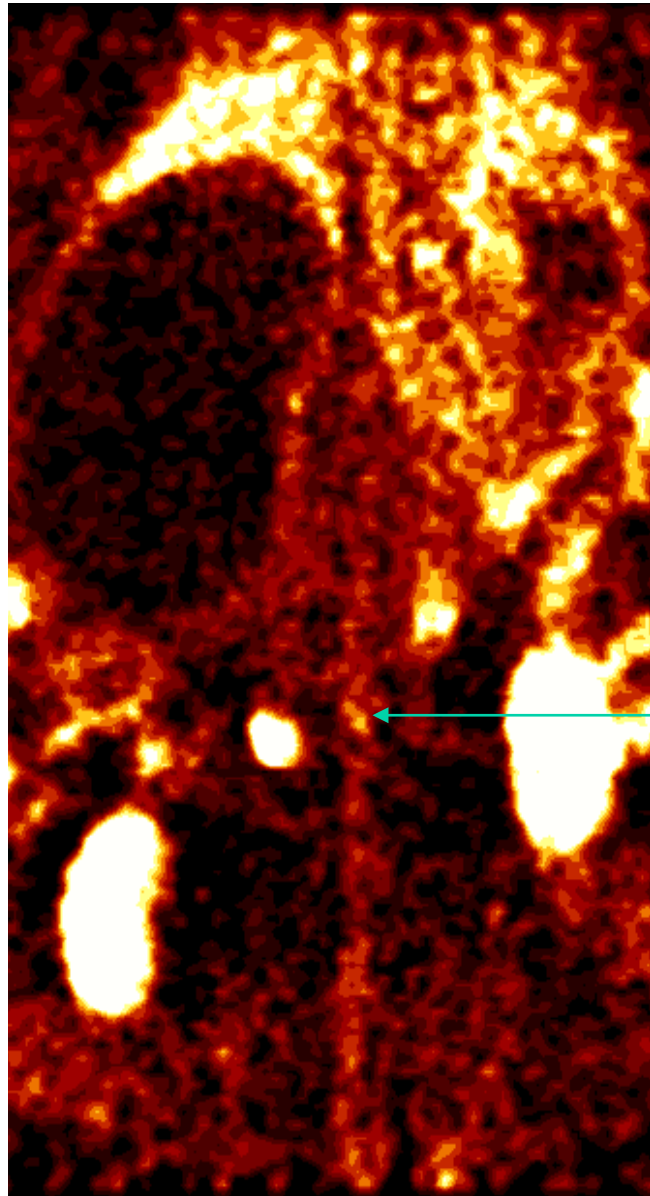


Figure 6.7 FDG-PET imaging of NZWR atherosclerosis, after change to low cholesterol diet (1)

Coronal image of animal 2, taken early after FDG injection. This shows an image of blood within the aorta and kidneys.



Minimal
aortic FDG
uptake

Figure 6.8 FDG-PET imaging of NZWR atherosclerosis, after change to low cholesterol diet (2)

Coronal image of animal 2, taken 90 minutes after FDG injection. This shows low aortic FDG uptake in comparison to adjacent kidneys. This should be compared with Figure 6.5 which is the equivalent image of this animal whilst on high cholesterol diet.

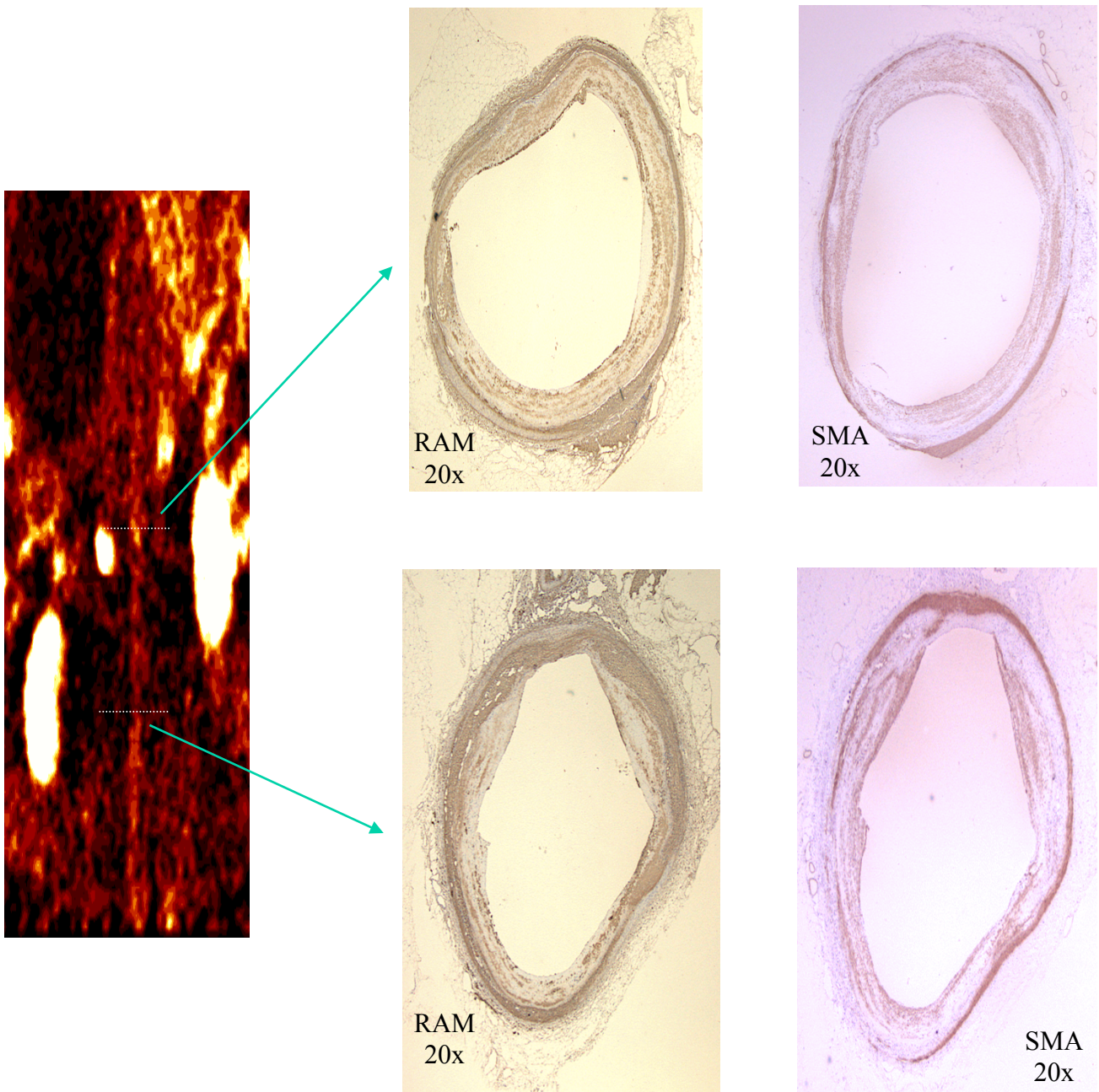
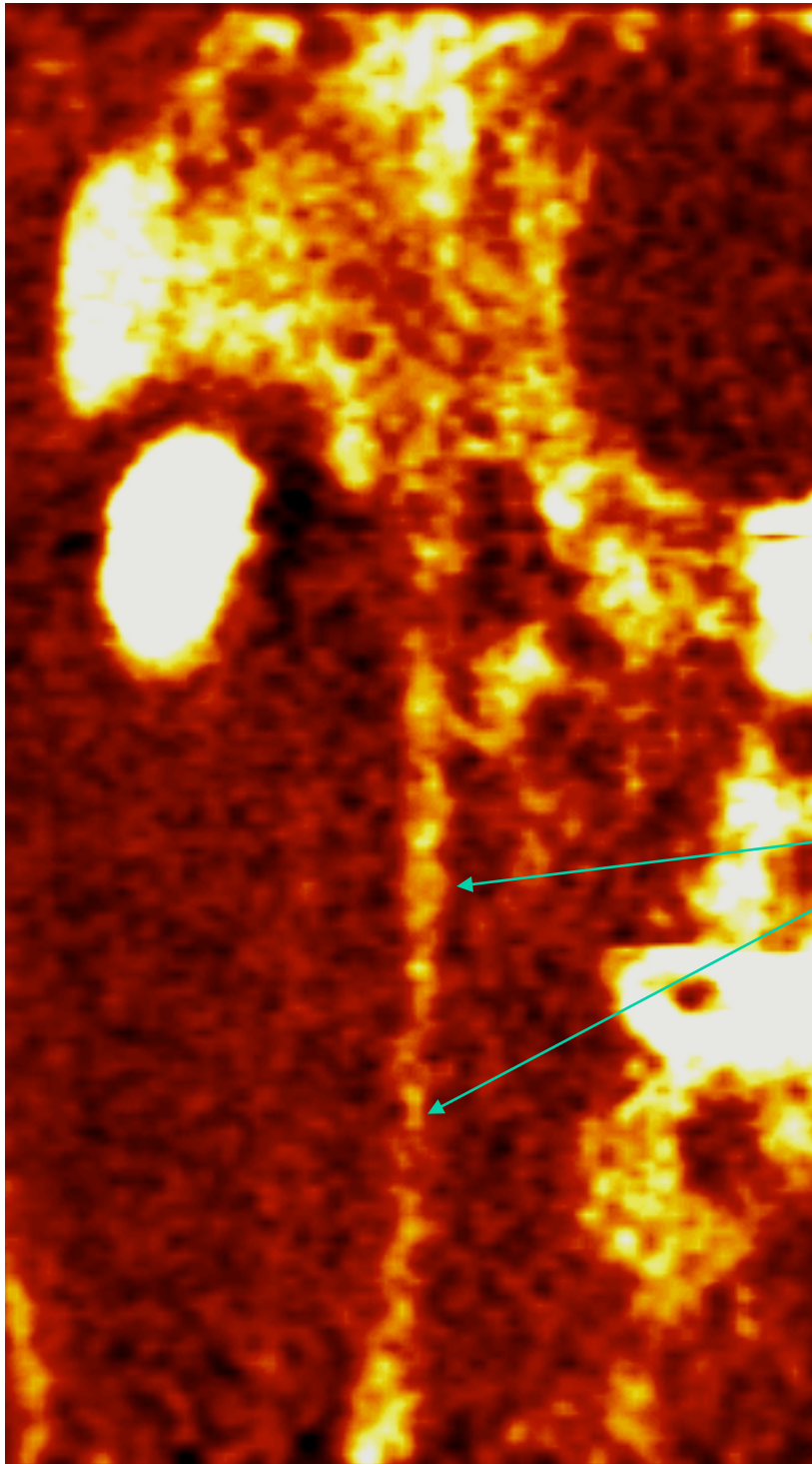


Figure 6.9 FDG-PET imaging of NZWR atherosclerosis, after change to low cholesterol diet, and subsequent histology

Coronal image of animal 2, taken 90 minutes after FDG injection. This shows low aortic FDG uptake in comparison to adjacent kidneys. Histological sections have been taken at two levels of the aorta. Rabbit anti-macrophage (RAM) and smooth muscle actin (SMA) immunohistochemistry have been used. At both levels there is a large neointimal region seen, with some macrophages present. Magnification is x20.



Late aortic
FDG uptake

Figure 6.10 FDG-PET imaging of NZWR atherosclerosis, after continued high cholesterol diet

Coronal image of animal 5, taken 90 minutes after FDG injection. This shows substantial aortic FDG uptake, illustrated by the blue arrows.

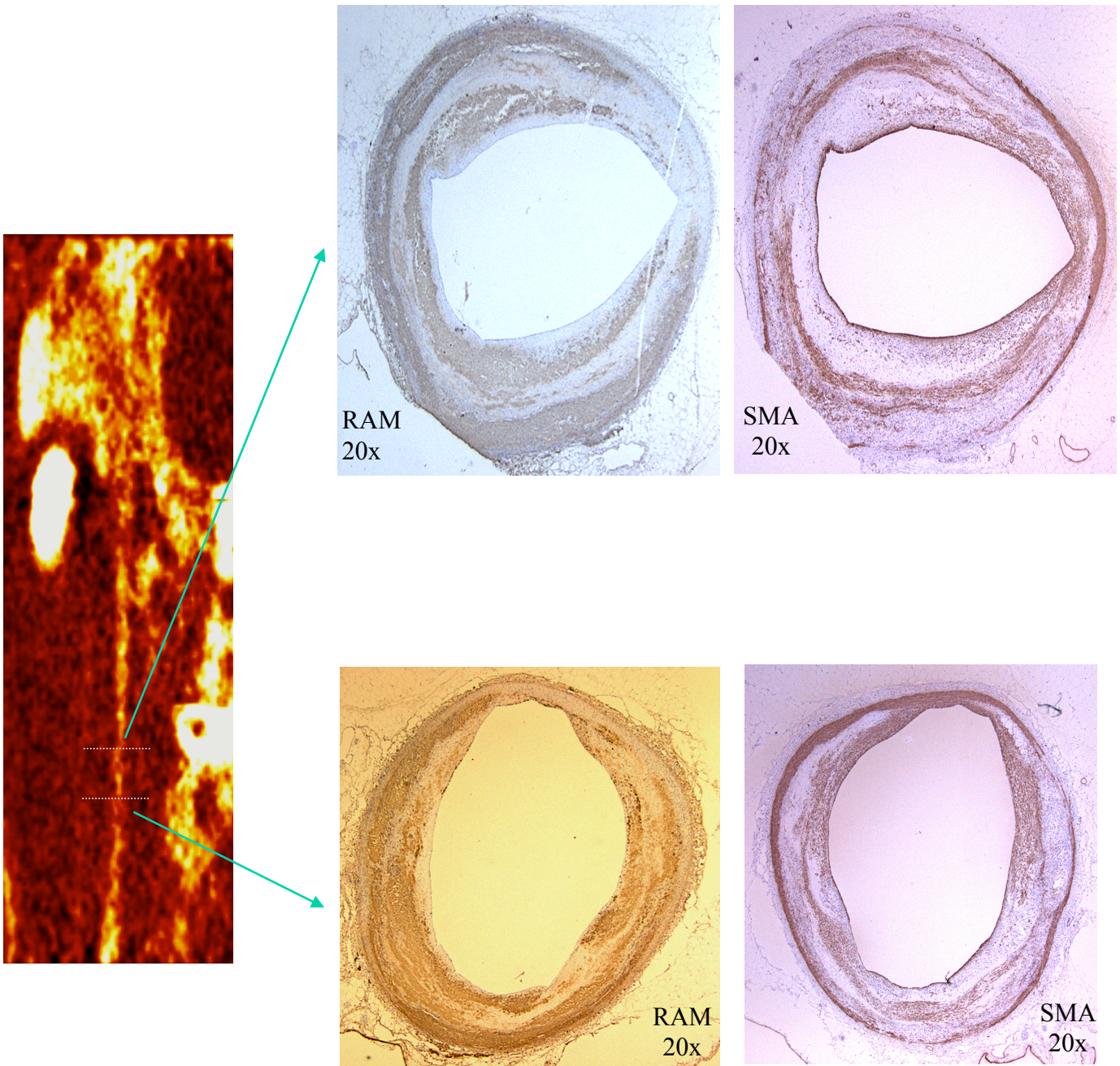


Figure 6.11 FDG-PET imaging of NZWR atherosclerosis, with continued high cholesterol diet, and subsequent histology

Coronal image of animal 5, taken 90 minutes after FDG injection. This shows high levels of aortic FDG uptake. Histological sections have been taken at two aortic levels. Rabbit anti-macrophage (RAM) and smooth muscle actin (SMA) immunohistochemistry have been used. At both levels there are numerous macrophages seen within a substantial neointima. Magnification is x20.

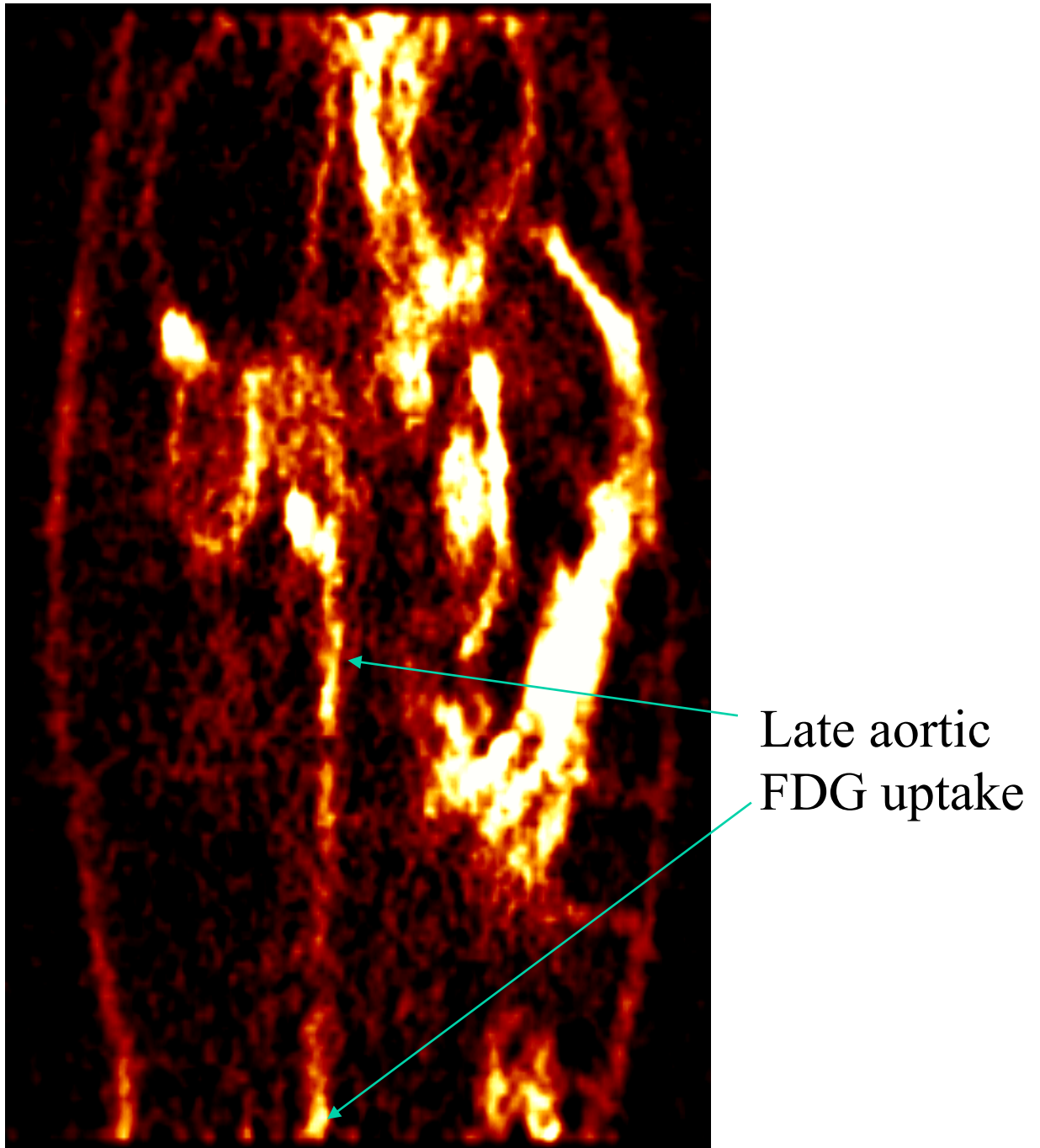


Figure 6.12 FDG-PET imaging of NZWR atherosclerosis, after continued high cholesterol diet

Coronal image of animal 8, taken 90 minutes after FDG injection. This substantial uptake of FDG within the aorta.

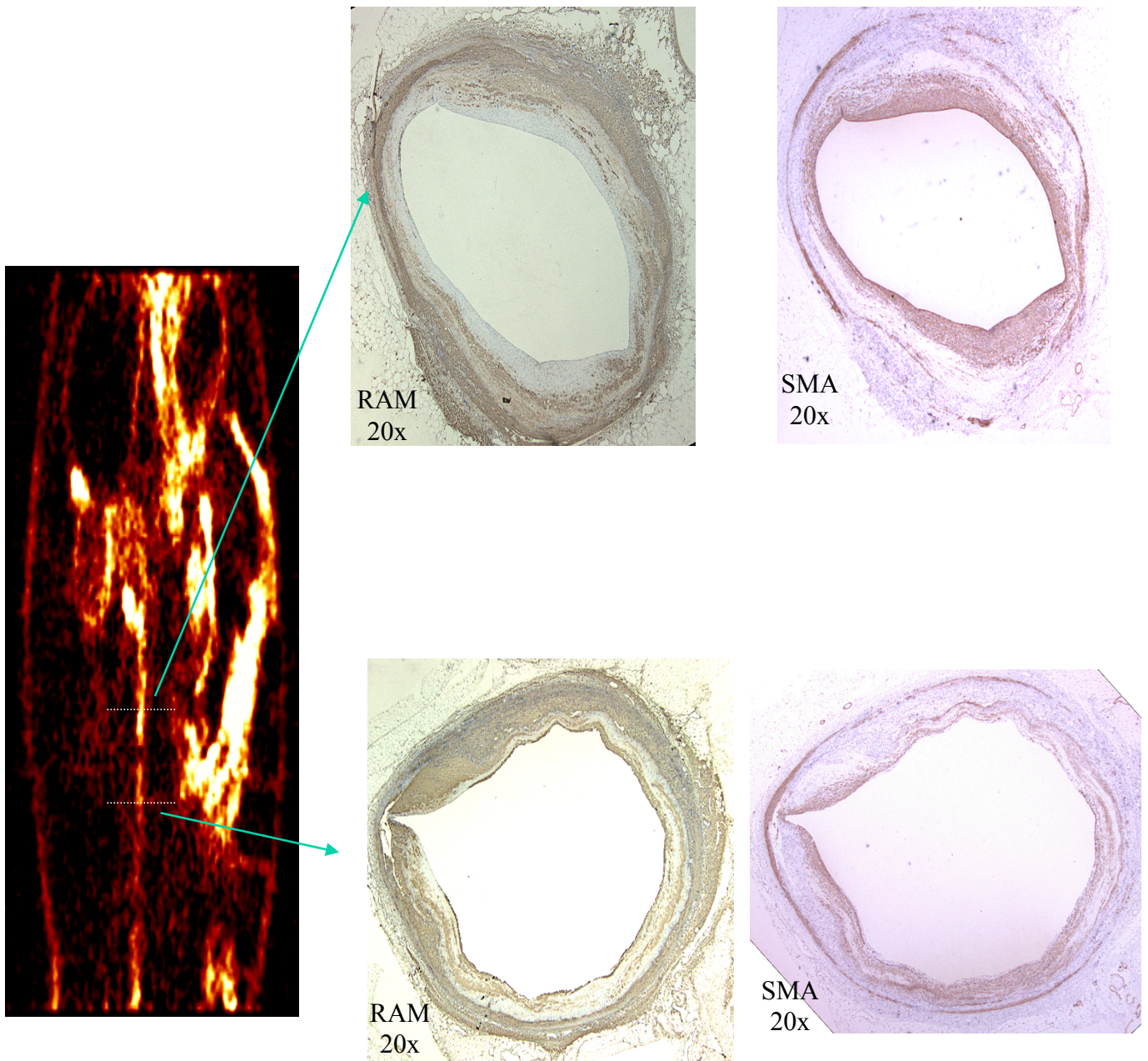


Figure 6.13 FDG-PET imaging of NZWR atherosclerosis, with continued high cholesterol diet, and subsequent histology

Coronal image of animal 8, taken 90 minutes after FDG injection. This shows high aortic FDG uptake. Histological sections have been taken at two aortic levels. Rabbit anti-macrophage (RAM) and smooth muscle actin (SMA) immunohistochemistry have been used. At both levels there are numerous macrophages seen. Magnification is x20.

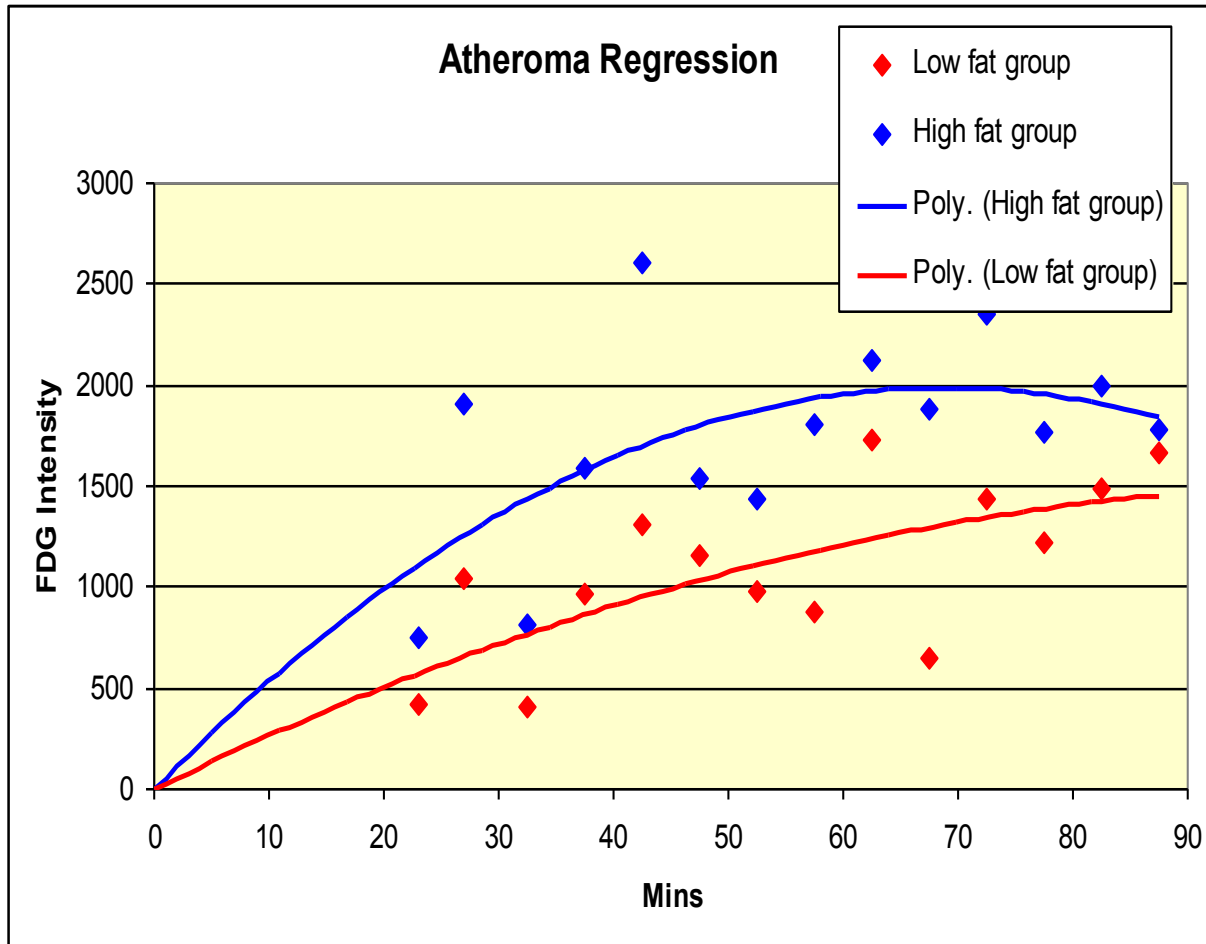


Figure 6.14 Graphical representation of average aortic FDG uptake after the dietary split after subtraction of FDG signal within the bloodstream

The average aortic FDG uptake in those animals on low cholesterol diet are shown in red, and those on high cholesterol diet are shown in blue. It can be seen that FDG accumulates within the aorta over time, and plateaus at around 70 minutes after injection. There was greater average FDG accumulation within the aorta of the high cholesterol group at all timepoints after FDG injection, but this did not reach statistical significance. Those animals in the blue group had a higher serum cholesterol than those in the red group. The lines are polynomial curves, fitted to the data points.

Chapter 7

CHAPTER 7

CONCLUSIONS AND FUTURE DIRECTIONS

Atherosclerosis with its complications remains an important cause of morbidity and mortality in the Western world, and is becoming increasingly problematic in developing countries. Inflammatory cell activity within the atherosclerotic plaque is a key determinant of subsequent fibrous cap rupture within the plaque, and this may lead to life-threatening vascular events.

Various imaging modalities currently exist for visualising the extent of atherosclerotic plaque burden within the individual patient. Contrast angiography, the most universally accepted technique, gives high-resolution images of the arterial lumen, but no information about the plaque itself, in terms of structure, inflammatory state or complications. The ideal imaging tool would inform about the arterial lumen, and also give some indication as to the inflammatory state of the plaque, to help determine its risk of rupture.

Advances in technology have enabled new strategies to get close to the clinical arena. The most likely candidate to emerge from the bunch is high-resolution magnetic resonance plaque imaging, which allows detailed plaque structure to be examined without exposing the patient to ionising radiation. However, despite high quality structural images, the inflammatory state of the plaque is not assessed by MR. Therefore, there is a need for an imaging technique that can assess the degree of plaque inflammation (and hence risk).

This work follows on from the knowledge that plaque inflammation is crucial to rupture (Ross, 1999), and sits alongside that of Casscells and others (Casscells et al., 1996; Verheye et al., 2002) who have demonstrated temperature variations both within the same plaque and between plaques in patients with different clinical presentations. These differences have been exploited to develop catheters that can map temperature contours within the coronary arteries.

This research project has investigated the potential role of FDG-PET to fulfil this requirement. FDG-PET is able to display areas of high metabolic activity within tissues. The hypothesis was that macrophages, driving inflammation within active, symptomatic plaques, would be detectable using FDG-PET, and further that this inflammation would be quantifiable. Initially, the ability of both monocyte THP-1 cells and human blood-derived monocytes to accumulate tritiated deoxyglucose in culture was studied. Results showed that these cells would take up FDG in proportion to their metabolic activity. Moving on from this, symptomatic plaques that had been excised from patients with recent plaque rupture were examined. It was shown using FDG phosphor imaging and autoradiography with tritiated deoxyglucose that these plaques were capable of taking up deoxyglucose, and that there was a co-localisation of deoxyglucose to macrophage-rich areas of the plaques – i.e. these areas of the plaque appeared to have the highest metabolic activity.

In parallel experiments, patients with symptomatic carotid artery disease were imaged using FDG-PET, in combination with computed tomography or MR to provide anatomical co-registration. Results clearly showed that symptomatic plaques accumulated significantly more FDG than did contralateral asymptomatic lesions, a conclusion that fits with the earlier work implicating macrophages as the most metabolically active cell type within the plaques. The combination of FDG-PET and MR imaging of carotid plaques allowed the detection of plaque inflammatory state (from PET) alongside high-resolution MR anatomical definition of the same plaque.

Finally, a small-animal PET scanner was used to image experimentally-induced atherosclerosis within the aortas of rabbits. Comparison of two groups of animals, with one on a high cholesterol diet and the other on normal diet showed some differences in signal intensity between the two groups; the limits of this prototype technology meant that absolute quantification of such differences was not possible. However, it is likely that with a more potent intervention such as the administration of HMG Co-A reductase inhibitors (statin class drugs), and with full data corrections available, clear differences would be shown between plaques that have been stabilised and those that remain at high risk of rupture.

Despite these promising early results, which have been obtained after overcoming many technical challenges, there remain some drawbacks with FDG-PET as a method of non-invasive imaging. It involves the use of ionising radiation, the imaging times are relatively long, and the reproducibility of the technique has not been demonstrated in humans as yet, although serial imaging was performed in the animal work described in Chapter 6. Future work will use less radioactivity (early studies have shown that a dose of 185MBq FDG gives almost as much information as the 370MBq used in this study). Additionally, dynamic protocols might allow both faster image acquisition and full kinetic modelling of FDG behaviour within the plaque. Finally, it is intended to perform an intervention study in patients with symptomatic carotid artery disease, using statin drugs to stabilise plaques, in order to ascertain whether this approach might be useful for monitoring the effect of atheroma-modifying therapies. Two low-dose FDG PET scans will be performed for each patient, one before and one during statin therapy. The PET data from both studies will be compared for evidence of a change in metabolic activity in the index carotid plaques.

It is hoped that by further studying the use of both FDG and more macrophage-specific ligands such as [¹¹C] PK11195, more light will be cast on the contribution of inflammation to plaque rupture. In addition, it is hoped that this work might pave the way for a novel approach to atherosclerosis imaging that reflects the cellular pathology of the disease rather than its anatomical consequences.

7.1 REFERENCES

1. Casscells, W., Hathorn, B., David, M., Krabach, T., Vaughn, W. K., McAllister, H. A., Bearman, G., & Willerson, J. T. (1996). Thermal detection of cellular infiltrates in living atherosclerotic plaques: possible implications for plaque rupture and thrombosis. *Lancet*, 347, 1447-1451.
2. Ross, R. (1999). Atherosclerosis--an inflammatory disease. *N.Engl.J.Med.*, 340, 115-126.
3. Verheye, S., De Meyer, G. R., Van Langenhove, G., Knaapen, M. W., & Kockx, M. M. (2002). In vivo temperature heterogeneity of atherosclerotic plaques is determined by plaque composition. *Circulation*, 105, 1596-1601.